SOHRAB NASIRI

INVESTIGATION OF THE PROPERTIES OF NEW ORGANIC ELECTROACTIVE COMPOUNDS EXHIBITING EITHER PROMPT OR DELAYED FLUORESCENCE

DOCTORAL DISSERTATION

Kaunas
2020

KAUNAS UNIVERSITY OF TECHNOLOGY

SOHRAB NASIRI

INVESTIGATION OF THE PROPERTIES OF NEW ORGANIC ELECTROACTIVE COMPOUNDS EXHIBITING EITHER PROMPT OR DELAYED FLUORESCENCE

Doctoral Dissertation

Technological Sciences, Materials Engineering (T 008)

2020, Kaunas

This doctoral dissertation was prepared at Kaunas University of Technology, Faculty of Chemical Technology, Department of Polymer Chemistry and Technology during the period of 2017−2020. The studies were supported by the Research Council of Lithuania.

Scientific Supervisor:
Prof. Habil. Dr. Juozas Vidas GRAŽULEVIČIUS (Kaunas University of Technology, Technological sciences, Materials Engineering T 008).

Scientific Advisor:
Dr. Dmytro VOLYNIUK (Kaunas University of Technology, Natural Sciences, Chemistry, N 003).

Editor:
Dr. Armandas RUMŠAS (Publishing House "Technologija")

Aurelija Gražina Rukšaitė (Publishing House "Technologija").

The official defence of the dissertation will be held at 1 p.m. 25th of January 2021 at the public meeting of the Dissertation Defence Board of Materials Engineering Scientific Field at the Rectorate Hall at Kaunas University of Technology.
Address: Donelaičio 73-403, LT-44249 Kaunas, Lithuania.
Phone: (+370) 37 30 00 42; fax: (+370) 37 32 41 44; email:doktorantura@ktu.lt.
This doctoral dissertation was sent out on 22 of December 2020.
The doctoral dissertation is available on the internet at http://ktu.edu and at the library of Kaunas University of Technology (Donelaičio 20, LT-44239, Kaunas, Lithuania).

KAUNO TECHNOLOGIJOS UNIVERSITETAS

SOHRAB NASIRI

NAUJŲ ORGANINIŲ ELEKTROAOKTYVIŲ JUNGINIŲ, PASIŽYMINČIŲ GREITĄJA ARBA UŽDELSTĄJA FLUORESCENCIJA, SAVYBIŲ TYRIMAI

Daktaro disertacija

Technologijos mokslai, medžiagų inžinerija (T 008)

2020, Kaunas

Disertacija rengta 2017−2020 metais Kauno technologijos universiteto Cheminės technologijos fakultete, Polimerų chemijos ir technologijos katedroje. Mokslinius tyrimus rėmė Lietuvos mokslo taryba.

Mokslinis vadovas:
Prof. habil dr. Juozas Vidas GRAŽULEVIČIUS (Kauno technologijos universitetas, technologijos mokslai, medžiagų inžinerija, T 008).

Mokslinis konsultantas:
Dr. Dmytro VOLYNIUK (Kauno technologijos universitetas, gamtos mokslai, chemija, N 003).

Redagavo:
Dr. Armandas RUMŠAS (leidykla „Technologija“).
Aurelija Gražina Rukšaitė (leidykla „Technologija“).

Medžiagų inžinerijos mokslo krypties disertacijos gynimo taryba:
Prof. dr. Saulius GRIGALEVIČIUS (Kauno technologijos universitetas, technologijos mokslai, medžiagų inžinerija, T 008) – **pirmininkas**;
Prof. dr. Arvaidas GALDIKAS (Kauno technologijos universitetas, technologijos mokslai, medžiagų inžinerija, T 008);
Prof. dr. Alexander KUKHTA (Baltarusijos valstybinis universitetas, Baltarusija, gamtos mokslai, fizika, N 002);
Dr. Šarūnas MEŠKINIS (Kauno technologijos universitetas, technologijos mokslai, medžiagų inžinerija, T 008);
Prof. dr. Rasa PAULIUKAITĖ (Fizinių ir technologijos mokslų centras, gamtos mokslai, fizika, N 002).

Disertacija bus ginama viešame medžiagų inžinerijos mokslo krypties disertacijos gynimo tarybos posėdyje 2021 m. sausio 25 d. 13.00 val. Kauno technologijos universiteto Diseretacijų gynimo salėje.

Adresas: K. Donelaičio g. 73-403, 44249 Kaunas, Lietuva.
Tel. (370) 37 300 042; faks. (370) 37 324 144; el. paštas doktorantura@ktu.lt.
Disertacija išsiųsta 2020 m. gruodžio 22 d.
Su disertacija galima susipažinti internetinėje svetainėje http://ktu.edu ir Kauno technologijos universiteto bibliotekoje (K. Donelaičio g. 20, 44239 Kaunas).

LIST OF ABBREVIATIONS

OLEDs	Organic light emitting diodes
PVD	Physical vacuum deposition
EIL	Electron injection layer
ETL	Electron transport layer
HTL	Hole transport layer
HIL	Hole injection layer
TM	Transition metal
ACQ	Aggregation-caused quenching
AIE	Aggregation-induced emission
AIEE	Aggregation-induced emission enhancement
CE	Current efficiency
CIE	Commission Internationale de l'Eclairage
CT	Charge transfer
CV	Cyclic voltammetry
D-A-D	Donor-acceptor-donor
DFT	Density functional theory
TG	Thermogravimetric
DSC	Differential scanning calorimetry
EA_{CV}	Electron affinity measured by CV
EL	Electroluminescent
EQE	External quantum efficiency
ES	Energy of singlet state
ET	Energy of triplet state
HOMO	Highest occupied molecular orbital
LUMO	Lowest unoccupied molecular orbital
HTM	Hole transporting materials
ICT	Intramolecular charge transfer
CT	Charge-transfer
IP_{CV}	Ionization potential measured by CV
IP_{PE}	Ionization potential measured by photoelectron emission method
IQE	Internal quantum efficiency
ITO	Indium-tin oxide
MCL	Mechanochromic luminescence
mCP	1,3-Bis(N-carbazolyl)benzene
MoO_3	Molybdenum trioxide
NPB	N,N'-Di(1-naphthyl)-N,N'-diphenyl-(1,1'-biphenyl)-4,4'-diamine
OLEDs	Organic light-emitting diodes
OPVs	Organic photovoltaic cells
PE	Power efficiency
PhOLEDs	Phosphorescent organic light-emitting diodes
PLQY	Photoluminescence quantum yield
ISC	Intersystem crossing
IC	Internal conversion
RISC	Reversed intersystem crossing

DF	Delayed fluorescence
TADF	Thermally activated delayed fluorescence
TTA	Triplet-triplet annihilation
TCTA	Tris(4-(carbazol-9-yl)phenyl)amine
TPBi	2,2',2''-(1,3,5-Benzinetriyl)-tris(1-phenyl-1-H-benzimidazole)
TSPO1	Diphenyl[4-(triphenylsilyl)phenyl]phosphine oxide
UV-VIS	Ultraviolet-visible
$\Delta E_{(S-T)}$	Singlet-triplet energy gap
Δf	Orientation polarizability of solvents
$\lambda_{abs}/\lambda_{em}$	Wavelength of maximum absorption/emission
τ	Excited-state lifetime
χ^2	Values of the accuracy of experiment
SOC	Spin orbit coupling
RTP	Room temperature phosphorescence
R&D	Research and development
S_1	Singlet state
T_1	Triplet state
THF	Tetrahydrofuran
m-MTDATA	4,4',4"-Tris[phenyl(m-tolyl)amino]triphenylamine
NMR	Nuclear magnetic resonance
FTIR	Fourier-transform infrared
OTQx	3,6-di-tert-butyl-9-(3-(3-methoxy-9H-carbazol-9-yl) quinoxalin-2-yl)-9H-carbazole
OCQx	9-(3-(9H-carbazol-9-yl) quinoxalin-2-yl)-3-methoxy-9Hcarbazole
XRD	X-Ray Diffraction
f_w	Water fractions
TOF	Time of Flight
μ_h	Hole mobility
TICT	Twisted ICT
PXZ	Phenoxazine
PTZ	Phenothiazine
ACR	Acridine
CZ	Carbazole
THDP	Tetrahydrodibenzophenanthridine
PI	Phenanthroimidazole
PE	Photoelectron
RIR	Restricted intramolecular rotation
RIV	Restricted intramolecular vibrations
RIM	Restricted intramolecular motions
TICT	Twisted intramolecular charge transfer
λ_F^{max}	Wavelength of maximum fluorescence
λ_{abs}^{max}	Wavelength of maximum absorption
V_{on}	Turn-on voltage
L_{max}	Maximum brightness
α	Field dependence parameter
E_g^{opt}	Optical band gap

k_{PF}	Rate of prompt fluorescence
k_{ISC}	Rate of intersystem crossing
k_{DF}	Rate of delayed fluorescence
k_{RISC}	Rate of reverse intersystem crossing
γ	Charge-balance factor
ϕ_{PL}	Photoluminescence quantum yield
χ	Efficiency of exciton production
η_{out}	Out coupling efficiency

TABLE OF CONTENTS

1. INTRODUCTION……..……..…9
2. RESULTS AND DISCUSSION……...17
2.1. Carbazole derivatives containing one or two tetra-/triphenylethenyl units as efficient hole-transporting OLED emitters……....17
2.2. Xanthenone based OLED emitters exhibiting both aggregation induced emission enhancement and thermally activated delayed fluorescence ……...…….23
2.3. Derivatives of tetrahydrodibenzophenanthridine and phenanthroimidazole as efficient blue emitters and its applications...…….. ……..32
2.4. Application in OLEDs of Tetra-/Triphenylethenyl Substituted 9,9-Dimethylacridine Derivatives …….…....38
2.5. Multifunctional D-A-D' type compounds: Mechanochromic Luminescence, Thermally Activated Delayed Fluorescence and Aggregation Enhanced Emission…….……...….48
3. CONCLUSIONS …….…....52
4. SANTRAUKA ……..…….…..54
4.1. ĮVADAS 54
4.2. REZULTATAI IR JŲ APTARIMAS.....56
4.2.1. Karbazolo dariniai, turintys vieną ar du tetra-/trifeniletenilpakaitus, kaip efektyvūs sky-les pernešantys OLED spinduoliai.....56
4.2.2 Ksantenono dariniai, pasižymintys agregacijos sustiprinta emisija ir termiškai aktyvint-ąja uždelstąja fluorescencija, kaip OLED spinduoliai.....59
4.2.3.Tetrahidrodibenzfenantridino ir fenantrimidazolo darinių fotofizikinės ir elektroliumin-escencinės savybės.....63
4.2.4.Tetra-/trifeniletenlpakeistų 9,9-dimetilakridino darinių fotofizikinės ir elektroliuminesc-encinės savybės.....65
4.2.5.Daugiafunkcinių D-A-D' tipo junginių, pasižyminčių mechanochromine liuminescencija, termiškai aktyvuotoji uždelstąja fluorescencija ir agregacijos sustiprinta emisija, elektroliuminescencinės savybės.....67
4.3. IŠVADOS.....70
5. REFERENCES ……...……...72
6. CURRICULUM VITAE…….....78
7. LIST OF PUBLICATIONS……..…...79
8.ACKNOWLEDGMENTS…….……...81
9. COPIES OF THE PUBLICATIONS …… 82

1. INTRODUCTION

Organic light-emitting diodes (OLEDs) emerged as one of the most dominant display technologies and potentially as the next generation solid-state light source[1]. The first approach to the OLED technology which caused a wide interest was conducted by researchers from Eastman-Kodak in 1987[2]. OLED has inspired the research of many scientists all over the world and has thus become an important component for the display and lighting technologies since its first commercialization in 1997[3]. Generally, OLEDs are double charge injection devices requiring simultaneous injection of both electrons and holes into the adjacent organic layer, which is followed by the emission of electroluminescence[4]. A facile, balanced charge transport, and a high conversion efficiency of excitons to light are required for an efficient OLED[5]. In order to achieve an efficient recombination of holes and electrons in the emitting layer, a π-conjugated structure of organic electroluminescent materials is required[6]. Also, suitable optical and photophysical properties, good thermal and morphological stability, as well as appropriate energy levels are the main requirements for the organic electroactive materials intended for the fabrication of highly efficient electroluminescent devices[5]. A combination of different donor (D) and acceptor (A) moieties in the structures of organic electroactive compounds offers possibility to achieve a broad range of the desired properties[7]. The basic structure of OLED consists of three layers: the anode, the cathode, and a thin layer of an organic emissive semiconducting compound placed in between them[8]. OLEDs can be exploited at low voltages to provide high brightness, wide viewing angles, a quick response and low energy consumption[7].

The principal ways for the fabrication of OLEDs are physical vacuum deposition (PVD) and solution-process deposition[9].

Both approaches have advantages as well as disadvantages. Thus, thermal evaporation appears to be a successful way to achieve high efficiency with such advantages as the immaculate deposition and precise layer thickness control[9]. However, huge wastage of compounds in the chamber makes it extremely expensive. Solution processing with such methods as coating or printing, which are highly cost-effective and feasible for mass manufacturing, provides a promising alternative to vacuum deposition. Nevertheless, such problems as the solubility of some organic materials in various organic solvents and the undesired blending of two organic layers during the subsequent coatings still remain the major challenges for the commercial application of solution-processing[10].

Recently, OLEDs have been designed via using the charge blocking principle to achieve efficient carrier recombination in the emitting layer (**Fig. 1.1**). By prevention of traveling electrons (holes) from the cathode (anode) to the host layer,

more electron-hole pairs could be generated in the host, and, hence more excitons would be available to be delivered to the dopants[11]. This is usually achieved by inserting a thin blocking layer, or a layer of some organic material that is particularly good for only one type of the carrier transport, adjacent to the host. This would effectively shift the exciton formation interface away from the host/transport layer interface to the host/blocking layer interface[12].

The following layers are typical for a modern OLED using materials suitable for each function:

- Electron injection layer (EIL);
- Electron transport layer (ETL);
- Hole blocking layer (HBL);
- Emission layer (EML), for electron/hole transport and their recombination to form an exciton which generates light emission;
- Hole transport layer (HTL);
- Hole injection layer (HIL);

EIL and HBL can also be used to control the location where the excitons are formed by blocking the hole transport. The charge transport layers ensure a good injection and transport of charge carriers towards the emission layer, where the excitons are formed[10]. To optimize the charge carrier balance, the EML is enclosed by two charge blocking layers which confine the charges inside the EML and thus ensure that all the charges recombine[13],[14]. Therefore, it is extremely important to design OLEDs while taking into account the relationships between the work function, the highest occupied molecular orbital (HOMO) level, and the lowest unoccupied molecular orbital (LUMO) level of each layer[15]. In addition, the values of the ionization potential and the charge mobility of the working materials are important.

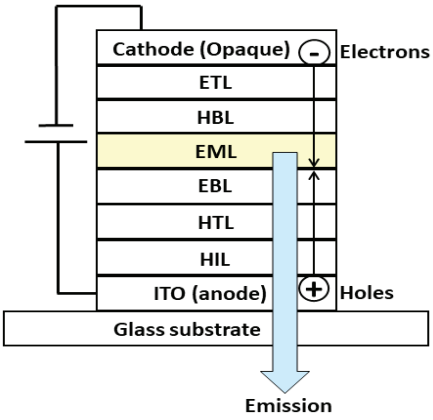

Fig. 1.1. Schematic representation of multilayer OLED structure

A huge impact on the development of OLEDs was made by Tang and Van Slyke who fabricated a device with an operating voltage of less than 10 V whose brightness exceeded 1000 cd/m^2, and whose efficiency was ca. 1%[2]. OLEDs of the first generation were fabricated by using prompt fluorescence compounds[2]. In this case, even when using molecules exhibiting photoluminescence quantum yield (PLQY) close to 100%, the maximum external quantum efficiency (EQE) of OLEDs possible is below 5%[16]. This is because of the limitation imposed by the spin statistics in organic emitters. In pure fluorescent emitters, the fraction of the emissive singlet excitons that are created from charge recombination in an OLED is below 25%, and the light extraction efficiency is often around 20%[13]. Therefore, mechanisms to harvest triplet excitons in organic emitters and to convert them to emissive singlet excitons are paramount in order to improve device efficiency.

Phosphorescent OLEDs (PHOLEDs) represent the second generation of OLEDs which emit light from the triplet state[17]. In these devices, precious noble metal complexes facilitate intersystem crossing (ISC) from the excited singlet state to the triplet state[17]. Typically, in phosphorescent OLEDs, the emitters are organometallic complexes with iridium (Ir) or platinum (Pt) cores[18]. Their excited singlet states undergo fast ISC to the lowest triplet state[17]. In PHOLEDs, IQE approaching 100% is possible through radiative recombination of both singlet and triplet excitons[19]. The main limitation of the phosphorescent dyes is their comparatively long radiative lifetime (in the microseconds range) which leads to undesirable side effects, namely, quenching processes[20].

The third generation of OLED emitters comprises organic donor-acceptor systems[21], as well as transition metal (TM) complexes with a small singlet-triplet energy gap ΔE_{ST} which lies within the range of thermal energy[22,23]. Because of the small ΔE_{ST}, reverse intersystem crossing (RISC) from the lowest excited triplet state to the lowest excited singlet state is reasonably done, and thermally activated delayed fluorescence (TADF) is performed, (TADF is called E-type delayed fluorescence (DF) in the older literature)[24]. Like PHOLEDs, TADF-based OLEDs show an internal quantum efficiency of up to 100%[25]. A disadvantage of many presently available TADF OLEDs that they share with the PHOLEDs is the rather low intrinsic radiative transition rate ($k_r=10^6$-10^7 s^{-1}) of the emitters which makes them sensitive to non-radiative decay processes[19]. Also, the emission from the states with the charge-transfer (CT) character is typically rather broad, which is not favorable for application in displays[15]. In order to realize high-efficiency OLEDs, two major factors have to be taken into account. First, the internal quantum efficiency (IQE) must be close to 100%, and, secondly, the extraction of light out of the device must be as efficient as possible.

By adding a small quantity of an emissive material to a host material, it is possible to improve the efficiency or to change the emission color. This method is called doping, and the materials used for doping are called dopants[26]. This technique is especially useful for materials in which the emission yield decreases at high density (concentration quenching)[20]. In addition, p and n type doping can lead to optimized charge carrier injection and transport[27]. Host materials increase the number of free charges in the organic layers so that the conductivity rises by several orders of magnitude[25]. For efficient TADF based EL devices, particularly for orange emissive exciplex-based OLEDs, host materials are usually necessary in order to prevent concentration quenching and triplet-triplet annihilation[27]. TADF based OLEDs can be fabricated with potentially lower costs, while maintaining efficiencies as high as those achieved for OLEDs based on phosphorescent emitters. Careful selection of the suitable host should generally be important, and the materials must possess suitable singlet (S_1) and triplet (T_1) energies so that to ensure efficient energy transfer from the host to the emitter[28,29]. In order to realize charge carrier injection from two electrodes and balance recombination of the two carriers in the emitting layer (EML), bipolar hosts are required for the reduction of exciton quenching and injection barriers[30,31].

Pure organic luminescent molecules whose energy gaps between S_1 and T_1 (**Fig. 1.2**) are generally large (above 0.5 eV) usually exhibit prompt fluorescence and do not show any phosphorescence. However, with the help of spin orbit coupling (SOC) from heavy metal atoms, the rate of ISC in organic metal complexes can be dramatically enhanced, resulting in strong room temperature phosphorescence[32].

TADF is a special radiative transition of excitons from the S_1 state, due to intersystem crossing (ISC) from T_1 state resulting in delayed emission with a longer life time than that of the prompt fluorescence[33]. As it is shown in **Fig. 1.2**, RISC from T_1 to S_1 generates the final emissive singlet excitons which are involved in the TADF.

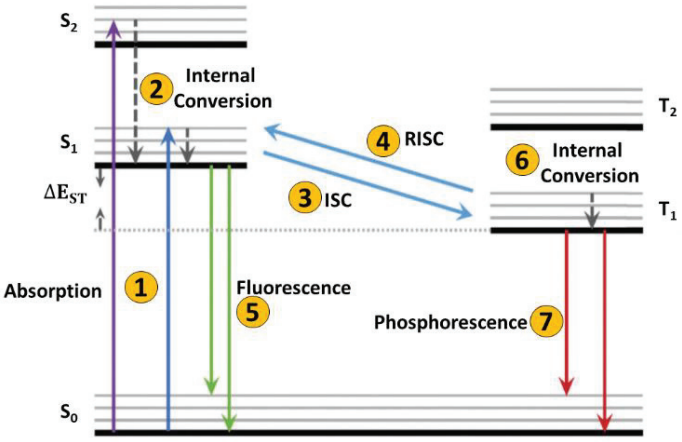

Fig. 1.2. Transition processes of photogenerated excitons for fluorescence (1→ 2 → 5), phosphorescence (1→ 2 → 3 → 6 → 7) and thermally active delayed fluorescence (1→ 2 → 3→ 4 → 5) in organic molecules[34]
1= absorption, 2 and 6 = internal conversion (IC), 3= intersystem crossing, 4 = reversible or reverse intersystem crossing, 5 = fluorescence, 7 = phosphorescence

The energy level of the S_1 state is usually located above that of the T_1 state, therefore, RISC is an endothermal process requiring thermal activation[34]. The intensity of TADF increases with the increase of the temperature[35]. Organic materials exhibiting TADF were also successfully exploited as hosts to yield high-performance OLEDs[35]. Since TADF is a thermally activated process, it is important to secure the intensive emission at lower temperatures. In order to minimize the temperature dependence of TADF, it is necessary to minimize the singlet-triplet energy splitting (ΔE_{ST}). RISC is not expected to occur for the emitters with ΔE (S_1-T_1) distinctly above ~0.13 eV[36,37]. Generally, TADF materials have a long delayed exciton lifetime and a strong intramolecular charge transfer (ICT) character[38]. Due to these characteristics, TADF OLEDs can exhibit high roll-off efficiency and broad emission spectra[38]. In order to obtain high efficiency, the selection of the suitable host materials is very important. In order to have suitable triplet energy (T_1) level and the balanced charge transport, care must be taken while designing the TADF host material. Meanwhile, to fabricate the TADF devices, host materials possessing high T_1 level over 3.0 eV are preferable[39].

Photoluminescence (PL) enhancement in the solid state and the higher values of PLQY of the solid samples than those of the corresponding solutions can be achieved due to aggregation induced emission (AIE) or aggregation induced emission enhancement (AIEE)[40,41]. AIE was first reported by Tang and his coworkers in the past decade, and it has continued to be one of the most active areas in the research on organic emitters[40,41]. Materials displaying AIE or AIEE are

strongly emissive in the aggregated or solid state[42]. The reasons of these phenomena are related to the restricted intramolecular rotation[43], restricted intramolecular vibrations and restricted intramolecular motions[44,45,46]. The AIE activity of compounds can be demonstrated by the emission behavior of the dispersions of emitters in the mixtures of tetrahydrofuran (THF) and water with the quantitative change of the water content[47,48].

Despite very active research in the design, synthesis and studies of organic emitters for OLEDs, including those exhibiting phosphorescence, TADF and AIEE, information on the relationship of the structure and properties of organic emitters and hosts and on their performance in OLEDs is still required. The 'critical amount' of such information will allow developing efficient, stable and cost effective OLEDs.

The aim of this work is the investigation and comprehensive analysis of the properties and performance in OLEDs of new organic electroactive compounds necessary for the establishment of the structure-properties relationship.

To achieve the aim of the work, the following tasks are formulated:

- Investigation of the photophysical and electroluminescent properties of carbazole derivatives containing one or two tetra-/triphenylethenyl units.
- Evaluation of the photophysical, photoelectrical and charge transporting properties of xanthenone derivatives.
- Investigation of the photophysical, electrochemical and electroluminescent properties of the derivatives tetrahydrodibenzophenanthridine and phenanthroimidazole.
- Investigation of the photophysical properties and performance in OLEDs of tetra-/triphenylethenyl substituted 9,9-dimethylacridine derivatives.
- Investigation of the electroluminescent properties of non-doped and doped devices based on unsymmetrical D-A-D' type TADF emitters in which differently substituted carbazole donor moieties are directly linked to the quinoxaline unit.

The novelty of the work:

- OLEDs containing new derivatives of carbazole containing one or two tetra-/triphenylethenyl units were fabricated and characterized.
- Investigation of the electroluminescence properties has proven that the compounds 9-ethyl-N,N-bis(4-(2,2-diphenylethenyl)phenyl)car-bazol-3-

amine and 9-ethyl-N,N-bis(4-(1,2,2-triphenylethenyl)phen-yl)carbazol-3-amine can be used for both hole-transporting and emissive layers.

- Blue, green and yellow OLEDs based on new xanthenone derivatives exhibiting both thermally activated delayed fluorescence and aggregation induced emission enhancement were fabricated and characterized.
- Derivatives of xanthenone containing di-tert-butyl-carbazolyl, di-tert-butylacridanyl, di-tert-butyl-phenothiazinyl and penoxazinyl moieties exhibited bipolar properties.
- Photophysical, electrochemical and electroluminescent properties of new derivatives tetrahydrodibenzophenanthridine and phenanthroi-midazole were studied.
- Aggregation induced emission enhancement was demonstrated for tetra-/triphenylethene-substituted 9,9-dimethylacridines for the first time and their electroluminescent properties were studied.
- Electroluminescent characterization of new series of asymmetrical D-A-D' type TADF emitters in which differently substituted carbazole donor moieties are directly linked to the quinoxaline unit was performed. It was shown that the efficiency of OLEDs can be improved, and the emission color can be modified when 9-(3-(9H-carbazol-9-yl)quinoxalin-2-yl)-3-methoxy-9H-carbazole and 3,6-di-tert-butyl-9-(3-(3-methoxy-9H-carbazol-9-yl)quinoxalin-2-yl)-9H-carbazole are used in the device structures.

Personal input of the author

The author investigated photophysical, electrochemical, photoelectron emission, charge transporting and electroluminescent properties of five series of organic electroactive compounds. dr. Monika Cekaviciute (Department of Polymer Chemistry and Technology, Kaunas University of Technology) synthesized tetra-/triphenylethenyl-substituted derivatives of carbazole. Measurements of the thermal propertieties by thermogravimetry (TG) and differential scanning calorimetry (DSC) were performed by dr. Jurate Simokaitiene (Department of Polymer Chemistry and Technology, Kaunas University of Technology). Ms. Aina Petrauskaite (Department of Polymer Chemistry and Technology, Kaunas University of Technology) performed cyclic voltammetry (CV) measurements. Charge mobility measurements were done in collaboration with dr. Dmytro Volyniuk (Department of Polymer Chemistry and Technology, Kaunas University of Technology). Theoretical calculations were performed by dr. Viktorija Andruleviciene (Department of Polymer Chemistry and Technology, Kaunas University of Technology). Eventually, the results were further analyzed by the author. Mr. Simas Macionis

(Department of Polymer Chemistry and Technology, Kaunas University of Technology) synthesized and purified derivatives of xanthenone. dr. Dalius Gudeika (Department of Polymer Chemistry and Technology, Kaunas University of Technology) designed derivatives of xanthenone and performed CV measurements. Mr. Manojkumar Dhanthala Thiyagarajan (Department of Chemistry, School of Advanced Sciences, Vellore Institute of Technology) synthesized and purified derivatives of tetrahydrodibenzophenanthridine and phenanthroimidazole. dr. Umamahesh Balijapalli (Department of Chemistry, School of Advanced Sciences, Vellore Institute of Technology) characterized derivatives of tetrahydrodibenzophenanthridine and phenanthroimidazole. Prof. Madhvesh Pathak (Department of Chemistry, School of Advanced Sciences, Vellore Institute of Technology) performed FTIR analysis of the compounds. Prof. Sathiyanarayanan Kulathu Iyer (Department of Chemistry, School of Advanced Sciences, Vellore Institute of Technology) designed the structures and routes of the synthesis of the compounds. dr. Galyna Sych (Department of Polymer Chemistry and Technology, Kaunas University of Technology) performed theoretical calculations of the derivatives of carbazole and quinoxaline. dr. Ramin Pashazadeh (Department of Polymer Chemistry and Technology, Kaunas University of Technology) designed and synthesized the compounds. Mr. Karolis Leitonas (Department of Polymer Chemistry and Technology, Kaunas University of Technology) investigated absorption and photoluminescence spectra. X-ray diffraction analysis was performed by dr. Algirdas Lazauskas (Institute of Materials Science, Kaunas University of Technology).

List of scientific publications on the topic of the dissertation

1. **Sohrab Nasiri**; Monika Cekaviciute; Jurate Simokaitiene; Aina Petrauskaite; Dmytro Volyniuk; Viktorija Andruleviciene; Oleksandr Bezvikonnyi; Juozas Vidas Grazulevicius. Carbazole derivatives containing one or two tetra-/triphenylethenyl units as efficient hole-transporting OLED emitters// Dyes and Pigments. ISSN 0143-7208. 2019, vol. 168, p. 93-102. [Web of Science].
   https://www.sciencedirect.com/science/article/pii/S0143720819301755

2. **Sohrab Nasiri**; Simas Macionis; Dalius Gudeika; Dmytro Volyniuk; Juozas V. Grazulevicius. Facile structure-modification of xanthenone based OLED emitters exhibiting both aggregation induced emission enhancement and thermally activated delayed fluorescence// Journal of Luminescence. ISSN

0022-2313. 2020, vol. 220. p. 116955. [Web of Science]. https://www.sciencedirect.com/science/article/pii/S0022231319316771

3. Manojkumar Dhanthala Thiyagarajan; Umamahesh Balijapalli; **Sohrab Nasiri**; DmytroVolyniuk; Jurate Simokaitienec; Madhvesh Pathak; Sathiyanarayanan Kulathu Iyer; Juozas Vidas Gražulevičius. Rational synthesis of tetrahydrodibenzophenanthridine and phenanthroimidazole as efficient blue emitters and its applications// European Journal of Organic Chemistry. ISSN 1434193X. 2020, p. 834-844. [Web of Science]. https://chemistryeurop.onlinelibrary.wiley.com/doi/full/10.1002/ejoc.201901711.

4. Monika Cekaviciute; Aina Petrauskaite; **Sohrab Nasiri**; Jurate Simokaitiene; Dmytro Volyniuk; Galyna Sych; Ruta Budreckiene; Juozas Vidas Grazulevicius. Towards blue AIE/AIEE: Synthesis and Applications in OLEDs of Tetra-/Triphenylethenyl Substituted 9,9-Dimethylacridine Derivatives//Molecules. ISSN 00249297,15-205835. 2020, vol.25. p. 445. [Web of Science]. https://www.mdpi.com/1420-3049/25/3/445.

5. Ramin Pashazadeh; Galyna Sych; **Sohrab Nasiri**; Karolis Leitonas; Algirdas Lazauskas; Dmytro Volyniuk; Peter J. Skabara; Juozas Vidas Grazulevicius. Multifunctional Characteristics from an Asymmetric D-A-D' Structure: Mechanochromic Luminescence, Thermally Activated Delayed Fluorescence and Aggregation Enhanced Emission// Chemical Engineering Journal. ISSN 1385-8947. 2020, vol.401. p. 125962. [Web of Science]. https://www.sciencedirect.com/science/article/pii/S1385894720320908.

2. RESULTS AND DISCUSSION

2.1. Carbazole derivatives containing one or two tetra-/triphenylethenyl units as efficient hole-transporting OLED emitters (Scientific publication No. 1, Q1, 4 quotations)

This chapter is based on the paper published in *Dyes and Pigments*, **2019**, *168*, 93-102[49]. New efficient carbazole-based emitters containing tetra-/triphenylethene units were developed for boosting the efficiency of non-doped fluorescent OLEDs. The molecular structures are shown in **Scheme 2.1**.

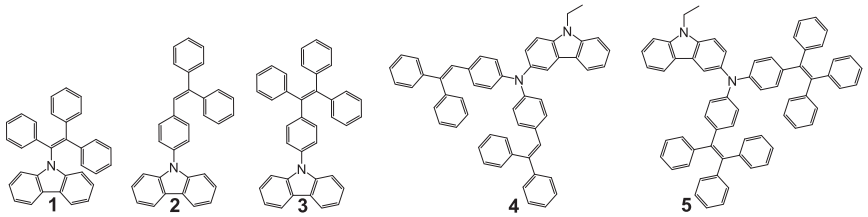

Scheme 2.1. Molecular structures of compounds **1**–**5**

The absorption and photoluminescence (PL) spectra of dilute solutions in toluene and THF, as well as vacuum-deposited films of the compounds are shown in **Fig. 2.1-a**. Their photophysical characteristics are summarized in **Table 2.1**. The red-shifts of low-energy absorption bands of solid films are attributed to the aggregation effects due to intermolecular interactions. Dilute solutions of mono-substituted carbazoles compounds **1**, **2** and **3** showed absorption maxima at ca. 342 nm, which is in accordance with the previously published data on tetra-/triphenylethenyl-substituted carbazole derivatives[50,51,52]. These absorption maxima are related to the π-π* transitions. The absorption maxima of dilute solutions of compounds **4** and **5** containing two tetra-/triphenylethenyl moieties were observed at ca. 404 and 382 nm, respectively (**Table 2.1**). The PL spectra of toluene and THF solutions of compounds **1–3** were found to be similar. Dilute solutions of compounds **1** and **2** showed blue emission with PL maxima at ca. 450-460 nm, while greenish-blue emission with the intensity maxima at ca. 500 nm was observed for solutions of compound **3**. Lower PLQY values were observed for dilute THF solutions of compounds **1**–**3** in comparison to their toluene solutions. This consideration can be explained by the slight polarity effect (ε=7.5 for THF and ε=2.38 for toluene) (**Table 2.1**). In case of the solutions of compounds **4** and **5** with two arylethenyl substituents, solvent polarity was affected on PLQY values and also the emission color. Thus, the PL spectra of THF solutions of compounds **4** and **5** were redshifted with respect of the spectra of toluene solutions.

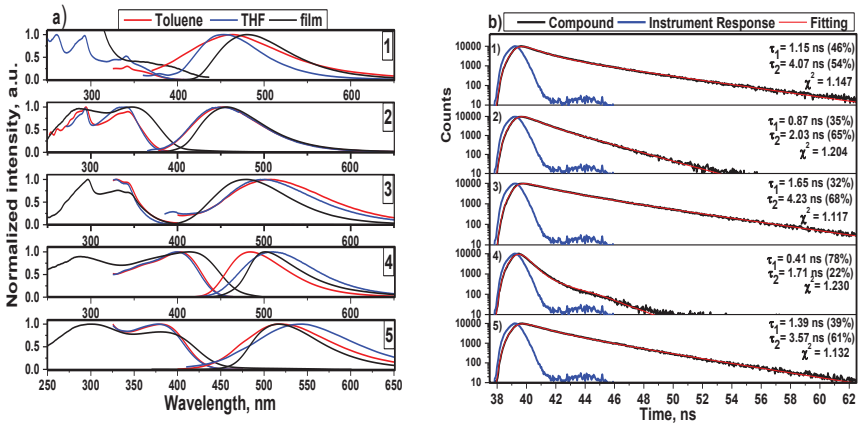

Fig. 2.1. **(a)** Normalized absorption and fluorescence spectra of dilute (10^{-5} M) toluene, THF solutions and solid films and **(b)** PL decay plots of solid films for compounds **1–5**

The PLQY values of the solid films of compounds **1–5** were recorded to be much higher than those of the corresponding solutions (**Table 2.1**). These results are apparently related to the AIEE effect which was previously proved for compounds **1** and **3**. It should be noted that the solid-state PLQY values of 55.7% and 100% previously reported for compounds **1** and **3**, and they are slightly higher than those obtained in this work (48% and 86%, respectively). These differences can apparently be related to reabsorption in solid films, which we did not take into account during PLQY measurements. PLQY values (which are close to unity in case of compound **3**) demonstrate high emission efficiency of the studied emitters **1–5** in the solid state (**Table 2.1**). Despite the very similar chemical structures of these compounds, big differences in their PLQYs were related to the twisting of the triphenylethene units relative to the triphenylamine core. In order to investigate the emission nature of compounds **1–5** in the solid state, PL decays were recorded. They are shown in **Fig. 2.1-b**. PL decays were well fitted giving PL lifetimes in nanosecond range, thus, compounds **1–5** were fluorescent. For adequate representation of PL decay curves, double exponential fits were required. This observation can evidently be explained by the formation of excited dimers in the solid state.

Table 2.1. Photophysical data for dilute solutions and solid films of compounds **1–5**

Compound	Toluene solution			THF solution			Film		
	λ_{abs}^{max}, nm	λ_{F}^{max}, nm	PLQY, %	λ_{abs}^{max}, nm	λ_{F}^{max}, nm	PLQY, %	λ_{abs}^{max}, nm	λ_{F}^{max}, nm	PLQY, %
1	342	462	4	342	454	2	366	480	48
2	342	448	3	342	448	2	354	458	52
3	342	507	3	342	499	1	345	479	86
4	404	484	17	404	508	15	420	500	28
5	382	517	9	382	542	6	397	517	35

The PL spectra of dispersions of the studied compounds in the mixtures of THF and water with various water fractions (f_w) were recorded in **Fig. 2.2-a**. Since the compounds were insoluble in water, their emissive aggregates were formed at certain f_w displaying the AIEE phenomenon. For illustration, the dispersion of compound **5** in THF/water mixtures showed weak emission at low water fractions. Until aggregates started to be formed, slight changes in emission intensities of the dispersions in THF/water mixtures were related to the changes in the solution polarity due to the increase of the water fraction. However, the emission intensity dramatically increased at f_w>80% when the formation of aggregates in THF/water mixtures occurred (**Fig 2.2-b**). As it is usually explained, such behavior is related to the AIEE effect due to the limitation of intramolecular motions.

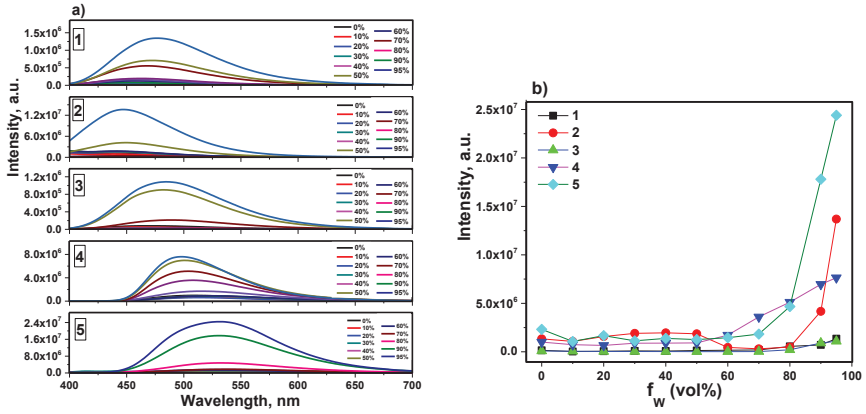

Fig. 2.2. (a) PL spectra of the dispersions of compound **5** in the THF/water mixtures and **(b)** PL maxima intensities versus water volume fraction in THF/water mixtures

The ionization potential (IP) values of carbazole derivatives with two arylethenyl moieties (**4**, **5**) were found to be lower than those of carbazole derivatives with a single arylethenyl substituent (**1-3**). In addition, the IP values of the compounds are presented in **Table 2.2**.

The time of flight (TOF) technique was used to estimate the charge transporting properties of compounds. The electric field dependencies of hole drift mobilities (μ_h)

for the layers of compounds **1**–**5** are exhibited in **Fig. 2.3**. All the compounds (**1**–**5**) displayed linear dependencies of hole mobilities to the square root of the electric field. Thus, μ_h for the layers of compounds **1**–**5** verify Poole-Frenkel type electric field dependence (Equation **2.1**) where μ_0 is the zero electric field charge mobility, and α is the field dependence parameter[53]. Hole-drift mobility values are listed in **Table 2.2**. The hole mobilities of compounds **4** and **5** exceeded 10^{-3} cm^2/V at high electric fields. μ_h values of the compounds were found to range in the order **1 > 2~3 > 4> 5**. Since the distances between molecules are shorter, the higher hole mobilities were observed for compound **1** relative to those of the other studied compounds.

2.1 $$\mu=\mu_0\times\exp(\alpha E)^{1/2}$$ [53]

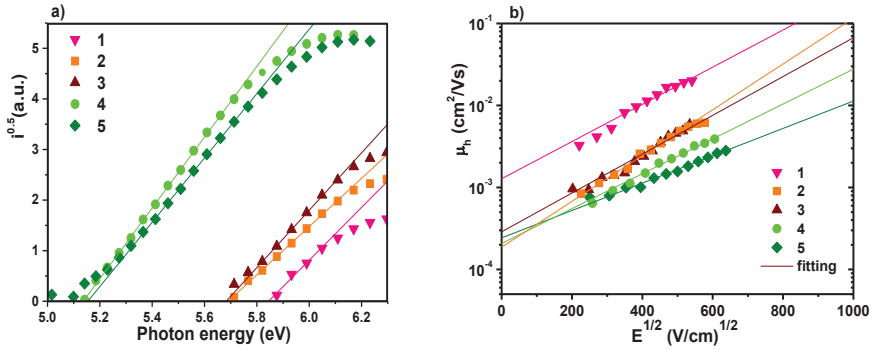

Fig. 2.3. (a) Photoelectron emission spectra of solid films and **(b)** hole mobility dependencies on applied electric field for the layers of compounds **1–5**

Table 2.2. Electrochemical characteristics and hole-transporting parameters of compounds **1–5**

Compound	E_g^{opt}, eV	I_P^{ep}, eV	μ_{h_0}, cm^2/Vs	μ_h, cm^2/Vs	α, $(cm/V)^{1/2}$
1	3.17	5.85	1.3×10^{-3}	2.1×10^{-2}	5.23×10^{-3}
2	3.27	5.70	1.93×10^{-4}	6×10^{-3}	5.43×10^{-3}
3	3.28	5.68	2.95×10^{-4}	6×10^{-3}	6.45×10^{-3}
4	2.75	5.14	2×10^{-4}	3×10^{-3}	4.9×10^{-3}
5	2.82	5.15	2.45×10^{-4}	1.9×10^{-3}	3.84×10^{-3}

Non-doped OLEDs were fabricated, and the structures of OLEDs were ITO/MoO_3 (1 nm)/ NPB (60 nm)/TCTA (5 nm)/non-doped light-emitting layer (30 nm)/TSPO1 (3 nm)/TPBi (40 nm)/LiF (0.5 nm)/Al, which were named as devices **D1–D5** depending on compounds **1**–**5** used as emitters. The fabricated OLEDs were characterized by electroluminescence with colors falling in the spectral range from blue to green with the corresponding standard Commission Internationale de l'Eclairage CIE coordinates, EL spectra of devices **D1–D5** was in agreement with the corresponding PL spectra of solid films of compounds **1–5** and the EL spectra

submitted in **Fig. 2.4-a**. The highest values of the maximum current (CE), power (PE) and external quantum efficiencies (EQE) of 5.88 cd/A, 3.15 lm/W, and 2.02%, respectively, were also obtained for device **D5** (**Fig. 2.4-c**, **Table. 2.3**). The device structure was further modified and optimized in order to make it more appropriate for compounds **4** and **5**. The modified device structure was ITO/MoO_3 (1 nm)/mMTDATA (50 nm)/light-emitting layer (30 nm)/TSPO1 (5 nm)/TPBi (65 nm)/LiF (0.5 nm)/Al, in which the hole-transporting layers were skipped since the HOMO of compounds **4** and **5** was appropriate for hole injection. The EL spectra of devices **D4a** and **D5a** were virtually the same as those of devices **D4** and **D5**. Moreover, the high barrier for holes at the interfaces m-MTDATA/compound **1**, m-MTDATA/compound **2** and m-MTDATA/ compound **3**, radiative recombination of the hole-electron pairs in devices **D1a**, **D2a** and **D3a** apparently occurs not only in the light-emitting layer but also in the m-MTDATA layer. Device **D5a** exhibited very high maximum brightness exceeding of 50000 cd/m^2 at 3.8 V. As a result, device **D5a** showed improved maximum EQE of 5.32% (**Fig. 2.4-c**).

Table 2.3. Non-doped OLED characteristics

Device	V_{on} (V)	λ_{max} (nm)	L_{max} (cd/m^2)	CE_{max} (cd/A)	PE_{max} (lm/W)	EQE_{max} (%)	CIE1931 coordinates (X,Y)
Device structure ITO/MoO_3/NPB/TCTA/light-emitting layer/TSPO1/TPBi/LiF/Al							
D1	3.81	470	4700	3	2.35	1.62	(0.168,0.209)
D2	3.99	441	4300	1.4	0.82	1.08	(0.159,0.126)
D3	3.99	479	2000	3.8	2.6	1.95	(0.174,0.244)
D4	4.19	499	12100	4.26	2.2	1.6	(0.194,0.463)
D5	3.79	518	15500	5.8	3	2	(0.248,0.514)
Device structure ITO/MoO_3/m-MTDATA/light-emitting layer/TSPO1/TPBi/LiF/Al							
D1a	4.1	497	6600	2.1	1.17	0.85	(0.202,0.34)
D3a	4.5	496	7700	2.76	1.38	1.16	(0.19,0.318)
D5a	3.8	518	52000	17	9.2	5.32	(0.242,0.52)

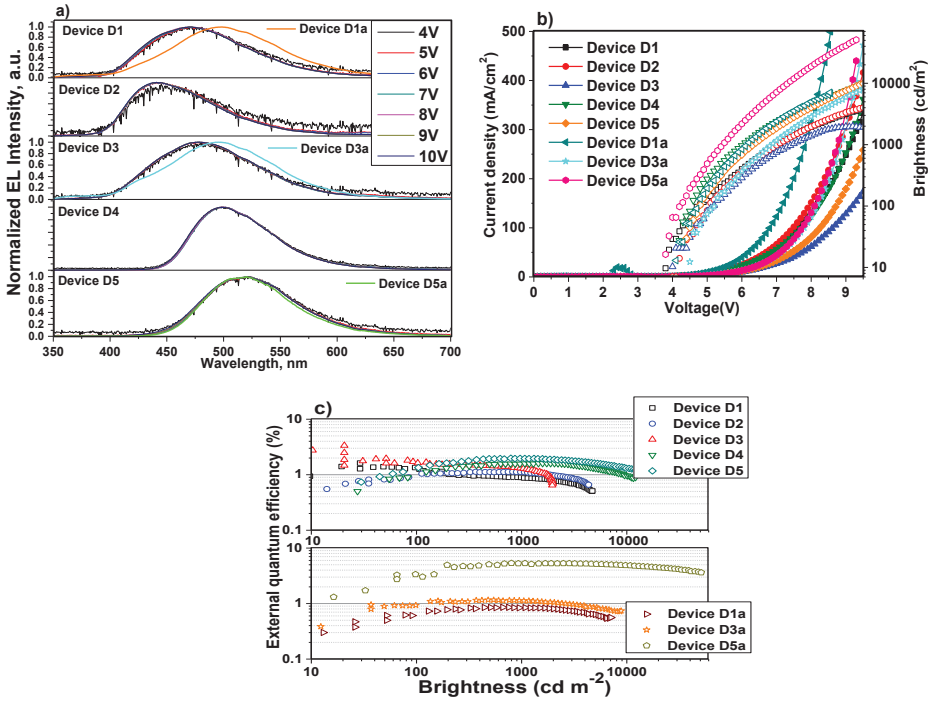

Fig. 2.4. (a) EL spectra recorded at different applied voltages, **(b)** current density-voltage, brightness-voltage and **(c)** external quantum efficiency- brightness characteristics of devices **D1**–**D5** and **D5a**

2.2. Xanthenone based OLED emitters exhibiting both aggregation induced emission enhancement and thermally activated delayed fluorescence (Scientific publication No. 2, Q2, 1 quotation)

This chapter is based on the paper published in *Journal of Luminescence,* **2020**, *220*, 116955[54]. Four new donor-acceptor compounds were investigated by theoretical and experimental approaches aiming to estimate the effect of the structure of a donor on the properties of potential OLED emitters. The molecular structures of derivatives **6–9** are shown in **Scheme 2.2**.

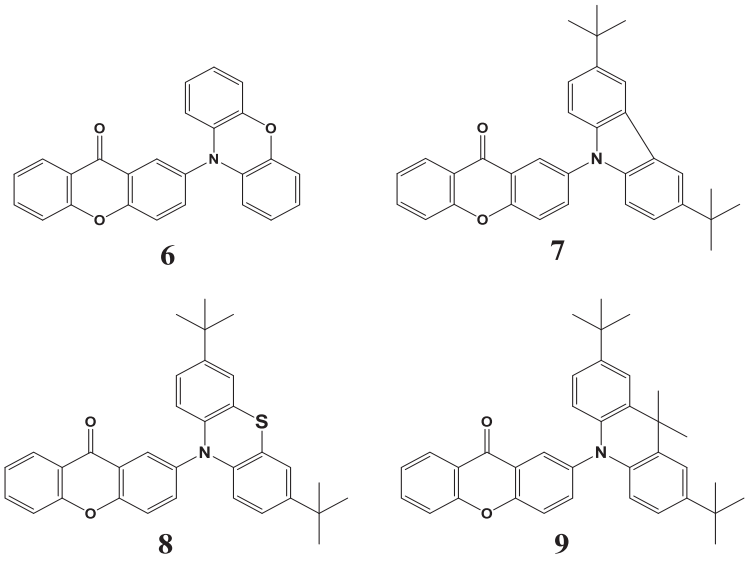

Scheme 2.2. Molecular structures of derivatives **6–9**

The molecular configuration and the frontier molecular orbital distributions of compounds **6–9** were analyzed by the density functional theory (DFT) calculations using Gaussian 09W software at the B3LYP/6-311G (d,p) level. The HOMO and LUMO orbital distributions and their energy values are presented in **Fig. 2.5**.

Compound	HOMO	LUMO
6	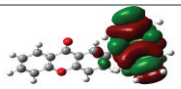 -4.52 eV	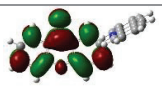 -2.65 eV
7	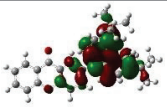 -5.51 eV	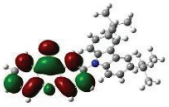 -2.37 eV
8	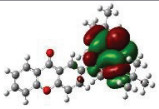 -4.94 eV	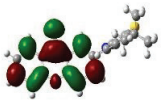 -2.48 eV
9	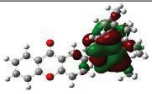 -5.02 eV	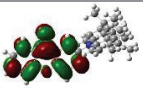 -2.36 eV

Fig. 2.5. HOMO and LUMO of compounds **6–9** calculated at B3LYP/6-311G (d,p) level

The absorption and PL spectra of the solutions in the solvents of different polarity (toluene, THF and chloroform) and the solid state (pure and doped films) media were recorded in **Fig. 2.6-a,b**. The absorption bands in the regions of ca. 250–300 nm and 300–350 nm are attributed to the superposition of the π→π* and n→π* transitions of the donor moieties and xanthenone units, respectively (**Fig. 2.6-a**). PL spectra were characterized by a single broad unstructured band which shifted to the low-energy region with increasing media of polarity (**Fig. 2.6-b**). For example, the PL spectrum of the THF solution of compound **9** was characterized by two bands with maxima at 432 and 626 nm which were related to the recombination of local (LE) and ICT (co-called twisted ICT (TICT)[55]) excitons, respectively. Indeed, the different twisting (rotation) of the donors interacting with solvents of different polarity could be expected, which resulted in media-dependent LE and TICT fluorescence.

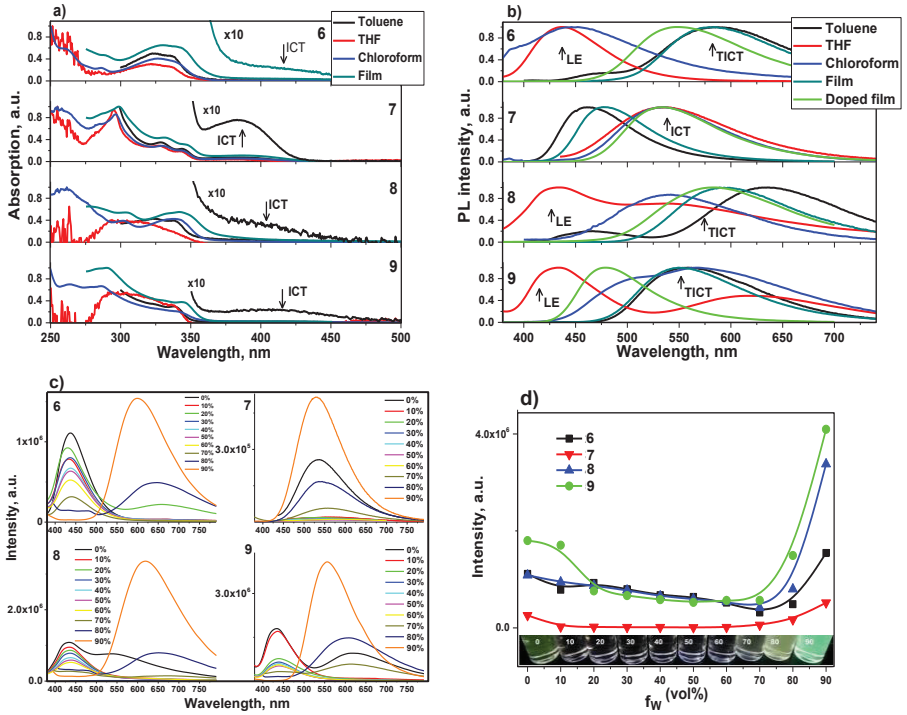

Fig. 2.6. (a) Absorption and **(b)** photoluminescence spectra of **6–9** dispersed in different media **(c)** PL spectra and **(d)** emission intensities versus volume fractions of water (f_W) of compounds **6–9** dispersed in THF/water mixtures

The PL spectra of compounds **6–9** in the solid state were characterized by the related single bands, most probably, to the emissive recombination of excited ICT states because of the restriction of free twisting (rotation) of the donors around the

N-C band in the solid state (**Fig. 2.6-b**). It should be noted that dual emission was previously observed for the derivatives of xanthenone substituted by electron donating units through the N-C bond[56]. The wavelengths maxima of the main absorption and fluorescence bands are shown in **Table 2.4**. The PLQY values of compounds **6–9** in solid film media were found to be higher than those of their toluene solutions (**Table 2.4**). This observation can apparently be attributed to the AIEE phenomenon which may be observed due to the restriction of movements of molecular units in solid state[57]. In order to prove this assumption, the PL spectra of the dispersions of the studied compounds in the THF/water mixtures with different volume water fractions (f_W) were recorded. They show emission intensities before and after the formation of aggregates at high f_W (**Fig. 2.6-c**). Indeed, a higher emission intensity was observed for the THF/water mixtures with high f_W in comparison to those of the THF solutions thus highlighting the AIEE effect for all the studied compounds (**Fig. 2.6-d**). The intensity monotonically decreased with increasing f_W, and it is related to the increasing polarity of the THF/water mixture (**Fig. 2.6-c**). When aggregates started to be formed at f_w ~60–70%, red-shifted PL spectra were obtained since TICT fluorescence dominated in the solid state.

Table 2.4. Spectroscopic characteristics of the solutions and solid films of compounds **6–9**

Compound	Solution			Solid Films					
	Toluene			Non-doped				Doped	
	λ_{abs}^{max}, nm	λ_F^{max}, nm	PLQY, %	λ_{abs}^{max}, nm	λ_F^{max}, nm	PLQY, %	E_T, eV	λ_F^{max}, nm	PLQY, %
6	327	590	0.6	330	580	4	2.34	549	14
7	293	457	15	298	476	19	2.74	534	38
8	331	638	0.3	277	595	5	2.39	585	7
9	331	563	2	290	549	14	2.51	479	36

Despite the identified AIEE effect for compounds **6–9**, PLQYs of their net films were much below unity (**Table 2.4**). In addition, more than two times lower PLQYs were obtained for derivatives **6** and **8** containing sulfur (S) and oxygen (O) heteroatoms in the donor moieties (di-tert-butyl-phenothiazine and penoxazine) than those observed for compounds **7** and **9** containing only a nitrogen heteroatom in the donor moieties. Relatively, low PLQYs may be related to special intermolecular interactions which are apparently different for compounds **6**, **8** and **7, 9**. This assumption is in good agreement with the enhanced PLQY values of compounds **6–9** molecularly dispersed in the mCP host in which the influence of intermolecular interactions was decreased (**Table 2.4**). Since relatively high dihedral angles between the donor and the acceptor were observed for compounds **6** and **7** by theoretical calculations (**Fig. 2.5**), triplets harvesting was expected via reverse

intersystem crossing. Furthermore, the intensity of the fluorescence spectra in toluene solution media of all the studied compounds considerably increased after deoxygenation (**Fig. 2.7-a**). This observation supports the above presumption about harvesting of triplets. In addition, long-lived components of PL decays were observed for pure and doped films of derivatives **6-9** (**Fig. 2.7-b**). In order to attribute these long-lived PL decay components to TADF, first of all, singlet (E_S) and triplet (E_T) energy levels had to be measured. Phosphorescence and photoluminescence spectra of compounds **6**–**9** in the solid film media were recorded at the temperature of liquid nitrogen (77 K), and E_S and E_T values were calculated by using the wavelengths of the onsets of these spectra by the empiric formula (Equation **2.2**) (**Fig. 2.7-c**). By using these energy levels, small values of the singlet-triplet splitting ΔE_{ST} ranging from 0.05 to 0.1 eV were obtained. Such small ΔE_{ST} values allow concluding that long-lived fluorescence corresponds to the TADF origin.

2.2 $$(E_S), (E_T) = 1240 \cdot \lambda^{-1} \text{ [58]}$$

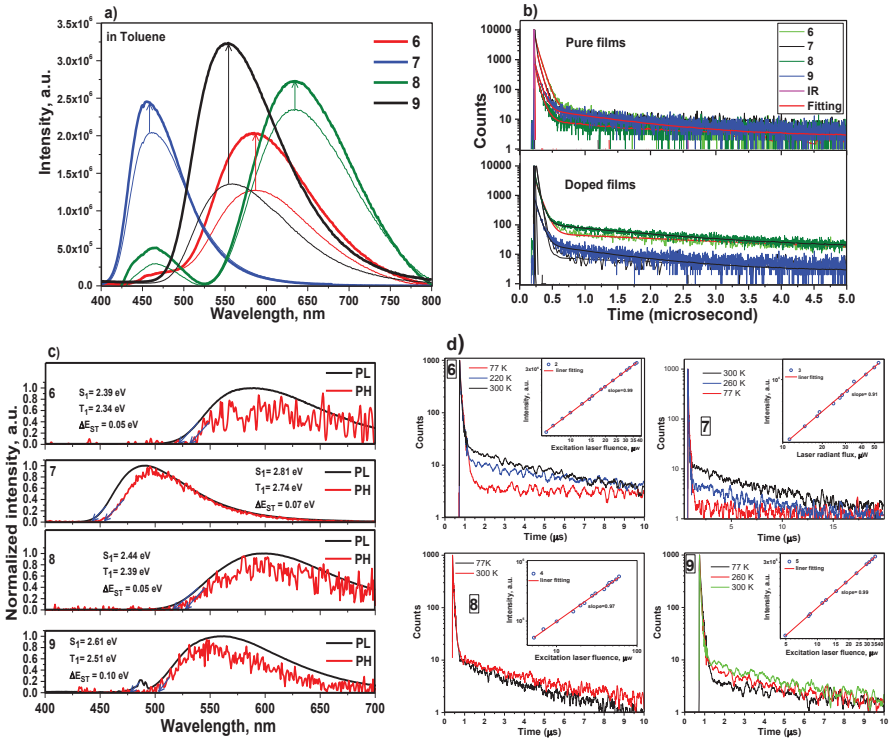

Fig. 2.7. (a) Emission spectra of compounds in vacuum and in an oxygenated environment, **(b)** PL decay curves of pure and doped (10 wt.% in mCP) films of compounds **6**–**9**, **(c)** PL and phosphorescence (Phos) spectra of solid films of the compounds recorded at 77 K and **(d)** PL decays of compounds doped in mCP (solid film) recorded at different temperatures.

The inset demonstrates dependence of delayed emission intensity on laser flux (delay of 1 μs)

In order to confirm this assumption, we additionally recorded PL decays at different temperatures and dependence of the emission intensity on the laser flux at room temperature for the films of the molecular mixtures of compounds **6–9** with mCP (**Fig. 2.7-d**). Both the increasing intensity of delayed emission with increasing temperatures and the linear dependencies of delayed emission intensity on the laser flux with a slope close to unity definitely proved the TADF origin of long-lived fluorescence. In order to investigate TADF properties of compounds **6–9**, we fitted PL decays of their non-doped and mCP-hosted films. The results of fitting are summarized in **Table 2.5**. Moreover, the radiation transition rates of doped compounds **6–9** in the films media were calculated by using Formulas **2.3**–**2.6**[59]:

2.3 $$k_{PF} = \frac{\eta_{PF}}{\tau_{PF}}$$ [59]

2.4 $$k_{ISC} = \frac{\eta_{DF}}{\eta_{PF}+\eta_{DF}} k_{PF}$$ [59]

2.5 $$k_{DF} = \frac{\eta_{DF}}{\tau_{DF}}$$ [59]

2.6 $$k_{RISC} = \frac{\eta_{DF}}{\eta_{PF}} \cdot \frac{k_{PF}.k_{DF}}{k_{ISC}}$$ [59]

where k_{PF}, k_{DF}, k_{ISC}, and k_{RISC} are rate constants of prompt and delayed components, intersystem crossing (ISC) and reverse intersystem crossing (RISC) processes, respectively. η_{PF} and η_{DF} are prompt and delayed PLQYs distinguished from the total PLQY values by comparing the integrated intensity of the prompt and delayed components. The obtained rate constants for the films of compounds **6–9** doped in mCP are collected in **Table 2.6**.

Table 2.5. Fitting data of PL decays of compounds **6–9** dispersed in different environments

Compound 6		
Parameters of PL Decay	**Solid film (Non-doped)**	**Solid film (Doped)**
τ_1, ns/(Value%)	19/19	74/53
τ_2, ns/(Value%)	62/75	5320/47
τ_3, ns/(Value%)	990/6	-
χ^2	1.233	1.174
Compound 7		
Parameters of PL Decay	**Solid film (Non-doped)**	**Solid film (Doped)**
τ_1, ns/(Value%)	30/96	51/78
τ_2, ns/(Value%)	3700/4	3700/22
χ^2	1.284	1.233
Compound 8		
Parameters of PL Decay	**Solid film (Non-doped)**	**Solid film (Doped)**
τ_1, ns/(Value%)	15/51	53/59
τ_2, ns/(Value%)	60/39	3200/41
τ_3, ns/(Value%)	1030/10	-
χ^2	1.274	1.281
Compound 9		
Parameters of PL Decay	**Solid film (Non-doped)**	**Solid film (Doped)**
τ_1, ns/(Value%)	58/67	60/74
τ_2, ns/(Value%)	1160/33	1570/26
χ^2	1.299	1.287

Table 2.6. Rate constants of prompt and delayed components of doped films of compounds **6–9**

Compound	τ_{PF}, ns	τ_{DF}, μs	η_{PF}	η_{DF}	k_{PF}, s^{-1}	k_{ISC}, s^{-1}	k_{DF}, s^{-1}	k_{RISC}, s^{-1}
6	74 (53%)	5.32 (47%)	0.074	0.066	1×10^{6}	0.47×10^{6}	0.12×10^{5}	0.23×10^{5}
7	51 (78%)	3.7 (22%)	0.296	0.084	5.8×10^{6}	1.28×10^{6}	0.23×10^{5}	0.3×10^{5}
8	53 (59%)	3.2 (41%)	0.041	0.029	0.8×10^{6}	0.33×10^{6}	0.1×10^{5}	0.17×10^{5}
9	60 (74%)	1.57 (26%)	0.266	0.094	4.4×10^{6}	1.15×10^{6}	0.6×10^{5}	0.8×10^{5}

Ionization potentials (IPPE) of compounds **6–9** coated on fluorine tin oxide (FTO) were obtained by electron photoemission spectroscopy in the air. IPPE values of 5.70, 5.95, 5.77, and 5.70 eV were obtained for compounds **6**, **7**, **8**, and **9**, respectively (**Fig. 2.8-a**). The highest ionization potential was observed for compound **7** containing tert-butyl-carbazolyl donor moiety. Furthermore, hole and electron mobility were detected by TOF measurements, and the plot is presented in **Fig. 2.8-b**. In addition, the values obtained from the optical energy gap, IP_{PE} and mobility are listed in **Table 2.7**.

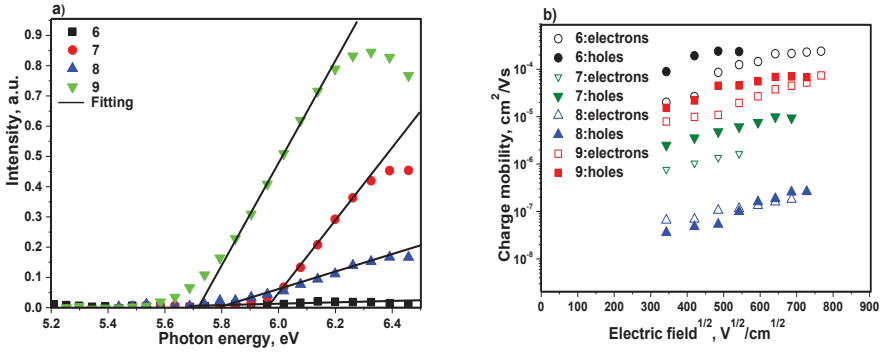

Fig. 2.8. (a) Photoelectron emission spectra, **(b)** electric fields dependences of electron and hole mobilities for the layers of compounds **6–9**

Table 2.7. Optical, photoelectrical and charge-transporting characteristics of compounds **6–9**

Compound	E_g^{opt} (eV) in Toluene	IP_{PE} (eV)	μ_h ($cm^2\ V^{-1}\ s^{-1}$)	μ_e ($cm^2\ V^{-1}\ s^{-1}$)
6	3.45	5.70	2.6×10^{-4}	1.3×10^{-4}
7	2.98	5.95	6.4×10^{-6}	1.7×10^{-6}
8	2.89	5.77	1×10^{-7}	1.2×10^{-7}
9	3.48	5.70	4.6×10^{-5}	2×10^{-5}

Values of Eg^{opt} estimated as the ratio 1240/λ of UV spectra (in toluene), IP_{PE} estimated from electron photoemission spectra, μ_h and μ_e are hole and electron mobility, respectively

Since compounds **6–9** were characterized by the appropriate HOMO/LUMO values for charge injections, bipolar charge-transporting properties, and relatively high PLQYs in mCP-based guest-host systems, they were employed as emitters in electroluminescent devices. The fabricated devices were named **PXZ, CZ, PTZ** and **ACR** depending on the emitters used in OLED structures ITO/MoO3 (1nm)/NPB (65nm)/ **6, 7, 8** or **9** (10 wt %):mCP (30nm)/TPBi (40nm)/LiF (0.5nm)/Al. As a result, the EL spectra of devices **PXZ, CZ, PTZ** and **ACR** were in good agreement with the PL spectra of emitters **6**, **7**, **8**, and **9**, respectively. Furthermore, the EL spectra and electroluminescence characterization obtained from the voltage-current density and voltage-brightness dependencies, the external quantum efficiencies and the CIE coordinates of devices presented in **Fig. 2.9**. Meanwhile, low-intensity bands appeared in the EL spectra of devices **PXZ** and **PTZ** at higher voltages since charge-blocking layers were not used in the device structure. This observation can be attributed to the emission of NPB (or TPBi) due to the shift of the recombination zone to the hole or electron transporting layer NPB or TPBi. The EL spectra of device **CZ** were blue-shifted in comparison to the PL spectrum of compound **7.** This observation shows that the hole-electron recombination did not occur within the light emitting layer. It was completely shifted to the electron transporting layer TPBi related to the energy barrier between the LUMO-LUMO energy levels of compound **7** and TPBi. Thus, device **CZ** did not reflect electroluminescent properties of emitter **7**. The lowest turn-on voltage of 3.2 V was observed for device **PXZ** based on compound **6** due to its highest and balanced hole and electron mobilities. The maximum brightness of devices **PXZ** and **ACR** exceeded 10000 cd.m^{-2} due to the high PLQY value of the light-emitting layers and their emission in the green-yellow region to which human eyes are sensitive (**Fig. 2-9-d**). The best external quantum efficiency value (EQE) of 3.5% was demonstrated by device **ACR** since emitter **9** showed high PLQY in the doped film and relatively high charge mobilities. Furthermore, the electroluminescence values are submitted in **Table 2.8.**

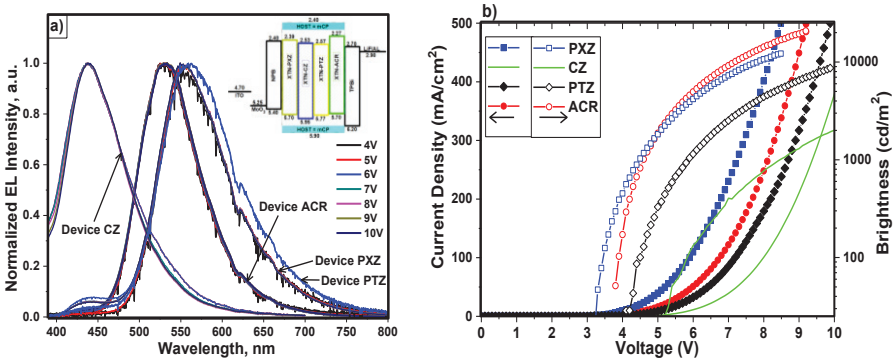

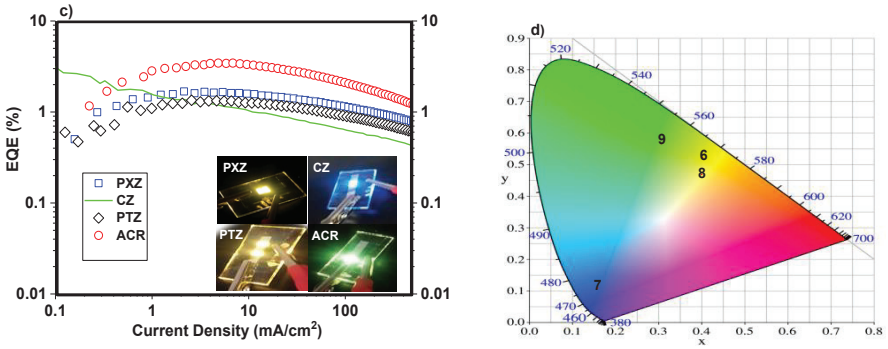

Fig. 2.9. (a) EL spectra recorded at different voltages, **(b)** voltage-current density and voltage-brightness dependencies **(c)** external quantum efficiencies and **(d)** CIE coordinates of devices

Table 2.8. Output parameters of OLEDs

Device	V_{on} (V)	L_{max} (cd/m²)	L at 8 V (cd/m²)	PE_{max} (lm/W)	CE_{max} (cd/A)	EQE_{max} (%)	CIE coordinates (X,Y)
PXZ	3.2	12500 (8.5 V)	10900	4.2	5.3	1.7	(0.403,0.526)
CZ	4.9	2400 (10.6 V)	820	3.7	2.8	1.8	(0.159,0.111)
PTZ	3.9	8800 (9.9 V)	4600	2.4	3.9	1.4	(0.401,0.473)
ACR	3.8	20900 (9.2 V)	14800	7.6	11.7	3.5	(0.307,0.571)

2.3. Derivatives of tetrahydrodibenzophenanthridine and phenanthroimidazole as efficient blue emitters and their applications (Scientific publication No. 3, Q1, 1 quotation)

This chapter is based on the paper published in *European Journal of Organic Chemistry,* **2020**, *2020*, 834–844[60]. The molecular structures of the compounds are presented in **Scheme 2.3**.

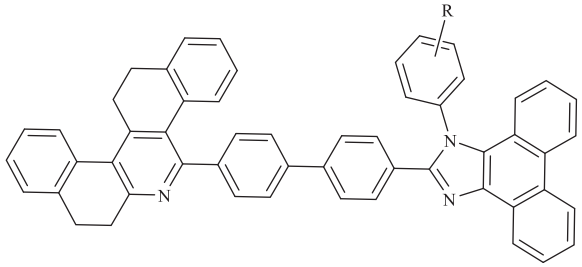

10: R = H
11: R = 4-Me
12: R = 4-F
13: R = 4-Cl
14: R = 3,5-Me
15: R = 4-MeO
16: R = 4-CN
17: R = 3,5-MeO
18: R = 4-NO_2
19: R = 2-pyridine

Scheme 2.3. Molecular structures of compounds **10–19**

In order to investigate the effect of the substitution pattern on the photophysical properties of the THDPs and PI derivatives, the absorption and photoluminescent (PL) spectra of their solutions and solid films were recorded (**Fig. 2.10-a,b**). The low energy bands absorption spectra of the solution (toluene) of compounds were characterized by the maxima at 346–361 nm and the low-intensity shoulder at 365–375 nm. These absorption bands can be mainly attributed to the absorption of the PI moiety since the lowest energy band is situated at the same region (with its maximum at 364 nm), and it is red-shifted in comparison to the lowest energy band (with maximum at 318 nm) of BTHDPs (**Table 2.9**)[61,62]. The small blue-shifts of the maxima of the lowest energy bands of compounds **10**–**19** relative to PI are apparently a result of the superposition of the absorption spectra of both donating and accepting units. Additional red-shifted energy bands (shoulders) which indicate intramolecular charge transfer (ICT) transitions in the ground states between the donor and acceptor units were practically not observed because of the presence of diphenyl spacers between THDP and PI moieties. As a result, similar optical energy band gap values (E_g^{opt}) were obtained for the studied compounds **10–19** (**Table 2.9**). Slight differences in the position of the lowest absorption bands were observed for the toluene solutions of derivatives **10–19** due to their post-functionalizations by different moieties inducing different steric and polar effects which affected electron delocalization. A similar absorption behavior of derivatives **10–19** was also observed in polar solvents than toluene thus revealing their weak solvatochromic effects in the ground states. Intensive deep-blue fluorescence with a high photoluminescence quantum yield (PLQY) was observed for the toluene solutions of compounds **10–19** (**Table 2.9**). The highest PLQY value of 93% was recorded for the toluene solution of compound **15** containing a methoxy substituent. PL decays of the toluene solution of the compounds agreed well with the mono-exponential law (**Fig. 2.10-c**). For adequate description of the PL decay curves of the films of compounds **10–19**, double or triple exponentials fits were required. The reasons of different PL decays of the films from those solutions could be due to the aggregation induced quenching and/or excimer formation. Different shapes of PL decays of compounds **10–19** in the solid films media may partly be related to non-radiative losses in the solid state. Moreover, much lower PLQY values of solid samples of compounds **10–19** were obtained in comparison to those of their toluene solutions (**Table 2.9**). Compound **15** containing a methoxy group demonstrated a relatively high PLQY of 59% in the solid state. A high PLQY of the solid sample of compound **15** can be related to the restriction of excimer formation which may occur between planar moieties as it was shown elsewhere. As a result, different variations of stokes shifts ($\Delta\upsilon=\upsilon_{abs}-\upsilon_{em}$) displaying positive solvatofluorochromism and

consistently proving CT character of their emission (**Table 2.9**) were obtained from the studied compounds. Non-structured PL spectra of the polar chloroform, THF, and acetone solutions of compounds **10–19** support the presumption that emission is a result of the recombination of the CT excited states. In order to investigate the effect of the substitution pattern of derivatives THDP and PI on their emission behavior, the dependence of their stokes shifts versus orientation polarizability of the chosen solvents (Δf) were linearly fitted (**Fig. 2.10-d**). The different slopes (ranging from 2633 to 8511 cm^{-1}) of these linear dependencies demonstrated differences in the dipole moments of the excited singlet states of compounds **10–19** according to the Lippert-Mataga law (**Table 2.9**)[63]. Different electron-donating or electron-accepting substituents of the phenyl group attached to the PI moiety resulted in a slightly different ICT behavior of compounds **10–19**. Because of the relatively low Lippert-Mataga slopes for compounds **10–19**, some contribution of the recombination of the locally-excited states to their emission is possible.

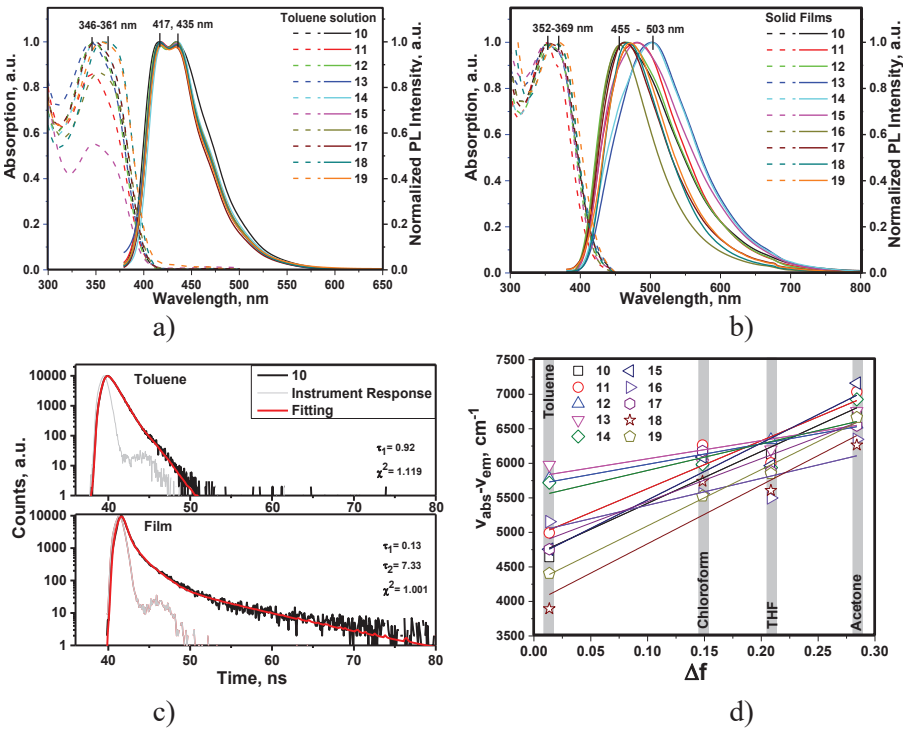

Fig. 2.10. (a) Absorption (dashed lines), and PL spectra (solid lines) of the solutions of compounds **10–19** in toluene **(b)** of solid-state samples, **(c)** PL decays of toluene solution and solid film of compound **10** and **(d)** Lippert-Mataga plots displaying correlation between orientation polarizability of the solvent (Δf) and stokes shifts ($\Delta\upsilon=\upsilon_{abs}-\upsilon_{em}$) for compounds **10–19**

Table 2.9. Photophysical parameters of the solutions of compounds **10-19** in toluene and solid films media

Compounds	λ_{abs}^{max}, nm	E_g^{opt}, eV	λ_F^{max}, nm	τ, ns	PLQY, %	FWHM, nm	CIE1931, (x, y)	Slope, cm^{-1}
	Toluene/film							
10	348/352	3.03/2.76	417,435/463	0.92/0.13, 7.33	93/27	77/125	(0.154, 0.059)/(0.202, 0.249)	7513
11	346/351	3.01/2.79	417,434/480	0.96/0.68, 4.43	67/11	67/126	(0.156, 0.063)/(0.204, 0.176)	6931
12	347/355	3.05/2.79	415,434/465	0.95/0.21, 2.048.12	87/32	69/128	(0.156, 0.056)/(0.202, 0.249)	2958
13	345/355	3.02/2.78	416,434/502	1.02/0.09, 1.727.49	66/8	67/131	(0.157, 0.063)/(0.236, 0.349)	2633
14	348/352	3.01/2.78	418,435/503	1.02/0.11, 1.907.89	75/12	68/135	(0.157, 0.065)/(0.230, 0.335)	3846
15	349/351	3.02/2.77	418,434/480	0.93/0.13, 1.568.27	93/59	66/137	(0.155, 0.059)/(0.214, 0.275)	8240
16	352/362	3.02/2.80	417,434/455	1.05/0.06, 1.519.74	73/16	68/91	(0.156, 0.062)/(0.173, 0.179)	3893
17	349/355	3.01/2.78	417,432/463	0.89/0.55, 3.0810.6	88/12	63/106	(0.155, 0.065)/(0.186, 0.222)	6229
18	357/362	3.01/2.79	416,434/469	0.95/0.05, 1.036.37	72/5	66/98	(0.155, 0.059)/(0.179, 0.233)	8511
19	355/367	2.96/2.76	418,434/471	0.95/0.03, 1.639.19	74/6	64/105	(0.156, 0.060)/(0.187, 0.245)	8146

IP_{PE} measurements for the compounds were performed (**Fig. 2.11**). IP_{PE} values and the results of charge mobility measurements are presented in **Table 2.10**.

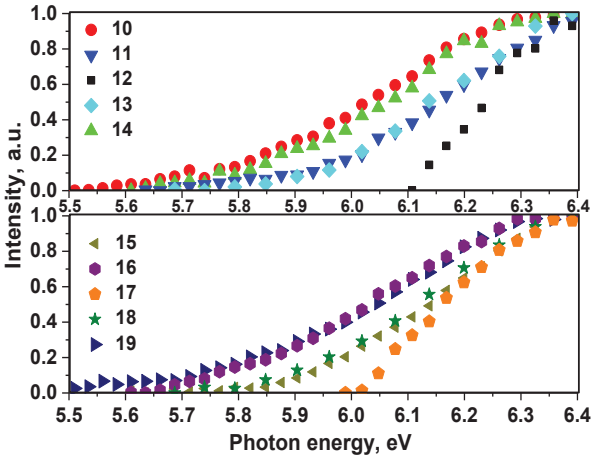

Fig. 2.11. Photoelectron emission spectra of vacuum-deposited layers of compounds **10–19** on FTO

Table 2.10. Ionization potential and charge-transporting characteristics of compounds **10–19**

Compound	Ip^{PE}, eV	μ_h, cm^2/Vs
10	5.74	$5.8 \cdot 10^{-6}$
11	5.90	-
12	6.11	$9 \cdot 10^{-6}$
13	5.92	-
14	5.81	-
15	5.92	$2.4 \cdot 10^{-6}$
16	5.88	-
17	5.99	$3.7 \cdot 10^{-6}$
18	5.77	-
19	5.75	-

Time-of-flight (TOF) technique was used for testing diode-like samples with the structure of ITO/vacuum-deposited compounds on the ITO/aluminum. Compound **10** showed hole mobility of 5.8×10^{-6} $cm^2/V.S$ at electric fields higher than 10^6 V/cm (**Fig. 2.12**). Compounds **12**, **15** and **17** showed hole mobilities similar to those of

compound **10** at the same electric field. This result indicated the absence of any significant effects of post functionalization on the hole mobilities of the studied derivatives. It was not possible to obtain the transit times (required for the calculations of charge mobility) from the photocurrent transients for the other compounds, apparently due to the strong charge-transport dispersion which is typical for good emitters[64]. For the same reasons, the transit times for electrons were also not detected in the corresponding photocurrent transients.

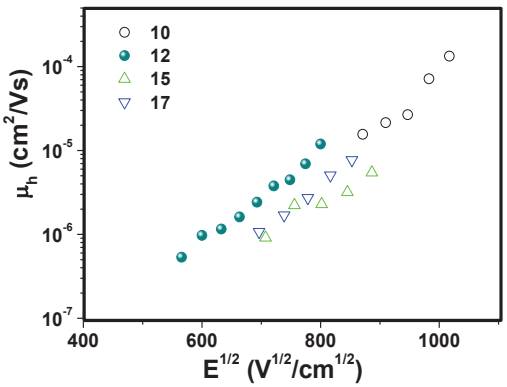

Fig. 2.12. Electric field dependences of hole mobility in vacuum-deposited films of compounds **10**, **12**, **15** and **17**

Taking into account that compounds **10, 12, 15** and **17** are characterized by relatively high PLQYs in the solid state and that they are capable of transporting charges, electroluminescent properties of the non-doped OLEDs. The OLED structure was ITO/MoO_3(1 nm)/NPB (30 nm)/**10, 12, 15** and **17** (18 nm)/BPhen (33 nm)/LiF(0.5 nm)/Al (**Fig. 2.13-a**). Similar EL spectra with the intensity maxima at 474 nm were observed for all the fabricated devices in contrast to the high roll-off efficiency of blue phosphorescent OLEDs which suffered from the formation of 'hot excitons' due to the presence of long-lived triplet excitons[65]. The fabricated blue fluorescent device **15** showed low roll-off efficiency (**Fig. 2.13-d**). The maximum external quantum efficiency (EQE) at very high brightness (L) of 10000 cd/m^2 for blue OLED gained 1.6% (**Fig. 2.13-d**). Better OLED performances of devices based on compounds **12** and **15,** in comparison with that of the device based on **10,** were mainly related to the higher PLQY values of the films of compounds **12** and **15** in comparison with that of the film of compound **10**. In addition, the differences between the charge-injection and charge-transporting properties of compounds **10, 12, 15** and **17** should also play important roles. The differences between the current density versus the applied voltages characteristics were observed for the studied devices (**Fig. 2.13-c**). Slightly different turn-on voltages (V_{on}= 4.9–5.4V) was

obtained from the fabricated devices (**Table 2.11**). Furthermore, improvement of the EQE of a device based on **15** can be expected. Nevertheless, the performed electroluminescent investigations not only testify the potential of the derivatives of tetrahydrodibenzophenanthridine and phenanthroimidazole in blue fluorescent OLEDs, but also demonstrate the requirements of their modifications through the smart molecule design.

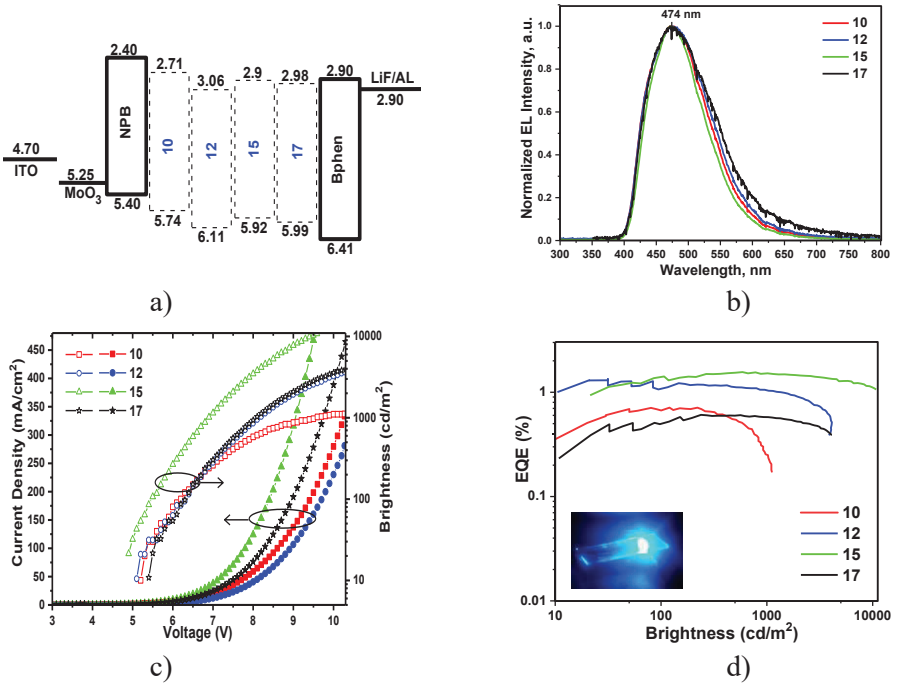

Fig. 2.13. (a) Equilibrium energy diagram, **(b)** EL spectra recorded at 7 V, **(c)** plots of current density and brightness versus applied voltages and **(d)** dependences of EQEs versus brightness of OLEDs, (the inset is photo of device **15**)

Table 2.11. Characteristics of non-doped OLEDs based on compounds **10, 12, 15** and **17**

Device	V_{on} (V)	L^{max} (cd/m^2)	L at 9 V (cd/m2)	PE^{max} (lm/W)	CE^{max} (cd/A)	EQE_{max} (%)	CIE1931 coordinates (x, y) at 10V
10: ITO/MoO_3/NPB/3a/TPBi/LiF/Al	5.2	1100	900	0.8	1.9	0.8	(0.194, 0.256)
12: ITO/MoO_3/NPB/3c/TPBi/LiF/Al	5.1	4100	2100	1.2	1.9	1.2	(0.185, 0.244)
15: ITO/MoO_3/NPB/3f/TPBi/LiF/Al	4.9	11300	8300	1.6	1.9	1.6	(0.179, 0.246)
17: ITO/MoO_3/NPB/3h/TPBi/LiF/Al	5.4	4100	2200	0.6	0.7	0.6	(0.201, 0.267)

2.4. Application in OLEDs of Tetra-/Triphenylethenyl substituted 9,9-Dimethylacridine derivatives (Scientific publication No. 4, Q1)

This chapter is based on the paper published in *Molecules*, **2020**, *25*, 445[66]. The photophysical and electroluminescent properties of six compounds were investigated. The molecular structures of the compounds are shown in **Scheme 2.4.**

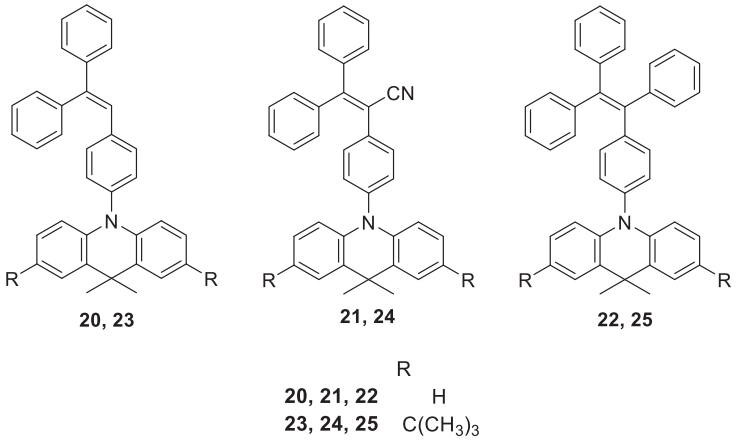

Scheme 2.4. Molecular structures of compounds **20–25**

In order to investigate differently substituted compounds **20-25** in the ground state, the absorption spectra of their dilute toluene and THF solutions were recorded (**Fig. 2.14**). The wavelengths of the absorption spectra of the solutions of compounds **20-25** were not particularly sensitive to the solvents in use and were observed at ca. 290 nm. The position of this UV band is close to that of acridan (**Fig. 2.14-a**). This observation shows that the low energy bands of compounds **20-25** can be mainly attributed to the local acridan transitions. The shoulders (maxima) at ca. 310-320 nm are attributed to the influence of tetra-/triphenylethenyl moieties. Weak lower-energy absorption bands in the range of 350-450 nm are apparently related to the intermolecular charge transfer (ICT) between acridan and tetra-/triphenylethenyl moieties. Compounds **21** and **24** displayed the most red-shifted ICT bands due to the presence of relatively strong electron acceptors. The UV absorption spectra of the vacuum-deposited films of compounds **20-25** replicated the spectra of the corresponding solutions well (**Fig. 2.14-b**). Slightly shifted low energy edges of the UV absorption spectra of vacuum-deposited films in comparison to those of the solutions can be explained either by the stronger ICT of compounds **20-25** in the solid state or by aggregation effects. Because of ICT, the PL spectra of compounds **20–25** were found to be sensitive to the polarity of the media. Thus, the PL spectra of the THF solutions of compounds **21** and **24** were significantly red-shifted in comparison to their toluene solutions (**Fig. 2.14-c**). Weak red-shifts were also observed for compounds **20**, **22**, **23**, and **25** containing no cyano groups, induced by molecular twisting. The PL spectra of the solid films of compounds **20-25** were

found to be similar to the PL spectra of the corresponding toluene solutions, apparently, and the reason is related to the low dielectric constants of the solid samples. The blue-shifted emission of the solid films of compounds **20-25** with respect to that of THF solutions may be explained by the influence of the relaxation of the local excited (LE) states. This assumption is in agreement with the double exponential photoluminescence decays of the films of compounds **20-25** that can be related to the overlapping of the relaxation of the LE and ICT states (**Fig. 2.14-d**). The solid films of compounds **20**, **22**, **23**, and **25** emitted in the blue region with the PL spectra peaked at 458–482 nm (**Fig. 2.14-b**). However, yellowish-green emission was observed for the films of compounds **21** and **24** due to the presence of cyano groups. The PL decays of compounds **20–25** were observed in the nanosecond range that ~ proves the simple fluorescent nature of emission (**Fig. 2.14-d**). Faster fluorescence transients mostly with mono exponential fitting were observed for the solutions of compounds **20-25** relative to those of the solid samples. Moreover, the normalized PL spectra of the doped solid films of compounds **20-25**:mCP are presented in **Fig. 2.15**.

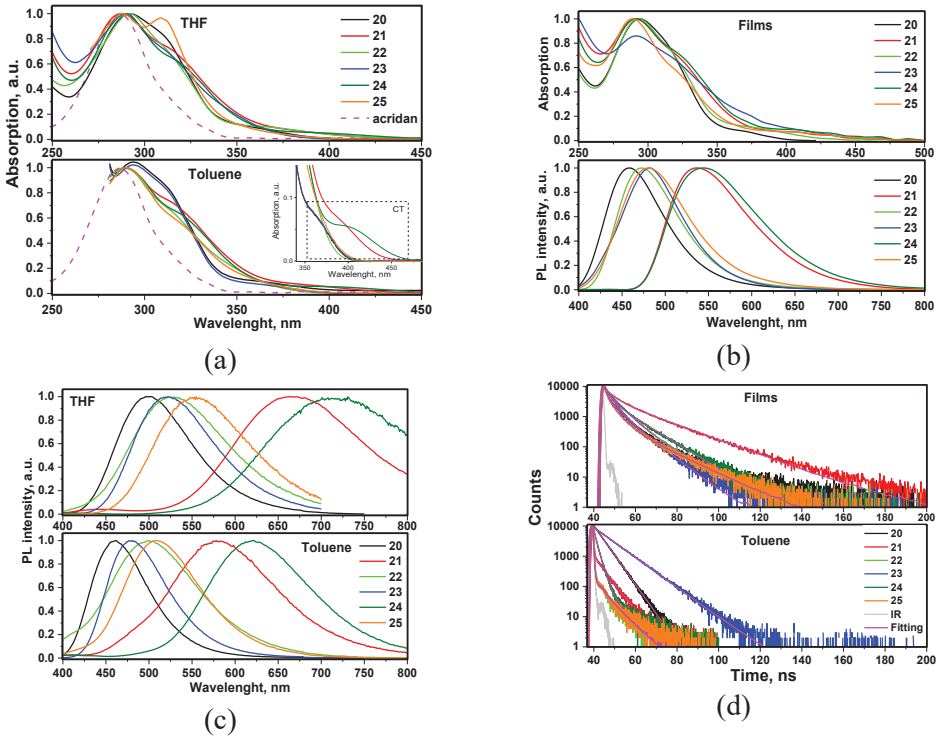

Fig. 2.14. (a) UV-vis absorption spectra of THF and toluene solutions (10^{-5} M) of compounds **20-25.** Low-energy ICT absorption bands of the solutions in toluene are zoomed in the inset, **(b)** UV-vis absorption and PL spectra of the films of compounds **20-25**, (**c**)

Steady-state PL spectra of THF and toluene solutions of compounds **20–25**, (**d**) PL decays of solid samples and toluene solutions of compounds **20–25** recorded at excitation wavelength of 374 nm

Table 2.12. Photophysical characteristics of compounds **20–25**

Compound	Toluene			THF		Non-doped film			Doped film	
	λ_{abs}^{max}, nm	λ_{PL}^{max}, nm	PLQY, %	λ_{abs}^{max}, nm	λ_{PL}^{max}, nm	λ_{abs}^{max}, nm	λ_{PL}^{max}, nm	PLQY, %	λ_{PL}^{max}, nm	PLQY, %
20	294	460	32	292	499	290	451	51	438	72
21	289	578	1	287	665	290	481	53	522	88
22	289	499	<1	289	527	288	452	44	442	71
23	294	477	39	290	522	290	464	40	440	52
24	290	622	2	288	715	289	531	26	550	38
25	290	508	1	289	553	288	475	53	445	83

The fluorescence quantum yields (PLQY) of dilute solutions in toluene and of non-doped and doped films media of compounds **20–25** are given in **Table 2.12**. The films of all the studied compounds exhibited considerably higher PLQY than the corresponding dilute solutions. This observation indicates aggregation induced emission (AIE) and aggregation induced emission enhancement (AIEE) for the compounds. In addition, the photophysical characteristics of compounds **20–25** are reported in **Table 2.12**. PLQY values (26–53%) of the non-doped films of the compounds were still much below unity apparently because of intermolecular quenching which may be partly overcome by appropriate hosting[67].

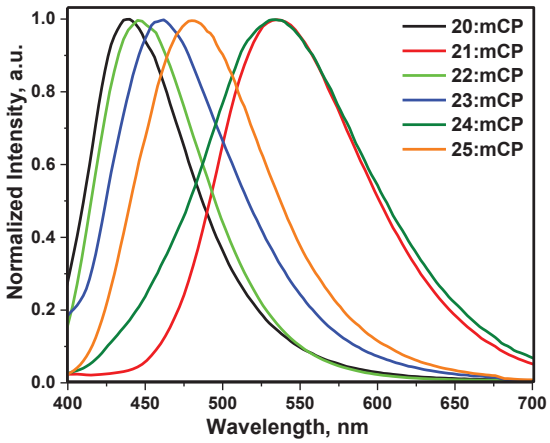

Fig. 2.15. Normalized PL spectra of solid films of compounds **20–25** doped in mCP (excitation wavelength 330 nm)

In order to investigate the AIE/AIEE of compounds **20–25**, the PL spectra of their dispersions in the THF-water mixtures with various water fractions (f_w) were

recorded (**Figs. 2.16** and **2.17**). By virtue of being insoluble in water, emissive aggregates of compounds **20–25** were formed at certain concentration of water thus highlighting the AIE/AIEE phenomena. The relative dependences of intensities and wavelengths of PL peaks of compounds **20–25** versus water fractions are shown in **Fig. 2.16** respectively. For example, with an increase of the water fraction in the THF-water mixture, the emission intensity of the dispersion of compound **20** constantly decreased and the PL maximum wavelength red-shifted until the aggregates were formed. These effects were caused by the increasing polarity of the THF-water mixtures to which ICT fluorescence is very sensitive. The further increase of f_w led to the increase of emission intensity and the blue shifts of the PL spectra due to the increasing amount of the aggregates. Similar regularities were observed for compounds **21, 22, 23** and **25**, and they were in good agreement with those reported for many other AIE/AIEE compounds[68]. However, a slightly different behavior was observed for compound **24**. The dispersion of compound **24** showed maximum emission intensity and a higher blue shift at f_w=70%. A similar observation was previously produced for compounds with AIE/AIEE effects, yet its cause is not clear yet[69,70]. In our opinion, this observation can apparently be explained by the structural modification of aggregates when their sizes were further increased.

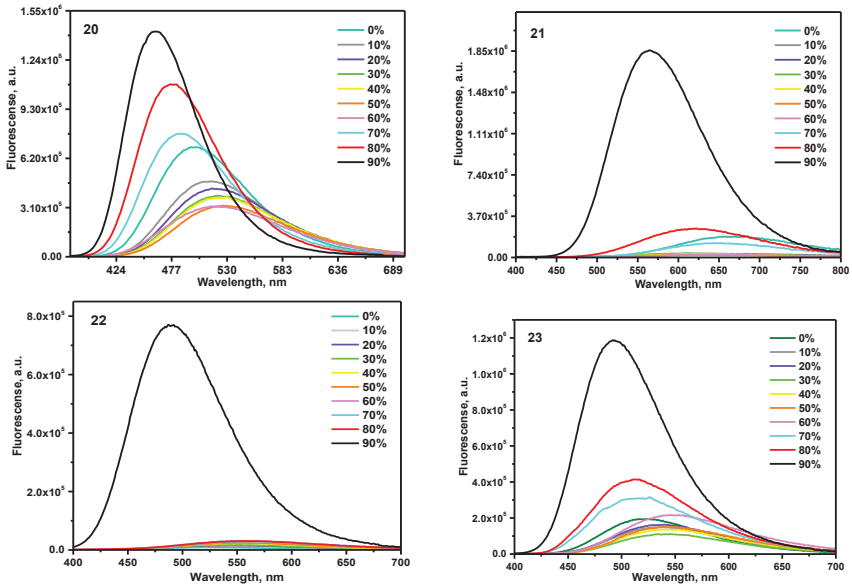

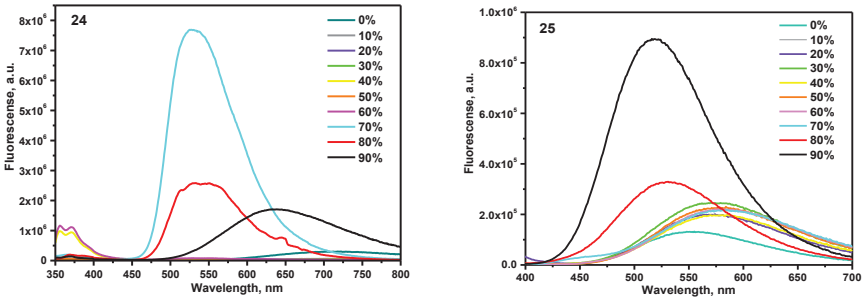

Fig. 2.16. Emission spectra of the dispersions of compounds **20–25** in THF/water mixtures (0–90%)

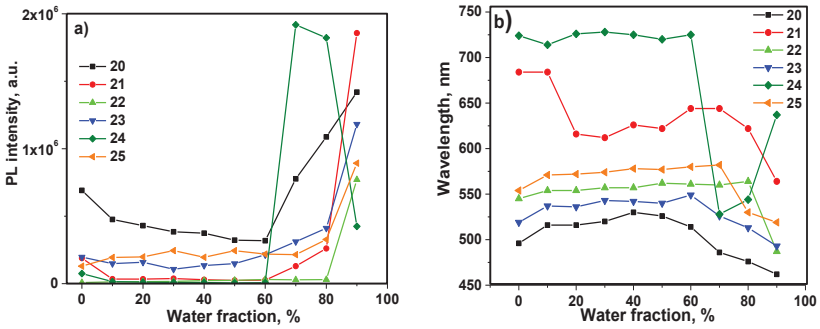

Fig. 2.17. Plots of **(a)** maximum emission intensity and **(b)** wavelength versus water fraction for the dispersions of compounds **20–25** in the mixtures of THF and water

The ionization potentials of vacuum deposited films (IP_{EP}) of compounds **20–25** were also determined with the electron photoemission method in air (**Fig. 2.18**). IP_{EP} values were recorded 5.70, 5.81, 5.66, 5.50, 5.63 and 5.43 for compounds **20, 21, 22, 23, 24** and **25** tandemly. The ionization potential values of tert-butyl substituted compounds **23–25** were found to be lower than those of compounds containing no tert-butyl groups (**20–22**) due to the slight donating effect of these groups. The IP value of compound **21** is higher than those of the remaining compounds due to the accepting properties of the cyano group.

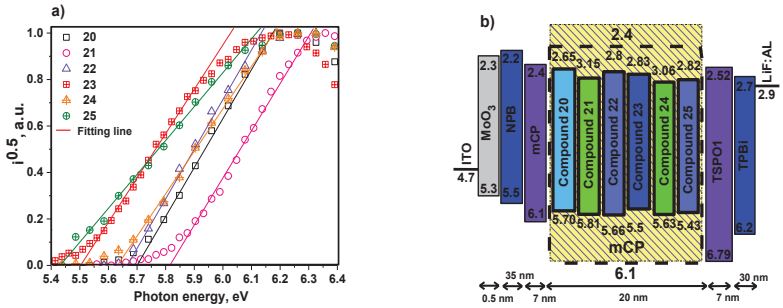

Fig. 2.18. (a) Photoelectron emission spectra of solid films of compounds **20–25**; **(b)** the structures of the non-doped and doped devices

Since compounds **20–25** showed high PLQYs in the solid state, they were tested as emitters in non-doped fluorescent OLEDs. Taking into account the values of the ionization potentials and electron affinities obtained for vacuum-deposited films of compounds **20–25**, their electroluminescent properties were studied via the following device structure: ITO/MoO_3 (0.5 nm)/NPB (35 nm)/mCP (7 nm)/ light-emitting layer (20 nm)/TSPO1 (7 nm)/TPBi (30 nm)/LiF (0.5 nm)/Al. Non-doped light-emitting layers of compounds **20–25** were used in devices **20N-25N**, respectively. The layers of MoO_3, NPB, mCP, TSPO1, TPBi, and LiF were used as the hole-injecting layer, the hole transporting layer, the exciton blocking layer, the hole/exciton blocking layer, the electron transporting layer, and the electron-injecting layer, respectively. According to the equilibrium energy diagram (**Fig. 2.18-b**) of the devices which demonstrates the absence of big energy barriers for the transported charges under applied external voltages, both holes and electrons were effectively injected to the light-emitting layers. Light-emitting recombination of the formed excitons occurred within the light-emitting layers. Thus, it is evident from the shapes of the electroluminescence (EL) spectra of devices **20N-25N** which were very similar to the shapes of the PL spectra of vacuum-deposited films **20–25**, respectively. The EL spectra of devices **20N-25N** were found to be similar under different applied voltages thus proving the main contribution of emitters **20–25** in electroluminescence (**Fig. 2.20**). Blue EL with close CIE coordinates (x from 0.15 to 0.17 and y from 0.13 to 0.25) was observed for devices **20N**, **22N**, **23N** and **25N** based on acridan and tetra-/triphenylethenyl-based emitters **20**, **22**, **23** and **25** containing no cyano groups (**Table 2.13.**). Meanwhile, OLEDs with the emitting layers of compounds **21** and **24** demonstrated yellow EL with CIE of (0.34, 0.56) and (0.41, 0.53) for devices **21N** and **24N** (**Fig 2.21**) similarly to the PL of vacuum-deposited films.

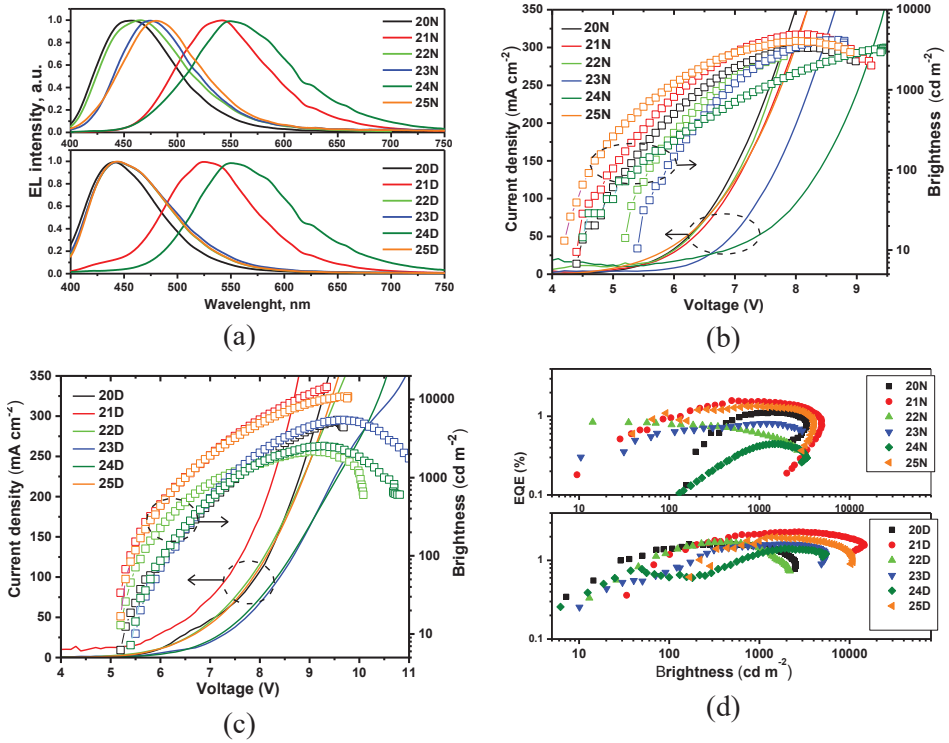

Fig. 2.19. (a) EL spectra, **(b, c)** current density-voltage-brightness and **(d)** external quantum efficiency-brightness characteristics of non-doped (**20N–25N**) and doped (**20D–25D**) OLEDs

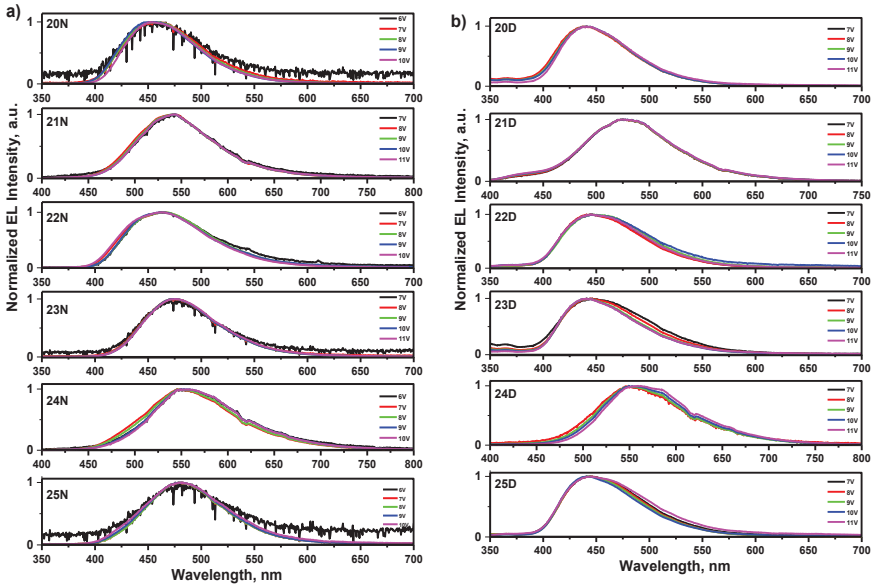

Fig. 2.20. Electroluminescence spectra of the devices at

different applied voltages **(a)** non-doped and **(b)** doped

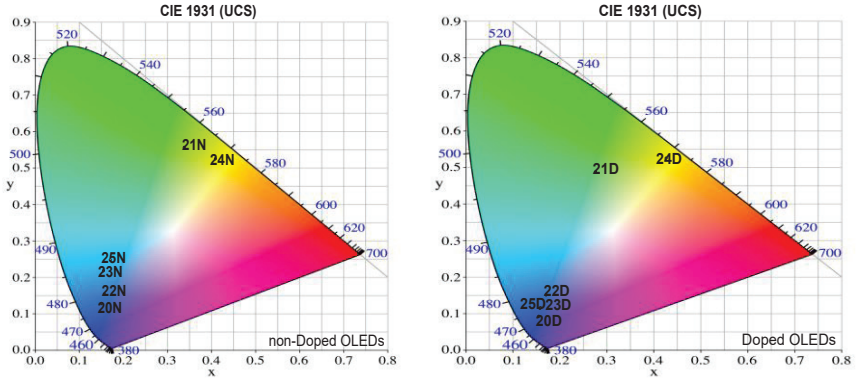

Fig 2.21. CIE coordinates of non-doped and doped OLEDs at 10V

Brightness exceeded 1000 cd/m^2 for all non-doped devices **20N–25N**. It reached the maximum value of 4940 cd/m^2 for device **21N**. The EL spectrum of this device was the closest to the sensitivity of the human eye. In addition, the film of emitter **21** was characterized by high PLQY of 53% (**Table 2.12**). The turn on voltages of devices **20N–25N** were observed in the range of 4.2–5.4 V demonstrating satisfactory charge-injecting and charge-transporting properties of the devices. The maximum external quantum efficiency (EQE) values of devices **20N–25N** were roughly proportional to the PLQY values of the non-doped films of the corresponding emitters. These EQEs are close to those of blue/green devices based on carbazole/triphenylamine and tetra-/triphenylethenyl-containing derivatives[71]. The highest EQE of 1.59% was obtained for device **21N**. This value is lower than 2.65%, which is the theoretical maximum of EQE for a device with a fluorescent emitter having PLQY of 53%. The theoretical EQE for device **21N** was calculated with a formula (Equation **2.7**) using the charge-balance factor γ=1, the efficiency of exciton production χ=0.25 (as for a fluorescent emitter), out-coupling efficiency η_{out}=0.2, and ϕ_{PL}=0.53 for the film of compound **21**. Apparently, the charge-balance factor of the studied devices is lower than unity. This presumption can be supported by the poor charge-transporting properties of emitters **20-25**. We tried to measure the charge mobilities in the vacuum-deposited films of compounds **20-25** by the time of flight (TOF) method, however, the transit times were not observed possibly because of the fast relaxation of charges in their layers. TOF measurements roughly demonstrated the charge transporting 'problems' of the non-doped films of compounds **20-25**. Therefore, the usage of the appropriate host was essential. The commonly used host mCP was chosen for the fabrication of doped OLEDs

exploiting the same device structure as the non-doped devices. In doped devices **20D-25D**, light-emitting layers **20-25** (10 wt. %) doped in mCP were used. The selection of the host was based not only on its appropriate HOMO/LUMO energy levels but also on the high PLQYs of the films of compounds **20-25** (10 wt. %) doped in mCP which ranged from 38% to 88%. The usage of the host allowed to increase the PLQY of compounds **20-25** in the solid state, apparently, due to the decrease of intermolecular interactions (restrictions of π–π* stacking) between neighboring molecules. The PL spectra of doped films were slightly blue-shifted in comparison to the PL spectra of the corresponding non-doped films. The EL spectra of doped devices **20D-25D** were in good agreement with the PL spectra of light-emitting layers **20-25**:mCP (**Fig. 2.15**). The shapes of the EL spectra of the doped devices were virtually the same under different external voltages (**Fig. 2.20**). The CIE coordinates of doped devices **20D–25D** were slightly shifted to the deeper blue region in comparison to those of non-doped devices **20N–25N** (**Table 2.13**).

As it was expected, the maximum EQEs of all the doped devices (**20D–25D**) were improved in comparison to those of the non-doped ones mainly due to the incensed PLQYs of the emitters dispersed in the host and due to the satisfactory charge-transporting properties of mCP (**Table 2.13**). The highest maximum EQE of 2.32% was also obtained for device **21D** based on compound **21**, which showed the highest PLQY of 88% when dispersed in mCP. However, the charge-injection properties of the doped devices were not improved. This is evident when taking into account the higher turn on voltages of devices **20D–25D** compared to those of devices **20N–25N**. This observation can be attributed to the induced energy barrier in the device structure by the relatively deep HOMO of mCP. Nevertheless, it was demonstrated that compounds **20–25** can be used as the fluorescent emitters in doped OLEDs. With the appropriate host exhibiting thermally activated delayed fluorescence (TADF), it is possible and sensible to test compounds **20–25** as fluorescent emitters in three component systems of **20–25**:TADF host:host for increasing the efficiencies of **20–25** based OLEDs, while still keeping in mind that exciton production probability is χ=1 for TADF based systems[72]. In addition, compounds **20–25** are potential candidates for sensing applications since they exhibit different emission intensities in liquids and solids.

2.7 $$\eta_{ext}=\gamma\times\phi_{PL}\times\chi\times\eta_{out}$$ [73]

Table 2.13. Electroluminescent parameters of non-doped (**20N–25N**) and doped (**20D–25D**) devices

Device	V_{on} (V)	L_{max} (cd/m^2)	CE_{max} (cd/A)	PE_{max} (lm/W)	EQE_{max} (%)	EL peak (nm)	CIE coordinates (x, y)
Non-doped devices 20N-25N							
20N	4.4	3350	2.23	1.07	1.10	456	0.15, 0.13
21N	4.4	4940	2.90	1.60	1.59	540	0.34, 0.56
22N	5.2	2630	2.83	1.78	0.86	465	0.16, 0.16
23N	5.4	4200	1.10	0.51	0.82	475	0.15, 0.22
24N	4.5	3360	1.30	0.53	0.45	550	0.41, 0.53
25N	4.2	4090	1.55	0.89	1.35	480	0.17, 0.25
Doped devices 20D-25D							
20D	5.2	5460	2.48	1.18	1.63	439	0.16, 0.10
21D	5.2	14400	4.67	2.13	2.32	525	0.28, 0.49
22D	5.2	2180	2.11	1.06	1.72	444	0.17, 0.16
23D	5.5	5460	3.10	1.29	1.62	444	0.16, 0.12
24D	5.4	2540	1.65	0.64	1.42	550	0.43, 0.53
25D	5.2	10900	1.95	0.94	1.93	444	0.16, 0.12

2.5. Multifunctional D-A-D' type compounds: mechanochromic luminescence, thermally activated delayed fluorescence and aggregation enhanced emission (Scientific publication No. 5, Q1)

This chapter is based on the paper published in *Chemical Engineering Journal*., **2020**, *401*, 125962[74]. Herein, we investigated the electroluminescence of new asymmetrical D-A-D' derivatives in which differently substituted carbazole donor moieties are directly linked to the quinoxaline unit (**Scheme 2.5.**). The compounds exhibit thermally activated delayed fluorescence, luminescence variation in response to external stresses (from green to orange) and emission enhancement in the aggregated state. The molecular structures of the compounds are presented in **Scheme 2.5**.

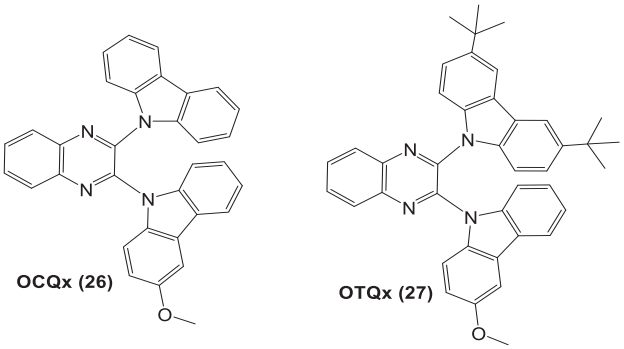

Scheme 2.5. Molecular structures of compounds **26** and **27**

The absorption and emission spectra of the solutions and films of compounds **26** and **27** are shown in **Fig. 2.22**. The photophysical data is summarized in **Table 2.14**. The absorption spectra of the compounds depict π-π* transitions of the aromatic rings at ca. 240 and 290 nm, and n-π* transitions of the nitrogen and oxygen atoms at ca. 330 nm and 347 nm[75]. The broad band at ca. 420 nm is attributed to the intramolecular charge transfer (ICT) transition from the donor to the acceptor moieties in each compound.

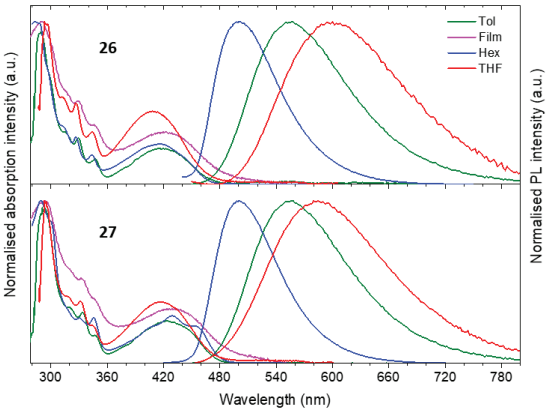

Fig. 2.22. Absorption and photoluminescence spectra of thin films and solutions of compounds **26** and **27** in solvents of various polarities

The optical band gaps obtained from the edge of the ICT transition peak were found to be close between the compounds, ~2.61 eV for compound **26** and ~2.59 eV for compound **27**. These values were obtained for solutions in toluene. In addition, the photoluminescence spectra of the compounds in hexane have the same wavelength maxima at 500 nm.

Table 2.14. Photophysical characteristics of compounds **26** and **27**

Compound	**Abs (nm)** (Hex, Tol, THF)	**PL (nm)** (Hex, Tol, THF, Doped film, Non-doped Film)	**S_1/T_1 (eV)**	**ΔE_{ST} (eV)**	**τ / τ[a] (ns/μs)**	**PLQY** doped film (mCP) (air/deg)	**PLQY** doped film (TCTA)(air/deg)
26	289, 328, 346	500, 547, 601, 546, 563	2.60/2.51	0.10	2.6/1340	0.19/0.23	0.17/0.24
27	291, 333, 347	500, 541, 583, 539, 567	2.61/2.55	0.06	4.4/1422	0.17/0.38	0.25/0.51

a) PL lifetime of compounds blended in host at RT

In order to examine the electroluminescence (EL) properties of compounds **26** and **27**, doped and non-doped OLEDs were fabricated having the device structure of ITO/MoO_3 (0.5 nm)/NPB (35 nm)/ compounds **26** or **27** (10 wt.%):TCTA (20 nm)/TSPO1 (7 nm)/TPBi (30 nm)/LiF (0.5 nm)/Al, where the light-emitting layer of respectively marked devices **26** and **27** consisted of compounds **26** or **27** as the TADF emitter and Tris(4-carbazoyl-9-ylphenyl)amine (TCTA) as the host. The

charge/exciton recombination zones were located within the light-emitting layer of devices **26** and **27** owing the additional layers of hole-injecting (molybdenum trioxide (MoO_3)), hole transporting (N,N′-di(1-naphthyl)-N,N′-diphenyl-(1,1′-biphenyl)-4,4′-diamine (NPB)), hole/exciton blocking (diphenyl[4-(triphenylsilyl)phenyl]phosphine oxide (TSPO1)), electron transporting (2,2',2''-(1,3,5-benzinetriyl)-tris(1-phenyl-1-H-benzimidazole) (TPBi)), and electron-injecting Lithium fluoride (LiF) ones involved to the OLED structure (**Fig. 2.23-a**). This statement is evident since the EL spectra of doped devices **26** (λ_{max}=535 nm) and **27** (λ_{max}=544 nm) are very similar to the PL spectra of the corresponding layers emitter **26**:TCTA (λ_{max}=546 nm) and emitter **27**:TCTA (λ_{max}=539 nm). The EL spectra of compound **27** are slightly red-shifted in comparison to the EL spectra of the device base of compound **26** due to the tert-substitution. Green and yellowish-green electroluminescence with a high maximum brightness of 41500 and 44500 cd/m^2 and with the CIE color coordinates of (0.338, 0.556) and (0.374, 0.572) was obtained for doped devices **26** and **27** (concentration=10%), respectively (**Fig. 2.23-b** (insets), **Fig. 2.23-c**). Good color stability of the electroluminescence of devices **26** and **27** was obtained under different applied voltages owing good host-guest energy transfer. Since the EL spectra do not include bands in the blue spectral region, there is no evidence of any emission of the host TCTA and/or charge-transporting layers NPB and TPBi.

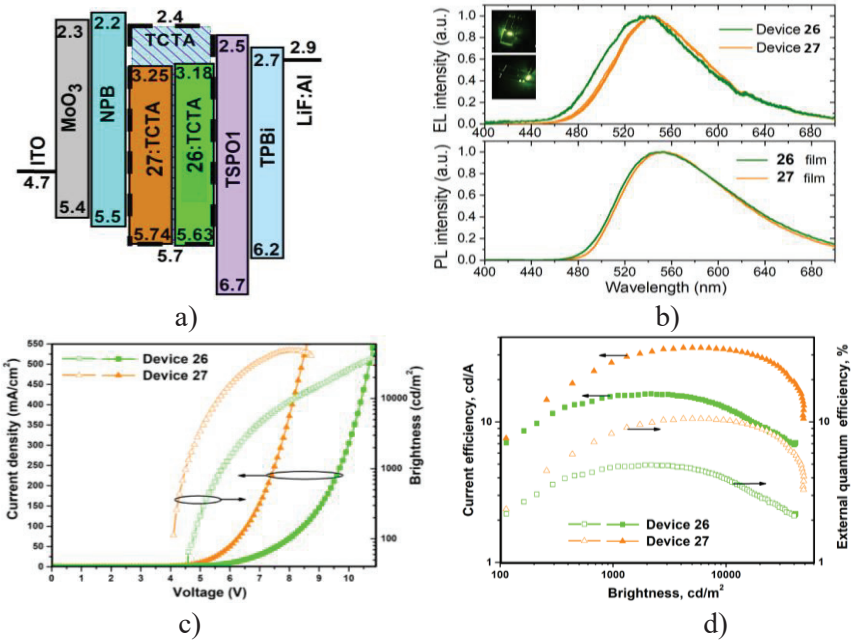

Fig. 2.23. (a) Equilibrium energy diagram, **(b)** EL spectra at different voltages ranging from 6 to 11 V with a step of 1V, **(c)** current density and brightness versus voltage and **(d)** current and external quantum efficiencies versus brightness for devices **26** and **27**

The fabricated doped devices (the concentration of the dopant was 10%) obtained from compounds **26** and **27** exhibited the maximum EQE of 4.95% and 10.53%; this trend is in good agreement with the trend of PLQYs (24% and 51%) of the light-emitting layers **26** (10wt. %):TCTA and **27** (10wt.%):TCTA, respectively (**Fig. 2.24-d**, **Table 2.15**). The EQE^{max} values dramatically decreased with the increasing concentration of the guest (**26** or **27**) in the light-emitting layer (**Fig. 2.24-e,f, Table 2.15**). This observation is apparently attributed to both the decrease of PLQYs under aggregate-induced quenching and charge disbalance at a high concentration of dopant **26** or **27**. As a result, non-doped devices based on compounds **26** and **27** were characterized by EQE^{max} of 0.48% and 0.71%, respectively (**Table 2.15**). Interestingly, shifts of the EL spectra (changed EL color) and increased EQE^{max} were obtained when the light-emitting layers of non-doped devices were treated by vapor of toluene (**Fig. 2.24, Table 2.15**). This means that the OLED efficiency and their emission color can be improved when mechanochromic luminophores are used in their device structure.

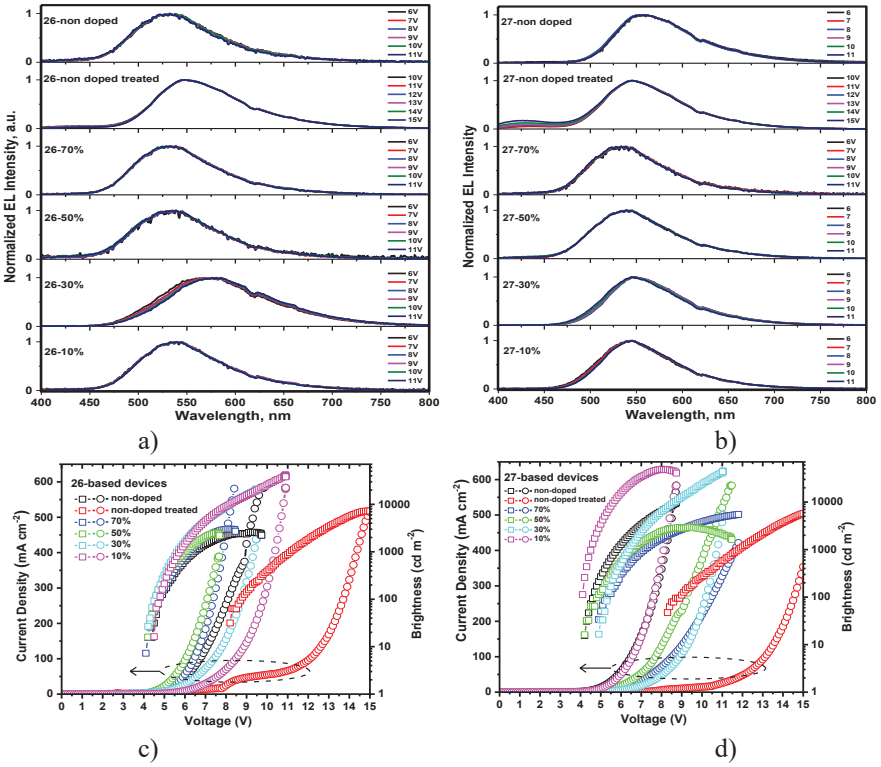

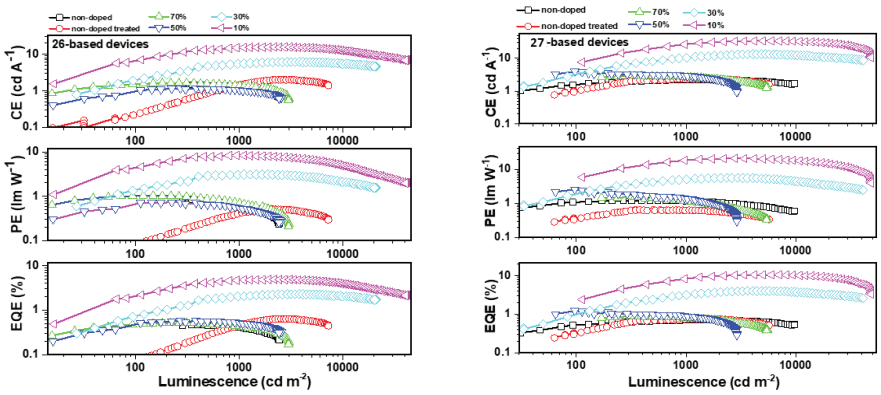

e) f)

Fig. 2.24. (a, b) EL spectra, **(c, d)** current density and brightness versus voltage and **(e, f)** current and external quantum efficiencies versus brightness for non-doped and doped devices based on **26** and **27**

Table 2.15. Characteristics of non-doped and doped devices based on **26** and **27**

Device		V_{on} (V)	L_{max} (cd/m^2)	CE_{max} (cd/A)	PE_{max} (lm/W)	EQE_{max} (%)	CIE coordinates (X, Y)
26	**non-doped**	4.43	2577	1.48	0.85	0.48	(0.313, 0.535)
	non-doped treated	8.18	7241	2.03	0.52	0.64	(0.397, 0.545)
	70%	4.12	3008	1.66	1.04	0.52	(0.315, 0.554)
	50%	4.20	2543	1.18	0.74	0.59	(0.312, 0.520)
	30%	4.19	20918	6.23	3.09	2.31	(0.456, 0.506)
	10%	4.49	41488	15.83	8.36	4.95	(0.338, 0.556)
27	**non-doped**	4.21	9661	2.19	1.23	0.71	(0.434, 0.540)
	non-doped treated	8.29	5725	2.42	0.66	0.77	(0.361, 0.512)
	70%	4.89	5412	3.04	1.59	0.91	(0.319, 0.549)
	50%	4.17	2937	3.96	2.59	1.23	(0.339, 0.542)
	30%	4.90	44888	13.38	5.68	4.05	(0.392, 0.562)
	10%	4.08	48809	33.64	21.08	10.53	(0.374, 0.572)

3. CONCLUSIONS

1. The photophysical and electroluminescence properties of carbazole derivatives containing one or two tri/tetraphenylethenyl moieties as the fluorescent OLED emitters were studied. It was determined that:

1.1. The ionization potentials of ca. 5.15 eV and hole mobilities reaching 10^{-3} cm^2/V were observed for the compounds with two tri/tetraphenylethenyl substituents; 9-ethyl-N,N-bis(4-(2,2-diphenylethenyl)phenyl)carbazol-3-amine and 9-ethyl-N,N-bis(4-(1,2,2-triphenylethenyl)phenyl)carbazol-3-amine were suitable for utilizing in OLED structures as the hole-transporting and emissive materials.

1.2. OLED based on a carbazole derivative with two tetraphenylethenyl substituents linked through the nitrogen atom in the C-3 position of the carbazole moiety showed the highest maximum brightness exceeding of 50000 cd/m^2, as well as high maximum current, power and external quantum efficiencies of 17 cd/A, 9.2 lm/W, and 5.32%, respectively.

2. Photophysical and electroluminescent properties of new derivatives of xanthenone containing di-tert-butyl-carbazolyl, di-tert-butylacridanyl, di-tert-butyl phenothiazinyl and penoxazinyl substituents were investigated. It was established that:

2.1. Because of the big dihedral angles between the donors and the acceptor as well as because of the possibility of rotation around the N-C bond, the compounds were characterized by thermally activated delayed fluorescence and aggregation induced emission enhancement.

2.2. Two times higher photoluminesce quantum yields reaching 38% for doped films were observed for compounds containing di-tert-butyl-carbazolyl and di-tert-butyl-acridanyl moieties as compared to those observed for the compounds with the donors containing S and O hetematoms.

2.3. The ionization potential values in the range of 5.67–5.96 eV and hole and electron mobilities were in the range from 6.3×10^{-8} to 6.3×10^{-4} cm^{2}V^{-1}s^{-1} at the electric field of 2.5×10^5 V·cm^{-1} were detected.

2.4. Differently substituted compounds were utilized as emitters in OLEDs; the highest maximum values of external quantum efficiency (up to 3.5%) were observed for OLEDs based on emitters containing di-tert-butyl-carbazolyl, di-tert-butylacridanyl groups.

3. Electro optical, charge-transporting and electroluminescent properties of ten compounds based on tetrahydrodibenzophenanthridine and phenanthroimidazole were evaluated.

3.1. The blue luminophores exhibited high photoluminescence quantum yields of 66–93% in toluene solutions and 5–59% in solid films.

3.2. The ionization potential values of the compounds were in the range of 5.74 to 6.11 eV.

3.3. The best blue OLED exhibited brightness exceeding 10000 cd/m^2 and a relatively low roll of efficiency.

4. The photophysical and electroluminescent properties of six new tetra-/triphenylethenyl-substituted 9,9-dimethylacridines were investigated. It was established that:

4.1. The emitters demonstrated fluorescence quantum yields of 26–53% in non-doped films and of 52–88% in doped films. In the solid state, the compounds

emitted in the blue region (451–481 nm) without doping and in the deep-blue range (438–445 nm) after doping.

4.3. The ionization potential values of the derivatives were found to be in the range of 5.43–5.81 eV.

4.4. Utilizing the compounds deep-blue OLEDs with the chromaticity coordinates of (0.16, 0.10), close to the blue color standard (0.14, 0.08) of the National Television System Committee, were obtained. The devices exhibited external quantum efficiencies up to 2.3%.

5. The electroluminescent properties of new asymmetric multifunctional compounds containing quinoxaline as an acceptor and differently substituted carbazole moieties as the donors were investigated.

5.1. Doped and non-doped OLEDs were fabricated and characterized. The maximum brightness, current efficiency and power efficiency values of 48809 cd/m^2, 33.64 cd/A and 21.08 lm/W respectively were observed.

5.2. By choosing the appropriate concentrations of the host, the external quantum efficiency of 10.53% was achieved.

4. SANTRAUKA

4.1. ĮVADAS

Organinių šviesos diodų (toliau – OLED) technologija tapo viena iš labiausiai dominuojančių ekranų technologijų ir potencialiai galinti tapti naujos kartos šviesos šaltinių technologija[1]. Eastman-Kodak tyrėjų 1987 m. sukurtas pirmasis OLED sukėlė didelį susidomėjimą[2]. OLED-ai, pradedant jų pirmuoju komercializuotu pavyzdžiu 1997 m., paskatino daugelio mokslininkų tyrimus visame pasaulyje ir tapo svarbiu ekranų ir apšvietimo technologijų komponentu[3]. OLED-ai yra dvigubos krūvininkų injekcijos prietaisai, paremti tuo pačiu metu vykstančia elektronų ir skylių pernaša į gretimus organinius sluoksnius, dėl ko pasireiškia elektroliuminescencija[4]. Norint, kad OLED-ai būtų efektyvūs, reikalinga subalansuota krūvininkų pernaša ir didelis eksitonų konversijos į šviesą efektyvumas[5]. Norint pasiekti efektyvią skylių ir elektronų rekombinaciją emisiniame sluoksnyje, reikalingi organiniai spinduoliai su π-konjuguota struktūra[6]. Organinėms elektroaktyvioms medžiagoms, naudojamoms efektyviuose elektroliuminescenciniuose prietaisuose, keliami tokie reikalavimai: tinkamos optinės ir fotofizikinės savybės, geras terminis ir morfologinis stabilumas, taip pat tinkami energetiniai lygmenys[5]. Organinių elektroaktyvių junginių struktūrose esančių skirtingų donorinių (toliau – D) ir akceptorinių (toliau – A) fragmentų deriniai suteikia tikimybę pasiekti platų norimų savybių diapazoną[7].

Naujesnės kartos OLED-ai konstruojami naudojant krūvininkų blokavimo principą, kad būtų užtikrinta efektyvi krūvininkų rekombinacija emisiniame sluoksnyje (**4.1 pav.**). Taip užkertamas kelias katodo (anodo) elektronams (skylėms) praeiti pro matricinį sluoksnį. Tokiu atveju matricoje susidaro daugiau elektronų ir skylių porų, taigi turėtume daugiau eksitonų ir didesnį prietaisų efektyvumą[11]. Tai

dažnai pasiekiama greta matricos įterpiant ploną blokuojantį sluoksnį arba organinės medžiagos, kuri pasižymi ypač gera tik vieno tipo krūvininkų pernaša, sluoksnį. Tai efektyviai perkelia eksitonų formavimosi zoną nuo matricos ir pernašos sluoksnių sąlyčio į matricos ir blokuojančio sluoksnio sąlytį[12].

OLED-ams būdingi sluoksniai sudaromi naudojant medžiagas, tinkamas atitinkamai funkcijai:

- Elektronų injekcijos sluoksnis (toliau – EIL);
- Elektronų pernašos sluoksnis (toliau – ETL);
- Skyles blokuojantis sluoksnis (toliau – HBL);
- Emisinis sluoksnis (toliau – EML), elektronų / skylių pernašai ir jų rekombinacijai susidarant eksitonui, kuris generuoja šviesos emisiją;
- Skylių pernašos sluoksnis (toliau – HTL);
- Skylių injekcijos sluoksnis (toliau – HIL).

EIL ir HBL taip pat gali būti naudojami eksitonų susidarymo zonai kontroliuoti, blokuojant skylių pernašą. Krūvininkų pernašos sluoksniai užtikrina gerą krūvininkų injekciją ir pernašą link emisinio sluoksnio, kuriame susidaro eksitonai[10]. Siekiant optimizuoti krūvininkų balansą, EML iš abiejų pusių yra atribojamas dviem krūvininkus blokuojančiais sluoksniais, kurie apriboja krūvininkus EML viduje ir taip užtikrina, kad visi krūvininkai rekombinuotų[13,14]. Todėl, kuriant OLED-us, labai svarbu atsižvelgti į santykius tarp darbinės funkcijos ir sluoksnius sudarančių junginių HOMO ir LUMO lygmens[15].

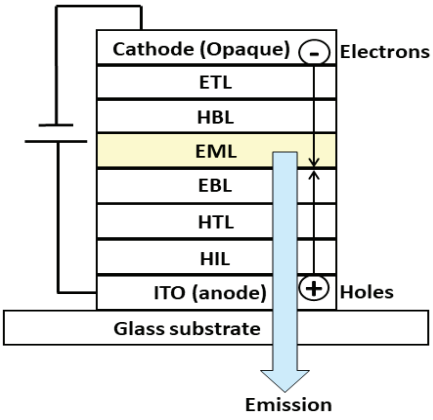

4.1 pav. Daugiasluoksnio OLED-o struktūros schema

Šio darbo tikslas – ištirti ir išsamiai išanalizuoti naujų organinių elektroaktyvių junginių savybes ir jų veikimą OLED-uose, siekiant nustatyti struktūros ir savybių tarpusavio priklausomybes.

Tikslui pasiekti buvo suformuluoti šie **uždaviniai:**

- Karbazolo darinių, turinčių vieną ar du tetra-/trifeniletenilpakaitus, fotofizikinių ir elektroliuminescencinių savybių tyrimas.
- Ksantenono darinių fotofizikinių, fotoelektrinių ir krūvininkus pernešančių savybių tyrimas.

- Tetrahidrodibenzfenantridino ir fenantrimidazolo darinių fotofizikinių, elektrocheminių ir elektroliuminescencinių savybių tyrimas.
- Tetra-/trifeniletenilpakeistų 9,9-dimetilakridino darinių fotofizikinių savybių tyrimas ir šių darinių išbandymas OLED struktūrose.
- Nelegiruotų ir legiruotų prietaisų, turinčių D-A-D' tipo TADF spinduolius, kuriuose skirtingus pakaitus turintys donoriniai karbazolo fragmentai tiesiogiai sujungti su chinoksalino fragmentu, elektroliuminescencinių savybių tyrimas.

Darbo naujumas:

- Panaudojant naujus vienu ar dviem tetra-/trifeniletenilo fragmentais pakeistus karbazolo darinius, suformuoti OLED-ai ir nustatytos jų charakteristikos.
- Suformuoti ir apibūdinti mėlyną, žalią ir geltoną šviesą skleidžiantys OLED-ai, turintys naujus ksantenono darinius, pasižyminčius termiškai aktyvuotąja uždelstąja fluorescencija ir agregacijos sustiprinta emisija.
- Ištirtos naujų tetrahidrodibenzfenantridino ir fenantrimidazolo darinių fotofizikinės, elektrocheminės ir elektroliuminescencinės savybės.
- Pirmą kartą įrodyta agregacijos sustiprinta emisija tetra-/trifeniletililpakeistiems 9,9-dimetilakridinams ir ištirtos šių junginių elektroliuminescencinės savybės.
- Atliktas naujų asimetrinio D-A-D' tipo TADF spinduolių, kuriuose skirtingai pakeisti donoriniai karbazolo fragmentai tiesiogiai sujungti su chinoksalino fragmentu, elektroliuminescencinis charakterizavimas.

4.2. REZULTATAI IR JŲ APTARIMAS

4.2.1. Karbazolo dariniai, turintys vieną ar du tetra-/trifeniletenilpakaitus, kaip efektyvūs skyles pernešantys OLED spinduoliai

Tiriamų junginių molekulinės struktūros pavaizduotos **4.1 schemoje**.

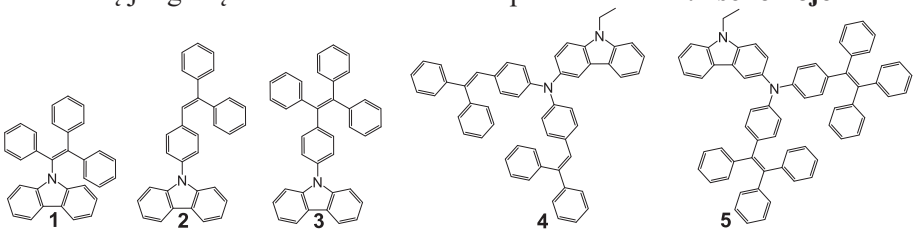

4.1 schema. Junginių **1**–**5** molekulinės struktūros

Junginių **1**–**5** praskiestų tirpalų toluene ir THF bei vakuume nusodintų sluoksnių absorbcijos ir fotoliuminescencijos (toliau – PL) spektrai atvaizduoti **4.2 pav., a.** Junginių kietųjų sluoksnių PL gesimo kreivės pateiktos **4.2 pav., b.** Fotofizikinės charakteristikos apibendrintos **4.1** len**telėje**. Junginių absorbcijos

maksimumai susiję su π-π* šuoliais. Junginių **4** ir **5**, turinčių dvi tetra-/trifenileteniilpakaitus, praskiestų tirpalų absorbcijos maksimumai pastebėti atitinkamai ties 404 ir 382 nm (**4.1 lentelė**). Nustatyta, kad junginių **1–3** tirpalų toluene ir THF PL spektrai yra panašūs.

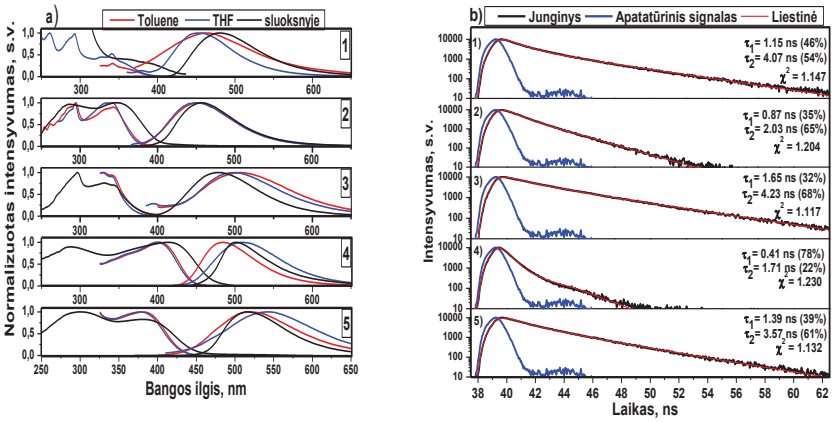

4.2 pav. (a) Junginių **1–5** praskiestų tirpalų (10^{-5} M) toluene ir THF bei sluoksnių normalizuoti absorbcijos ir fluorescencijos spektrai ir **(b)** kietųjų sluoksnių PL gesimo kreivės

Junginių **1–5** kietųjų sluoksnių fluorescencijos kvantinių našumų (toliau – *PLQY*) vertės yra daug didesnės nei atitinkamų tirpalų (**4.1 lentelė**). Šie rezultatai yra susiję su agregacijos sustiprinta emisija (toliau – AIEE).

4.1 lentelė. Junginių **1–5** praskiestų tirpalų ir sluoksnių fotofizikiniai duomenys

Junginys	**Toluene tirpalas**			**THF tirpalas**			**Sluoksnis**		
	λ_{abs}^{max}, **nm**	λ_{F}^{max}, **nm**	***PLQY*, %**	λ_{abs}^{max}, **nm**	λ_{F}^{max}, **nm**	***PLQY*, %**	λ_{abs}^{max}, **nm**	λ_{F}^{max}, **nm**	***PLQY*, %**
1	342	462	4	342	454	2	366	480	48
2	342	448	3	342	448	2	354	458	52
3	342	507	3	342	499	1	345	479	86
4	404	484	17	404	508	15	420	500	28
5	382	517	9	382	542	6	397	517	35

4.2 lentelėje pateiktos junginių jonizacijos potencialų (toliau – IP) vertės. Lėkio trukmės metodu (TOF) ištirtos junginių krūvininkų pernašos savybės. Junginių **1–5** sluoksnių skylių dreifinio judrio (μ_h) priklausomybės nuo elektrinio lauko pavaizduotos **4.3 pav.**

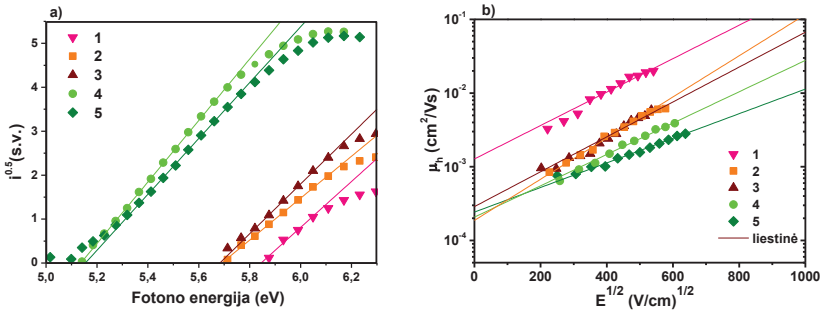

4.3 pav. (a) Junginių **1–5** sluoksnių fotoelektroninės emisijos spektrai ir **(b)** skylių dreifinio judrio priklausomybės nuo elektros lauko stiprio

4.2 lentelė. Junginių **1–5** elektrocheminės charakteristikos ir skylių pernašos parametrai

Junginys	E_g^{opt}, eV	I_P^{ep}, eV	μ_{h_0}, cm^2/Vs	μ_h, cm^2/Vs	α, (cm/V)$^{1/2}$
1	3,17	5,85	$1{,}3\times10^{-3}$	$2{,}1\times10^{-2}$	$5{,}23\times10^{-3}$
2	3,27	5,70	$1{,}93\times10^{-4}$	6×10^{-3}	$5{,}43\times10^{-3}$
3	3,28	5,68	$2{,}95\times10^{-4}$	6×10^{-3}	$6{,}45\times10^{-3}$
4	2,75	5,14	2×10^{-4}	3×10^{-3}	$4{,}9\times10^{-3}$
5	2,82	5,15	$2{,}45\times10^{-4}$	$1{,}9\times10^{-3}$	$3{,}84\times10^{-3}$

Nelegiruoti OLED-ai formuoti kelių skirtingų struktūrų. ITO/MoO_3 (1 nm)/ NPB (60 nm)/TCTA (5 nm)/ emisinis sluoksnis (30 nm)/TSPO1 (3 nm)/TPBi (40 nm)/LiF (0,5 nm)/Al struktūros prietaisai pavadinti **D1–D5**. O prietaisų **D1a**, **D3a** ir **D5a** struktūrose ITO/MoO_3 (1 nm)/mMTDATA (50 nm)/emisinis sluoksnis (30 nm)/TSPO1 (5 nm)/TPBi (65 nm)/LiF (0,5 nm)/Al, skylių pernašos sluoksniai praleisti, nes junginių **4** ir **5** HOMO tinkamas skylių injekcijai. Prietaiso **D5a** maksimalus skaistis viršijo 50000 cd/m^2 ties 3,8 V. Dėl to prietaiso **D5a** maksimalus išorinis kvantinis efektyvumas (toliau – *EQE*) siekė 5,32 % (**4.3 lentelė** ir **4.4 pav.**).

4.3 lentelė. Nelegiruotų OLED-ų charakteristikos

Prietaisas	V_{on} (V)	λ_{max} (nm)	L_{max} (cd/m^2)	CE_{max} (cd/A)	PE_{max} (lm/W)	EQE_{max} (%)	CIE1931 koordinatės (X,Y)
Prietaiso struktūra ITO/MoO_3/NPB/TCTA/emisinis sluoksnis/TSPO1/TPBi/LiF/Al							
D1	3,81	470	4700	3	2,35	1,62	(0,168;0,209)
D2	3,99	441	4300	1,4	0,82	1,08	(0,159;0,126)
D3	3,99	479	2000	3,8	2,6	1,95	(0,174;0,244)
D4	4,19	499	12100	4,26	2,2	1,6	(0,194;0,463)
D5	3,79	518	15500	5,8	3	2	(0,248;0,514)
Prietaiso struktūra ITO/MoO_3/m-MTDATA/emisinis sluoksnis/TSPO1/TPBi/LiF/Al							
D1a	4,1	497	6600	2,1	1,17	0,85	(0,202;0,34)
D3a	4,5	496	7700	2,76	1,38	1,16	(0,19;0,318)
D5a	3,8	518	52000	17	9,2	5,32	(0,242;0,52)

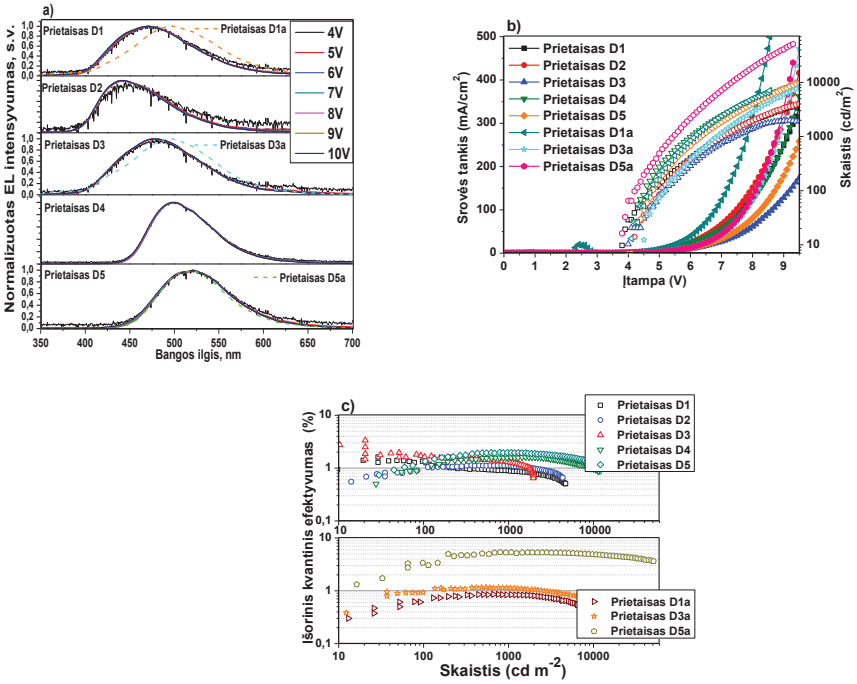

4.4 pav. (a) Prietaisų **D1-D5** ir **D5a** elektroliuminescencijos (EL) spektrai, užrašyti esant skirtingoms įtampoms, **(b)** srovės tankio, įtampos ir skaisčio bei **(c)** *EQE* ir skaisčio tarpusavio priklausomybės

4.2.2. Ksantenono dariniai, pasižymintys agregacijos sustiprinta emisija ir termiškai aktyvintąja uždelstąja fluorescencija, kaip OLED spinduoliai

Junginių **6–9** molekulinės struktūros pateiktos **4.2 schemoje**.

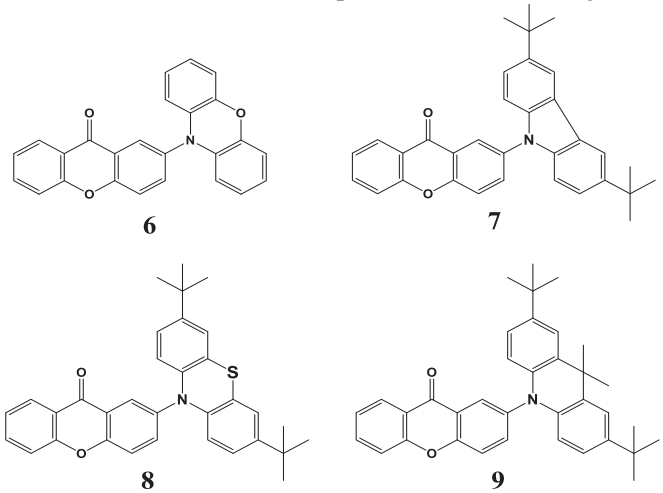

4.2 schema. Junginių **6–9** molekulinės struktūros

Junginių **6–9** tirpalų skirtingo poliškumo (toluene, THF ir chloroforme) tirpikliuose bei kietųjų bandinių (grynų ir legiruotų sluoksnių) absorbcijos ir PL spektrai pateikti **4.5 pav., a, b.**Junginių absorbcijos juostas ties 250–300 nm ir 300–350 nm galima priskirti donorinių ksantenono fragmentų atitinkamiems π→π* ir n→π* šuoliams (**4.5 pav., a**). Užfiksuotiems PL spektrams būdinga viena plati nestruktūrizuota juosta, kuri slenka mažesnės energetinės srities link, didėjant terpės poliškumui (**4.5 pav., b**).

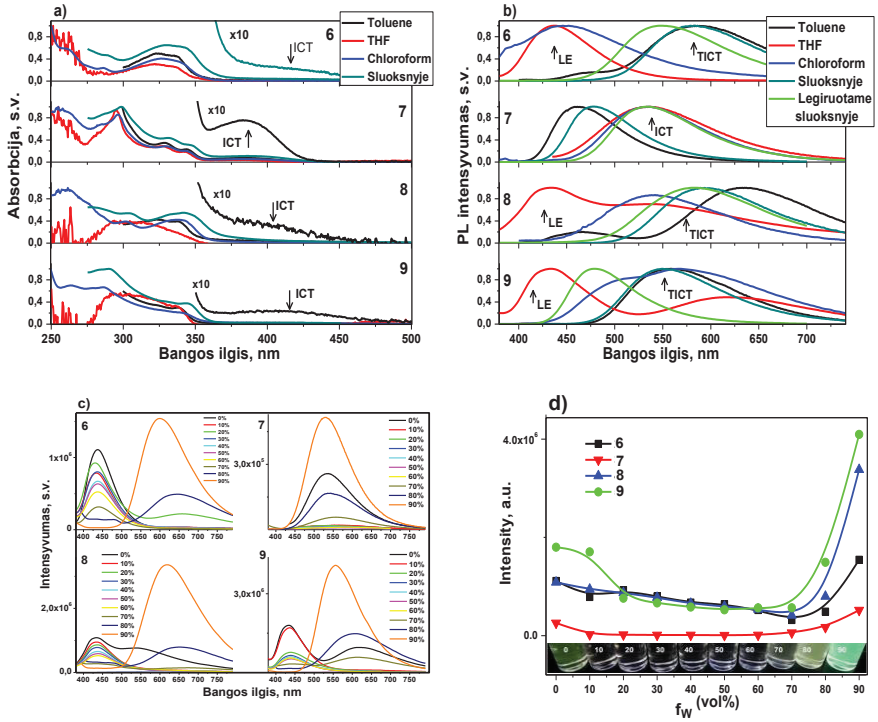

4.5 pav. (a) Junginių **6–9,** disperguotų skirtingose terpėse, absorbcijos ir **(b)** fotoliuminescencijos spektrai, **(c)** junginių **6**–**9** dispersijų THF/vandens mišiniuose PL spektrai ir **(d)** emisijos intensyvumo bei vandens tūrinės frakcijos (f_W) priklausomybė

Junginių **6–9** kietųjų sluoksnių *PLQY* vertės yra didesnės nei jų tirpalų toluene (**4.4 lentelė**), todėl junginiai sukėlė AIEE. Junginių **6–9** dispersijų THF/vandens mišiniuose PL spektrai ir emisijos priklausomybė nuo vandens frakcijos tūrio pateikta **4.5 pav., c, d.**

4.4 lentelė. Junginių **6**–**9** tirpalų ir sluoksnių spektrinės charakteristikos

Junginys	Tirpale			Sluoksnyje					
	Toluene			Nelegiruotame				Legiruotame	
	λ_{abs}^{max}, nm	λ_{F}^{max}, nm	*PLQY*, %	λ_{abs}^{max}, nm	λ_{F}^{max}, nm	*PLQY*, %	E_T, eV	λ_{F}^{max}, nm	*PLQY*, %
6	327	590	0,6	330	580	4	2,34	549	14
7	293	457	15	298	476	19	2,74	534	38
8	331	638	0,3	277	595	5	2,39	585	7
9	331	563	2	290	549	14	2,51	479	36

Visų tirtų junginių tirpalų toluene fluorescencijos spektrų intensyvumas padidėjo pašalinus deguonį (**4.6 pav., a**). Junginių **6**–**9** nelegiruotų ir legiruotų sluoksnių PL gesimo kreivėse pastebėtas ilgasis komponentas (**4.6 pav., b**). Junginių **6–9** sluoksnių fosforescencijos ir fotoliuminescencijos spektrai užrašyti skysto azoto temperatūroje (77 K), o E_S ir E_T vertės apskaičiuotos naudojant šių spektrų pradžios bangos ilgius pagal empirinę formulę (E_S), (E_T) = $1240 \cdot \lambda^{-1}$ (**4.6 pav., c.**). Junginių **6–9** molekulinių mišinių su mCP sluoksnių PL gesimas skirtingose temperatūrose ir emisijos intensyvumo priklausomybė nuo lazerio srauto kambario temperatūroje pateikti **4.6 pav., d.** Didėjantis uždelstosios emisijos intensyvumas didėjant temperatūrai bei uždelstosios emisijos intensyvumo tiesinės priklausomybės nuo lazerio srauto, kurios nuolydžio kampas artimas vienetui, neabejotinai įrodė ilgalaikės fluorescencijos TADF pobūdį.

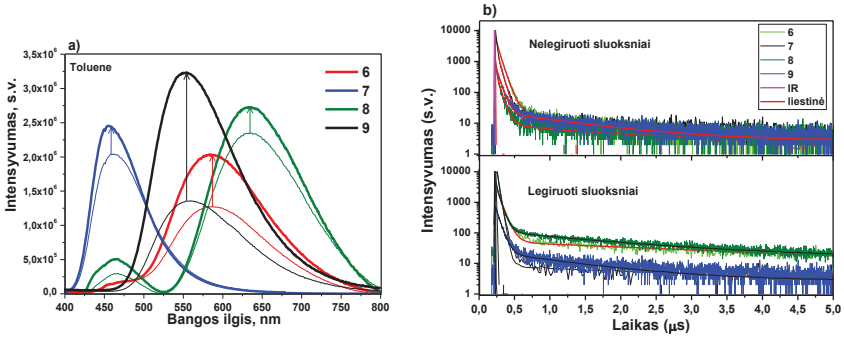

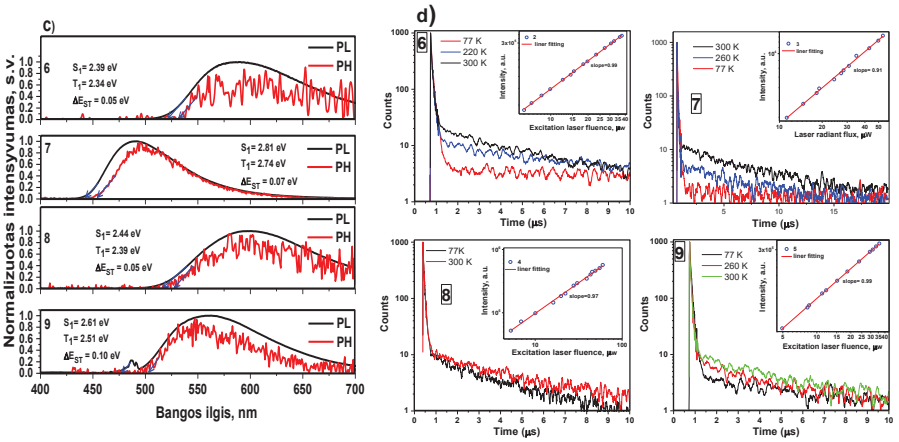

4.6 pav. (a) Junginių tirpalų toluene emisijos spektrai vakuume ir deguonies aplinkoje, **(b)** junginių **6**–**9** nelegiruotų ir legiruotų (10 % mCP) sluoksnių PL gesimo kreivės, **(c)** junginių sluoksnių PL ir fosforescencijos (PH) spektrai esant 77 K, **(d)** junginių legiruotų mCP sluoksnių PL gesimo kreivės, užfiksuotos skirtingose temperatūrose. Įklijose pateikta uždelstosios emisijos intensyvumo priklausomybė nuo lazerio srauto (uždelsta 1 μs).

Suformuoti OLED-ai pavadinti **PXZ, CZ, PTZ** ir **ACR,** priklausomai nuo struktūroje naudoto spinduolio: ITO/MoO3 (1 nm)/NPB (65 nm)/ **6, 7, 8** arba **9** (10 %):mCP (30 nm)/TPBi (40 nm)/LiF (0,5 nm)/Al. Prietaisų **PXZ**, **CZ**, **PTZ** ir **ACR** EL spektrai gerai koreliuoja, atitinkamai su **6**, **7**, **8** ir **9** spinduolių PL spektrais. Mažiausia 3,2 V įjungimo įtampa nustatyta prietaiso **PXZ**, turinčio junginį **2**, dėl jo aukščiausio ir subalansuoto skylių ir elektronų judrio. Prietaisų **PXZ** ir **ACR** maksimalus skaistis viršijo 10000 cd·m^{-2} dėl didelių emisinių sluoksnių *PLQY* verčių ir jų emisijos yra žaliai geltonoje regimojo spektro srityje (**4.7 pav., d**). Geriausią *EQE* vertę – 3,5 % turėjo prietaisas **ACR**, nes spinduolis **9** legiruotame sluoksnyje turėjo aukštą *PLQY* ir santykinai didelius krūvininkų judrius. Elektroliuminescencijos vertės pateiktos **4.5 lentelėje**.

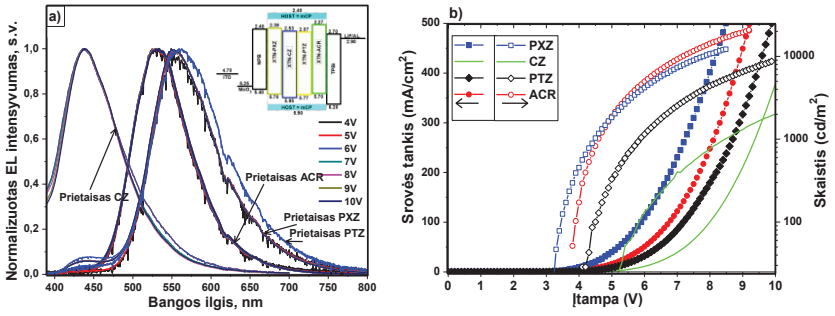

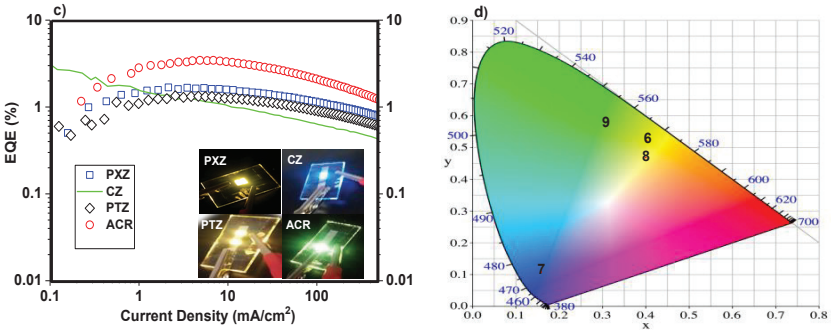

4.7 pav. (a) Prietaisų EL spektrai, užfiksuoti esant įvairiai įtampai, **(b)** įtampos, srovės tankio ir skaisčio tarpusavio priklausomybės bei **(c)** EQE ir srovės tankio tarpusavio priklausomybė ir **(d)** CIE koordinatės

4.5 lentelė. OLED-ų parametrai

Prietaisas	V_{on} **(V)**	L_{max} **(cd/m²)**	L **ties 8** V **(cd/m²)**	PE_{max} **(lm/W)**	CE_{max} **(cd/A)**	EQE_{max} **(%)**	**CIE koordinatės** ($X;Y$)
PXZ	3,2	12500 (8,5 V)	10900	4,2	5,3	1,7	(0,403;0,526)
CZ	4,9	2400 (10,6 V)	820	3,7	2,8	1,8	(0,159;0,111)
PTZ	3,9	8800 (9,9 V)	4600	2,4	3,9	1,4	(0,401;0,473)
ACR	3,8	20900 (9,2 V)	14800	7,6	11,7	3,5	(0,307;0,571)

4.2.3. Tetrahidrodibenzfenantridino ir fenantrimidazolo darinių fotofizikinės ir elektroliuminescencinės savybės

Junginių molekulinės struktūros pateiktos **4.3 schemoje**.

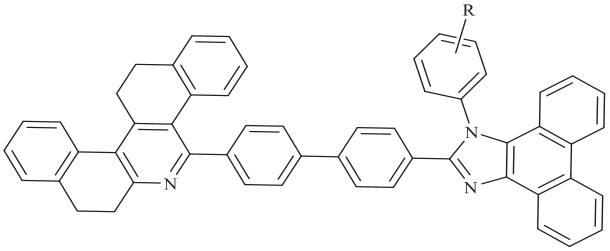

10: R = H
11: R = 4-Me
12: R = 4-F
13: R = 4-Cl
14: R = 3,5-Me
15: R = 4-MeO
16: R = 4-CN
17: R = 3,5-MeO
18: R = 4-NO_2
19: R = 2-pyridine

4.3 schema. Junginių **10–19** molekulinės struktūros

Siekiant ištirti pakaitų įtaką tetrahidrodibenzfenantridino (toliau – THDP) ir fenantrimidazolo (toliau PI) darinių fotofizikinėms savybėms, užfiksuoti junginių

tirpalų ir sluoksnių absorbcijos ir PL spektrai (**4.8 pav., a, b**). Junginių **10–19** tirpalų toluene absorbcija labai panaši. Panaši tendencija matoma ir polinių tirpiklių tirpaluose, parodanti silpną junginių solvatochromizmo efektą pagrindinėse būsenose. Skirtingi Lippert-Mataga tiesinių priklausomybių nuolydžiai (svyruoja nuo 2633 iki 8511 cm^{-1}) parodė, kad junginių **10–19** sužadintų singletinių būsenų dipolio momentai skiriasi (4.8 pav., d)[63]. Be to, gana maži junginių **10–19** Lippert-Mataga nuolydžiai rodo lokaliai sužadintų būsenų rekombinacijos galimą indėlį junginių emisijoje.

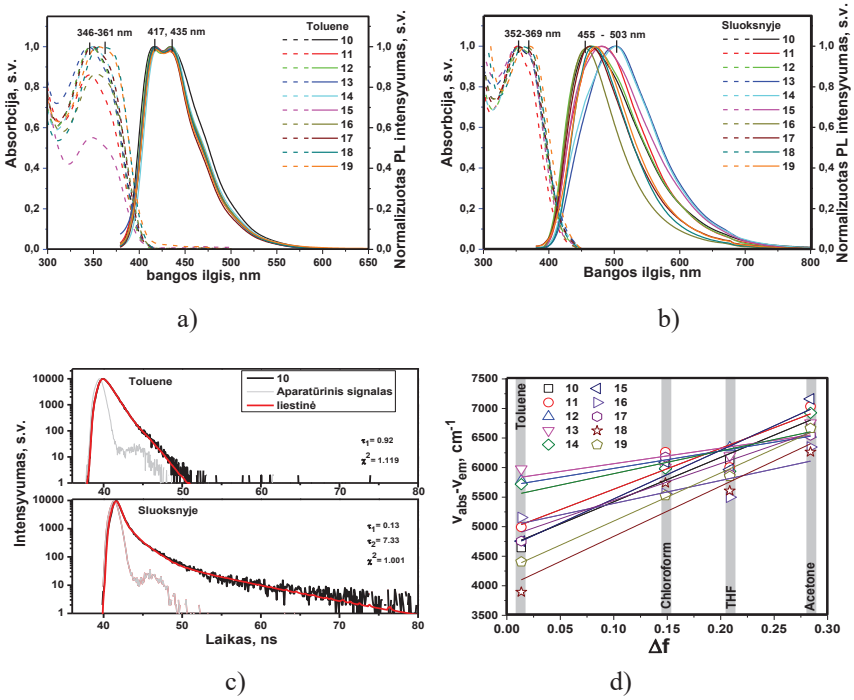

4.8 pav. (a) Junginių **10–19** tirpalų toluene ir **(b)** sluoksnių absorbcijos (brūkšninės linijos) bei PL (vientisos linijos) spektrai, **(c)** junginio **10** tirpalo toluene ir sluoksnio PL gesimo kreivės, **(d)** junginių **10–19** Lippert-Mataga diagramos, rodančios koreliaciją tarp tirpiklio poliškumo (Δf) ir Stokso poslinkių ($\Delta \upsilon = \upsilon_{abs} - \upsilon_{em}$)

Junginiai **10, 12, 15** ir **17** išbandyti nelegiruotų OLED-ų struktūrose, atsižvelgiant į jų sluoksnių gana dideles *PLQY* vertes ir tai, kad jie gali pernešti krūvininkus. Suformuotų OLED-ų struktūra ITO/MoO_3(1 nm)/NPB (30 nm)/**10, 12, 15** ar **17** (18 nm)/BPhen (33 nm)/LiF(0,5 nm)/Al (**4.9 pav., a**). Mėlynas OLED pasiekė 1,6 % *EQE* esant 10000 cd/m^2 skaisčiui (*L*) (**4.9 pav., d**).

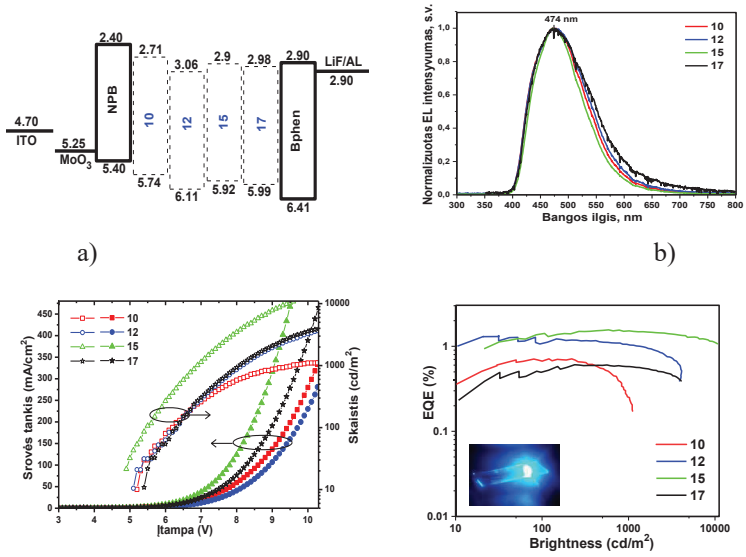

4.9 pav. Prietaisų **(a)** energetinių lygmenų diagrama, **(b)** EL spektrai esant 7 V, **(c)** srovės stiprio ir skaisčio priklausomybė nuo įtampos bei **(d)** EQE priklausomybė nuo skaisčio (įklijoje prietaiso **15** nuotrauka)

4.2.4. Tetra-/trifeniletenlpakeistų 9,9-dimetilakridino darinių fotofizikinės ir elektroliuminescencinės savybės

Tiriamų junginių molekulinės struktūros pateiktos **4.4 schemoje**.

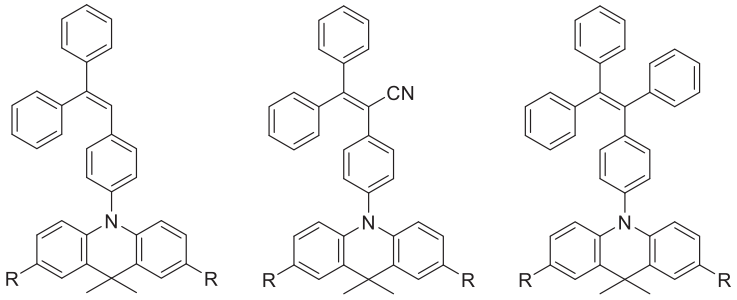

	R
20, 21, 22	H
23, 24, 25	$C(CH_3)_3$

4.4 schema. Junginių **20–25** molekulinės struktūros

Užrašyti junginių **20–-25** praskiestų tirpalų toluene ir THF absorbcijos spektrai (**4.10 pav.**). Junginių **20–25** tirpalų absorbcijos juostos nebuvo ypač jautrios naudojamiems tirpikliams ir matomos maždaug ties 290 nm. Junginių **20–25**

vakuumu nusodintų sluoksnių UV absorbcijos spektrai gerai koreliavo su atitinkamais tirpalų spektrais (**4.10 pav., b**). Junginių **20**, **22**, **23** ir **25** sluoksniai emituoja mėlyname regione su PL pikais intervale 458–482 nm (**4.10 pav., b**). Junginių **20–25** PL gesimas pastebėtas nanosekundžių diapazone, tai įrodo emisijos paprastąjį fluorescencinį pobūdį (**4.10 pav., d**). Junginių **20–25** tirpalų, palyginti su sluoksniais, pastebėti greitesni fluorescencijos gesimai, dažniausiai aprašomi monoeksponentine funkcija.

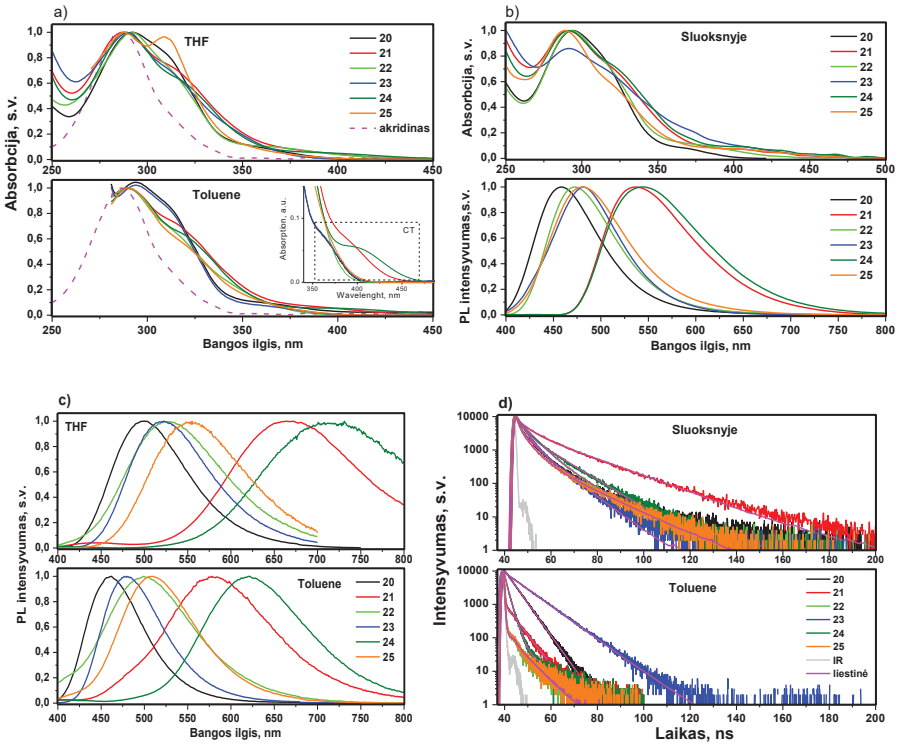

4.10 pav. (a) Junginių **20–25** tirpalų (10^{-5} M) THF ir toluene UV-vis absorbcijos spektrai. Įklijoje pavaizduota padidintos junginių tirpalų toluene mažos energijos absorbcijos juostos, **(b)** junginių **20–25** sluoksnių UV-vis absorbcijos ir PL spektrai, **(c)** junginių **20–25** tirpalų toluene ir THF PL spektrai, **(d)** junginių **20–25** sluoksnių ir tirpalų PL gesimo kreivės, kai sužadinimo bangos ilgis 374 nm

Junginių elektroliuminescencinės savybės (**4.11 pav.**) tirtos suformavus prietaisus, kurių struktūra: ITO/MoO_3 (0,5 nm)/NPB (35 nm)/mCP (7 nm) / emisinis sluoksnis (20 nm)/TSPO1 (7 nm)/TPBi (30 nm)/LiF (0,5 nm)/Al. Junginiai **20–25** panaudoti kaip nelegiruoti emisiniai sluoksniai atitinkamuose prietaisuose **20N–25N**. MoO_3, NPB, mCP, TSPO1, TPBi, ir LiF sluoksniai atitinkamai panaudoti kaip skylių injekcinis, skylių pernašos, eksitonus blokuojantis, skyles / elektronus blokuojantis, elektronų pernašos ir elektronų injekcinis sluoksniai (**4.11 pav.**).

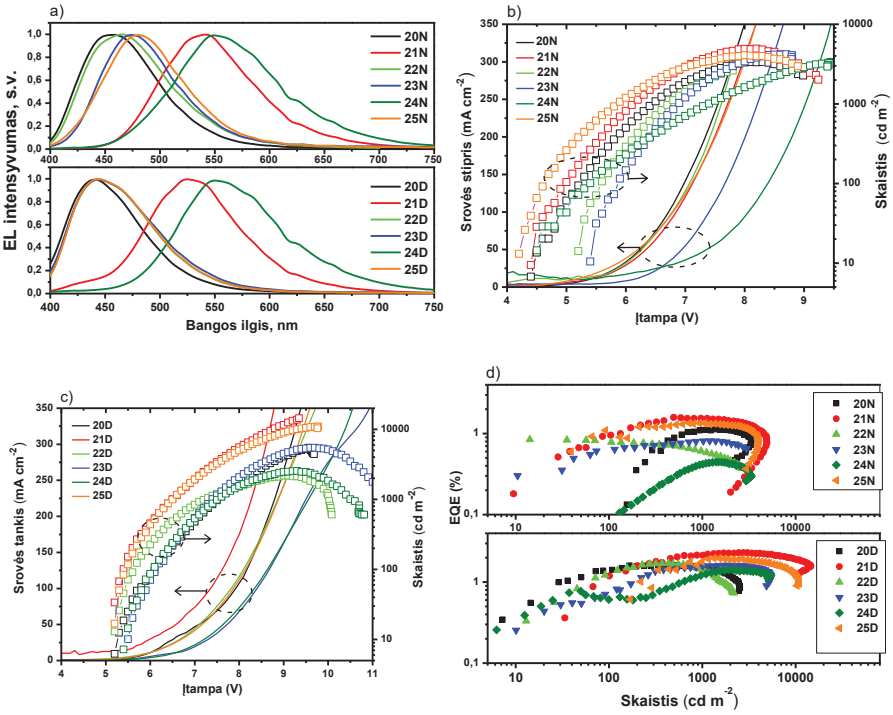

4.11 pav. Nelegiruotų (**20N-25N**) ir legiruotų (**20D-25D**) OLED-ų **(a)** EL spektrai, **(b, c)** srovės stiprio ir skaisčio priklausomybės nuo įtampos, **(d)** EQE ir skaisčio tarpusavio priklausomybė

4.2.5. Daugiafunkcinių D-A-D' tipo junginių, pasižyminčių mechanochromine liuminescencija, termiškai aktyvuotąja uždelstąja fluorescencija ir agregacijos sustiprinta emisija, elektroliuminescencinės savybės

Tiriamųjų junginių molekulinės struktūros pateiktos **4.5 schemoje**.

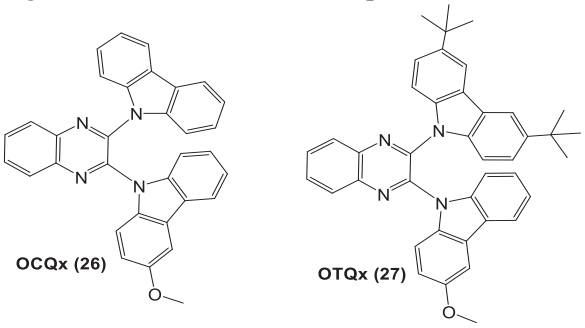

4.5 schema. Junginių **26** ir **27** molekulinės struktūros

Siekiant ištirti junginių **26** ir **27** elektroliuminescencines savybes, suformuoti legiruoti ir nelegiruoti OLED-ai, kurių struktūra: ITO/MoO_3(0,5 nm)/NPB (35 nm) /

junginys **26** ar **27** (10 %):TCTA (20 nm)/TSPO1 (7 nm)/TPBi (30 nm)/LiF (0,5 nm)/Al. Prietaisuose **26** ir **27** emisinį sluoksnį sudarė atitinkamai junginiai **26** ar **27,** disperguoti tri(4-karbazoil-9-ilfenil)amino (TCTA) matricoje.

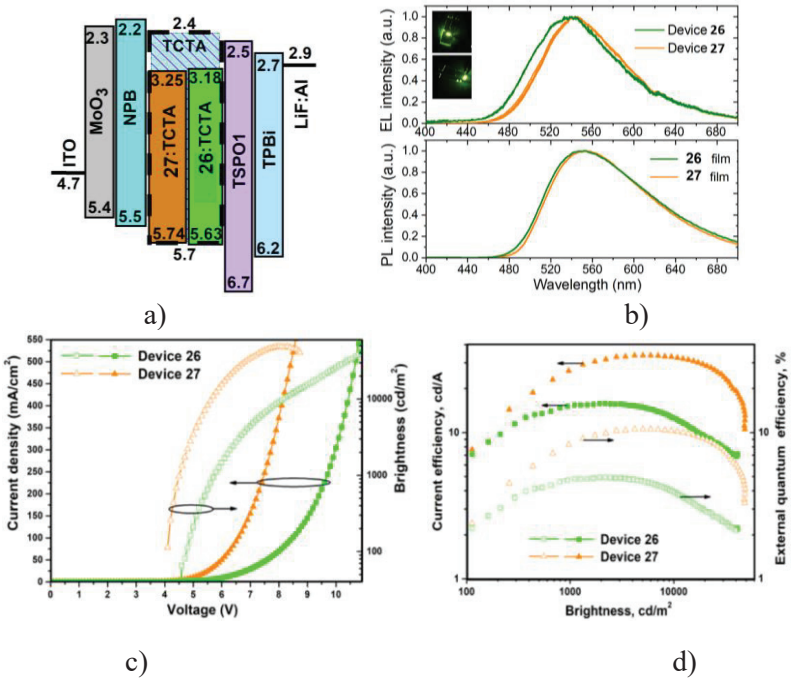

4.12 pav. Prietaisų **26** ir **27 (a)** energetinių lygmenų diagrama, **(b)** EL spektrai esant skirtingoms įtampoms intervale nuo 6 iki 11 V, žingsnis 1V, **(c)** srovės stiprio ir skaisčio priklausomybė nuo įtampos bei **(d)** srovės ir EQE priklausomybė nuo skaisčio

Legiruotų prietaisų (spinduolio koncentracija 10 %), turinčių junginius **26** ir **27**, *EQE* vertės atitinkamai buvo 4,95 ir 10,53 %, šios vertės gerai koreliuoja su emisinių sluoksnių *PLQY* vertėmis (24 ir 51 %) (**4.12 pav., d**, **4.6 lentelė**). EQE^{max} vertės smarkiai sumažėja didinant spinduolio (**26** ar **27**) koncentraciją emisiniame sluoksnyje (**4.13 pav., e, f**, **4.6 lentelė**). Šis pastebėjimas siejamas su *PLQY* mažėjimu dėl agregatų sukelto gesinimo ir dėl krūvininkų disbalanso esant didelei spinduolių **26** ar **27** koncentracijai. Dėl to nelegiruotų prietaisų, turinčių junginius **26** ir **27**, EQE^{max} vertės atitinkamai yra 0,48 ir 0,71 % (**4.6 lentelė**). Įdomu tai, kad nelegiruotų prietaisų EL spektrų poslinkiai (pakeičia EL spalvą) ir padidėję EQE^{max}, gauti emisinius sluoksnius apdorojus tolueno garais (**4.13 pav., 4.6 lentelė**). Tai reiškia, kad OLED-ų efektyvumą ir jų emisijos spalvą galima pagerinti jų struktūroje naudojant mechanochrominius luminoforus.

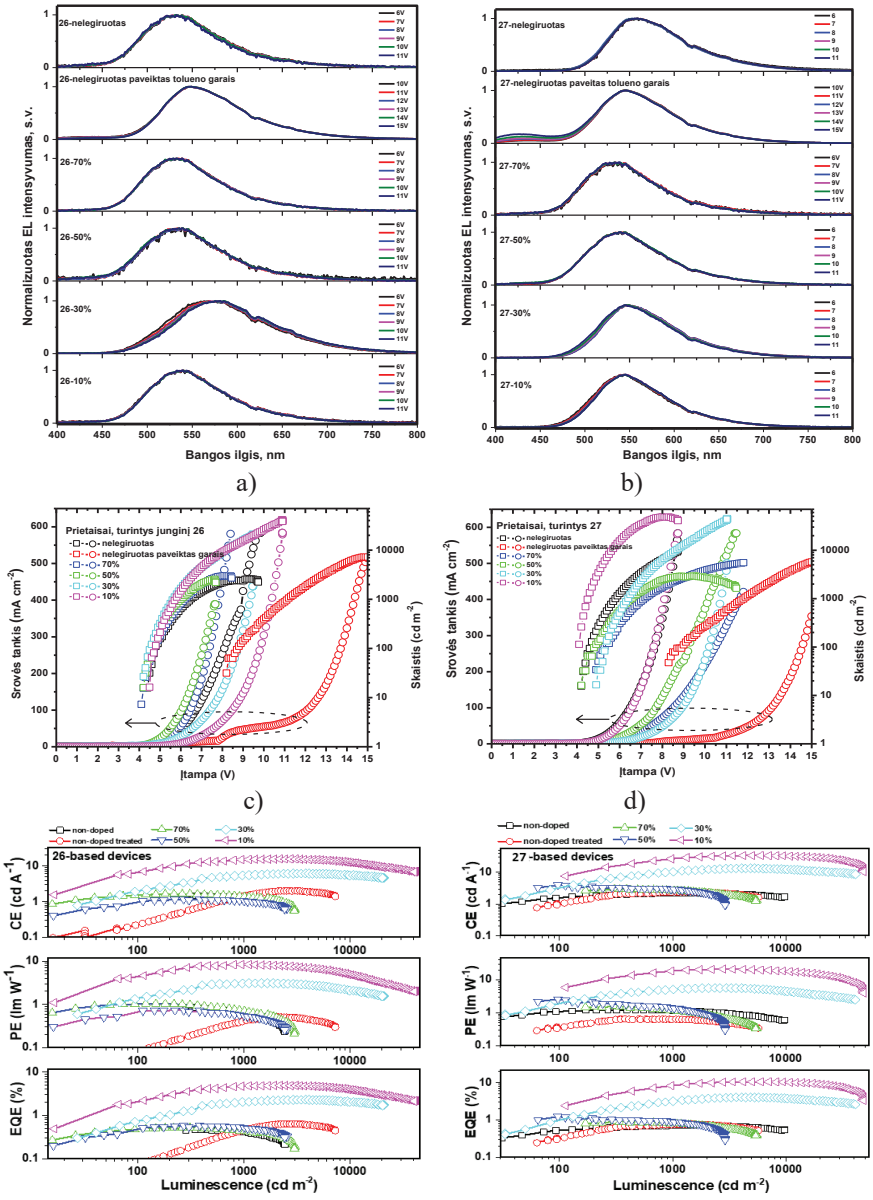

4.13 pav. Nelegiruotų ir legiruotų prietaisų, turinčių junginius **26** ir **27 (a, b)** EL spektrai, **(c, d)** srovės tankio ir skaisčio priklausomybės nuo įtampos bei **(e, f)** srovės ir *EQE* priklausomybė nuo skaisčio

4.6 lentelė. Nelegiruotų ir legiruotų prietaisų, suformuotų panaudojant junginius **26** ir **27,** charakteristikos

Prietaisas		Įjungimo įtampa, (V)	Maks. skaistis, (cd/m^2)	Maks. srovės efektyvumas, (cd/A)	Maks. galios efektyvumas, (lm/W)	Maks. išorinis kvantinis efektyvumas (%)	CIE koordinatės (*X; Y*)
26	**nelegiruotas**	4,43	2577	1,48	0,85	0,48	(0,313; 0,535)
	nelegiruotas paveiktas tol. garais	8,18	7241	2,03	0,52	0,64	(0,397; 0,545)
	70 %	4,12	3008	1,66	1,04	0,52	(0,315; 0,554)
	50 %	4,20	2543	1,18	0,74	0,59	(0,312; 0,520)
	30 %	4,19	20918	6,23	3,09	2,31	(0,456; 0,506)
	10 %	4,49	41488	15,83	8,36	4,95	(0,338; 0,556)
27	**nelegiruotas**	4,21	9661	2,19	1,23	0,71	(0,434; 0,540)
	nelegiruotas paveiktas tol. garais	8,29	5725	2,42	0,66	0,77	(0,361; 0,512)
	70 %	4,89	5412	3,04	1,59	0,91	(0,319; 0,549)
	50 %	4,17	2937	3,96	2,59	1,23	(0,339; 0,542)
	30 %	4,90	44888	13,38	5,68	4,05	(0,392; 0,562)
	10 %	4,08	48809	33,64	21,08	10,53	(0,374; 0,572)

4.3. IŠVADOS

1. Ištirtos karbazolo darinių, turinčių vieną arba du tri-/tetrafeniletenilpakaitus, kaip fluorescencinių OLED-ų spinduolių, fotofizikinės ir elektroliuminescencijos savybės. Nustatyta, kad:

1.1. Junginiams, turintiems du tri-/tetafeniletenil fragmentus, būdingi apie 5,15 eV jonizacijos potencialai ir skylių judriai, siekiantys 10^{-3} cm^2/V.

1.2. Junginiai išbandyti OLED-uose, kai skyles injektuojančios ir pernešančios medžiagos OLED-ui, turinčiam karbazolo darinį su dviem tetrafeniletenilpakaitais, sujungtais per azoto atomą karbazolo fragmento C-3 padėtyje, būdingas maksimalus 50000 cd/m^2 skaistis, taip pat didelis srovės, galios ir išorinis kvantinis efektyvumas, atitinkamai 17 cd/A, 9,2 lm/W, ir 5,32 %.

2. Ištirtos naujų ksantenono darinių, turinčių di-*tret*-butilkarbazolo, di-*tret*-butilakridano, di-*tret*-butilfentiazino ir fenoksazino fragmentus, fotofizikinės ir elektroliuminescencinės savybės. Nustatyta, kad:

2.1. Junginių jonizacijos potencialų vertės išsidėsto intervale 5,67–5,96 eV, o skylių ir elektronų judriai išsidėsto plačiame intervale nuo $6{,}3\times10^{-8}$ iki $6{,}3\times10^{-4}$ cm^{2}V^{-1}s^{-1}, esant $2{,}5\times10^{5}$ V·cm^{-1} elektrinio lauko stipriui.

2.2. Junginiai panaudoti kaip spinduoliai OLED-uose. Didžiausios maksimalaus išorinio kvantinio efektyvumo vertės (iki 3,5 %) nustatytos OLED-ų, kurių spinduoliai turėjo di-*tret*-butilkarbazolil- ir di-*tret*-butilakridanilgrupes.

3. Ištirtos dešimties tetrahidrodibenzfenantridino ir fenantrimidazolo darinių elektrooptinės, krūvininkų pernašos ir elektroliuminescencinės savybės. Nustatyta, kad:
3.1. Mėlynųjų luminoforų tirpalų toluene fotoliuminescencijos kvantiniai našumai siekia 66–93 %, o sluoksnių – 5–59 %.
3.2. Junginiams būdingos artimos jonizacijos potencialų (5,74-6,11 eV) ir gimiringumo elektronui (2,71–3,06 eV) vertės.
3.3. Mėlyna elektroliuminescencija pasižyminčio OLED-o skaistis viršijo 10000 cd/m^2. Jam būdingas santykinai mažas efektyvumo mažėjimas. Junginys, turintis metoksigrupes, pasižymi geriausiomis fotoliuminescencijos ir elektroliuminescencijos charakteristikomis.
4. Ištirtos šešių tetra-/trifeniletenilpakeistų 9,9-dimetilakridinų fotofizikinės ir elektroliuminescencinės savybės.
Nustatyta, kad:
4.1. Junginių nelegiruotų sluoksnių fluorescencijos kvantiniai našumai išsidėsto intervale 26–53 %, o legiruotų – 52–88 %, dėl agregacijos sustiprintos emisijos.
4.2. Junginių jonizacijos potencialo vertės yra santykinai plačiame diapazone 5,43–5,81 eV.
4.3. Suformuotų prietaisų išorinis kvantinis efektyvumas siekė 2,3 %.
5. Ištirtos naujų asimetrinių daugiafunkcinių junginių, turinčių akceptorinį chinoksalino ir donorinius skirtingai pakeistus karbazolo fragmentus, elektroliuminescencinės savybės.
5.1. Suformuoti ir charakterizuoti legiruoti ir nelegiruoti OLED-ai.
5.2. Nustatytos maksimalios skaisčio, srovės ir galios efektyvumų vertės atitinkamai siekia 48809 cd/m^2, 33,64 cd/A ir 21,08 lm/W.
5.2. Parinkus tinkamas matricinio junginio koncentracijas, pasiektas 10,53 % OLED-o išorinis kvantinis efektyvumas.

5. REFERENCES

1. Geffroy, B., et al. Organic light-emitting diode (OLED) technology: materials, devices and display technologies. *Polymer. Int*. **2006**, *55*, 572-582. <https:// 10.1002/pi.1974>.
2. Tang, CW., et al. Organic electroluminescent diodes. *Appl. Phys. Lett*. **1987**, *51*, 913-915. <https://doi.org/10.1063/1.98799>.
3. Kulkarni, A.P., et al. Electron Transport Materials for Organic Light-Emitting Diodes. *Chem. Mater.* **2004**, *16*, 4556-4573. <https://doi.org/10.1021/cm049473l>.
4. Shirota, Y., et al. Charge Carrier Transporting Molecular Materials and Their Applications in Devices. *Chem. Rev.* **2007**. *107,* 953-1010. <https://doi.org/10.1021/cr050143+>.
5. Lundin, N.J., et al. Synthesis and characterization of a multicomponent rhenium (I) complex for application as an OLED dopant. *Angewandte. Chem. Int. Edition.* **2006**, *45*, 2582-2584. <https://doi.org/10.1002/anie.200504532>.
6. Tian, F., et al. Efficient electroluminescence from twistacene-modified π-conjugated compounds. *Dyes Pigm*. **2020**, *177*, 108298. < https://doi.org/10.1016/j.dyepig.2020.108298>.
7. Takimiya, K., et al. π-Building blocks for organic electronics: revaluation of "inductive" and "resonance" effects of π-electron deficient units. *Chem.Mater*. **2013**, *26*, 587-593. <https://dx.doi.org/10.1021/cm4021063>.
8. Ko, C.W., et al. Bright white organic light-emitting diode. *Appl. Phys. Lett*. **2011**, *79*, 4234-4236. <https://doi.org/10.1063/1.1425454>.
9. LEE, T.W. et al. Characteristics of Solution-Processed Small-Molecule Organic Films and Light-Emitting Diodes Compared with their Vacuum-Deposited Counterparts. *Adv. Funct. Mater.* **2009**. *19*, 1625-1630. <http://doi.wiley.com/10.1002/adfm.200801045>.
10. Earmme, T., et al. High-performance multilayered phosphorescent OLEDs by solution-processed commercial electron-transport materials. *Mater. Chem*. **2012**, *22*, 4660. <http://xlink.rsc.org/?DOI=c2jm14347j>.
11. Su, S.J., et al. Highly efficient organic blue- and white-light-emitting devices having a carrier and exciton confining structure for reduced efficiency roll-off. *Adv. Mater*. **2008**, *20*, 4189-4194. <https://doi.org/10.1002/adma.200801375>.
12. Sasabe, H., et al. High-efficiency blue and white organic light-emitting devices incorporating a blue iridium carbene complex. *Adv. Mater*. **2010**, *22*, 5003-5007. <https://doi.org/10.1002/adma.201002254>.
13. Walzer, K., et al. Highly efficient organic devices based on electrically doped transport layers. *Chem. Rev.* **2007**, *107*, 1233-1271. <https://doi.org/10.1021/cr050156n>.
14. Meerheim, R., et al. Efficiency and stability of p-i-n type organic light emitting diodes for display and lighting applications. *Proc. IEEE*. **2009**, *97*, 1606-1626.

<https://doi.org/10.1109/JPROC.2009.2022418>.
15. JOU, J.-H., et al. Approaches for fabricating high efficiency organic light emitting diodes. *Mater. Chem. C*. **2015**, *3*, 2974-3002.
<https://doi.org/10.1039/C4TC02495H>.
16. Kondakov, D.Y. Role of triplet-triplet annihilation in highly efficient fluorescent devices. *Soci. Info. Disp*. **2009**, *17*, 137-144.
<https://doi.org/10.1889/JSID17.2.137>.
17. Adachi, C., Third-generation organic electroluminescence materials. *Jpn. J. Appl. Phys.* **2014***, 53,* 060101- 060111.
<http://dx.doi.org/10.7567/JJAP.53.060101>.
18. Wagenknecht, P.S., et al. Metal centered ligand field excited states: their roles in the design and performance of transition metal based photochemical molecular devices. *Coord. Chem. Rev.* **2011***, 255*, 591-616.
< https://doi.org/10.1016/j.ccr.2010.11.016>.
19 . Wang, B.Z., et al. Unlocking the full potential of organic light-emitting diodes on flexible plastic. *Nat. Photo*. **2011**, *5*, 753-757.
<https://doi.org/10.1038/nphoton.2011.259>
20. Baldo, M.A., et al. Highly efficient phosphorescent emission from organic electroluminescent devices. *Nat.* **1998***, 395*, 151-154.
21. Adachi, C., et al. High performance TADF for OLEDs. *Presentation at the **2015** SSL R&D WORKSHOP in San Francisco, CA*.
<http://energy.gov/sites/prod/files/2015/02/f19/adachi_oled-tadf_sanfrancisco2015.pdf>.
22. Cariati, E., et al. Cu(I) hybrid inorganic-organic materials with intriguing stimuli responsive and optoelectronic properties. *Coord. Chem. Rev.* **2016***, 306*, 566-614.
< https://doi.org/10.1016/j.ccr.2015.03.004>.
23. Leitl, M.J., et al. Copper(I) complexes for thermally activated delayed fluorescence: from photophysical to device properties. *Top. Curr. Chem.* **2016***, 374*, 25.
<https://doi.org/10.1007/s41061-016-0019-1>.
24. Parker, C.A., et al. Triplet-singlet emission in fluid solutions. phosphorescence of eosin. *Trans. Fara. Soc.* **1961***, 57*, 1894-1904.
< https://doi.org/10.1039/TF9615701894>.
25. Uoyama, H., et al. Highly efficient organic light-emitting diodes from delayed fluorescence. *Natu*. **2012**, *492*, 234-238.
< https://doi.org/10.1038/nature11687>.
26. Tang, C.W., et al. Electroluminescent Device with Modified Thin Film Luminescent Zone, US Patent 4, 769, 292 (**1988**).
27. Buckley, A. Organic light emitting diodes (OLEDs), materials, devices and applications. Woodhead Publishing Series in Electronic and Optical Materials number 36 (**2013**).

28. Zheng, C., et al. Highly efficient green and red OLEDs based on a new exciplex system with simple structures. *Org.Elec*. **2017**, *43*, 136-141. <https://doi.org/10.1016/j.orgel.2017.01.020>.
29. Yuan, S., etal. High-performance red organic light-emitting devices based on an exciplex system with thermally activated delayed fluorescence characteristic. *Org. Elec*. **2016**, *39*, 10-15. <https://doi.org/10.1016/j.orgel.2016.09.020>.
30. Y. Nagai, H. Sasabe, J. Takahashi, N. Onuma, T. Ito, S. Ohisaab, J. Kido, Highly efficient, deep-red organic light-emitting devices using energy transfer from exciplexes. *Mater. Chem. C*. **2014**, *5*, 527-530. <https://doi.org/10.1039/C6TC04979F>.
31. Kim, B., Engineering of Mixed Host for High External Quantum Efficiency above 25% in Green Thermally Activated Delayed Fluorescence Device. *Adv. Funct. Mater*. **2014**, *24*, 3970-3977. <https://doi.org/10.1002/adfm.201303730>.
32. Levy, D., et al. Room temperature phosphorescence and delayed fluorescence of organic molecules trapped in silica sol–gel glasses. *Photoc. Photobio. A*. **1991**, *57*, 41-63. < https://doi.org/10.1016/1010-6030(91)85006-3>.
33. Fukagawa, H., et al. Highly efficient and stable organic light-emitting diodes with a greatly reduced amount of phosphorescent emitter. *Sci. Rep.* **2015**, *5*, 9855/1-7. <https://doi.org/10.1038/srep09855>.
34. Yang, Z., et al. Recent advances in organic thermally activated delayed fluorescence materials. *Chem. Soc. Rev.* **2017**, *46*, 915. < https://doi.org/10.1039/c6cs00368k>.
35. Deaton, J.C., et al. E-type delayed fluorescence of a phosphine-supported Cu_2(mu-NAr_2)$_2$ diamond core: harvesting singlet and triplet excitons in OLEDs. *Am. Chem Soc*. **2010**, *132*, 9499-508. <https://doi.org/10.1021/ja1004575>.
36. Li, G., et al. Highly efficient and stable narrow-band phosphorescent emitters for oled applications. *Adv. Opt.Mater.* **2015**, *3*, 390-397. <https://10.1002/adom.201400341>.
37. Sun, J.W., et al. Thermally Activated Delayed Fluorescence from Azasiline Based Intramolecular Charge-Transfer Emitter (DTPDDA) and a Highly Efficient Blue Light Emitting Diode. *Chem. Mater*. **2015**, *27*, 6675-6681. <https://doi.org/10.1021/acs.chemmater.5b02515>.
38. Lin, T.A., et al. Sky-Blue Organic Light Emitting Diode with 37% External Quantum Efficiency Using Thermally Activated Delayed Fluorescence from Spiroacridine-Triazine Hybrid. *Adv. Mater*. **2016**, *28*, 6976-6983. <https://doi.org/10.1002/adma.201601675>.
39. Lee, J., et al. Effect of various host characteristics on blue thermally activated delayed fluorescent devices. *Org. Elec*. **2018**, *59*, 39-44. <https://doi.org/10.1016/j.orgel.2018.04.034>.
40. Marks, T.J., et al. Toward the Ideal Organic Light-Emitting Diode. The Versatility and Utility of Interfacial Tailoring by Cross-Linked Siloxane Interlayers. *Americ. Chem. Soci*. **2005**, *38*, 632-643. <https://doi.org/10.1021/ar030210r>.

41. Ning, Z., et al. Aggregation-induced Emission (AIE)-active Starburst Triarylamine Fluorophores as Potential Non-doped Red Emitters for Organic Light-emitting Diodes and Cl_2 Gas Chemodosimeter. *Adv. Funct. Mater*. **2007**, *17*, 3799-3807. <https://doi.org/10.1002/adfm.200700649>.
42. Sunil, D., et al. Aggregation-induced emission of azines: An up-to-date review. *Molec. Liq*. **2019**, *292*, 111371. <https://doi.org/10.1016/j.molliq.2019.111371>.
43. Samanta, S., et al. An aggregation-induced emission (AIE) active probe for multiple targets: a fluorescent sensor for Zn2+ and Al3+ & a colorimetric sensor for Cu^{2+} and F^{-}. *Dalt. Tran*. **2015**, *44*, 18902-18910. <https://doi.org/10.1039/C5DT03186A>.
44. Park, S., et al. Enhanced Emission and Its Switching in Fluorescent Organic Nanoparticles. *Am. Chem. Soc.* **2002**, *124*, 48, 14410-14415. <https://doi.org/10.1021/ja0269082>.
45. Lager, E., et al. Twisted Intramolecular Charge Transfer and Aggregation-Induced Emission of BODIPY Derivatives. *Phys. Chem. C*. **2009**, *36*, 15845-15853. <https://doi.org/10.1021/jp902962h>.
46. Yan, X., et al. More than Restriction of Twisted Intramolecular Charge Transfer: Three-Dimensional Expanded Shaped Cross-Molecular Packing for Emission Enhancement in Aggregates. *Phys. Chem. C*. **2012**, *116*, 12187-12195. <https://doi.org/10.1021/jp212257f>.
47. Xu, S., et al. An Organic Molecule with Asymmetric Structure Exhibiting Aggregation-Induced Emission, Delayed Fluorescence, and Mechanoluminescence. *Angew. Chem. Int.* **2015**, *54*, 874-878. <https://doi.org/10.1002/anie.201409767>.
48. Kukhta, N.A., et al. Can Fluorenone-Based Compounds Emit in the Blue Region? Impact of the Conjugation Length and the Ground-State Aggregation. *Chem. Mater.* **2017**, *29*, 1695-1707. <https://doi.org/10.1021/acs.chemmater.6b05158>.
49. Nasiri, S., et al. Carbazole derivatives containing one or two tetra-/triphenylethenyl units as efficient hole-transporting OLED emitters. *Dyes Pigm*. **2019**, *168*, 93-102. <https://doi.org/10.1016/j.dyepig.2019.04.045>
50. Zhao, Z., et al. Molecular anchors in the solid state: restriction of intramolecular rotation boosts emission efficiency of luminogen aggregates to unity. *Chem. Sci*. **2011**, *2*, 672-675. <https://doi.org/10.1039/C0SC00521E>.
51. Zhao, Z., et al. Using tetraphenylethene and carbazole to create efficient luminophores with aggregation-induced emission, high thermal stability, and good hole-transporting property. *Mater. Chem*.**2012**, *22*, 4527-34. <https://doi.org/10.1039/C2JM14914A>.
52. Jou, J-H., et al. Approaches for fabricating high efficiency organic light emitting diodes. *Mater. Chem. C*. **2015**, *3*, 2974-3002. <https:// doi.org/10.1039/c4tc02495h>.
53. Borsenberger, PM., et al. Hole Transport in a vapor deposited phenylenediamine molecular glass. *Phys. Status. Solid. B*. **1995**, *191*, 461-469. <https://doi.org/10.1002/pssb.2221910219>.

54. Nasiri, S., et al. Facile structure-modification of xanthenone based OLED emitters exhibiting both aggregation induced emission enhancement and thermally activated delayed fluorescence. *Lumin.* **2020***, 220*, 116955. <https://doi.org/10.1016/j.jlumin.2019.116955>.
55. Sasaki, S., et al., Recent advances in twisted intramolecular charge transfer (TICT) fluorescence and related phenomena in materials chemistry. *Mater. Chem*. **2016**, 2731-2743. <https://doi.org/10.1039/C5TC03933A>.
56. Lee, J., et al. Thermally activated delayed fluorescence properties of regioisomeric xanthone-based twisted intramolecular charge-transfer luminophores. *Bull. Chem. Soc. Jpn.* **2017**, *90*, 231-236. <https://doi.org/10.1246/bcsj.20160380>.
57. Chen, Y., et al. Aggregation-induced emission: fundamental understanding and future developments, Mater. *Horizons*. **2019**, *6*, 428-433. <https://doi.org/10.1039/c8mh01331d>.
58. Stanford, A.L., et al. Early Quantum Physics. *Phys. Stud. Sci. Eng*. **1985**, 691-716. < https://doi.org/10.1016/B978-0-12-663380-1.50026-4>.
59. Han, C., et al. Dipole-dipole interaction management for efficient blue thermally activated delayed fluorescence diodes. *Chem*. **2018**, *4*, 2154-2167. <https://doi.org/10.1016/j.chempr.2018.06.005>
60. Nasiri, S., et al. Rational synthesis of tetrahydrodibenzophenanthridine and phenathroimidazo-le as efficient blue emitters and its applications. *Eur. J. Org. Chem.* **2020** (7).<http://dx.doi.org/10.1002/ejoc.201901711>
61. Qin, W., et al. Construction of Efficient Deep Blue Aggregation-Induced Emission Luminogen from Triphenylethene for Nondoped Organic Light-Emitting Diodes. *Chem. Mat*. **2015**, *27*, 3892-3901. <https://doi.org/10.1021/acs.chemmater.5b00568>.
62. Venkatesan, M., et al. Highly selective chemosensor for the detection of Ru^{3+} ion by fluorescent turn-on response and its bioimaging recognition in living cells. *Sens. Actu. B: Chem.* **2018**, *267*, 373-380. < https://doi.org/10.1016/j.snb.2018.03.077>
63. Patra, D., et al. Synchronous fluorescence spectroscopic study of solvatochromic curcumin dye. *Spectro. Acta. P. A: Molec & Bio. Spec*. **2011**, *79*, 1034-1041. < https://doi.org/10.1016/j.saa.2011.04.016>.
64. Lee, J., et al. Hot excited state management for long-lived blue phosphorescent organic light-emitting diodes. *Natu Commu*. **2017**, 8, article number: 15566. < https://doi.org/10.1038/ncomms15566>.
65. Amorim, C.A., et al. Determination of carrier mobility in MEH-PPV thin-films by stationary and transient current techniques. *Non-Cryst. Solid*. **2012**, *358*, 484-491. <https://doi.org/10.1016/j.jnoncrysol.2011.11.001>.
66. Nasiri, S., et al. Towards blue AIE/AIEE: Synthesis and Applications in OLEDs of Tetra-/Triphenylethenyl Substituted 9,9-Dimethylacridine Derivatives. *Molec*. **2020**, *25*, 445. https://doi.org/10.3390/molecules25030445.

67. Tomkeviciene, A., et al. Thianthrene and acridan-substituted benzophenone or diphenylsulf one: Effect of triplet harvesting via TADF and phosphorescence on efficiency of all-organic OLEDs. *Org. Electron.* **2019**, *70*, 227-239. < https://doi.org/10.1016/j.orgel.2019.04.025>.
68. Huo, J., et al. Design and development of highly efficient lightemitting layersin OLEDs with dimesitylboranes: an updated review. *Chem. Rec.* **2019**,*19*, 1-15. <https://doi.org/10.1002/tcr.201900068>.
69. Han, T., et al. Aggregation-induced emission: phenomenon, mechanism and applications. *Chem. Commun.* **2009**, *2009*, 4332-4353. <https://doi.org/10.1039/B904665H>.
70. Zhang, X., et al. End-group effects of piezofluorochromic aggregation-induced enhanced emission compounds containing distyrylanthracene. *Mater. Chem.* **2012**, *22*, 18505-18513. <https://doi.org/10.1039/C2JM33140C>.
71. Liu, Y., et al. Tuning the electronic nature of aggregation-induced emission luminogens with enhanced hole-transporting property. *Chem. Mater*. **2011**, *23*, 2536-2544. <https://doi.org/10.1021/cm2003269>.
72. Nakanotani, H., et al. High-efficiency organic light-emitting diodes with fluorescent emitters. *Nat Commun*. **2014**, *30*, 5, 4016. <https://10.1038/ncomms5016>.
73. Yersin, H., et al. Highly Efficient OLEDs with Phosphorescent Materials. Wiley-VCH, **2008**.
74. Pashazadeh, R., et al. Multifunctional Characteristics from an Asymmetric D-A-D' Structure: Mechanochromic Luminescence, Thermally Activated Delayed Fluorescence and Aggregation Enhanced Emission. *Chem. Eng*. **2020**, *401*, 125962. <https://doi.org/10.1016/j.cej.2020.125962>.
75. Sych, G., et al. Structure-properties relationship of tetrafluorostyrene-based monomers and polymers containing different donor moieties. *React. Func. Poly*. **2019**, *143*, 104323. < https://doi.org/10.1016/j.reactfunctpolym.2019.104323>.

6. CURRICULUM VITAE

Name, Surname: Sohrab Nasiri
E-mail: sohrab.nasiri@ktu.edu

Education

2004-2008
Bachelor's Degree in Materials Engineering, Islamic Azad University , Najafabad Branch, Faculty of Materials Engineering

2009-2011
Master's Degree in Materials Engineering, Islamic Azad University, Najafabad Branch, Faculty of Materials Engineering

2017-2021
PhD studies in Materials Engineering, Kaunas University of Technology, Faculty of Chemical Technology

Work experience

May 01, 2020 – December 18, 2020
Project: "Bipolar semiconductors exhibiting aggregation induced emission enhancement for multi colored thermally activated delayed fluorescent OLEDs (BLIX4LED)", Kaunas University of Technology, Faculty of Chemical Technology

7. LIST OF PUBLICATIONS

1. **Nasiri, S.**, Cekaviciute, Monika., Simokaitiene, Jurate., Petrauskaite, Aina., Volyniuk, D., Andruleviciene, V., Bezvikonnyi O., Grazulevicius J.V. Carbazole derivatives containing one or two tetra-/triphenylethenyl units as efficient hole-transporting OLED emitters// Journal of Dyes and pigments. ISSN 0143-7208. 2019, vol. 168, p. 93-102. https://www.sciencedirect.com/science/article/pii/S0143720819301755

2. **Nasiri, S.**, Macionis, S., Gudeika, D., Volyniuk, D., Grazulevicius, J.V. Facile structure-modification of xanthenone based OLED emitters exhibiting both aggregation induced emission enhancement and thermally activated delayed fluorescence// Journal of Luminescence. ISSN 0022-2313. 2020, vol. 220. p. 116955. https://www.sciencedirect.com/science/article/pii/S0022231319316771

3. Thiyagarajan, M.D., Balijapalli, Umamahesh., **Nasiri, S.**, Volyniuk, D., Simokaitienec, J., Pathak, M., Iye, S.K., Gražulevičius, J.V. Rational synthesis of tetrahydrodibenzophenan-thridine and phenanthroimidazole as efficient blue emitters and its applications// Europian Journal Organic Chemistry (Eur.J.Org. Chem). ISSN 1434193X. 2020, p. 834-844. https://chemistryeurop.onlinelibrary.wiley.com/doi/full/10.1002/ejo.20191711

4. Cekaviciute, M., Petrauskaite, A., **Nasiri, S.**, Simokaitiene, J., Volyniuk, D., Sych, G., Budreckiene, R., Grazulevicius, J.V. Towards blue AIE/AIEE: Synthesis and Applications in OLEDs of Tetra-/Triphenylethenyl Substituted 9,9-Dimethylacridine Derivatives// Journal Molecules. ISSN 00249297,15205835. 2020, vol.25. p. 445. https://www.mdpi.com/1420-3049/25/3/445

5. Pashazadeh, R., Sych, G., **Nasiri, S.**, Leitonas, K., Lazauskas, Algirdas., Volyniuk, D., Skabara, P.J., Grazulevicius, J.V. Multifunctional Characteristics from an Asymmetric D-A-D' Structure: Mechanochromic Luminescence, Thermally Activated Delayed Fluorescence and Aggregation Enhanced Emission// Chemical Engineering Journal. ISSN 1385-8947. 2020, vol. 401. 125962. https://www.sciencedirect.com/science/article/pii/S1385894720320908

Attendance of international conferences:

1. **Nasiri, Sohrab**; Čekavičiūtė, Monika; Simokaitienė, Jūratė; Petrauskaitė, Aina; Volyniuk, Dmytro; Andrulevičienė, Viktorija; Bezvikonnyi, Oleksandr; Gražulevičius, Juozas Vidas. Tri and tetraphenylethenyl, substituted carbazole derivatives: synthesis, characterization and exhibiting AIEE as efficient hole-transporting OLED emitters// Baltic polymer symposium 2019, Vilnius, Lithuania, September 18-20, 2019: programme and proceedings. Vilnius: s.n. 2019. p. 56.
2. **Nasiri, Sohrab**; Mačionis, Simas; Gudeika, Dalius; Volyniuk, Dmytro; Gražulevičius, Juozas Vidas. Synthesis and investigation of xanthenone based OLED emitters exhibiting both AIEE and TADF// Open Readings 2020: 63rd international conference for students of physics and natural sciences, March 17-20, Vilnius, Lithuania. Vilnius: Vilnius University. 2020, P2-19, p. 1.
3. **Nasiri, Sohrab**; Mačionis, Simas; Gudeika, Dalius; Volyniuk, Dmytro; Gražulevičius, Juozas Vidas. Facile structure-modification of xanthenone and thioxanthenone based OLED emitters exhibiting both aggregation induced emission enhancement and thermally activated delayed fluorescence// 22nd International Conference Advanced Materials and Technologies, August 24-28, Palanga, Lithuania: 2020.

8. ACKNOWLEDGMENTS

Prof. Habil. dr. Juozas Vidas Gražulevičius (Department of Polymer Chemistry and Technology, Kaunas University of Technology) is sincerely thanked for the supervision of my doctoral research, consultations, valuable advice and great support.

dr. Dmytro Volyniuk (Department of Polymer Chemistry and Technology, Kaunas University of Technology) is kindly thanked for the advising of my study, measurements of charge-transporting, photoelectron emission properties, OLEDs characteristics, for sharing knowledge in photophysics and for valuable scientific discussion.

Dyes and Pigments 168 (2019) 93–102

Contents lists available at ScienceDirect

Dyes and Pigments

journal homepage: www.elsevier.com/locate/dyepig

Carbazole derivatives containing one or two tetra-/triphenylethenyl units as efficient hole-transporting OLED emitters

Sohrab Nasiri, Monika Cekaviciute, Jurate Simokaitiene, Aina Petrauskaite, Dmytro Volyniuk, Viktorija Andruleviciene, Oleksandr Bezvikonnyi, Juozas Vidas Grazulevicius*

Department of Polymer Chemistry and Technology, Kaunas University of Technology, Radvilenu rd. 19, LT-50254, Kaunas, Lithuania

ARTICLE INFO

Keywords:
Tetra-/triphenylethene
Carbazole
Aggregation induced emission enhancement
Hole mobility
Electroluminescence

ABSTRACT

New efficient carbazole-based emitters containing tetra-/triphenylethene units were developed for boosting efficiency of non-doped fluorescent organic light-emitting diodes. Comparable study of the properties of derivatives containing one or two tetra-/triphenylethenyl units was performed using various experimental and theoretical techniques. Depending on the substitution pattern, emitters exhibited strong blue or green emission, which was enhanced by aggregation. Compounds with two substituents showed higher glass transition temperatures (up to 120 °C) and lower ionization potentials (of ca. 5.15 eV) comparing to mono substituted derivatives. Time-of-flight hole drift mobility values of the studied compounds with two substituents reached 10^{-3} cm^2/V at high electric fields. Non-doped fluorescent OLEDs based on carbazole derivative containing two tetraphenylethenyl units demonstrated extremely high external quantum efficiency as for simple fluorescent organic light-emitting devices, which reached 5.32%.

1. Introduction

Development of organic luminescent materials exhibiting aggregation induced emission enhancement (AIEE) is hot research topic because of their wide possible applications ranging from biological imaging including specific cancer cell imaging, photothermal therapy, physical and chemical sensing to optoelectronics [1–4]. Intensity of emission of such organic luminescent materials dramatically increase in solid-state in comparison to that of solutions due to either the restriction of intramolecular motions or intermolecular through-space interaction upon clustering or aggregation [5]. Since high emission efficiency in solid-state is required for emitters of advance organic light emitting diodes (OLEDs), many AIEE compounds were utilized as electroluminescent materials [6]. Such emitters typically contain AIEE active tetra- or triphenylethene units, which may boost emission efficiency of solid films to unity [7]. Most of such emitters are characterized by prompt fluorescence. Because of the spin-statistic limit efficiencies of OLED based on such emitters are rather low compared to those of devices based on thermally activated delayed fluorescence or phosphorescent OLEDs. However, they are unquestioningly important active OLED materials allowing to achieve long-term stability and emission color purity [8–10]. In addition, simple molecular structure of tetra- or triphenylethenyl moieties allows facile preparation and easy chemical modification of OLED emitters with AIEE phenomenon [11]. For instance, photoluminescence quantum yields (PLQY) close to unity were observed for tetraphenylethenyl-substituted carbazole derivatives [7,12]. However, no impressive maximum external quantum efficiencies (EQEs) were observed for non-doped devices based on these such derivatives [7]. EQE reached only 2.3%. Study of another example of tetraphenylethenyl-substituted carbazole derivatives showed that hole-transporting properties of these derivatives are very sensitive to the position of tetraphenylethenyl moieties [13]. As a result, EQEs of non-doped OLEDs based on these derivatives ranged from 0.4 to 3.2% [14]. This observation was explained by poor charge-injection properties of the materials. In such case, additional hole-transporting layers are required. Simple fluorescent OLEDs based on triphenylethenyl-substituted carbazole derivatives showed relatively high EQEs up to 3.8% [15]. It is expected that further modification of tetra-/triphenylethenyl-substituted carbazole derivatives as AIEE active OLED materials may lead to improvement of their properties including charge-injection and charge-transporting characteristics [16,17].

With the aim of boosting efficiency of non-doped fluorescent OLEDs, new AIEE emitters were designed in this work. The design was based on exploitation two tetra-/triphenylethene substitutuents linked through the nitrogen atom in C-3 position of carbazole moiety and compared with previously published carbazole derivatives [12,18,19] when

* Corresponding author.
E-mail address: juozas.grazulevicius@ktu.lt (J.V. Grazulevicius).

https://doi.org/10.1016/j.dyepig.2019.04.045
Received 22 January 2019; Received in revised form 9 April 2019; Accepted 17 April 2019
Available online 21 April 2019

substituent is in N-9 carbazole position. The choice of such substitution strategy was supported by the fact that previously reported tetra-/triphenylethenyl-substituted derivatives were found as effective OLED materials with very high PLQYs and good hole transporting properties [12,15]. Attachment of two donating tetra-/triphenylethene units to carbazole moiety can lead to decrease of oxidation potential and increase of molar mass. This may lead to improved hole-injection properties, thermal stability and increased glass transition temperature. To demonstrate efficiency of the proposed design strategy, comparable study of new carbazole derivatives containing two tetra-/triphenylethenyl moieties and previously reported carbazole derivatives with single tetra-/triphenylethene unit was performed [7,12,18]. As it was expected, improved hole-injection abilities were observed for the compounds containing two tetra-/triphenylethenyl moieties in comparison to mono-substituted ones. All the studied compounds were characterized by relatively high hole mobilities reaching 10^{-2} cm^2/V in high electric fields. Simple non-doped fluorescent OLED based on newly developed carbazole derivative containing two tetrahenylethenyl moieties as light-emitting material exhibited impressive maximum EQE of 5.32%.

2. Results and discussion

2.1. Synthesis

The synthetic routes towards appropriate tetra- or triphenylethenyl-substituted carbazole derivatives are shown in Scheme 1. The compounds were synthesized by the Buchwald-Hartwig method [20,21] in the presence of palladium complex or by the Buchwald procedure [22] in the presence of CuI and 2,2,6,6-tetramethyl-3,5-heptanedione as ligand. The synthesized compounds were identified by mass-, IR- and ^1H, ^{13}C NMR spectrometries and elemental analysis. The details of synthesis and characterization data are given in Supporting Information.

2.2. Geometries and frontier orbitals

The geometrical structures of compounds **1–5** were analyzed employing quantum chemical calculations (Fig. 1). Density functional theory (DFT) for **1–5** showed that arylethenyl substituents are rotated with respect to carbazole moiety. In the case of compound **1**, the dihedral angle between carbazole moiety and ethenyl linkage was of 64°. Dihedral angles between carbazole units and phenyl ring planes in compounds **2** and **3** were found to be of 55°, while dihedral angles between phenyl ring planes and ethenyl linkages were of 28° and 49°, respectively. For compounds **4** and **5** in which arylethenyl substituents are connected through the nitrogen atom in C-3 positions of carbazole moiety dihedral angles between carbazole unit and C—N—C bonds range from 54° to 55°. The dihedral angles between phenyl ring planes and C—N—C bonds in compounds **4** and **5** were 37° and 36°, respectively, while dihedral angles between phenyl ring and ethenyl linkages are similar to those observed for compounds **2** and **3**.

The frontier orbitals of the molecules are shown in Fig. 1. HOMO is localized throughout all molecule. HOMO of compounds **1–3** with single arylethenyl substituent is more prominent on carbazole moiety, while HOMO of compounds **4**, **5** with two arylethenyl substituents is more localized on inner triphenylamine moiety. The LUMO main electron density of compounds **1–5** is essentially on the arylethenyl fragments, with small contribution from the carbazole moiety. The electronic properties related to these orbitals consequently were expected to exhibit some similarities.

2.3. Photophysical properties

Absorption and photoluminescence (PL) spectra of dilute solutions in toluene and THF as well as of vacuum-deposited films of the compounds are shown in Fig. 2. Their photophysical characteristics are summarized in Table 1. The low-energy absorption bands for all compounds **1–5** were practically not sensitive to the solvent used (toluene or THF). The low-energy absorption bands of solid films were red-shifted in comparison to those of the corresponding diluted solutions. The red-shifts are attributed to the aggregation effects due to the intermolecular interactions in solid state. Dilute solutions of mono-substituted carbazoles (**1–3**) showed absorption maxima at ca. 342 nm, which are in accordance with previously published data on tetra-/

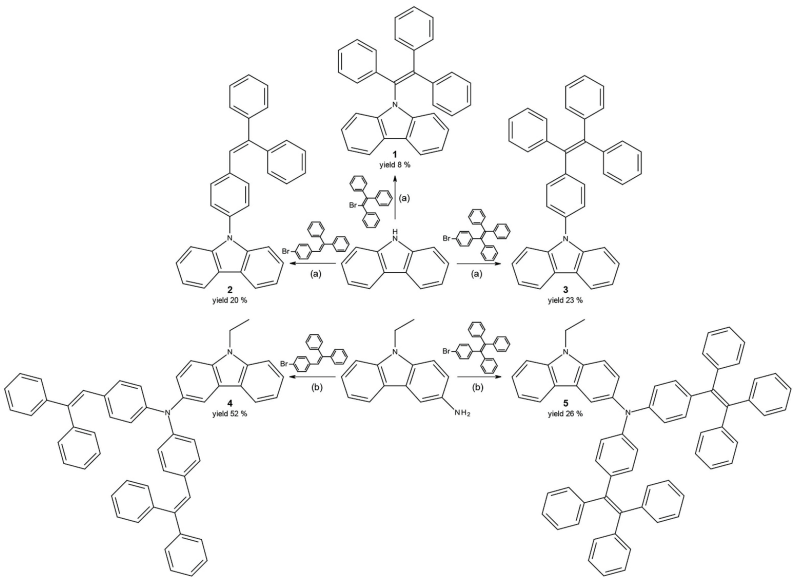

Scheme 1. Synthetic routes for compounds **1–5**. (a) CuI, TMHD, K_2CO_3, DMF, reflux; (b) *t*-Bu_3P, Pd_2dba_3, *t*-BuOK, anhydrous toluene, 90 °C.

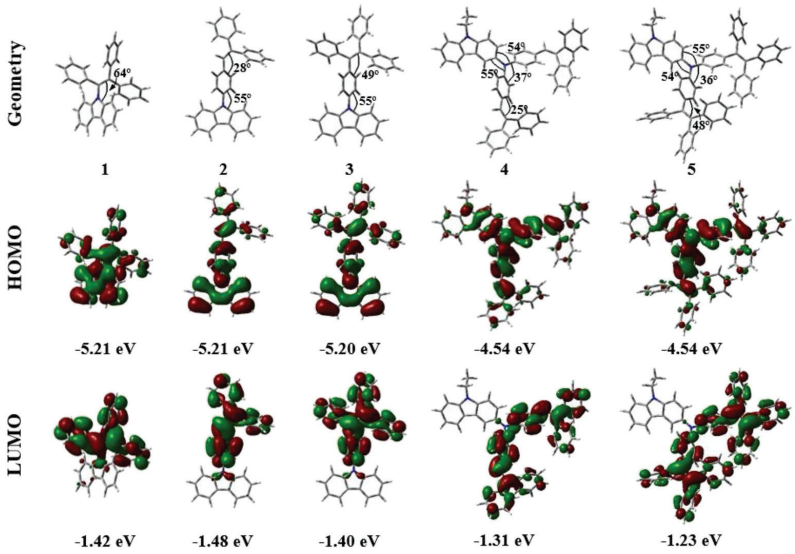

Fig. 1. Optimized geometries, HOMO and LUMO of compounds **1–5** calculated at B3LYP/6-31G (d,p) level.

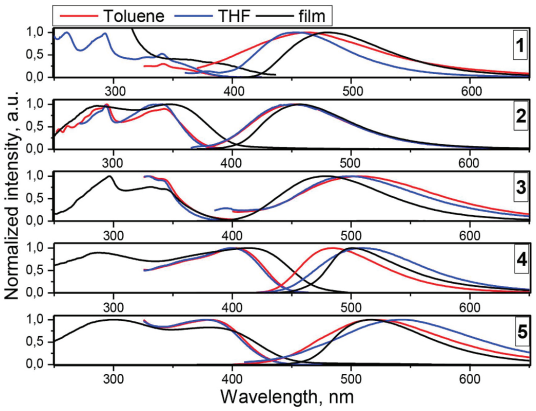

Fig. 2. Normalized absorption and fluorescence spectra of dilute (10^{-5} M) toluene, THF solutions and solid films of compounds **1–5**.

triphenylethenyl-substituted carbazole derivatives [7,12,16]. These absorption maxima are related to the π–π* transitions. Absorption maxima of dilute solutions of compounds **4** and **5** containing two tetra-/triphenylethenyl moieties were observed at ca. 404 and 382 nm, respectively (Table 1). Time dependent (TD) DFT calculations carried out to interpret impact of tetra-/triphenylethene units to the optical properties of the synthesized compounds. The experimental UV spectra of compounds **1–5** were found to accord with the theoretical UV spectra. The lowest energy absorption bands of compounds **4** and **5** having two tetra-/triphenylethenyl moieties are red-shifted relative to those of compounds **1–3** containing one arylethenyl moiety (Figure S1) indicating the decrease of optical band gap from 3.80 eV to 3.31 eV as well as increase of extent of conjugation. Corresponding to the results of quantum chemical calculations, the lowest energy absorption bands of derivatives **1–5** are characterized as transitions from ground state (S_0) to first excited state (S_1). In case of compound **5** transition from ground state (S_0) to second excited state (S_2) also contributes (Figure S1, Table S1). The transitions from ground state to the first excited state (S_0/S_1) for compounds **1–5** correspond to the transitions from HOMO to LUMO.

Dilute toluene and THF solutions of all studied compounds showed weak emission (Fig. 2). PL spectra of toluene and THF solutions of compounds **1–3** were found to be similar. Dilute solutions of **1** and **2** showed blue emission with PL maxima at ca. 450–460 nm, while greenish-blue emission with the intensity maxima at ca. 500 nm was observed for solutions of **3**. Lower PL quantum yields (Φ_F) were observed for dilute THF solutions of **1–3** in comparison to their toluene solutions. This consideration can be explained by the slight polarity effect (ε = 7.5 for THF and ε = 2.38 for toluene) (Table 1). In case of solutions of compounds **4** and **5** with two arylethenyl substituents, solvent polarity affected not only Φ_F values but also emission color.

Table 1
Photophysical data for dilute solutions and solid films of compounds **1–5**.

Compound	Toluene solution			THF solution			Film		
	λ_{abs}^{max}, nm	λ_F^{max}, nm	Φ_F, %	λ_{abs}^{max}, nm	λ_F^{max}, nm	Φ_F, %	λ_{abs}^{max}, nm	λ_F^{max}, nm	Φ_F, %
1	342	462	4	342	454	2	366	480	48
2	342	448	3	342	448	2	354	458	52
3	342	507	3	342	499	1	345	479	86
4	404	484	17	404	508	15	420	500	28
5	382	517	9	382	542	6	397	517	35

λ_{abs}^{max} – wavelength of absorption maximum. λ_F^{max} – wavelength of emission maximum (λ_{ex}: 350 nm). Φ_F – quantum yield.

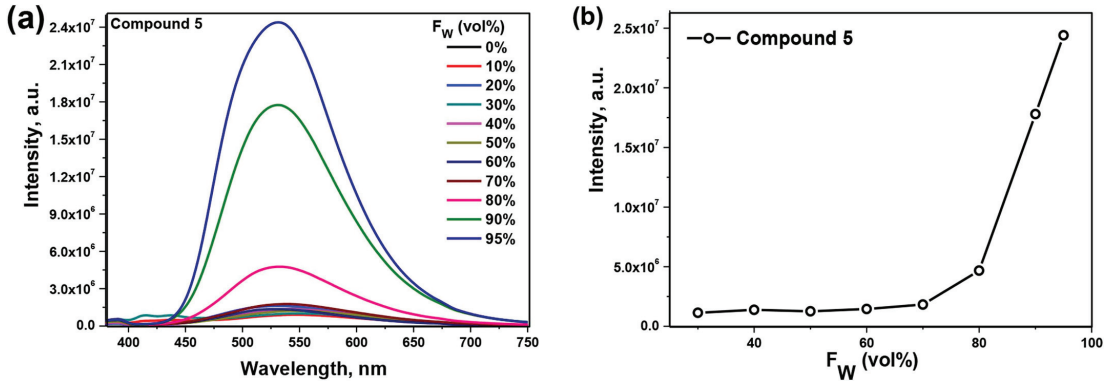

Fig. 3. Non-normalized PL spectra of the dispersions of compound **5** in the THF/water mixtures (a) and PL maximum intensities versus water volume fraction in THF/water solutions (b).

Thus, PL spectra of THF solutions of compounds **4** and **5** were red-shifted with respect of the spectra of toluene solutions (Fig. 2). Compounds **2** and **3** have tetra-/triphenylethenene units incorporated through heterocyclic nitrogen atom of carbazole moiety, while in compounds **4** and **5** tetra-/triphenylethenene units are attached through nitrogen atom attached to C-6 position. Therefore, different strength of electron donating ability of nitrogen atoms to which tetra-/triphenylethenene units are attached can be the reason of different PL behavior of these compounds. In addition, this deliberation can be explained by charge-transfer (CT) character of emission due to the twisted molecular structures of compounds **4** and **5**. Similarly to that of solutions of compounds with one arylethenyl substituent, emission spectra of solutions of tetraphenylethenyl-substituted carbazole derivative **5** were red-shifted in correlation to those of compound **4** containing triphenylethenyl substituents.

Solid films of compounds **1**–**5** shown strong emissions stretching from blue to green region of visible spectra (Fig. 2, Table 1). The wavelengths of PL maxima of solid films of the compounds were found to range in the order **2** < **1** ≈ **3** < **4** < **5**, reflecting impacts of configuration and amount of arylethenyl moieties. Φ_F values of the solid films of compounds **1**–**5** were recorded to be much higher, than those of the corresponding solutions (Table 1). These results are apparently related to AIEE effect which previously proved for compounds **1** and **3** [12,16]. It should be noted that solid-state Φ_F values of 55.7 and 100% previously reported for compounds **1** and **3** are slightly higher than those obtained in this work (48 and 86%, respectively). These differences can apparently be related to reabsorption in solid films, which we did not take into account during Φ_F measurements. Additionally, different methods of preparation of films in two different laboratories can be reason for different Φ_F values. Nevertheless, Φ_F values (which is close to unity in case of compound **3**) demonstrate high emission efficiency of the studied emitters **1**–**5** in solid-state (Table 1). It was expected that on increasing the number of tetra-/triphenylethene units increase the PLQY induced by AIEE effect. However, PLQY of **4** and **5** in film state is decreased compared to **1, 2** and **3** which are possessing one tetra-/triphenylethene unit. PLQYs of solid films of organic materials are very sensitive to many factors including molecular structure, intermolecular interactions, film-forming properties, dipole moments of molecule which may increase with increasing the number of tetra-/triphenylethene units, etc. Therefore, the increasing number of tetra-/triphenylethene units should not obligatory increase PLQY induced by AIEE effect. For example, PQLY values in the order of 93, 78, and 99% of PLQY were obtained for the films of compounds containing one, two and four tetraphenylethene units, respectively [23]. PLQYs ranging from 33.9 to 73.9% were observed for the films of compounds based on triphenylamine core and three triphenylethene units [24]. Despite the very similar chemical structures of these compounds, big differences in their PLQYs were related to the twisting of the triphenylethene units relative to the triphenylamine core. The increasing extent of molecular conjugation, taking place with increasing number of tetra-/triphenylethene units, may lead to enhancement of PLQY and charge mobilities of such molecules. However, higher number of substituents induce more steric hindrance, which subsequently may lead to decrease of PLQYs [25]. Thus, to our opinion, overlapping of different effects results in lower PLQY of the films of **4** and **5** in comparison to that of the films of compounds **1, 2** and **3**.

To investigate emission nature of compounds **1**–**5** in solid-state, PL decays were recorded (Figure S2). Since these PL decays were well-fitted giving PL lifetimes in nanosecond range, it could be concluded that solid compounds of **1**–**5** were characterized by fluorescence. For adequate representation of PL decay curves double exponential fits were required. This observation can evidently be explained by the formation of excited dimers in solid state.

2.4. Aggregation induced emission enhancement

PL spectra of dispersions of the studied compounds in the mixtures of THF and water with various water fractions (f_w) were recorded (Fig. 3, S2−S5). Since the compounds were insoluble in water, their emissive aggregates were formed at the certain f_w displaying AIEE phenomenon. For instance, dispersion of compound **5** in THF/water mixtures shown weak emission at low water fractions. This emission intensity essentially did not change within large range of water fraction (up to 80%). Until aggregates started to be formed, slight changes in emission intensities of the dispersions in THF/water mixtures were related to the changes in solution polarity due to the increase of water fraction. However, emission intensity dramatically increased at f_w > 80% when formation of aggregates in THF/water mixtures occurred (Fig. 3). As it usually explained [1], such behavior is related to AIEE effect due to the limitation of intramolecular motions in solid-state. The similar effects were observed for other studied compounds Figure S2-S5).

2.5. Thermal properties

The thermal characterization of the synthesized compounds was carried out by DSC and TGA under nitrogen atmosphere. The thermal properties are summarized in Table 2. All the synthesized compounds (**1**–**5**) exhibited moderately high thermal stability. The temperatures of five percent of weight loss ($T_{des\text{-}5\%}$) ranged from 275 °C to 440 °C, as

Table 2
Thermal properties of compounds **1–5**.

Compound	T_{cr}, °C	T_m, °C	T_g, °C	$T_{des\text{-}5\%}$,°C
1		174	70	275
2	119	170, 178	53	315
3	136	255		340
4			108	410
5		205	120	440

T_m, T_{cr} and T_g estimated by DSC at heating rate of 10 °C/min, N_2 atmosphere; [a] second heating scan.
$T_{des\text{-}5\%}$ estimated by TGA at heating rate of 20 °C/min; N_2 atmosphere.

confirmed by TGA with a heating rate of 20 °C/min. Carbazole derivatives usually possess high thermal stability and their thermal decomposition usually starts above 300 °C [26]. Rather low $T_{des\text{-}5\%}$ of compounds **1–3** can be explained by their lower molar mass which is favorable for sublimation.

Compounds **1–3** and **5** were obtained as crystalline substances, while **4** was separated after the synthesis as amorphous powder. When the melt samples of carbazole derivatives **1**, **2** and **5** were cooled down during DSC experiments, they formed molecular glasses with glass transition temperatures (T_g) of 70, 53 and 120 °C, respectively. The higher T_g of compound **1**, when compared with that of compound **2**, can evidently be explained by its more compact structure which prevents freedom of movement of molecular fragments. It was impossible to transform compound **3** into the glassy state due to its strong tendency to crystallize. T_g of compounds **4** and **5** with two arylethenyl moieties were found to be greater than those of compounds **1** and **2** containing single arylethenyl substituent. Compound **2** showed polymorphism. Two endothermic melting peaks (T_m) were observed in the first DSC heating scan at 170 and 178 °C (Fig. 4). Upon second heating, compound **2** showed besides glass transition at 53 °C but also crystallization (T_{cr}) at 119 °C and melting at 170 °C.

2.6. Electrochemical, photoelectrical and charge transporting properties

Ionization potentials, electron affinities and charge mobilities are important characteristics for evaluation of applicability of compounds in optoelectronic devices. Electrochemical properties of the compounds were analyzed by cyclic voltammetry (CV). Cyclic voltammograms of compounds **1–5** presented in Fig. 5. The electrochemical properties are resumed in Table 3. Compounds **1–3** underwent irreversible oxidation. However, compounds **4** and **5**, having an open reactive C-6 position, showed reversible oxidation similarly as previously reported [13,27]. We assume that the formation of radical cations leading to the formation of the dimers, which is generally observed in CV experiments of 3-monosubstituted carbazole derivatives, did not occur in this case [13,27,28]. The ionization potential values (I_p^{cv}) were determined from the values of the onset oxidation potential considering ferrocene (Fc). The I_p^{cv} values of the carbazole derivatives ranged from 4.98 to 5.62 eV. Electron affinities (EA^{cv}) were found from optical band gaps and ionization energy values [29]. They ranged from 2.16 to 2.45 eV.

Ionization potentials of vacuum deposited layers (I_p^{ep}) of compounds **1–5** also determined by electron photoemission method in air (Fig. 4b). The I_p^{ep} values of **1–5** ranged from 5.14 to 5.85 eV. The ionization potential values of carbazole derivatives with two arylethenyl moieties (**4**, **5**) were found to be lower than, those of carbazole derivatives with single arylethenyl substituent (**1–3**). Both methods of estimation of ionization potentials as well as HOMO energy values (see Fig. 1) revealed the same trend. As it is mentioned above, the ionization potential values (5.14 and 5.15 eV) of carbazole derivatives with two arylethenyl moieties (**4**, **5**) were found to be much lower than, those of carbazole derivatives with single arylethenyl substituent (**1–3**) (5.62, 5,62 and 5,61 eV), respectively. Such improvement in hole-injection properties of compounds **4** and **5** derives from nitrogen attached to C-3 atom of carbazole moiety because of its donating ability. Most probably, such improvement in hole-injection properties of compounds **4** and **5** (ionization potential values of 5.14 and 5.15 eV) could not be obtained by incorporating only tetra-/triphenylethene units to carbazole moiety. However, we believe that the achieved hole-injection properties of compounds **4** and **5** are related to both the C-3 nitrogen atom and tetra-/triphenylethene units because of relatively big differences between ionization potential values of carbazole derivatives with two arylethenyl moieties (**4**, **5**) and carbazole derivatives with single arylethenyl substituent (**1–3**).

Time of flight (TOF) technique was used to estimate charge transporting properties of the compounds. Transit times (t_{tr}) were well observed for holes in the corresponding low-dispersive photocurrent transients of the layers of compounds **1–5** (Fig. 6a and S9). Transit times were not observed for electrons indicating absence of electron transport in the films of compounds **1–5**. Electric field dependencies of hole drift mobilities (μ_h) for the layers of compounds **1–5** are exhibited in Fig. 6. All the compounds displayed linear dependencies of hole mobilities to the square root of electric field. Thus, μ_h for the layers of compounds **1–5** verify Poole–Frenkel type electric field dependence $\mu = \mu_o \times \exp(\alpha E)^{1/2}$, where μ_o is the zero electric field charge mobility, and α is the field dependence parameter [30]. Organic semiconductors typically confirmed this dependence (Fig. 6) [31,32]. Hole-drift mobility values are collected in Table 3. Hole mobilities of compounds **4** and

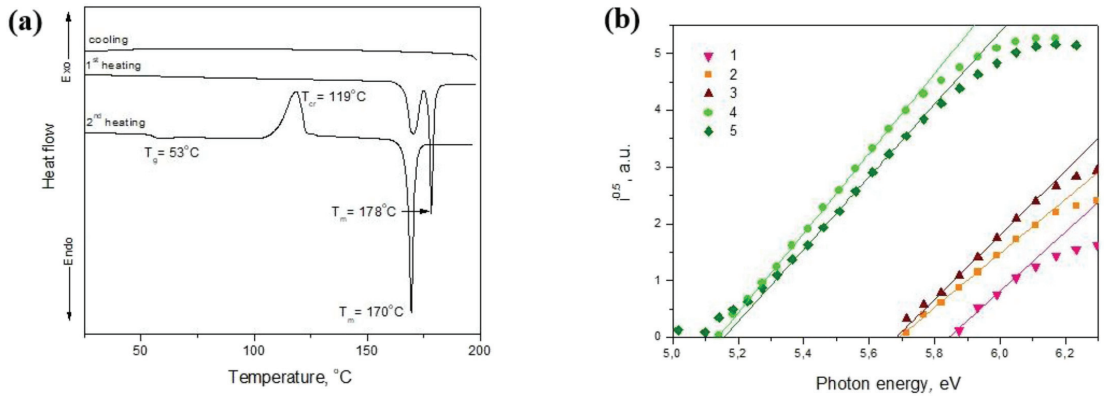

Fig. 4. DSC curves of compound **2** (scan rate of 10 °C/min. N_2 atmosphere) (a) and photoelectron emission spectra of solid films of compounds **1–5** (b).

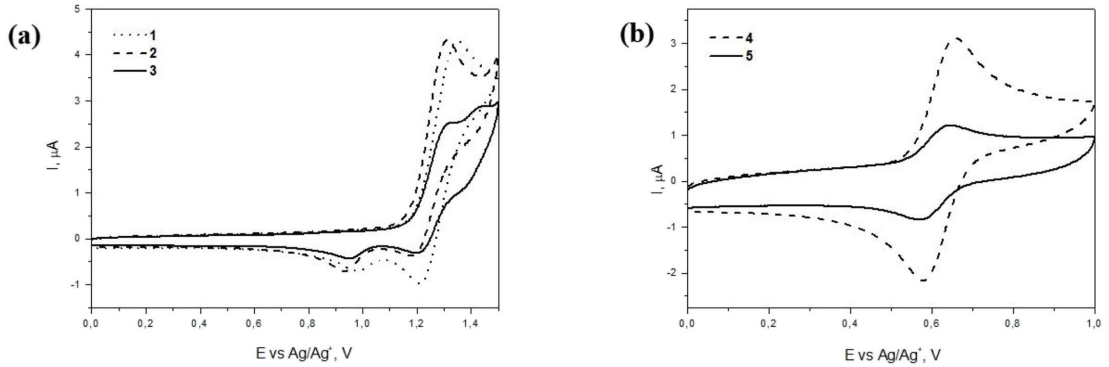

Fig. 5. Cyclic voltammograms of dilute solutions of compounds **1–3** (a) and **4**, **5** (b) in dichloromethane (room temperature) recorded at sweep rate of 0.1 V/s.

5 exceeded 10^{-3} cm^2/V at high electric fields. μ_h values of the compounds were found to range in order **1** > **2**~**3** > **4** > **5**. According to the previously published crystal structure of compound **3** multiple C—H···π hydrogen bonds with distances of 2.719–3.090 Å are formed between hydrogen atoms of phenyl rings of tetraphenylethenyl unit in one molecule and the π cloud of planar aromatic ring in another molecule [7]. Such molecular packing may provide good HOMO-HOMO overlapping of neighboring molecules, which results in good hole-transporting properties of compound **3**. Apparently, distances between neighboring molecules of compound **1** are even shorter, multiple C—H···π hydrogen bonds with distances of 2.620 and 3.075 Å are formed between carbazole protons of one molecule and the π cloud of the carbazole of the neighboring molecule [21]. Since distances between molecules are shorter, the higher hole mobilities were observed for compound **1** relative to those of other studied compounds.

2.7. Electroluminescent devices

Non-doped OLEDs were fabricated to explore the effect of substitution pattern of the studied carbazole derivatives on their electroluminescent properties and to demonstrate potential of the compounds as electroactive functional materials (mainly emitters) in organic electronics. The structures of the fabricated OLEDs were ITO/MoO_3 (1 nm)/NPB (60 nm)/TCTA (5 nm)/non-doped light-emitting layer (30 nm)/TSPO1 (3 nm)/TPBi (40 nm)/LiF (0.5 nm)/Al, which were named as devices **D1–D5** depending on compounds **1–5** used as emitters. In these OLED structures, molybdenum trioxide (MoO_3) and lithium fluoride (LiF) were utilized for the deposition of hole and electron injecting layers, respectively. *N,N′*-di(1-naphthyl)-*N,N′*-diphenyl-(1,1′-biphenyl)-4,4′-diamine (NPB)/tris(4-carbazoyl-9-ylphenyl)amine (TCTA) and 2,2′,2″-(1,3,5-benzinetriyl)-tris(1-phenyl-1H-benzimidazole) (TPBi)/diphenyl-4-triphenylsilyl-phenylphosphineoxide (TSPO1) were exploited as hole and electron transporting layers, respectively. Tandemly, TCTA and TSPO1 played roles of electron and hole blocking layers, respectively. As their usual roles, indium-tin-oxide (ITO) was optically transparent anode and LiF/Al was cathode. Using these device structures, good charge-injection and charge-transport were ensured for devices **D1–D5**, despite the different HOMO/LUMO energy levels of compounds **1–5** (Fig. 7). Moreover, HOMO (I_p^{ep}) values of solid films were used in the design of the devices.

The fabricated OLEDs were characterized by electroluminescence with colors falling in spectral range from blue to green with corresponding CIE coordinates, which are presented in Table 4 (Figure S10). EL spectra of devices D1–D5 were in agreement with corresponding PL spectra of solid films of compounds **1–5** (Figure S11). Small differences between them are related to the different optical and electrical excitation sources used. EL spectra were stable at different applied voltages showing that hole-electron recombination occurred only within light-emitting layer and electroluminescence of devices **D1–D5** was related to emission of solid films of compounds **1–5**, respectively (Fig. 8a).

Comparable turn-on voltages ranging from 3.7 to 4.5 V were noticed for all devices (Fig. 8b). The small differences of turn-on voltages and voltage-current density characteristics were apparently related to the differences in charge transporting properties and HOMO/LUMO values of light-emitting layers (Table 3). The highest maximum brightness exceeding 15000 cd/m^2 was noted for device **D5** (Fig. 8c, Table 4). The highest values of the maximum current, power and external quantum efficiencies (EQE) of 5.88 cd/A, 3.15 lm/W, and 2.02% respectively were also obtained for the device **D5** (Fig. 8c, Table 4). The studied devices exhibited very low efficiency roll-off apparently because of good stability of the fluorescent emitters **1–5** under electrical excitation. In case of some devices, higher EQE values were observed at high brightness of 1000 cd/m^2 in comparison to those recorded at lower brightness of 100 cd/m^2 (Table 4). This observation is apparently related to the balance of hole and electron transport in the non-doped

Table 3
I_p^{cv}, EA^{cv}, band gap energies, electrochemical characteristics and hole-transporting parameters of compounds **1–5**.

Compound	E_{onset}^{ox}, V	E_g^{opt}, eV	I_P^{ep}, eV	I_p^{cv}, eV	E_A^{cv}, eV	μ_{h0}, cm^2/Vs	μ_h, cm^2/Vs	α, $(cm/V)^{1/2}$
1	0.82	3.17	5.85	5.62	2.45	1.3×10^{-3}	2.1×10^{-2}	5.23×10^{-3}
2	0.82	3.27	5.70	5.62	2.35	1.93×10^{-4}	6×10^{-3}	5.43×10^{-3}
3	0.81	3.28	5.68	5.61	2.33	2.95×10^{-4}	6×10^{-3}	6.45×10^{-3}
4	0.18	2.75	5.14	4.98	2.23	2×10^{-4}	3×10^{-3}	4.9×10^{-3}
5	0.18	2.82	5.15	4.98	2.16	2.45×10^{-4}	1.9×10^{-3}	3.84×10^{-3}

The onset oxidation potentials (E_{onset}^{ox}) versus Fc measured by CV from the first redox cycle. The optical band gap (E_g^{opt}) estimated from the edges of absorption spectra of THF solutions of compounds ($E_g^{opt} = 1240/\lambda_{onset.}$). Ionization potentials (I_P^{ep}) measured by photoelectron emission in air method. Ionization potentials (I_p^{cv}) measured by CV.: $I_p^{cv} = 4.8 + E_{onset}^{ox}$ [29]. Electron affinities calculated using equation $EA^{cv} = I_p^{cv} - E_g^{opt}$. Hole mobility ($\mu_h$) values at electric field of 2.9×10^5 V/cm. Zero-field hole mobility (μ_{h0}) values and field dependence parameter (α) are indicated as well.

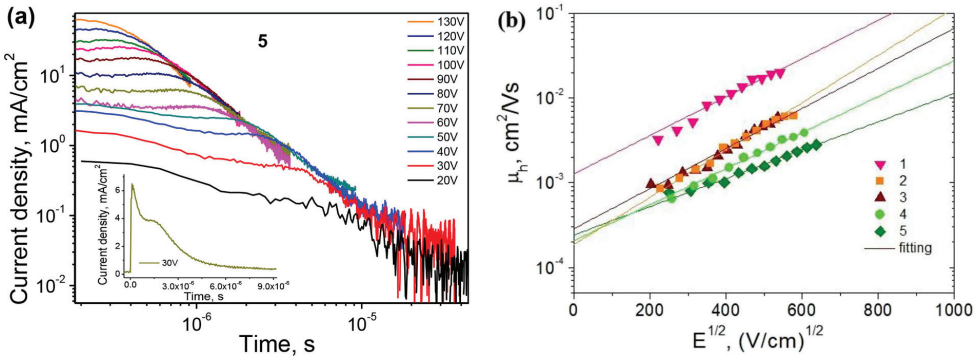

Fig. 6. TOF pulses for holes in the layers of compound **5** at different electric fields (a) and hole mobility dependences on applied electric field for the layers of compounds **1–5** (b).

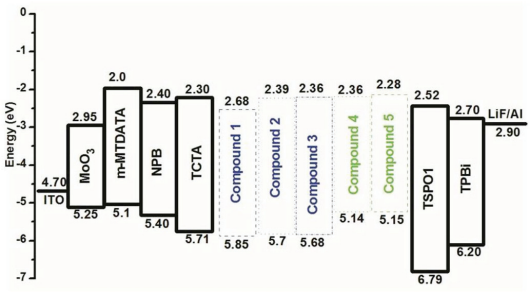

Fig. 7. Equilibrium energy diagrams for devices **D1–D5**.

light-emitting layers at higher current densities.

The device structure was further modified and optimized in order to make it more appropriate for compounds **4** and **5**. The modified device structure was ITO/MoO_3 (1 nm)/mMTDATA (50 nm)/light-emitting layer (30 nm)/TSPO1 (5 nm)/TPBi (65 nm)/LiF (0.5 nm)/Al in which hole-transporting layers were skipped since HOMO of compounds **4** and **5** was appropriate for hole injection (Fig. 7). In these devices, compounds **1**–5 were tested, and the corresponding devices were named as **D1a**-**D5a**, respectively. EL spectra of devices **D4a** and **D5a** were practically the same as those of devices **D4** and **D5**. Both corresponded to PL spectra of compounds **4** or **5** (Fig. 8a, Figure S12). However, EL spectra of devices **D1a**, **D2a** and **D3a** were different from those of devices **D1**, **D2** and **D3.** Because of the high barrier for holes at the interfaces m-MTDATA/compound **1**, m-MTDATA/compound **2** and m-MTDATA/compound **3**, radiative recombination of hole-electron pairs in devices **D1a**, **D2a** and **D3a** apparently occurs not only in the light-emitting layer but also in m-MTDATA layer. Device **D5a** exhibited very high maximum brightness exceeding of 50000 cd/m^2 at 9.3 V (Figure 8b, Table 4). As a result, device **D5a** showed improved maximum EQE of 5.32% (Fig. 8c). This value is very high as for simple non-doped fluorescent devices. The theoretical maximum of such devices is of 5–7.5% taking out-coupling efficiency of 20–30% [33]. It worth of noting that maximum EQEs of device **D5a** based on carbazole derivative **5** with two tetraphenylethenyl moieties is considerably higher than those of previously reported OLEDs based on carbazole derivatives, containing single tetra-/triphenylethenyl substituent (Table S2). Since PLQY values are below unity for the films of the fluorescent compounds **4** and **5,** which harvest only singlet excitons to light under electrical excitation, it is not clear how such high EQE values of devices **D4a** and **D5a** were achieved even if the charge-balance factor was close to unity. To check the possible pathway of triplet harvesting, interface exciplex emission was identified between the layer of m-MTDATA and light-emitting layer of devices **D1a-D5a** (Figure S13). The shapes of PL spectra and PL decays of the solid mixtures of m-MTDATA(50%) and compounds **1–5** (50%) were obtained such as those typically observed for exciplexes [34,35]. It was recently shown that device performance of OLEDs based on emitting layers of materials exhibiting AIEE can be enhanced by triplet harvesting due to utilization of interface exciplex-host [36]. Apparently, relatively high EQE values of devices **D4a** and **D5a** were achieved due to the utilization of interface exciplexes m-

Table 4
Non-doped OLED characteristics.

Device	V_{on} (V)	λ_{max} (nm)	L_{max} (cd/m^2)	CE_{max} (cd/A)	PE_{max} (lm/W)	EQE_{max} (%)	EQE (%) at 100/1000 cd/m^2	CIE1931 coordinates (X,Y)
Device structure ITO/MoO_3/NPB/TCTA/light-emitting layer/TSPO1/TPBi/LiF/Al								
D1	3.81	470	4700	3	2.35	1.62	1.29/0.86	(0.168,0.209)
D2	3.99	441	4300	1.4	0.82	1.08	1.04/1.09	(0.159,0.126)
D3	3.99	479	2000	3.8	2.6	1.95	1.7/1.3	(0.174,0.244)
D4	4.19	499	12100	4.26	2.2	1.6	0.99/1.52	(0.194,0.463)
D5	3.79	518	15500	5.8	3	2	1.3/1.97	(0.248,0.514)
Device structure ITO/MoO_3/m-MTDATA/light-emitting layer/TSPO1/TPBi/LiF/Al								
D1a	4.1	497	6600	2.1	1.17	0.85	0.66/0.84	(0.202,0.34)
D2a	5.3	521	10300	3.9	1.7	1.3	1.06/1.28	(0.252,0.456)
D3a	4.5	496	7700	2.76	1.38	1.16	0.9/1.09	(0.19,0.318)
D4a	5.1	500	28000	9.6	4.6	3.3	3.1/3.25	(0.21, 0.464)
D5a	3.8	518	52000	17	9.2	5.32	3.1/5.22	(0.242,0.52)
Device structure ITO/MoO_3/light-emitting layer/TSPO1/TPBi/LiF/Al								
D4b	5.0	500	25300	8.0	4.3	2.7	2.24/2.63	(0.205,0.483)
D5b	5.9	521	37600	12.6	5.3	4.0	2.43/3.99	(0.24,0.52)

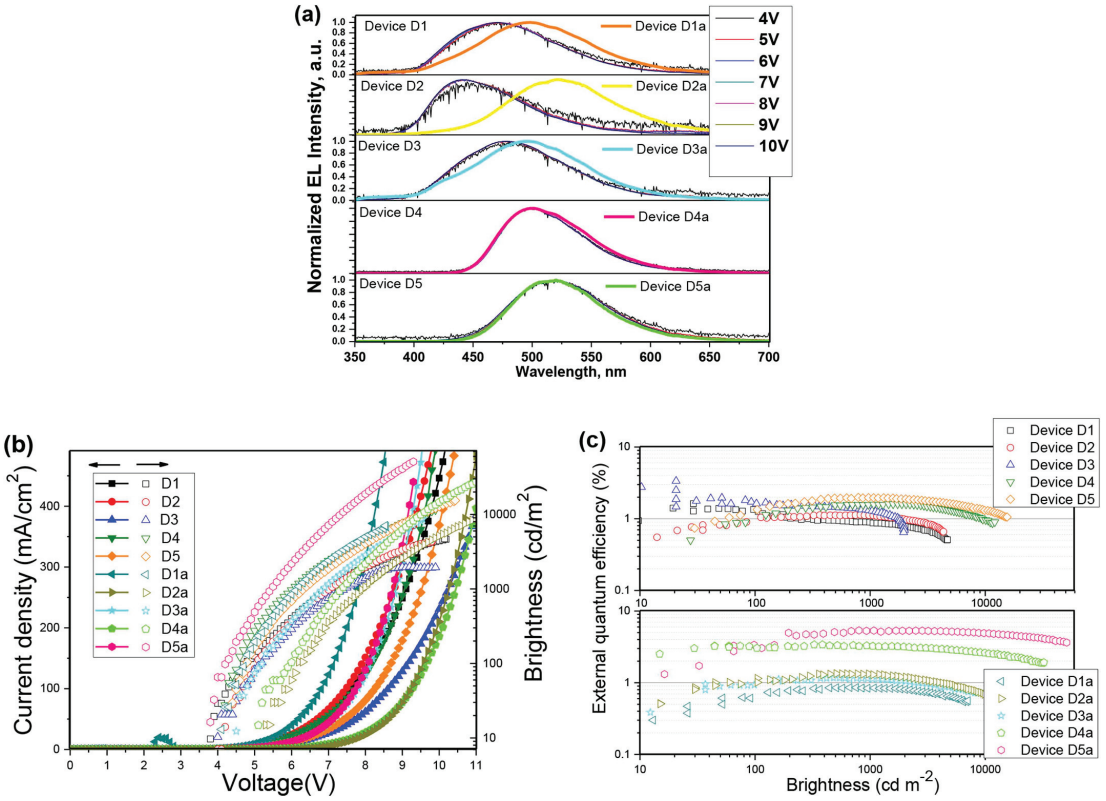

Fig. 8. EL spectra recorded at the different applied voltages (a), current density-voltage and brightness-voltage (b) and external quantum efficiency-brightness characteristics (c) of devices **D1–D5** and **D5a**.

MTDATA:**4** and m-MTDATA:**5**. Since PL spectra of solid films **4** (***5***) and solid mixtures m-MTDATA:**4** (m-MTDATA:**5)** were observed in the same region, enhancement of EQE of devices **D4a** and **D5a** was apparently achieved due to the triplet energy transfer from the exciplex-host to emitter **4** (***5***). In contract, the corresponding PL spectra of exciplexes m-MTDATA:**1,** m-MTDATA:**2,** and m-MTDATA:**3** were red-shifted in comparison to PL spectra of solid films of **1–3**. As a result, lower EQE values and red-shifted EL spectra of devices **D1a**, **D2a** and **D3a** in comparison to those of devices **D1**, **D2** and **D3** were observed due to the exciplex-formation. Thus, formation of exciplexes m-MTDATA:**1–3** resulted in poor performances of devices **D1a**, **D2a** and **D3a.** On the other hand, EQE efficiencies of devices **D4a** and **D5a** were enhanced owing to exciplex-hosts m-MTDATA:**4** and m-MTDATA:**5** (Table 4).

In addition, the designed compounds are very good candidates to be used as multifunctional OLED materials. Thus, compounds **4** and **5** may be used for both hole-transporting (HTM) and emissive (EM) layers due to their relatively high PLQYs, relatively high hole mobilities and high HOMO values for good hole injection from either anode or hole-injection layers. To prove this concept, devices **D4b** and **D5b** having a structure ITO/MoO_3 (1 nm)/light-emitting layer (60 nm)/TSPO1 (5 nm)/TPBi (60 nm)/LiF (0.5 nm)/Al without m-MTADATA layer were fabricated exploiting compounds **4** or **5** for the preparation of the light-emitting and hole-transporting layers, respectively. Stable at different voltages, EL spectra of devices **D4b** and **D5b** were practically the same as those observed for other **4** or **5**-based devices **D4**, **D5, D4a** and **D5a** (Figure S14, Table 4). Displaying potential of compounds **4** or **5** as multifunctional OLED materials, relatively high OLED performances were observed for fluorescent devices **D4b** and **D5b** (Table 4). Their maximum EQE values reached 2.7 and 4.0% (Figure S15, S16). However, these EQE values were lower than maximum EQE values of devices **D4a** and **D5a** with m-MTADATA layer. In the case of devices **D4a** and **D5a,** there are energy barriers of ca. 0.68–0.28 eV for electrons between m-MTADATA and **4** or **5** (Fig. 7). Thus, no leakage of electrons from the light-emitting layer to anode take place because of electron-blocking properties of m-MTADATA layer. Since electron-blocking layer was not used in case of devices **D4b** and **D5b** slightly lower EQE values in were observed relative to those recorded for devices **D4a** and **D5a** (Table 4).

3. Experimental

3.1. Methods

^{1}H NMR and ^{13}C NMR spectra were registered with Varian Unity Inova [300 MHz (^{1}H), 75.4 MHz (^{13}C)] and Bruker Avance III [400 MHz (^{1}H), 100 MHz (^{13}C)] spectrometers at room temperature. All the data are provided as chemical shifts δ (ppm) downfield from $Si(CH_3)_4$. Infrared (IR) spectra were registered using PerkinElmer Spectrum GX II FT-IR System. The samples of the solid compounds were prepared in form of KBr pellets. Mass spectra (MS) were obtained on the Waters SQ Detector 2. Elemental analysis was performed with an Exeter Analytical

CE-440 Elemental Analyzer. Differential scanning calorimetry (DSC) measurements were recorded in nitrogen atmosphere with a PerkinElmer at DSC 8500 equipment at heating rate of 10 °C/min. Thermogravimetric analysis (TGA) was executed on a PerkinElmer TGA 4000 apparatus in a nitrogen atmosphere at heating rate of 20 °C/min. Melting points were measured with Electrothermal MEL-TEMP melting point apparatus. Absorption spectra of dilute (10^{-5} M) solutions in tetrahydrofuran (THF) were registered on an UV–vis–NIR spectrophotometer Lambda 950 (PerkinElmer). Fluorescence spectra, fluorescence quantum yields (Φ_F) and fluorescence transients of dilute solutions in THF (10^{-5} M) or solid films of the compounds were registered with Edinburgh Instruments LS980 spectrometer. Cyclic voltammetry (CV) measurements were recorded using a micro-Autolab III (Metrohm Autolab) potentiostat equipped with a standard three-electrode configuration. A three-electrode cell equipped with a glassy carbon-working electrode, an $Ag/AgNO_3$ (0.01 M in anhydrous acetonitrile) reference electrode and a Pt wire counter electrode were employed. The measurements were carried out in anhydrous dichloromethane with tetrabutylammonium hexafluorophosphate (0.1 M) as supporting electrolyte under nitrogen atmosphere at scan rate of 0.05 V/s [37]. The measurements were calibrated using an internal standard, ferrocene/ferrocenium (Fc) system. Oxidation potentials ($E_{1/2}$ vs Fc) for reversible oxidation were collected as average values of the anodic and cathodic peak potentials, E_{pa} and E_{pc}, respectively. Ionization potentials (I_P^{ep}) of the vacuum-deposited films of the synthesized compounds were measured by electron photoemission method in air as described before [38,39]. Hole drift mobilities were measured by a time of-flight (TOF) method as reported earlier [40]. The pulsed Nd:YAG laser (EKSPLA NL300, 355 nm, 3–6 ns), Keithley 6517B electrometer, Tektronix TDS 3052C oscilloscope were exploited in the TOF experimental setup. Hole mobility was calculated as $\mu = d^2/U{\cdot}t_t$ using transit time (t_t) with the applied bias (U) and the entire thickness (d) of the samples.

Thermo-vacuum deposition technique (Kurt J. Lesker in-built in an MB EcoVap4G glove box) was used for fabrication of electroluminescent devices under pressure lower than 2×10^{-6} mBar. Density-voltage and luminance-voltage characteristics were registered using Keithley 2400C sourcemeter and certificated photodiode PH100−Si-HA-D0 together with the PC-Based Power and Energy Monitor 11S-LINK as it was previously described [41,42]. External quantum efficiency was estimated using the luminance, current density, and EL spectrum. Electroluminescence (EL) spectra were recorded by an Aventes AvaSpec-2048XL spectrometer. EL spectra were used for calculations of chromaticity coordinates (x, y) of the devices.

The computations were carried out in the frame of density functional theory (DFT) engaging the B3LYP functional with Gaussian 16 program [43–46]. The functional was exploited in conjunction with the 6-31G(d,p) basis set. The spectroscopic properties and of the molecules was calculated by mean of time dependent density functional theory method (TDDFT) [47–51]. Up to 40 excited states were calculated and the theoretical absorption bands were gained by considering a band half-width at half-maximum 0.3 eV.

4. Conclusion

We synthesized and characterized carbazole derivatives containing on or two tri/tetraphenylethenyl moieties as fluorescent OLED emitters showing high photoluminescence quantum yields in solid-state due to the aggregation induced emission enhancement. The synthesized compounds formed glasses with glass transition temperatures in the range of 53–120 °C. Ionization potentials of ca. 5.15 eV and hole mobilities reaching 10^{-3} cm^2/V were observed for the compounds with two tri/tetraphenylethenyl substituents. They showed both good hole-injecting and hole-transporting properties. OLED, based on carbazole derivative with two tetraphenylethenyl substituents linked through the nitrogen atom in C-3 position of carbazole moiety, showed the highest maximum brightness exceeding of 50000 cd/m^2 as well as high maximum current, power and external quantum efficiencies of 17 cd/A, 9.2 lm/W, and 5.32% respectively.

Acknowledgements

This research was funded by the European Regional Development Fund according to the supported activity 'Research Projects Implemented by World-class Researcher Groups' under Measure No. 01.2.2-LMT-K-718. Nataliya Kostiv is acknowledged for the initial tests of photophysical properties of the compounds.

Appendix A. Supplementary data

Supplementary data to this article can be found online at https://doi.org/10.1016/j.dyepig.2019.04.045.

References

[1] Mei J, Leung NLC, Kwok RTK, Lam JWY, Tang BZ. Aggregation-induced emission: together we shine, united we soar!. Chem Rev 2015;115(21):11718–940https://doi.org/10.1021/acs.chemrev.5b00263.
[2] Shi X, Yu C, Su H, Kwok R, Jiang M, He Z, et al. A red-emissive antibody–AIEgen conjugate for turn-on and wash-free imaging of specific cancer cells. Chem Sci 2017;8:7014–24https://doi.org/10.1039/C7SC01054K.
[3] Qi J, Fang Y, Kwok RTK, Zhang X, Hu X, Lam JWY, et al. Highly stable organic small molecular nanoparticles as an advanced and biocompatible phototheranostic agent of tumor in living mice. ACS Nano 2017;11(7):7177–88https://doi.org/10.1021/acsnano.7b03062.
[4] Grybauskaite-Kaminskiene G, Volyniuk D, Mimaite V, Bezvikonnyi O, Bucinskas A, Bagdziunas G, Grazulevicius JV. Aggregation-enhanced emission and thermally activated delayed fluorescence of derivatives of 9-phenyl-9H-carbazole: effects of methoxy and *tret*-butyl substituents. Chem Eur J 2018;24:9581–91https://doi.org/10.1002/chem.201800822.
[5] Chen Y, Lam JWY, Kwok RTK, Liu B, Tang BZ. Aggregation-induced emission: fundamental understanding and future developments. Mater Horizons 2019;6:428–33. https://doi.org/10.1039/C8MH01331D.
[6] He BR, Chang ZF, Jiang YB, Xu XF, Lu P, Kwok HS, et al. Piezochromic luminescentand electroluminescent materials comprised of tetraphenylethene plus spirobifluorene or 9,9-diphenylfluorene. Dyes Pigments 2014;106:87–93https://doi.org/10.1016/j.dyepig.2014.02.026.
[7] Zhao Z, Lu P, Lam JWY, Wang Z, Chan CYK, Sung HH, et al. Molecular anchors in the solid state: restriction of intramolecular rotation boosts emission efficiency of luminogen aggregates to unity. Chem Sci 2011;2:672–5https://doi.org/10.1039/C0SC00521E.
[8] Okumoto K, Kanno H, Hamaa Y, Takahashi H, Shibata K. Green fluorescent organic light-emitting device with external quantum efficiency of nearly 10%. Appl Phys Lett 2006;89:063504 1–3https://doi.org/10.1063/1.2266452.
[9] Wen S-W, Lee M-T, Chen CH. Recent development of blue fluorescent OLED materials and devices. IEEE/OSA J Disp Technol 2005;1(1):90–9https://doi.org/10.1109/JDT.2005.852802.
[10] Butkute R, Lygaitis R, Mimaite V, Gudeika D, Volyniuk D, Sini G, Grazulevicius JV. Bipolar highly solid-state luminescent phenanthroimidazole derivatives as materials for blue and white organic light emitting diodes exploiting either monomer, exciplex or electroplex emission. Dyes Pigments 2017;146:425–37https://doi.org/10.1016/j.dyepig.2017.07.029.
[11] Dong SH, Li ZH, Qin J. New carbazole-based fluorophores: synthesis, characterization, and aggregation-induced emission enhancement. J Phys Chem B 2009;113:434–41https://doi.org/10.1021/jp807510a.
[12] Zhao Z, Chan CYK, Chen S, Deng C, Lam JWY, Jim CKW, et al. Using tetraphenylethene and carbazole to create efficient luminophores with aggregation-induced emission, high thermal stability, and good hole-transporting property. J Mater Chem 2012;22:4527–34https://doi.org/10.1039/C2JM14914A.
[13] Tomkeviciene A, Sutaite J, Volyniuk D, Kostiv N, Simkus G, Mimaite V, Grazulevicius JV. Aggregation-induced emission enhancement in charge-transporting derivatives of carbazole and tetra(tri)phenylethylene. Dyes Pigments 2017;140:363–74https://doi.org/10.1016/j.dyepig.2017.01.056.
[14] Volyniuk D, Sutaite J, Tomkeviciene A, Kostiv N, Buika G, Grazulevicius JV. Organic light-emitting diodes exploiting aggregation-induced exciton and exciplex emissions. J Lumin 2017;192:534–40https://doi.org/10.1016/j.jlumin.2017.07.040.
[15] Lo D, Chang C-H, Krucaite G, Volyniuk D, Grazulevicius JV, Grigalevicius S. Sky-blue aggregation-induced emission molecules for non-doped organic light-emitting diodes. J Mater Chem C 2017;5:6054–60https://doi.org/10.1039/C7TC01659J.
[16] Jou J-H, Kumar S, Agrawal A, Lia T-H, Sahoo S. Approaches for fabricating high efficiency organic light emitting diodes. J Mater Chem C 2015;3:2974–3002https://doi.org/10.1039/c4tc02495h.
[17] Jhulki S, Moorthy JN. Small molecular hole-transporting materials (HTMs) in organic light-emitting diodes (OLEDs): structural diversity and classification. J Mater Chem C 2018;6:8280–325https://doi.org/10.1039/c8tc01300d.
[18] Chan CYK, Lam JWY, Zhao Z, Chen S, Lu P, Sung HHY, et al. Aggregation-induced

emission, mechanochromism and blue electroluminescence of carbazole and triphenylamine-substituted ethenes. J Mater Chem C 2014;2. 4320-4321-7 https://doi.org/10.1039/C4TC00097H.
[19] Kim WY, Yoon K-B. Synthesis of novel carbazole-based blue light-emitting copolymers containing (diphenylene)vinylene pendants. Polym Kor 2013;37(6):736–43https://doi.org/10.7317/pk.2013.37.6.736.
[20] Hartwig JF. Palladium-catalyzed amination of aryl halides: mechanism and rational catalyst design. Synlett 1997;4:329–40http://doi.org/10.1055/s-1997-789.
[21] Mitra S, Darira H, Chattopadhyay P. Efficient synthesis of imidazole-fused benzodiazepines using palladium-catalyzed intramolecular C-N bond formation reaction. Synthesis 2013;45:85–92http://doi.org/10.1055/s-0032-1316828.
[22] Shafir A, Buchwald SL. Highly selective room-temperature copper-catalyzed C − N coupling reactions. J Am Chem Soc 2006;128:8742–3http://doi.org/10.1021/ja063063b.
[23] Liu Y, Chen X, Lv Y, Chen S, Lam JWY, et al. Systemic studies of tetraphenylethene–triphenylamine oligomers and a polymer: achieving both efficient solid-state emissions and hole-transporting capability. Chem Eur J 2012;18:9929–38https://doi.org/10.1002/chem.201201400.
[24] Huang J, Sun N, Yang J, Tang R, Li Q, et al. Blue aggregation-induced emission luminogens: high external quantum efficiencies up to 3.99% in led device, and restriction of the conjugation length through rational molecular design. Adv Funct Mater 2014;24:7645–54https://doi.org/10.1002/adfm.201401867.
[25] Chen G, Li W, Zhou T, Peng Q, Zhai D, et al. Conjugation-induced rigidity in twisting molecules: filling the gap between aggregation-caused quenching and aggregation-induced emission. Adv Mater 2015;27:4496–501https://doi.org/10.1002/adma.201501981.
[26] Zhang YX, Ding L, Liu XY, Jiang ZQ, Chen H, Liao S, Ji SJ. Spiro-fused N-phenylcarbazole-based host materials for blue phosphorescent organic light-emitting diodes. Org Electron 2015;20:112–8https://doi.org/10.1016/j.orgel.2015.02.014.
[27] Lav TX, Tran-Van F, Vidal F, Peralta S, Chevrot C, Teyssie D, et al. Synthesis and characterization of p and n dopable interpenetrating polymer networks for organic photovoltaic devices. Thin Solid Films 2008;516:17223–9https://doi.org/10.1016/j.tsf.2007.12.126.
[28] Karon K, Lapkowski M. Carbazole electrochemistry: a short review. J Solid State Electrochem 2015;19:2601–10https://doi.org/10.1007/s10008-015-2973-x.
[29] Kaafanari BL, El-Ballouli AO, Trattnig R, Fonari A, Sax S, Wex B, et al. Bis(carbazolyl) derivatives of pyrene and tetrahydropyrene: synthesis, structures, optical properties, electrochemistry, and electroluminescence. J Mater Chem C 2013;1:1638–50https://doi.org/10.1039/C2TC00474G.
[30] Borsenberger PM, Shi J. Hole Transport in a vapor deposited phenylenediamine molecular glass. Phys Status Solidi B 1995;191(2):461–9https://doi.org/10.1002/pssb.2221910219.
[31] Reig M, Bagdziunas G, Volyniuk D, Grazulevicius JV, Velasco D. Tuning the ambipolar charge transport properties of tricyanovinyl-substituted carbazole-based materials. Phys Chem Chem Phys 2017;19:6721–30https://doi.org/10.1039/C6CP08078B.
[32] Bucinskas A, Volyniuk D, Danyliv Y, Grazulevicius JV, Baryshnikov G, Minaev B, et al. N-annelated perylenes as effective green emitters for OLEDs. RSC Adv 2015;5:78150–9https://doi.org/10.1039/C5RA15075B.
[33] Furno M, Meerheim R, Hofmann S, Lussem B, Leo K. Efficiency and rate of spontaneous emission in organic electroluminescent devices. Phys Rev B 2012;85:115205 1–21https://doi.org/10.1103/PhysRevB.85.115205.
[34] Guzauskas M, Volyniuk D, Tomkeviciene A, Pidluzhna A, Lazauskas A, et al. Dual nature of exciplexes: exciplex-forming properties of carbazole and fluorene hybrid trimers. J Mater Chem C 2019;7:25–32https://doi.org/10.1039/C8TC04708A.
[35] Chapran M, Pander PH, Vasylieva M, Wiosna-Sałyga G, Ulanski J, et al. Realizing 20% external quantum efficiency in electroluminescence with efficient thermally activated delayed fluorescence from an exciplex. ACS Appl Mater Interfaces 2019;11(14):13460–71https://doi.org/10.1021/acsami.8b18284.
[36] Sych G, Simokaitiene J, Bezvikonnyi O, Tsiko U, Volyniuk D, et al. Exciplex-enhanced singlet emission efficiency of nondoped organic light emitting diodes based on derivatives of tetrafluorophenylcarbazole and tri/tetraphenylethylene exhibiting aggregation-induced emission enhancement. J Phys Chem C 2018;122(26):14827–37https://doi.org/10.1021/acs.jpcc.8b03895.
[37] Shirota Y, Kageyama H. Charge carrier transporting molecular materials and their applications in devices charge carrier transporting molecular materials and their applications in devices. Chem Rev 2007;107:953–1010https://doi.org/10.1021/cr050143+.
[38] Malinauskas T, Daskeviciene M, Kazlauskas K, Su HC, Grazulevicius JV, Jursenas S, et al. Multifunctional red phosphorescent bis-cyclometallated iridium complexes based on 2-phenyl-1,2,3-benzotriazole ligand and carbazolyl moieties. Tetrahedron 2011;67:1852–61https://doi.org/10.1016/j.tet.2011.01.026.
[39] Kukhta NA, Volyniuk D, Peciulyte L, Ostrauskaite J, Juska G, Grazulevicius JV. Structure-property relationships of star-shaped blue-emitting charge-transporting 1,3,5-triphenylbenzene derivatives. Dyes Pigments 2015;117:122–32https://doi.org/10.1016/j.dyepig.2015.02.013.
[40] Mimaite V, Grazulevicius JV, Laurinaviciute R, Volyniuk D, Jankauskas V, Sini G. Can hydrogen bonds improve the hole-mobility in amorphous organic semiconductors? Experimental and theoretical insights. J Mater Chem C 2015;3:11660–74https://doi.org/10.1039/C5TC02534F.
[41] Greenham N, Friend R, Bradley D. Angular dependence of the emission from a conjugated polymer, light-emitting diode: implications for efficiency calculations. Adv Mater 1994;6:491–4https://doi.org/10.1002/adma.19940060612.
[42] Cekaviciute M, Simokaitiene J, Volyniuk D, Sini G, Grazulevicius JV. Arylfluorenyl-substituted metoxytriphenylamines as deep blue exciplex forming bipolar semiconductors for white and blue organic light emitting diodes. Dyes Pigments 2017;140:187–202https://doi.org/10.1016/j.dyepig.2017.01.023.
[43] Kohn W, Sham L. Self-consistent equations including exchange and correlation effects. Phys Rev 1965;140:A1133https://doi.org/10.1103/PhysRev.140.A1133.
[44] Lee CTW, Yang T, Parr RG. Development of the Colle-Salvetti correlation-energy formula into a functional of the electron density. Phys Rev B 1988;37:785–9https://doi.org/10.1103/PhysRevB.37.785.
[45] Becke AD. Density-functional thermochemistry. III. The role of exact exchange. J Chem Phys 1993;98:5648–52https://doi.org/10.1063/1.464913.
[46] Frisch MJ, Trucks GW, Schlegel HB, Scuseria GE, Robb MA, Cheeseman JR, et al. Gaussian 09, revision B.01. Wallingford CT: Gaussian Inc.; 2009.
[47] Casida ME, Jamorski C, Casida KC, Salahub DR. Molecular excitation energies to high-lying bound states from time-dependent density-functional response theory: characterization and correction of the time-dependent local density approximation ionization threshold. J Chem Phys 1998;108:4439–49https://doi.org/10.1063/1.475855.
[48] Bauernschmitt R, Ahlrichs R. Treatment of electronic excitations within the adiabatic approximation of time dependent density functional theory. Chem Phys Lett 1996;256:454–64https://doi.org/10.1016/0009-2614(96)00440-X.
[49] Gross EKU, Kohn W. Time-dependent density-functional theory. Adv Quant Chem 1990;21:255–91https://doi.org/10.1016/S0065-3276(08)60600-0.
[50] Gross EKU, Kohn W. Local density-functional theory of frequency-dependent linear response. Phys Rev Lett 1985;55:2850–2https://doi.org/10.1103/PhysRevLett.55.2850.
[51] Runge E, Gross EKU. Density-functional theory for time-dependent systems. Phys Rev Lett 1984;52:997–1000https://doi.org/10.1103/PhysRevLett.52.997.

Journal of Luminescence 220 (2020) 116955

Contents lists available at ScienceDirect

Journal of Luminescence

journal homepage: http://www.elsevier.com/locate/jlumin

Facile structure-modification of xanthenone based OLED emitters exhibiting both aggregation induced emission enhancement and thermally activated delayed fluorescence

Sohrab Nasiri, Simas Macionis, Dalius Gudeika, Dmytro Volyniuk, Juozas V. Grazulevicius *

Department of Polymer Chemistry and Technology, Kaunas University of Technology, Radvilenu pl. 19, LT-50254, Kaunas, Lithuania

ARTICLE INFO

Keywords:
Organic light-emitting diode
Xanthenone
Thermally activated delayed fluorescence
Aggregation induced emission enhancement

ABSTRACT

Four new donor-acceptor compounds were designed, synthesized and investigated by theoretical and experimental approaches aiming to estimate effect of the structure of a donor on the properties of potential OLED emitters. Because of the different electron-donating abilities of the nitrogen-containing heterocycles, derivatives of xanthenone containing di-*tert*-butyl-carbazolyl, di-*tert*-butyl-acridanyl, di-*tert*-butyl-phenothiazinyl and penoxazinyl moieties exhibited different photophysical behavior. Because of big dihedral angles between the donors and acceptor as well as because of possibility of rotation around N–C bond, the designed compounds were characterized by thermally activated delayed fluorescence and aggregation induced emission enhancement effect. Twice higher photoluminesce quantum yields reaching 38% in doped films were obtained for compounds containing di-*tert*-butyl-carbazolyl and di-*tert*-butyl-acridanyl moieties as compared to those observed for compounds with the donors containing S and O heteroatoms. Strong effect of the donor substituents on charge injection (ionization potentials were in the range of 5.67–5.96 eV) and charge-transporting properties (hole and electron mobilities were in a wide range from 6.3×10^{-8} to 6.3×10^{-4} $cm^2V^{-1}s^{-1}$ at electric field of 2.5×10^5 V cm^{-1}) was detected. The differently substituted compounds were utilized as emitters in OLEDs. Higher maximum values of external quantum efficiency (up to 3.5%) were observed for OLEDs based on emitters with nitrogen containing donors relative to estimated for OLEDs based on emitters containing di-*tert*-butyl-phenothiazinyl and penoxazinyl moieties.

1. Introduction

Because of the possibly of full exciton harvesting in organic light emitting diodes (OLEDs) and absence of toxic and rare-earth atoms in molecule structures of organic materials exhibiting thermally activated delayed fluorescence (TADF), they have attracted great attention [1–4]. Many interesting combinations of donor and acceptor moieties resulting in efficient TADF compounds were reported [5,6]. Some TADF emitters are characterized by close to unity photoluminescence quantum yields (PLQYs) in host-guest systems (light-emitting layers of OLEDs) where hosts are used to overcome aggregation-induced quenching which is commonly observed for organic dyes [7,8]. Donor-acceptor (D-A) compounds containing xanthenone acceptor unit and the different donor moieties showed efficient TADF with PLQYs in the range of 81–99% in an appropriate host [9–11]. These studies have revealed, the xanthenone is well suitable acceptor for design of efficient TADF emitters apparently due to its structure rigidity, high triplet level (*ca.* 3.19 eV [12]), and high electron affinity caused by carbonyl group. Therefore, it is predictable that further structural modification of donor-containing xanthenone derivatives may lead to development of TADF emitters with aggregation-induced emission enhancement (AIEE) property [13]. Because of complicated deposition process of host-guest systems with no gradient of concentration of TADF emitter within OLED light-emitting layer, it is a hot topic to develop emitters with the combination TADF and AIEE properties which results in high PLQYs of neat films. Such compounds can be used for the preparation of emitting layers of OLEDs with the simple structure [14].

In most of D-A molecular structure of TADF emitters, donors directly or *via* appropriate spacers are linked to acceptors mostly through N–C bond [9–11]. Because of the steric repulsion (restriction), such linkage allows to get high dihedral angle between the electron donating and accepting units resulting in enhanced intramolecular charge transfer

* Corresponding author.
E-mail address: juozas.grazulevicius@ktu.lt (J.V. Grazulevicius).

https://doi.org/10.1016/j.jlumin.2019.116955
Received 27 August 2019; Received in revised form 19 November 2019; Accepted 6 December 2019
Available online 9 December 2019

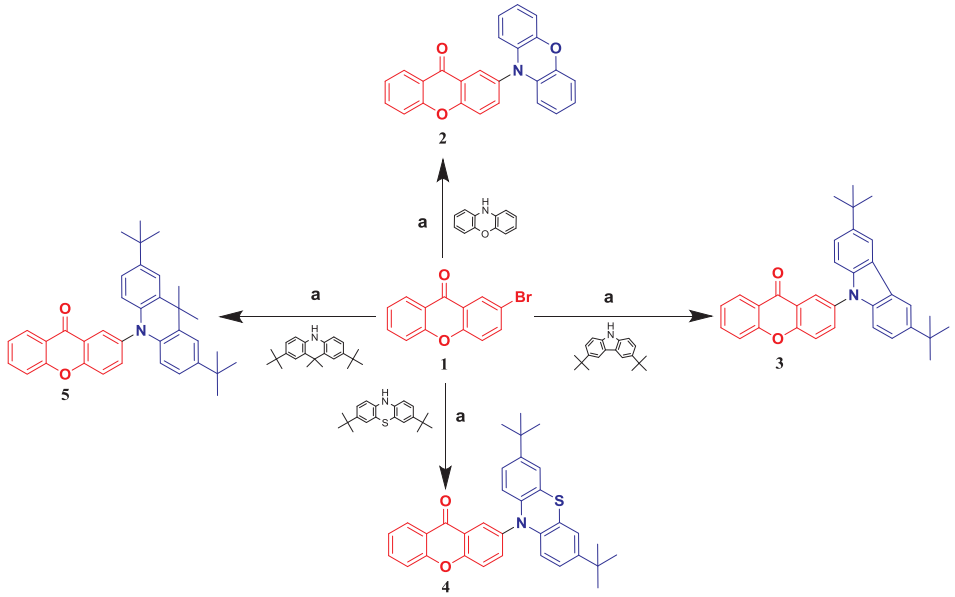

Scheme 1. The synthetic routes to xanthenone-based derivatives **2**–**5.** Reagents and conditions: a) $Pd(OAc)_2$, P (*t*-Bu)$_3$·HBF_4, *t*-BuONa, toluene, 120 °C, 24 h.

(ICT), effective HOMO-LUMO separation and small singlet-triplet splitting ($\Delta E_{ST} < 0.1$ eV) [15,16]. All these properties are required for efficient TADF. On the other hand, "free" movements of D(A) units around N–C bond may result in AIEE effect when these movements are completely stuck in solid-state [17,18]. We partly aimed to prove this assumption in the current work. Although there are examples of usage of xanthenone acceptor in design of TADF emitters [19–22], xanthenone-based TADF compounds containing *tert*-butyl-substituted donor units linked through N–C bond are absent in the literature, to the best of our knowledge. Aiming to develop xanthenone-based compounds with combination of both TADF and AIEE properties in this study, xanthenone as acceptor was linked through N–C bond with the different donor moieties (carbazole, acridan, phenothiazine or phenoxazine). TADF and AIEE properties of new xanthenone-based emitters were investigated by steady-stay and time resolved luminescence spectroscopy at different conditions. Considerably better electroluminescent performances were observed for devices based on xanthenone emitters containing di-*tert*-butyl-carbazolyl and di-*tert*-butyl-acridanyl moieties in comparison to those of devices based on xanthenone emitters containing di-*tert*-butyl-phenothiazinyl and penoxazinyl moieties. These findings provide hints for further synthesis of efficient TADF emitters.

2. Experimental

2.1. Instrumentation

^{13}C NMR, ^{1}H NMR spectra were obtained using a Varrian Unity Inova (300 MHz (^{1}H) and 75 MHz (^{13}C)). Mass (MS) spectra, infrared (IR), elemental, differential scanning calorimetry (DSC), thermogravimetric analysis (TGA) measurements were carried out as described earlier [23]. Absorption, photoluminescence (PL) spectra of dilute solutions and of the films were recorded as described previously [24]. To record PL and phosphorescence spectra as well as PL decays at different temperatures, variable temperature liquid nitrogen cryostat (Optistat DN2) was used. To record the dependencies of delayed emission intensity on laser flux of the samples, the Edinburgh Instruments FLS980 spectrometer and a PicoQuantLDH-D-C-375 laser (wavelength 374 nm) were utilized. Theoretical calculations had been carried with Gaussian 16 and Gaussview 6 softwares. Ionization potential measurements of the solid samples were performed by photoelectron emission method in air [25]. Cyclic voltammetry (CV) measurements of the liquid samples were carried out as described earlier [26]. Electron and hole mobilities (μ_e, μ_h) were studied by time of flight technique [27]. OLEDs were created with vacuum deposition of inorganic and organic layers onto cleaned ITO coated glass, vacuum of 10^{-6} Torr was used. The active area of the obtained devices was 3×6 mm^2, furthermore measurement was made after the creation of the device, in the air without passivation. The luminance voltage and current density voltage dependences were measured with brightness and semiconductor parameters analyzer (HP 4145A) was measured using a calibrated photodiode and electroluminescence spectra were recorded with an Ocean Optics modular spectrometer [28].

3. Results and discussion

3.1. Synthesis and characterization

The synthesis route to **1**–**5** derivatives is shown in Scheme 1. The starting compound (**1**) was prepared according to the earlier reported procedure [29]. Final compounds **2**–**5** were synthesized by a Buchwald-Hartwig coupling of **1** with the corresponding donors (10*H*-phenoxazine, 3,6-di-*tert*-butyl-9*H*-carbazole, 3,7-di-*tert*-butyl-10*H*-phenothiazine and 2,7-di-*tert*-butyl-9,9-dimethyl-9,10-dihydroacridine, see Supporting Information). The chemical structures were confirmed by NMR, IR spectroscopies, mass spectrometry and elemental analysis. The results were in agreement with the theoretical values. All the compounds showed good solubility in organic solvents.

3.2. Geometries and frontier orbitals

The molecular configuration and the frontier molecular orbital distribution of **2**–**5** were analyzed by density functional theory (DFT)

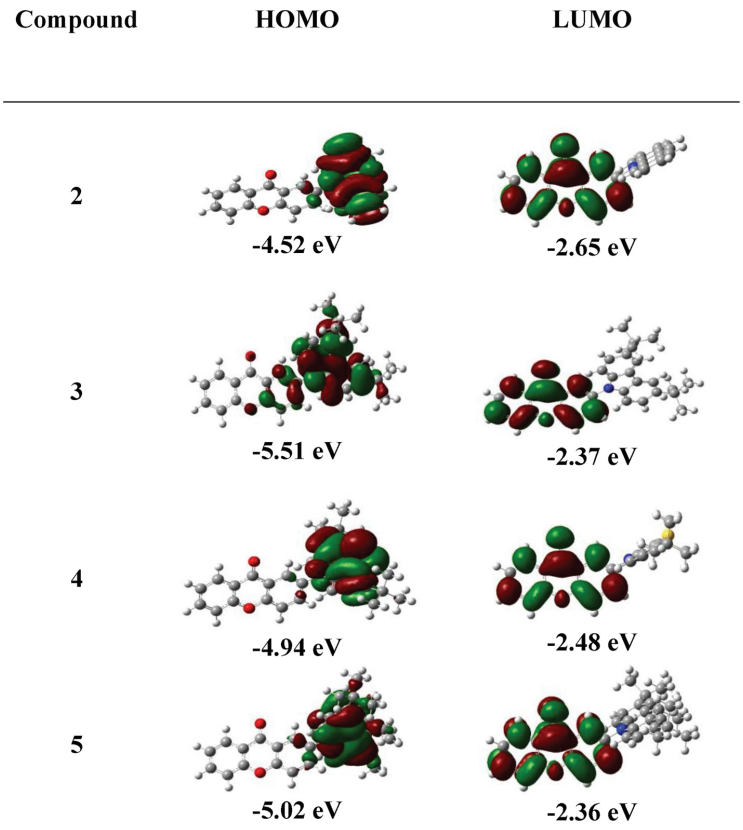

Fig. 1. HOMO and LUMO of **2**–**5** calculated at B3LYP/6-311G (d,p) level.

Table 1
Thermal characteristics of **2**–**5**.

Derivative	T_m (°C)[a]	T_{cr} (°C)[b]	T_g (°C)[c]	T_d (°C)[d]
2	196	123	70	331
3	255	193	116	351
4	174	–	108	336
5	235	165	100	311

Determined by DSC, scan rate 10 °C/min, nitrogen atmosphere.
[a] T_m is melting temperature.
[b] T_{cr} - crystallization temperature.
[c] T_g is glass-transition temperature.
[d] T_d is the temperature of the onset of thermal degradation; scan rate 20 °C/min, nitrogen atmosphere.

calculations using Gaussian 16 software at the B3LYP/6-311G (d,p) level. The theoretical geometries and the distribution of the highest occupied molecular orbital (HOMO) and the lowest unoccupied molecular orbital (LUMO) of compounds **2**–**5** are presented in Fig. 1. HOMO are mainly localized on di-*tert*-butyl carbazolyl, di-*tert*-butyl acridanyl, di-*tert*-butyl phenothiazinyl and penoxazinyl moieties, while LUMO mainly locate on xanthenone moiety. The clear separation of HOMO and LUMO molecular orbitals determined small calculated ΔE_{ST} values of (0.09, 0.11, 0.10 and 0.15) eV for **2**, **3**, **4** and **5**, respectively. The HOMO energy levels of the compounds were in the range of −5.51 to −4.52 eV. The LUMO energy levels of the four molecules were found to be close due to the same acceptor moiety of xanthenone. The deepest HOMO was observed for compound **3** containing di-*tert*-butyl-carbazolyl donor moiety, while the most shallow HOMO was observed for compound **2**, containing phenoxazine donor unit.

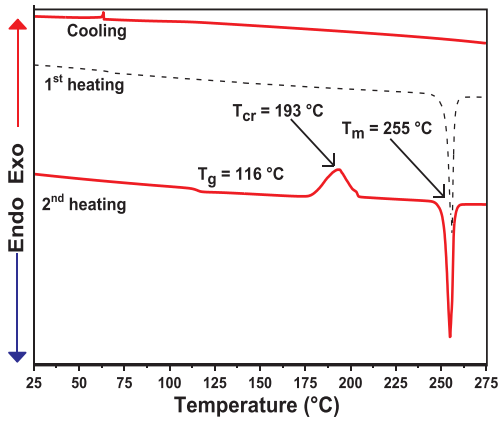

Fig. 2. DSC curves of compound 3.

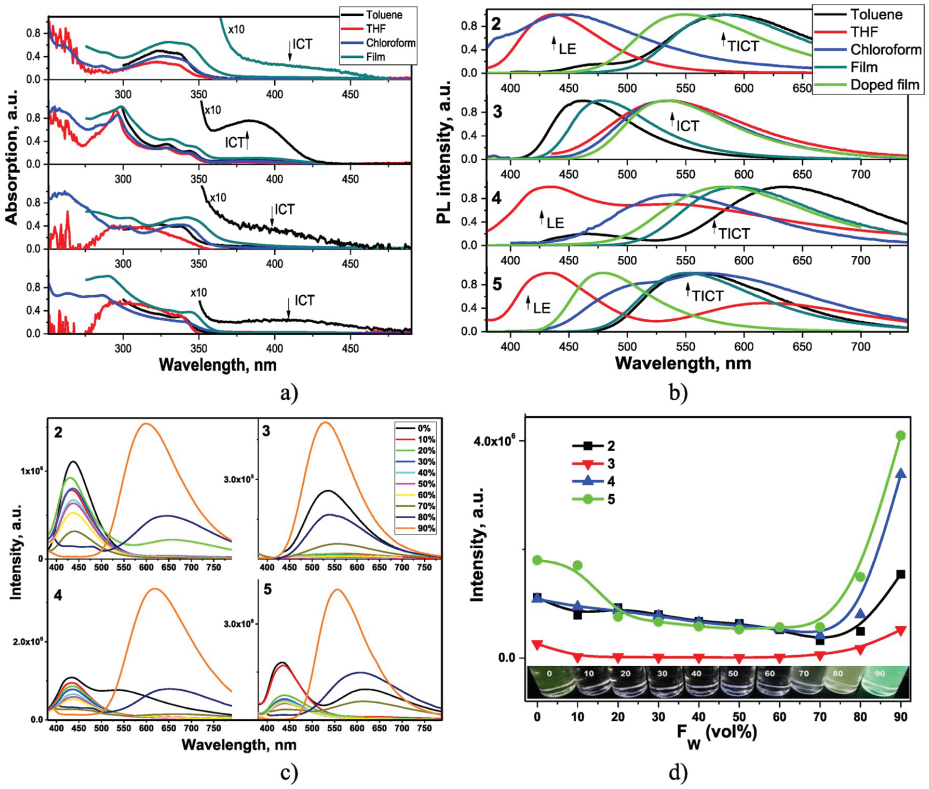

Fig. 3. Absorption (a) and photoluminescence (b) spectra of compounds **2**–**5** dispersed in different media. PL spectra (c) and emission intensities versus volume fractions of water (F_W) (d) of compounds **2**–**5** dispersed in THF/water mixtures (the inset is photo of samples under UV excitation for compound **3**). Doped films were spin-coated taking 10 wt% dopant concentration in *m*CP.

3.3. Thermal properties

The behavior under heating of compounds **2**–**5** were studied by DSC and TGA under nitrogen atmosphere. The data are presented in Table 1. The compounds showed rather high thermal stability. The temperatures of the onsets of thermal degradation (T_d) were in the range of 311–351 °C (Fig. 2 and Fig. S6). Compound **3** with di-*tert*-butyl-carbazolyl moieties exhibited the highest T_d of 351 °C.

Compounds **2**–**5** were obtained after purification as crystalline substances. They showed endothermic melting (T_m) signals in the initial heating scans. However, all of them could be transformed into the glassy state by cooling from the melts. DSC thermograms of derivative **3** are shown in Fig. 2. The crystalline sample of **3** showed T_m signal at 255 °C on the first heating and formed glass upon cooling. In the second heating scan, the glass transition temperature (T_g) was observed at 116 °C, and on further heating an exothermic peak due to crystallization signal appeared at 193 °C to give crystals, which melted at 255 °C. Derivatives **2** and **5** demonstrated the analogous behavior during the DSC scans (Table 1, Figs. S6a and c). In the first heating scan of derivative **2**, T_m signal was observed at 196 °C. When the molten sample was cooled down, it formed glass. During the second DSC scan, the amorphous sample demonstrated T_g signal at 70 °C followed by crystallization signal at 123 °C and T_m signal at 196 °C. Compound **5** melted at 235 °C and formed amorphous material upon cooling. The amorphous sample demonstrated T_g signal at 100 °C followed by crystallization at 165 °C and T_m at 235 °C. Derivative **4** was also obtained after the synthesis and purification as crystalline material, however it demonstrated slightly different behavior in the DSC measurements (Fig. S6b). The crystalline sample of **4** melted at 174 °C on the first heating scan. It formed solid amorphous material upon cooling. When the amorphous sample was heated again, the T_g was observed at 108 °C and on further heating no peaks due to crystallization and melting appeared.

The established T_g values for **3**–**5** ranged from 70 to 116 °C. The lowest T_g was observed for compound **2**, having no *tert*-butyl substituents. Derivatives **3**–**5** containing *tert*-butyl-substituted donor moieties exhibited elevated glass transition temperatures. The presence of relatively bulky *tert*-butyl substituents apparently enhances intermolecular interaction and hiders intermolecular rotations. Compound **3** containing di-*tert*-butyl-carbazolyl moiety exhibited the highest T_g. It also showed the highest melting point and the highest temperature of the onset of thermal degradation.

3.4. Photophysical properties

Effects of the different donor substituents of xanthenone in derivatives **2**–**5** on their electronic structures were investigated by steady-state absorption and photoluminescence (PL) spectroscopy. Absorption and/or PL spectra of the solutions in the solvents of different polarity (toluene, THF, chloroform) and solid-state (pure and doped films) media were recorded (Fig. 3). Absorption bands in the regions of *ca.* 250–300 nm and 300–350 nm are attributed to superposition of the π→π* and n→π* transitions of the donor moieties and xanthenone units,

Table 2
Spectroscopic characterisctics of the solutions and solid films of compounds **2**–**5**.

Compound	Solution			Solid Films							
	Toluene			Non-doped						Doped	
	λ_{abs}^{max}, nm	λ_{F}^{max}, nm	Φ_F, %	λ_{abs}^{max}, nm	λ_{F}^{max}, nm	Φ_F, %	E_S, eV	E_T, eV	ΔE_{ST}, eV	λ_{F}^{max}, nm	Φ_F, %
2	327	590	0.6	330	580	4	2.39 (2.14)	2.34 (2.12)	0.05 (0.02)	549	14
3	293	457	15	298	476	19	2.81 (2.80)	2.74 (2.60)	0.07 (0.2)	534	38
4	331	638	0.3	277	595	5	2.44 (2.35)	2.39 (2.33)	0.05 (0.02)	585	7
5	331	563	2	290	549	14	2.61 (2.30)	2.51 (2.28)	0.10 (0.02)	479	36

respectively (Fig. 3a). Low-energy absorption bands (tails), located in 350–470 nm region, can be attributed to intramolecular charge transfer (ICT) between xanthenone and the donor moieties in the ground state. The strongest ICT absorption band was detected for xanthenone derivative **3** containing *tert*-butylated carbazole units (Fig. 3a). As a result, pure ICT emission with broad non-structured PL spectrum with full width at half maximum (FWHM) of 78–130 nm was observed for the solutions and film of compound **3** (Fig. 3a). Its PL spectra were characterized by single broad unstructured band which shifted to low-energy region with increasing media polarity (Fig. 3b). In case of the dispersions of compounds **4**, and **5** in different media, rather weak ICT absorption bands were detected. ICT absorption transitions were not detected for the solutions of compound **2** but detected for its films. PL spectra of compounds **2**, **4**, and **5** dispersed in different media (Fig. 3b) were characterized by either high-energy or low-energy bands (or their overlapping). For example, PL spectrum of THF solution of compound **5** was characterized by two bands with maxima at 432 and 626 nm, which were related to recombination of local (LE) and ICT (co-called, twisted ICT (TICT) [30]) excitons, respectively. Indeed, the different twisting (rotation) of donors interacting with solvents of different polarity could be expected which resulted in media-dependent LE and TICT fluorescence. PL spectra of the films of compounds **2**–**5** were characterized by single bands related, most probably, to emissive recombination of excited ICT states because of the restriction of free twisting (rotation) of donors around N–C band in solid-state (Fig. 3b). It should be noted that dual emission was previously observed for the derivatives of xanthenone substituted by electron donating units through N–C bond [10]. The wavelengths of maxima of the main absorption and fluorescence bands

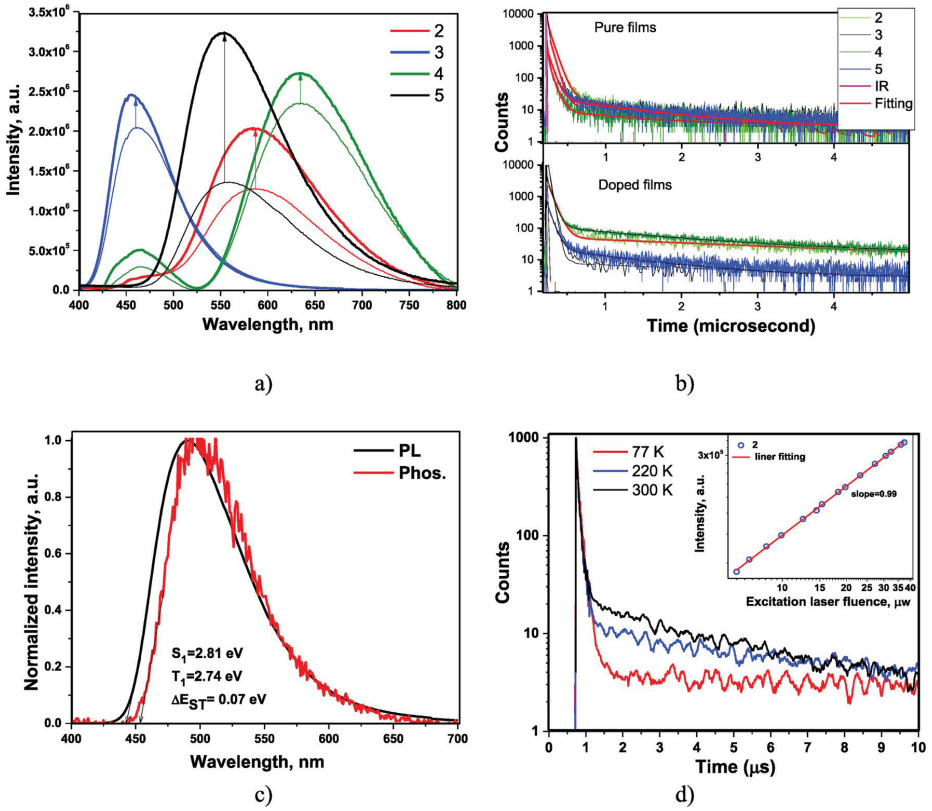

Fig. 4. PL spectra of as prepared (thin lines) and deoxygenated (thick lines) toluene solutions (a); PL decay curves of pure and doped (10 wt% in *m*CP) films of **2**–**5** (b); PL and phosphorescence (Phos) spectra (c) of film of compound **3** recorded at 77 K; and PL decays of the film of compound **2** doped in mCP recorded at different temperatures (d). The inset demonstrates dependence of delayed emission intensity on laser flux (delay of 1 μs).

Table 3
Electrochemical characteristics, HOMO/LUMO energies, and hole and electron mobilities of compounds **2**–**5**.

Compound	E^{ox}_{onset} *vs* Fc, (V)[a]	EA_{CV} (eV)[b]	IP_{CV} (eV)[c]	E_g^{opt} (eV)[d]	IP_{PE} (eV)[e]	μ_h ($cm^2\ V^{-1}\ s^{-1}$)[f]	μ_e ($cm^2\ V^{-1}\ s^{-1}$)[f]
2	0.30	1.57	5.02	3.45	5.70	$2.6{\cdot}10^{-4}$	$1.3{\cdot}10^{-4}$
3	0.31	2.05	5.03	2.98	5.95	$6.4{\cdot}10^{-6}$	$1.7{\cdot}10^{-6}$
4	0.16	1.93	4.82	2.89	5.77	$1{\cdot}10^{-7}$	$1.2{\cdot}10^{-7}$
5	0.44	1.73	5.21	3.48	5.70	$4.6{\cdot}10^{-5}$	$2{\cdot}10^{-5}$

[a] E^{ox}_{onset} as measured *vs*. ferrocene/ferrocenium.
[b] EA_{CV} was calculated by the equation $EA_{CV} = -(|IP_{CV}| - E_g^{opt})$.
[c] IP_{CV} are ionization potentials calculated by the formula $|-(1.4 \times 1e^- \times E^{ox}_{onset}$ *vs* Fc/V) − 4.6| eV [32].
[d] E_g^{opt} estimated as the ratio $1240/\lambda_{of\ UV\ spectra\ (in\ toluene)}$.
[e] IP_{PE} - ionization potential estimated from electron photoemission spectra.
[f] μ_h and μ_e are hole and electron mobility at electric field $3{\cdot}10^5$ V cm^{-1}, respectively.

are shown in Table 2.

PLQYs of solid films of compounds **2**–**5** were found to be higher than those of their toluene solutions (Table 2). This observation can apparently be attributed to AIEE phenomenon which may be observed due the restriction of movements of molecular units in solid-state [31]. To prove this assumption, PL spectra of the dispersions of the studied compounds in the THF/water mixtures with different volume water fractions (F_W) were recorded. They show emission intensities before and after formation of aggregates at high F_W (Fig. 3c). Indeed, higher emission intensity was observed for THF/water mixtures with high F_W in comparison to those of THF solutions highlighting AIEE effect for all the studied compounds (Fig. 3d). As it was discussed above, THF solutions of compounds **2, 4**, and **5** were characterized by LE fluorescence. Its intensity monotonically decreased with increasing F_W, thus with increasing polarity of THF/water mixture (Fig. 3c). When aggregates started to be formed at F_w ~60–70%, red-shifted PL spectra were obtained since TICT fluorescence dominated in solid-state.

E_S is singlet energy and E_T is triplet energy which were obtained from PL spectra and phosphorescence spectra (Fig. S7); $\Delta E_{ST} = E_S - E_T$. The theoretical values of E_{S1}, E_{T1}, ΔE_{ST} are depicted in parentheses.

Despite the identified AIEE effect for compounds **2**–**5**, PLQYs of their net films were much below the unity (Table 2). In addition, more than two times lower PLQYs were obtained for derivatives **2** and **4** containing S and O heteroatoms in the donor moieties (di-*tert*-butyl-phenothiazine and penoxazine) than those observed for compounds **3** and **5** containing only nitrogen heteroatom in the donor moieties. Relatively low PLQYs may be related to special intermolecular interactions which are apparently different for compounds **2**, **4** and **3, 5**. This assumption is in good agreement with enhanced PLQY values of compounds **2**–**5** molecularly dispersed in *m*CP host in which the influence of intermolecular interactions was decreased (Table 2).

Since relatively high dihedral angles between donor and acceptor were observed for compounds **2** and **3** by the theoretical calculations (Fig. 1), triplets harvesting was expected *via* reverse intersystem crossing. Indeed, intensity of fluorescence of toluene solutions of all the studied compounds considerably increased after deoxygenation (Fig. 4 a). This observation supports the above presumption about harvesting of triplets. In addition, long-lived components of PL decays were observed for pure and doped films of derivatives **2**–**5** (Fig. 4b). To attribute these long-lived PL decay components to TADF, first singlet (E_S) and triplet (E_T) energy levels had to be measured. Phosphorescence and photoluminescence spectra of the films of **2**–**5** were recorded at temperature of liquid nitrogen (77 K) and E_S and E_T were calculated using wavelengths of the on-sets of these spectra by empiric formula E_S (E_T) = $1240{\cdot}\lambda^{-1}$ (Fig. 3 and Fig. S7, Table 3). Using these energy levels, small values of singlet-triplet splitting ΔE_{ST} ranging from 0.05 to 0.1 eV were obtained for compounds 2–5 in non-doped films (Table 2). Such small ΔE_{ST} values, allow to assume that long-lived fluorescence is of TADF origin (Fig. 4 b). To confirm this assumption, we additionally recorded PL decays at different temperatures and dependence of delayed emission intensity on laser flux at room temperature for the films of molecular

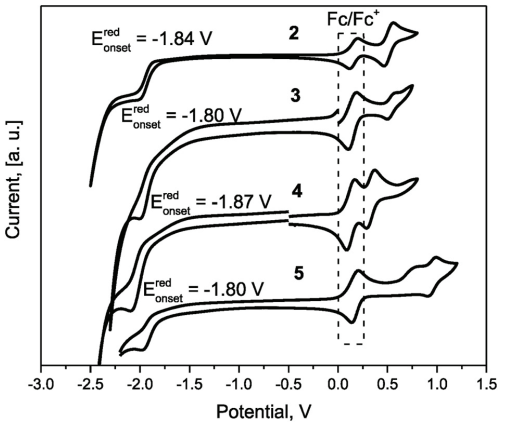

Fig. 5. Cyclic voltammograms of dilute solutions of compounds **2**–**5** in dichloromethane (sweep rate - 100 mV/s).

mixtures of compounds **2**–**5** with mCP (Fig. 4d and Fig. S8). Both increasing intensity of delayed emission with increasing temperatures and linear dependencies of delayed emission intensity on laser flux with slope close to unity definitely prove TADF origin of long-lived fluorescence.

To investigate TADF properties of compounds 2–5, we fitted PL decays of their non-doped and mCP-hosted films. Results of fitting of PL decays of compounds 2–5 are summarized in Table S1. In addition, the radiation transition rates for the films of the compounds 2–5 doped in mCP was calculated (Table S2). The studied compounds in solid-state exhibited relatively high K_{RISC} values which are only slightly lower than those of highly efficient TADF emitters [15].

3.5. Electrochemical properties

Electrochemical properties of compounds **2**–**5** were evaluated by cyclic voltammetry (CV) measurements using ferrocene as the internal standard. Derivatives **3** and **5** exhibited quasireversible oxidation behavior, while compounds **2** and **4** displayed reversible oxidation which could be assigned to the oxidation of appropriate donors (Fig. 5). All the derivatives showed similar quasireversible reduction signals with potentials of around −1.80 V, which could be attributed to the reduction of xanthenone moiety. Ionization potentials (IP_{CV}) of 5.02, 5.03, 4.82 and 5.21 eV were estimated for **2**, **3**, **4**, and **5**, respectively from the onset potentials of their oxidation curves. The highest ionization potential was observed for derivative **3**, having *tert*-butyl-carbazolyl moiety. Electron affinity (EA_{CV}) values were determined according to the equation $EA_{CV} = E_g^{opt} - (|IP_{CV}| -)$ eV. They were found to be of 1.57 eV,

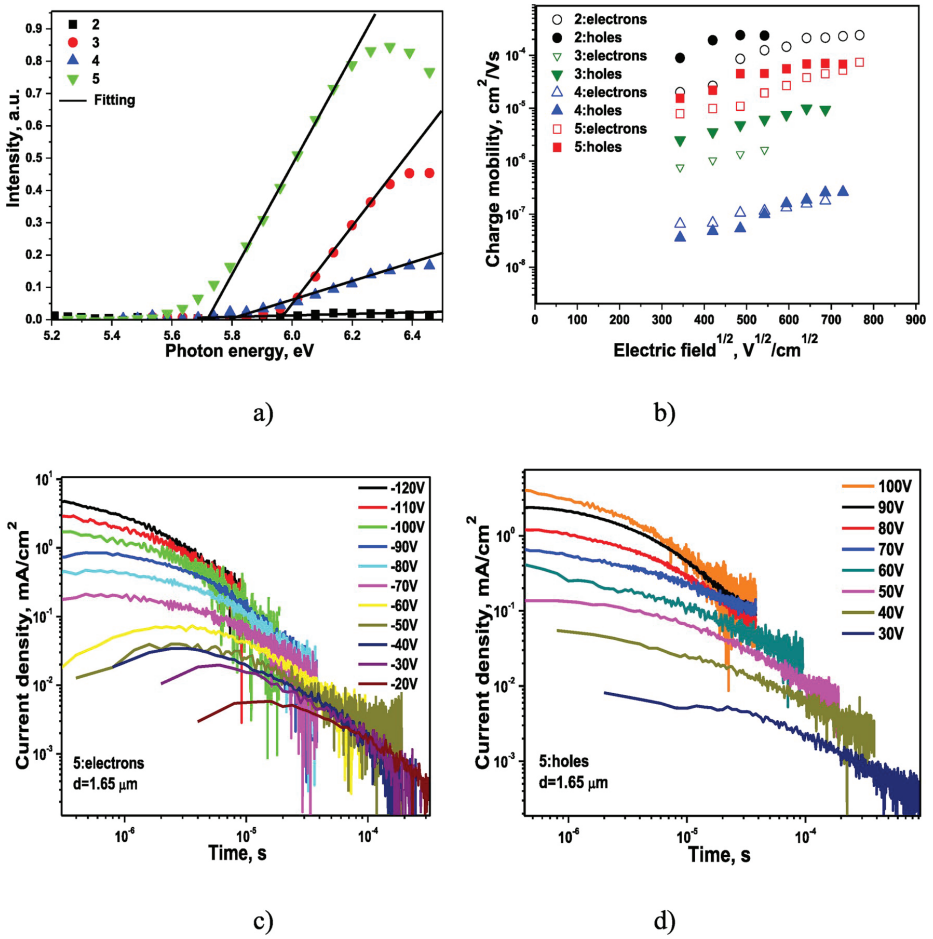

Fig. 6. Photoelectron emission spectra (a), electric fields dependences of electron and hole mobilities (b) for the layers of compounds **2**–**5**, and electric filed dependences of electron (c) and hole (d) TOF transients for the layer of compound **5**.

Table 4
Out-put parameters of OLEDs.

Device	V_{on} (V[a]	L_{max} (cd/m^2)[b]	L at 8 V (cd/m^2)	PE_{max} (lm/W)[c]	CE_{max} (cd/A)[d]	EQE_{max} (%)[e]	CIE coordinates (X,Y)
PXZ	3.2	12500 (8.5 V)	10900	4.2	5.3	1.7	(0.403,0.526)
CZ	4.9	2400 (10.6 V)	820	3.7	2.8	1.8	(0.159,0.111)
PTZ	3.9	8800 (9.9 V)	4600	2.4	3.9	1.4	(0.401,0.473)
ACR	3.8	20900 (9.2 V)	14800	7.6	11.7	3.5	(0.307,0.571)

[a] V_{on} is turn on voltage.
[b] L_{max} is maximum luminance achieved at the certain applied voltages.
[c] PE_{max} is maximum power efficiency.
[d] CE_{max} is maximum current efficiency.
[e] EQE_{max} is maximum external quantum efficiency.

2.05 eV, 1.93 eV and 1.73 eV, respectively.

3.6. Photoelectron emission and charge transporting properties

Ionization potentials (IP_{PE}) of compounds **2**–**5** in solid-state were obtained by electron photoemission spectroscopy in air. IP_{PE} values of 5.7, 5.95, 5.77, and 5.7 eV were acquired for the films of **2**, **3**, **4**, and **5**, respectively by extrapolation of linear parts of electron photoemission spectra to the abscissa axis (Fig. 6a). IP_{PE} values of the films of **2**–**5** were higher than IP_{CV} values but they followed the similar trends (Table 4). The highest ionization potential again was observed for compound **3**, containing *tert*-butyl-carbazolyl donor moiety. The IP_{PE} values of compounds **2**–**5** were in good agreement to those previously reported for non-doped films of xanthenone-based TADF emitters containing strong

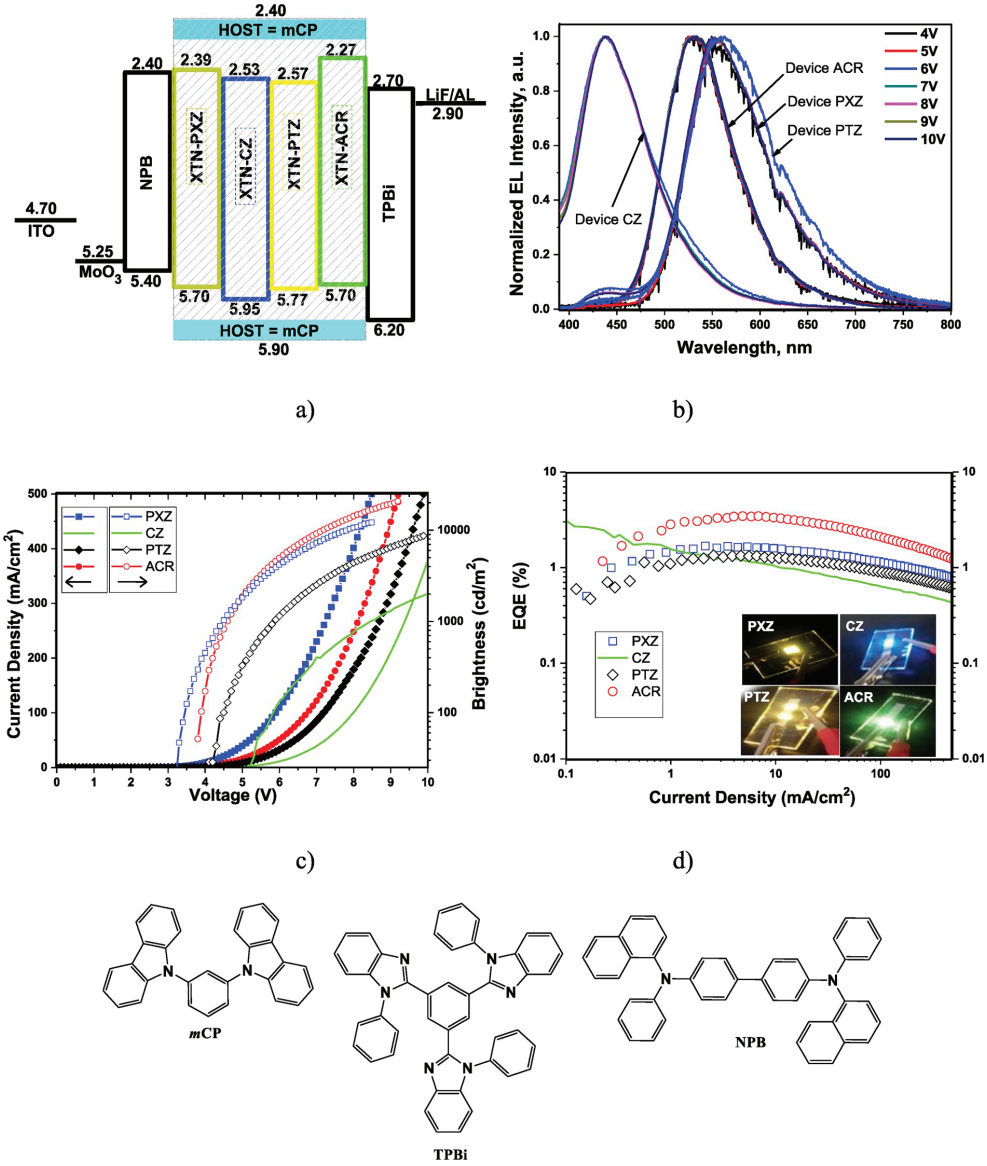

Fig. 7. Energy diagrams (a); EL spectra (b) at the different voltages; voltage-current density and voltage-brightness dependencies (c); and external quantum efficiencies (d) of the fabricated OLEDs. Insets are photos of the tested samples; (e) molecular structures of the organic compounds used in the devices.

donors [10].

Hole and electron transport was detected for compounds **2**–**5** by TOF measurements (Fig. 6 b). The transit times recorded at different positive (for holes) and negative (for electrons) external voltages on ITO electrode and at room temperatures were used to calculate charge mobilities (Fig. 6c,d and Fig.S9). The TOF transients were not characterized by well observed plateau and tail indicating low dispersive or even dispersive hole and electron transport in neat films of **2**–**5**. Dispersive charge transport is typical for highly twisted TADF compounds [33]. Hole and electron mobility values for compounds **2**–**5** were found to be strongly sensitive to the nature of donor substituents (Fig. 6b). Charge mobility values were found in very large range from *ca.* $9.6{\cdot}10^{-8}$ to $2.4{\cdot}10^{-4}$ $cm^2V^{-1}s^{-1}$ at applied electric field of 3×10^5 V cm^{-1} and decreased in the order **2**>**5**>**3**>**4** (Fig. 6b, Table 3). Such big differences can apparently be explained not only by the different donor substituents but also by the different molecular packing in solid-state. Since the highest charge mobilities were obtained for *tert*-butyl-group-free compound **2**, it seems that *tert*-butyl substituents slightly reduced charge mobilities apparently because of decreased HOMO-HOMO and LUMO-LUMO overlapping between neighboring molecules in vacuum-deposited

films. Up to *ca.* 4 times lower, electron mobility values were obtained for compounds **2**–**5** in comparison to their hole mobilities at electric field of 3×10^5 V cm^{-1} (Fig. 6b).

3.7. Electroluminescent properties

Since compounds **2**–**5** were characterized by appropriate HOMO/LUMO values for charge-injections, bipolar charge-transporting properties, and relatively high PLQYs in *m*CP-based guest-host systems, they were employed as emitters in electroluminescent devices. The fabricated devices were named as **PXZ, CZ, PTZ** and **ACR** depending on the emitters used in OLED structures ITO/MoO_3 (1 nm)/NPB (65 nm)/**2, 3, 4** or **5** (10 wt %):*m*CP (30 nm)/TPBi (40 nm)/LiF (0.5 nm)/Al. According to the equilibrium energy diagrams of these devices, good charge-injection processes from electrodes to light-emitting layers can be expected due to the presence of additional layers (MoO_3 and LiF as hole and electron injection layers and NPB and TPBi as hole and electron transporting layers, respectively) (Fig. 7 a). As a result, EL spectra of devices **PXZ, PTZ** and **ACR** were in agreement with PL spectra of emitters **2, 4**, and **5**, respectively. This observation indicates exciton radiative recombination within the light-emitting layers (Fig. 7b). The CIE coordinates of the emissions of the fabricated devices are collected in Table 4 and presented in the CIE color diagram (Fig. S10). The EL spectra of device **ACR** were found to be independent on the voltage. Meanwhile, low-intensity bands (the residual blue emission) appeared in EL spectra of devices **PXZ** and **PTZ** at higher voltages since charge-blocking layers were not used in the device structure (Fig. 7a). This observation can be attributed to the emission of NPB (or TPBi) due to the shift of recombination zone to hole- or electron-transporting layer NPB or TPBi. The EL spectra of device **CZ** was blue-shifted in comparison to PL spectrum of compound **3** (Table 2). This observation shows that hole-electron recombination did not occur within light-emitting layer. It was completely shifted to electron-transporting layer TPBi, apparently, because of the energy barrier between LUMO-LUMO energy levels of compound **3** and TPBi. Thus, device **CZ** did not reflect electroluminescent properties of emitter **3**, therefore, its characteristics are not compared with those of the other devices fabricated in this work. The lowest turn-on voltage of 3.2 V was observed for device **PXZ** based on compound **2** due to its highest and balanced hole and electron mobilities (Figs. 6b and 7c). The maximum brightness of devices **PXZ** and **ACR** exceeded 10000 cd m^{-2} due to high PLQY value of light-emitting layers and their emission in green-yellow region to which human eyes are sensitive (Fig. 7c). The best external quantum efficiencies (EQE) of 3.5% was demonstrated by device **ACR** since the emitter **5** showed high PLQY in its solid solution in *m*CP and relatively high charge mobilities (Fig. 7 d, Table 2). The fabricated device **ACR** did not demonstrate all potential of emitter **5** exhibiting TADF and AIEE effects. Experimental EQE was much lower than theoretically possible one. The theoretical EQE exceeding of 11% was calculated by the formula $\eta_{ext} = \gamma \times \varphi_{PL} \times \chi \times \eta_{out}$ using the charge-balance factor $\gamma = 1$, the efficiency of exciton production $\chi = 1$ (as for TADF emitter), the outcoupling efficiency $\eta_{out} = 0.3$, and $\varphi_{PL} = 0.36$ for the film *m*CP:**5** measured in air. Nevertheless, the results of this work suggests that usage of xanthenone emitters containing *tert*-butyl-acridanyl moieties can result in considerably better OLED characteristics in comparison to those of devices based on xanthenone emitters containing *tert*-butyl-carbazolyl moiety.

4. Conclusions

To establish the structure-property relationship between acceptor and four different donor moieties, we systematically studied their photophysical, thermal, electrochemical, and electroluminescent properties of donor disubstituted xanthenones. Some derivatives exhibited high thermal stability with the temperatures of decomposition onsets up to 351 °C. The compounds were found to be glass-forming with glass transition temperatures ranging from 70 to 116 °C. Twice higher solid-state photoluminesce quantum yields of 38% were observed for compounds containing *tert*-butyl-carbazolyl and *tert*-butyl-acridanyl moieties compared with those of compounds containing S and O heteroatoms in donor moieties. Ambipolar charge transport was detected in the layers of the synthesized compounds. Twice higher electroluminescent characteristics were obtained for electroluminescent devices based on xanthenone emitters containing *tert*-butyl-carbazolyl and *tert*-butyl-acridanyl moieties in comparison to those of devices based on xanthenone emitters containing *tert*-butyl-phenothiazinyl and penoxazinyl moieties. This observation provides useful information for further design of efficient TADF emitters. The highest external quantum efficiency of 3.5% was demonstrated by organic light emitting diode based on emitter containing *tert*-butyl-acridanyl and xanthenone moieties.

Declaration of competing interest

All authors confirm that there are no interests to declare.

CRediT authorship contribution statement

Sohrab Nasiri: Investigation, Data curation. **Simas Macionis:** Investigation, Visualization. **Dalius Gudeika:** Conceptualization, Methodology. **Dmytro Volyniuk:** Writing - original draft, Validation. **Juozas V. Grazulevicius:** Project administration, Supervision, Writing - review & editing.

Acknowledgements

This project has received funding from European Regional Development Fund (project No 01.2.2-LMT-K-718-01-0015) under grant agreement with the Research Council of Lithuania (LMTLT). Support of the Lithuanian Academy of Sciences is gratefully acknowledged. This project has received funding from the Research Council of Lithuania (LMTLT), agreement No [S-LU-20-3].

Appendix A. Supplementary data

Supplementary data to this article can be found online at https://doi.org/10.1016/j.jlumin.2019.116955.

References

[1] H. Uoyama, K. Goushi, K. Shizu, H. Nomura, C. Adachi, Highly efficient organic light–emitting diodes from delayed fluorescence, Nature 492 (2012) 234–240, https://doi.org/10.1038/nature11687.
[2] Y. Liu, C. Li, Z. Ren, S. Yan, M.R. Bryce, All-organic thermally activated delayed fluorescence materials for organic light-emitting diodes, Nat. Rev. Mater. 3 (2018) 1–20, https://doi.org/10.1038/natrevmats.2018.20.
[3] S. Kothavale, K.H. Lee, J.Y. Lee, Isomeric quinoxalinedicarbonitrile as color-managing acceptors of thermally activated delayed fluorescent emitters, ACS Appl. Mater. Interfaces 11 (2019) 17583–17591, https://doi.org/10.1021/acsami.9b02824.
[4] J. Jayakumar, T.L. Wu, M.J. Huang, P.Y. Huang, T.Y. Chou, H.W. Lin, C.H. Cheng, Pyridine-carbonitrile–carbazole-based delayed fluorescence materials with highly congested structures and excellent OLED performance, ACS Appl. Mater. Interfaces 11 (2019) 21042–21048, https://doi.org/10.1021/acsami.9b04664.
[5] Y. Im, M. Kim, Y.J. Cho, J.A. Seo, K.S. Yook, J.Y. Lee, Molecular design strategy of organic thermally activated delayed fluorescence emitters, Chem. Mater. 29 (2017) 1946–1963, https://doi.org/10.1021/acs.chemmater.6b05324.
[6] F. Gao, R. Du, C. Han, J. Zhang, Y. Wei, G. Lu, H. Xu, High-efficiency blue thermally activated delayed fluorescence from donor-acceptor-donor systems: via the through-space conjugation effect, Chem. Sci. 10 (2019) 5556–5567, https://doi.org/10.1039/c9sc01240k.
[7] M.Y. Wong, E. Zysman-Colman, Purely organic thermally activated delayed fluorescence materials for organic light-emitting diodes, Adv. Mater. 29 (2017) 1605444–1605454, https://doi.org/10.1002/adma.201605444.
[8] V. Jankus, P. Data, D. Graves, C. McGuinness, J. Santos, M.R. Bryce, F.B. Dias, A. P. Monkman, Highly efficient TADF OLEDs: how the emitter–host interaction controls both the excited state species and electrical properties of the devices to achieve near 100% triplet harvesting and high efficiency, Adv. Funct. Mater. 24 (2014) 6178–6186, https://doi.org/10.1002/adfm.201400948.

[9] J. Lee, N. Aizawa, M. Numata, C. Adachi, T. Yasuda, Versatile molecular functionalization for inhibiting concentration quenching of thermally activated delayed fluorescence, Adv. Mater. 29 (2017) 1604856 1–6, https://doi.org/10.1002/adma.201604856.
[10] J. Lee, I.S. Park, T. Yasuda, Thermally activated delayed fluorescence properties of regioisomeric xanthone-based twisted intramolecular charge-transfer luminophores, Bull. Chem. Soc. Jpn. 90 (2017) 231–236, https://doi.org/10.1246/bcsj.20160380.
[11] H. Nakanotani, T. Higuchi, T. Furukawa, K. Masui, K. Morimoto, M. Numata, H. Tanaka, Y. Sagara, T. Yasuda, C. Adachi, High-efficiency organic light-emitting diodes with fluorescent emitters, Nat. Commun. 5 (2014) 4016 1–7, https://doi.org/10.1246/bcsj.20160380.
[12] H.J. Pownall, R.E. Connors, J.R. Huberm, Origin of the anomalous phosphorescence of aromatic ketones. xanthone in 3-methylpentane, Chem. Phys. Lett. 22 (1973) 503–504, https://doi.org/10.1016/0009-2614(73)80578-0.
[13] Q. Wan, B. Zhang, J. Tong, Y. Li, H. Wu, H. Zhang, Z. Wang, Y. Pan, B.Z. Tang, Feasible structure-modification strategy for inhibiting aggregation-caused quenching effect and constructing exciton conversion channels in acridone-based emitters, Phys. Chem. Chem. Phys. 21 (2019) 9837–9844, https://doi.org/10.1039/C9CP01706B.
[14] J. Guo, Z. Zhao, B.Z. Tang, Purely organic materials with aggregation-induced delayed fluorescence for efficient nondoped OLEDs, Adv. Opt. Mater. (2018) 1–11, https://doi.org/10.1002/adom.201800264, 1800264.
[15] Q. Zhang, B. Li, S. Huang, H. Nomura, H. Tanaka, C. Adachi, Efficient blue organic light-emitting diodes employing thermally activated delayed fluorescence, Nat. Photonics 8 (2014) 326–332, https://doi.org/10.1038/nphoton.2014.12.
[16] B.K. Sharma, A.M. Shaikh, R.M. Kamble, Synthesis photophysical electrochemical and thermal investigation of triarylamines based on 9H-xanthen-9-one: yellow–green fluorescent materials, J. Chem. Sci. 127 (2015) 2063–2071, https://doi.org/10.1007/s12039-015-0973-0.
[17] F. Ma, Y. Cheng, X. Zhang, X. Gu, Y. Zheng, K. Hasrat, Z. Qi, Enhancing performance for blue TADF emitters by introducing intramolecular CH···N hydrogen bonding between donor and acceptor, Dyes Pigments 166 (2019) 245–253, https://doi.org/10.1016/j.dyepig.2019.03.016.
[18] S. Gong, J. Luo, Z. Wang, Y. Li, T. Chen, G. Xie, C. Yang, Tuning emissive characteristics and singlet-triplet energy splitting of fluorescent emitters by encapsulation group modification: yellow TADF emitter for solution-processed OLEDs with high luminance and ultraslow efficiency roll-off, Dyes Pigments 139 (2017) 593–600, https://doi.org/10.1016/j.dyepig.2016.12.058.
[19] Y. Zhang, H. Ma, S. Wang, Z. Li, K. Ye, J. Zhang, Y. Liu, Q. Peng, Y. Wang, Supramolecular structure dependent thermally activated delayed fluorescence (TADF) properties of organic polymorphs, J. Phys. Chem. C 120 (2016) 19759–19767, https://doi.org/10.1021/acs.jpcc.6b05537.
[20] T. Miwa, S. Kubo, K. Shizu, T. Komino, C. Adachi, H. Kaji, Blue organic light emitting diodes realizing external quantum efficiency over 25% using thermally activated delayed fluorescence emitters, Sci. Rep. 7 (2017) 284, https://doi.org/10.1038/s41598-017-00368-5.
[21] N. Aizawa, C.J. Tsou, I.S. Park, T. Yasuda, Aggregation-induced delayed fluorescence from phenothiazine-containing donor–acceptor molecules for high efficiency non-doped organic light-emitting diodes, Polym. J. 49 (2017) 197–202, https://doi.org/10.1038/pj.2016.82.
[22] M. Inoue, T. Serevičius, H. Nakanotani, K. Yoshida, T. Matsushima, S. Juršenas, C. Adachi, Effect of reverse intersystem crossing rate to suppress efficiency roll-off in organic light-emitting diodes with thermally activated delayed fluorescence emitters, Chem. Phys. Lett. 644 (2016) 62–67, https://doi.org/10.1016/j.cplett.2015.11.042.
[23] D. Gudeika, D. Volyniuk, J.V. Grazulevicius, E. Skuodis, S.Y. Yu, W.T. Liou, L. Y. Chen, Y.J. Shiu, Derivative of oxygafluorene and di-tert-butyl carbazole as the host with very high hole mobility for high-efficiency blue phosphorescent organic light-emitting diodes, Dyes Pigments 130 (2016) 298–305, https://doi.org/10.1016/j.dyepig.2016.03.039.
[24] D. Gudeika, J.V. Grazulevicius, D. Volyniuk, R. Butkute, G. Juska, A. Miasojedovas, A. Gruodis, S. Jursenas, Structure-properties relationship of the derivatives of carbazole and 1,8-naphthalimide: effects of the substitution and the linking topology, Dyes Pigments 114 (2015) 239–252, https://doi.org/10.1016/j.dyepig.2014.11.013.
[25] A. Ivanauskaite, R. Lygaitis, S. Raisys, K. Kazlauskas, G. Kreiza, D. Volyniuk, D. Gudeika, S. Jursenas, J.V. Grazulevicius, Structure–property relationship of blue solid state emissive phenanthroimidazole derivatives, Phys. Chem. Chem. Phys. 19 (2017) 16737–16748, https://doi.org/10.1039/c7cp02248d.
[26] (a) D. Gudeika, G. Sini, V. Jankauskas, G. Sych, J.V. Grazulevicius, Synthesis and properties of the derivatives of triphenylamine and 1,8-naphthalimide with the olefinic linkages between chromophores, RSC Adv. 6 (2016) 2191–2201, https://doi.org/10.1039/C5RA24820E;
(b) D. Gudeika, J.V. Grazulevicius, D. Volyniuk, G. Juska, V. Jankauskas, G. Sini, Effect of ethynyl linkages on the properties of the derivatives of triphenylamine and 1,8-naphthalimide, J. Phys. Chem. C 119 (2015) 28335–28346, https://doi.org/10.1021/acs.jpcc.5b10163.
[27] (a) R. Butkute, R. Lygaitis, V. Mimaite, D. Gudeika, D. Volyniuk, G. Sini, J. V. Grazulevicius, Bipolar highly solid-state luminescent phenanthroimidazole derivatives as materials for blue and white organic light emitting diodes exploiting either monomer, exciplex or electroplex emission, Dyes Pigments 146 (2017) 425–437, https://doi.org/10.1016/j.dyepig.2017.07.029;
(b) D. Gudeika, A. Ivanauskaite, R. Lygaitis, V. Kosach, D. Volyniuk, R. Butkute, A. P. Naumenko, V. Yashchuk, J.V. Grazulevicius, Charge-transporting blue emitters having donor and acceptor moieties, J. Photochem. Photobiol. A Chem. 315 (2016) 121–128, https://doi.org/10.1016/j.jphotochem.2015.10.002;
(c) D. Gudeika, R.R. Reghu, J.V. Grazulevicius, G. Buika, J. Simokaitiene, A. Miasojedovas, S. Jursenas, V. Jankauskas, Electron-transporting naphthalimide-substituted derivatives of fluorene, Dyes Pigments 99 (2013) 895–902, https://doi.org/10.1016/j.dyepig.2013.07.016.
[28] G. Sych, J. Simokaitiene, O. Bezvikonnyi, U. Tsiko, D. Volyniuk, D. Gudeika, J. V. Grazulevicius, Exciplex-enhanced singlet emission efficiency of nondoped organic light emitting diodes based on derivatives of tetrafluorophenylcarbazole and tri/tetraphenylethylene exhibiting aggregation-induced emission enhancement, J. Phys. Chem. C 122 (2018) 14827–14877, https://doi.org/10.1021/acs.jpcc.8b03895.
[29] S.N. Dhar, CXVIII. - a comparative study in the xanthone series. Part I, J. Chem. Soc. Trans. 117 (1920) 1053–1070, https://doi.org/10.1039/CT9201701053.
[30] S. Sasaki, G.P.C. Drummen, G.I. Konishi, Recent advances in twisted intramolecular charge transfer (TICT) fluorescence and related phenomena in materials chemistry, J. Mater. Chem. C 4 (2016) 2731–2743, https://doi.org/10.1039/C5TC03933A.
[31] Y. Chen, J.W.Y. Lam, R.T.K. Kwok, B. Liu, B.Z. Tang, Aggregation-induced emission: fundamental understanding and future developments, Mater. Horizons. 6 (2019) 428–433, https://doi.org/10.1039/c8mh01331d.
[32] B.W. D'Andrade, S. Datta, S.R. Forrest, P. Djurovich, E. Polikarpov, M. E. Thompson, Relationship between the ionization and oxidation potentials of molecular organic semiconductors, Org. Electron. 6 (2005) 11–20, https://doi.org/10.1016/j.orgel.2005.01.002.
[33] O. Bezvikonnyi, D. Gudeika, D. Volyniuk, V. Mimaite, B.R. Sebastine, J. V. Grazulevicius, Effect of donor substituents on thermally activated delayed fluorescence of diphenylsulfone derivatives, J. Lumin. 206 (2019) 250–259, https://doi.org/10.1016/j.jlumin.2018.10.018.

ChemPubSoc Europe

DOI: 10.1002/ejoc.201901711

EurJOC European Journal of Organic Chemistry

Full Paper

Electroluminescence

Rational Synthesis of Tetrahydrodibenzophenanthridine and Phenanthroimidazole as Efficient Blue Emitters and their Applications

Manojkumar Dhanthala Thiyagarajan,[a] Umamahesh Balijapalli,[a,b] Sohrab Nasiri,[c] Dmytro Volyniuk,[c] Jurate Simokaitienec,[c] Madhvesh Pathak,*[a] Sathiyanarayanan Kulathu Iyer,*[a] and Juozas Vidas Gražulevičius*[c]

Abstract: Ten luminophores based on tetrahydrodibenzophenanthridine (THDP) and phenanthroimidazole (PI) were designed, synthesized and characterized for their thermal, electrochemical, electro-optical, charge-transporting characteristics and electroluminescent properties. The blue luminophores exhibited high photoluminescence quantum yields of 66–93 % in toluene solutions and of 5–59 % in solid films. The highest values were observed for the derivative of THDP and PI containing methoxy group. The compounds showed close values of ionization potentials (5.74–6.11 eV) and electron affinities (2.71–3.06 eV). The selected compounds were tested in electroluminescent devices for the preparation of non-doped light-emitting layers. The best device fabricated using derivative of THDP and PI with methoxy groups showed blue electroluminescence with brightness of 10000 cd/m^2 at high applied voltages. We performed DFT calculations and observed lowest singlet–triplet gap (ΔE_{ST}) values of 0.33 and 0.03 eV, oscillator strength (f) values of 0.034 and 0.008 for CN and NO_2 derivatives. Interestingly, we also observed that compounds **3g** and **3i** showed HOMO and LUMO levels with similar energy gap (Eg) of 3.60 eV and deeper HOMO values of –5.30, –5.33 eV and LUMO values of –1.94, –2.77 eV.

Introduction

Organic light-emitting diodes (OLEDs) have drawn massive attention due to their increasing applications in flat-panel displays and lighting devices.[1] OLEDs can be driven at low voltages to produce high brightness, wide viewing angles, fast response, low power consumption light-weight,[2] industrial and professional displays and micro-display products have already been developed. Researchers have reported deep-blue phosphorescent materials.[3,4] Phosphorescent OLEDs can theoretically achieve 100 % internal quantum efficiency. However, blue phosphorescent OLEDs have short lifetime and sharp efficiency roll-off at high brightness.[5] The fabrication of OLEDs can be done by two distinct methods, namely wet and dry processes. Typically, dry-process is used to realize high efficiency OLEDs with high-quality light.[6–8] Shortcomings such as inefficient use of materials, high energy consumption and poor scalability are major issues in cost-effective, mass-production.

In contrast, some of the aforementioned approaches can be adopted in wet-process to fabricate high-quality light OLED devices, but with comparatively low efficiency. Nevertheless, wet-process is deemed far superior in enabling simple fabrication, large area-size and roll-to-roll production, and consequently more cost-effective. However, energetic doping often requires minute control of doping concentration and inescapably increases manufacturing cost and this type of phase separation in the dopant-host system can make energy transfer ineffective. Many recent researchers have reported a high efficiency of blue fluorescent materials.[9–12] Some of them offer deep-blue emission with CIEy < 0.10.[13] Recently, Benzimidazole-based materials that possess different functional chromophores have been demonstrated as deep-blue-light emitters.[14] However, these materials have deep HOMO, thereby leading to larger hole-injection barriers at the hole-transporter emitter junctions, and thus they require higher operation voltages and provide lower efficiencies.[15,16] In fact, deep-blue OLEDs with high efficiency, good color stability, and low working voltage are rare.[17–20]

Tetrahydrodibenzophenanthridine (**THDP**) is a well-known fluorophore with exceptional photophysical properties, used as intermediate for the construction of organometallics and also utilized as a ratiometric fluorescence sensor for the detection

[a] Department of Chemistry, School of Advanced Sciences, Vellore Institute of Technology,
Vellore-632014, Tamilnadu, India
E-mail: sathiya_kuna@hotmail.com
madhveshpathak@vit.ac.in
https://www.sites.google.com/site/sathiyanarayananresearchgroup/home?authuser=0
[b] Centre for Organic Photonics and Electronics Research (OPERA), Kyushu University,
744 Motooka, Nishi, Fukuoka 819-0395, Japan
http://www.cstf.kyushu-u.ac.jp/~adachilab/lab/
[c] Kaunas University of Technology, Department of Polymer Chemistry and Technology,
Radvilenu pl.19, LT 50254, Kaunas, Lithunania
E-mail: juozas.grazulevicius@ktu.it
https://fct.ktu.edu/department-of-polymer-chemistry-and-technology/

Supporting information and ORCID(s) from the author(s) for this article are available on the WWW under https://doi.org/10.1002/ejoc.201901711.

of aniline.[21] On the other hand, 1,3,5-tris(*N*-phenylbenzimidazol-2-yl)benzene (TPBi) was widely used as an electron-injection and hole-blocking material in OLEDs, However, due to localization of its emission in the ultraviolet spectral region (368 nm), TPBi cannot be used as an emitter. Phenanthro[9,10-*d*]imidazole (**PI**) containing imidazole unit exhibits excellent thermal stability, highly efficient photoluminescence (PL) quantum yields and balanced charge carrier injection properties which make derivatives of **PI** promising candidates for OLEDs.[22] This information inspired us to develop new derivatives of **THDP** and **PI** as blue materials by a facile synthetic processes followed by systematic studies of their thermal, photophysical, and charge injection properties. In addition, postfunctionalization of derivatives of **THDP** and **PI** was performed by functional groups such as NO_2, CN, methoxy, methyl, and by halogens.

In this work, we used the donor-π-acceptor approach to design new molecules with PI core as the acceptor for its good electron-transporting mobility and THDP as the donor for good hole transport mobility and for connecting them with different linkers.[23–26] New **THDP** and **PI** derivative containing methoxy group showed the highest photoluminescence quantum yields in both toluene solutions (93 %) and in solid state (59 %). The best device performance was observed using non-doped light-emitting layer of this compound.

Synthesis and Characterization

THDP was easily prepared by the one-pot condensation reaction of substituted aldehydes, ammonium acetate and 2-tetralone with good yields.[27] 5-[4-(4,4,5,5-tetramethyl-1,3,2-dioxaborolan-2-yl)phenyl]-7,8,13,14-tetrahydrodi benzo[*a*,*i*] phenanthridine **1** (**BTHDP**) which is a key intermediate (its chemical structure shown in Scheme 1) was synthesized in good yield of 65 % according to the previously reported procedure (see the experimental section for the details).[28] The reaction of 9,10-phenanthrenequinone, *p*-bromobenzaldehyde with substituted aniline derivatives in the presence of ammonium acetate, and acetic acid gave substituted bromophenyl phenanthroimidazoles (**BrPI**) as yellow solids with up to 90 % yields (see supporting information).

In the final step, we used palladium-catalyzed Suzuki coupling to couple **BTHDP** with **BrPI** derivatives to obtain **THDP-PI** bipolar fluorophores (**3a**–**3j**) as shown in Scheme 1. The optimized reaction conditions were established by the screening of catalyst, solvent, base, temperature. TThe details were given in Table S1 in supporting information. It found out that 10 mol-% $Pd(PPh_3)_4$ and 2 equiv. of Cs_2CO_3 in dioxane/H_2O (4:1) allowed to obtain compound **3a** in 78 % yield (Table S1). Functional groups such as NO_2, CN, methoxy, methyl, and halogens tolerated the reaction conditions and the coupling smoothly proceeded to produce the desired compounds in good yields. All the compounds were freely soluble in common organic solvents and were purified by column chromatography using a mixture of ethyl acetate/chloroform/*n*-hexane as the eluent. Further, the purity was improved by consecutive crystallization steps and the structures were ascertained by FTIR, NMR, and mass spectrometry analysis (see section 1, supporting information).

Photophysical Properties

To investigate the effect of the substitution pattern on photophysical properties of the THDPs and PI derivatives, absorption and photoluminescent (PL) spectra of their solutions and solid films were recorded (Figure 1a-d and Figure S1). Low-energy bands of absorption spectra of toluene solutions of all derivatives were characterized by maxima at 346–361 nm and low-intensity shoulder at 365–375 nm. These absorption bands can be mainly attributed to absorption of PI moiety, since the lowest energy band is situated at the same region (with maximum at 364 nm) and is red-shifted in comparison to the lowest energy band (with maximum at 318 nm) of BTHDPs (Table 1).[29–33] Small blue-shifts of the maxima of the lowest energy bands of compounds **3a**–**j** relative to that of PI is, apparently, the result of superposition of absorption spectra of both donating and accepting units. Additional red-shifted energy bands (shoulders) that indicate intramolecular charge transfer (ICT) transitions in ground states between donor and acceptor units were practically not observed because of the presence of diphenyl spacers between THDP and PI moieties. As a result,

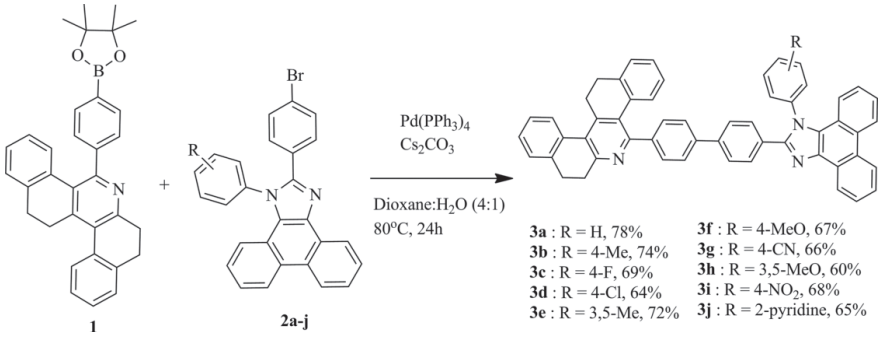

Scheme 1. Synthesis of 5-[4′-(1-phenyl-1*H*-phenanthro[9,10-*d*]imidazol-2-yl)-(1,1′-biphenyl)-4-yl]-7,8,13,14-tetrahydrodibenzo[*a*,*i*]phenanthridine and its derivatives.

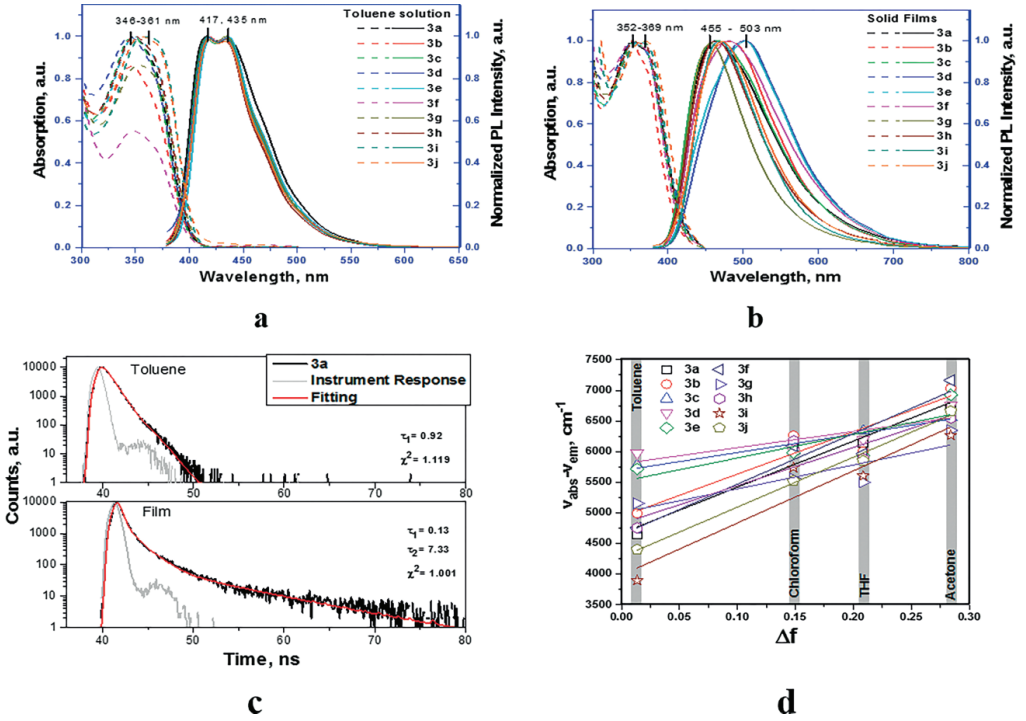

Figure 1. Absorption (dashed lines), and PL spectra (solid lines) of the solutions of compounds **3a**–**j** in toluene (a) and of solid-state samples (b); PL decays of toluene solution and solid film of compound **3a** (c) and Lippert–Mataga plots displaying correlation between orientation polarizability of the solvent (Δf) and the Stokes shifts ($\Delta \upsilon = \upsilon$abs-$\upsilon$em) for compounds **3a**–**j** (d).

similar optical energy band gaps (E_g^{opt}) were obtained for the studied compounds (Table 1). Slight differences in the position of the lowest absorption bands were observed for the toluene solutions of derivatives **3a**–**j** due to their post-functionalization's by different moieties inducing different steric and polar effects, which affected electron delocalization. A similar absorption behavior of the derivatives **3a**–**j** was also observed more in polar solvents than in toluene, revealing their weak solvatochromic effects in ground states. Absorption spectra of solid films of **3a**–**j** practically reconstituted the corresponding spectra which were only slightly red-shifted due to the aggregation effects of the solutions (Figure 1b).

Intensive, deep-blue fluorescence with high photoluminescence quantum yield (PLQY) was observe for toluene solutions of compounds **3a**–**j** (Table 1). The highest PLQY value of 93 % was recorded for toluene solution of compound **3f** containing metoxy substituent. PL decays of the toluene solutions were agreed well with the mono-exponential law (Figure 1c and Figure 2). Close to nanosecond, life times of fluorescence were observe for all the solutions, displaying weak effect of the substitution pattern (Table 1). For adequate description of PL decay curves of the films of compounds, double or triple exponentials fits were required. The reasons of different PL decays of the films from those solutions could be due to aggregation induced quenching and/or excimer formation. Clear effect of substitution pattern on PL decays of the films of **3a**–**j** was observed (Figure 1c, Figure 2 and Table 1). Different shapes of PL decays of the films **3a**–**j** may partly be related to non-radiative losses in solid-state. Indeed, much lower PLQY values of solid samples of **3a**–**j** were obtain in a comparison to those of their toluene solutions (Table 1). Compound **3f**, containing methoxy group, demonstrated relatively high PLQY of 59 % in solid-state. It was higher than that of compound **3a**, which did not have any substituent at phenyl group linked to PI moiety. High PLQY of solid sample of **3f** can be related to restriction of excimer formation, which may occur between planar moieties, as it was shown elsewhere.[34]

Vibronically structured PL spectra were recorded for the toluene solution of the compounds (Figure 1a). These PL spectra corresponded to pure deep-blue color with CIE1931 color coordinates of ($x < 0.16$, $y < 0.07$) and full width at half maximum (FWHM) < 77 nm (Table 1). Interestingly, FWHM of toluene solutions of substituted compounds **3b**–**j** was lower in comparison to FWHM of 77 nm observed for the solution of non-substituted compound **3a**. The shapes of PL spectra were similar to the shape of PL spectrum of DMF solution of PI.[35] PL spectra of the solutions of **3a**–**j** in toluene were red-shifted in comparison to PL spectrum of the solution of PI. Further, red-shift of emis-

Table 1. Photophysical parameters of the solutions of compounds **3a–j** in toluene and solid films.

Compounds	λ_{abs}^{max} [nm] Toluene/film	E_g^{opt} [eV]	λ_F^{max} [nm]	τ [ns]	PLQY [%]	FWHM [nm]	CIE1931 (x, y)	Slope[a] [cm^{-1}]
3a	348/352	3.03/2.76	417, 435/ 463	0.92/ 0.13, 7.33	93/27	77/125	(0.154, 0.059)/ (0.202, 0.249)	7513
3b	346/351	3.01/2.79	417,434/ 480	0.96/ 0.68, 4.43	67/11	67/126	(0.156, 0.063)/ (0.204, 0.176)	6931
3c	347/355	3.05/2.79	415,434/ 465	0.95/ 0.21, 2.04, 8.12	87/32	69/128	(0.156, 0.056)/ (0.202, 0.249)	2958
3d	345/355	3.02/2.78	416,434/ 502	1.02/ 0.09, 1.72, 7.49	66/8	67/131	(0.157, 0.063)/ (0.236, 0.349)	2633
3e	348/352	3.01/2.78	418,435/ 503	1.02/ 0.11, 1.90, 7.89	75/12	68/135	(0.157, 0.065)/ (0.230, 0.335)	3846
3f	349/351	3.02/2.77	418,434/ 480	0.93/ 0.13, 1.56, 8.27	93/59	66/137	(0.155, 0.059)/ (0.214, 0.275)	8240
3g	352/362	3.02/2.80	417,434/ 455	1.05/ 0.06, 1.51, 9.74	73/16	68/91	(0.156, 0.062)/ (0.173, 0.179)	3893
3h	349/355	3.01/2.78	417,432/ 463	0.89/ 0.55, 3.08, 10.6	88/12	63/106	(0.155, 0.065)/ (0.186, 0.222)	6229
3i	357/362	3.01/2.79	416,434/ 469	0.95/ 0.05, 1.03, 6.37	72/5	66/98	(0.155, 0.059)/ (0.179, 0.233)	8511
3j	355/367	2.96/2.76	418,434/ 471	0.95/ 0.03, 1.63, 9.19	74/6	64/105	(0.156, 0.060)/ (0.187, 0.245)	8146

[a] Absorbance and emission, photoluminescence quantum yield (PLQY), full width at half maximum (FWHM), life time decay (τ), color coordinates (CIE 1931).

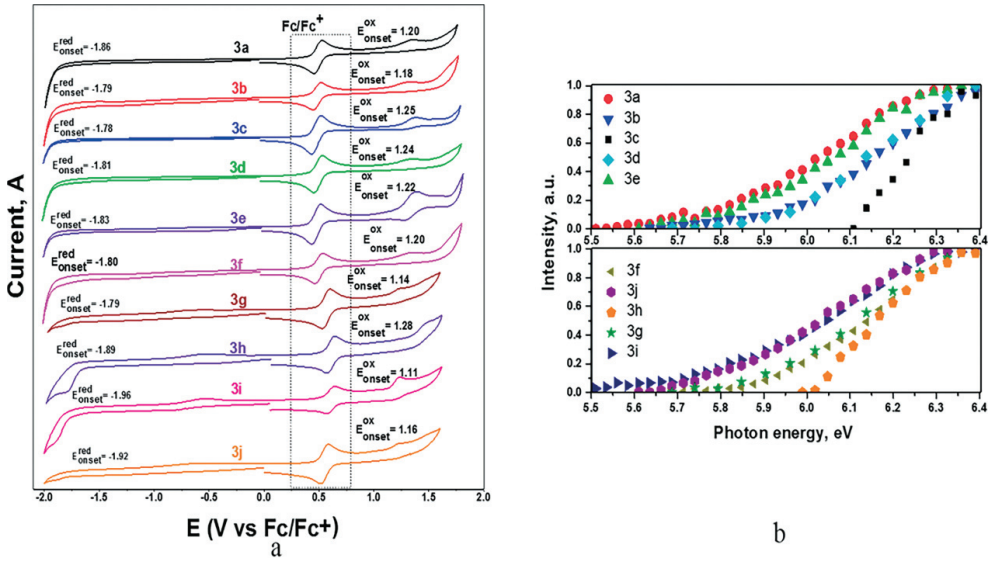

Figure 2. (a) Cyclic voltammograms of the solutions and (b) photoelectron emission spectra of vacuum-deposited films of compounds **3a–j**.

sion band of compounds **3a–j** was observed for the solution in chloroform, THF, and acetone, owing to an increase in the polarity of the solvents (Figure S2).

As a result, different variations of Stokes shifts ($\Delta\upsilon$=υ_{abs}-υ_{em}) displaying positive solvatofluorochromism and consistently proving CT character of their emission (Table 1) were obtained for the studied compounds. Non-structured PL spectra of the polar chloroform, THF, and acetone solutions of compounds **3a–j** support the presumption that emission is a result of recombination of CT exited states. To investigate the effect of the substitution pattern of the derivatives THDP and PI derivatives on their emission behavior, the dependence of their Stokes shifts vs. orientation polarizability of the chosen solvents (Δf) were linearly fitted (Figure 1d). The different slopes (ranging from 2633 to 8511 cm^{-1}) of these linear dependencies demonstrated differences in dipole moments of excited singlet states of compounds **3a–j** according to the Lippert–Mataga law (Table 1).[36] Different electron-donating or electron-accepting

substituents of phenyl group attached to PI moiety resulted in slightly different ICT behavior of compounds **3a**–**j**. Because of relatively low Lippert–Mataga slopes for compounds **3a**–**j**, some contribution of recombination of locally-exited states to their emission is possible. Non-structured nature of PL spectra of THF solutions of compounds **3a**–**j** at 77 K also suggests ICT emission (Figure 2). At 77 K, phosphorescence was not detect apparently due to the presence of bulky BTHDP unit. Broadening of PL spectra of the films of **3a**–**j** corresponds to some loss in deep-blue color purity in comparison to that of toluene solutions (Figure 1b). FWHM lower than 137 nm and CIE 1931 color coordinates of ($x < 0.16$, $y < 0.07$) were obtained for PL of **3a**–**j** in solid-state (Table 2). Nevertheless, more than twice the higher PLQY of compound **3f** containing appropriate substituent in comparison to PLQY of non-substituted counterpart **3a** demonstrated efficiency of post-functionalization in increase of potential for OLED applications.

Table 2. Thermal, electrochemical, electro optical and charge-transporting characteristics of compounds **3a**–**j**.

Compounds	T_g [°]C	T_m [°]C	$Ip^{CV[a]}/Ip^{PE}$ [eV]	$E_A{}^{CV[b]}/E_A{}^{PE}$ [eV]	μ_h [cm^2/Vs]
3a	185	348	6/5.74	2.94/2.71	5.8×10^{-6}
3b	179	341	5.98/5.90	3.01/2.89	–
3c	184	379	6.05/6.11	3.02/3.06	9×10^{-6}
3d	176	362	6.04/5.92	2.99/2.9	–
3e	189	324	6.02/5.81	2.97/2.8	–
3f	197	373	6/5.92	3/2.9	2.4×10^{-6}
3g	207	337	5.94/5.88	3.01/2.86	–
3h	176	286	6.08/5.99	2.91/2.98	3.7×10^{-6}
3i	205	–	5.91/5.77	2.84/2.76	–
3j	198	240	5.96/5.75	2.88/2.79	–

[a] IPCV = 4.8 + E_{ox}onset. [b] E_{ACV} = 4.8 – E_{red}onset; a taken at electric field of 6.4 × 105 V/cm.

Thermal, Electrochemical and Photoelectrical Characterization

Most of the synthesized compounds, except **3i**, were obtained after purification as crystalline or semi-crystalline substances, as confirmed by differential scanning calorimetry (DSC) measurements. Their melting temperatures (T_m) ranged from 240 to 379 °C. All the compounds were found to be capable of glass formation. They showed relatively high glass transition temperatures (T_g) of 176–205 °C (Figure S6, Table 2). Such high T_g values can apparently be explained by relatively high molecular weights and the rigid structures of the compounds. Small differences in T_g values of compounds **3a**–**j** can be attributed either to their different molecular weights or to different intermolecular interactions in solid states determined by different substituents of PI moiety.

To estimate energy levels of compounds **3a**–**j**, at the preliminary stage, cyclic voltammograms (CV) of their solutions were recorded (Figure 2a). The reversible oxidations and reductions were observed, which highlighted their good electrochemical stability of the compounds. Since all the studied compounds contain THDP and PI moieties, the similar values of oxidation and reduction potentials were obtained. Small differences were determined by the different substituents with weak electron-accepting or electron-donating abilities attached to PI moiety (Figure 2a). Oxidation of THDP moiety and reduction of PI moiety were responsible for observed oxidation and reduction peaks of compounds **3a**–**j**. Ionization potential (Ip^{CV}) and electron affinity (E_A^{CV}) values estimated from CV measurements were obtain in the ranges of 5.91–6.05 and 2.97–3.07 eV, respectively (Table 2). Since Ip^{CV} and E_A^{CV} energy levels are not directly related to the solid layers of organic semiconductors, vacuum-deposited films of **3a**–**j** were additionally tested by electron photoemission spectrometry in air (PES). The values of ionization potentials (I_p^{PES}) for **3a**–**j** in the condensed phase were estimate from the corresponding photoelectron emission spectra extrapolating their linear parts to zero of the ordinate axes (Figure 2b, Table 2).

Meanwhile, electron affinities (E_A^{PES}) were calculate using the equation $E_A = I_P^{PES} - E_g$, where E_g is optical band-gap energy obtain from the low-energy edge of absorption spectra of vacuum-deposited films of **3a**–**j** (Figure 3b, Table 2). Showing the similar trends, I_p^{PES} and E_A^{PES} values of compounds **3a**–**j** were slightly different from the corresponding I_p^{CV} and E_A^{CV} values (Table 2). The values of I_p^{PES} and E_A^{PES} of compounds **3a**–**j** were in good agreement with the corresponding energy levels of functional materials of OLEDs and efficient charge injection from the electrodes can be predicted.

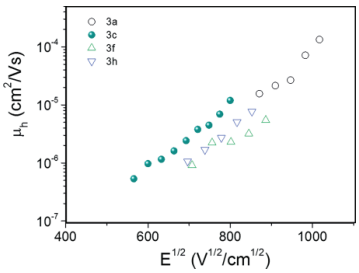

Figure 3. Electric field dependences of the hole mobility in vacuo-deposited film of compounds **3a**, **3c**, **3f** and **3h**.

Charge-Transporting Properties

Owing to donor–acceptor molecular structures of the studied PI and phenanthridine derivatives, we expected bipolar charge-transporting properties. Such expectations were partly grounded on the previously published phenanthridine/phenanthroimidazole based compounds which showed relatively good hole or electron-transporting properties.[37,38] To verify these expectations, time-of-flight (TOF) technique was used for testing diode-like samples with the structure of ITO/vacuum-deposited film/aluminum. Unsubstituted compound **3a** showed hole mobility of 1.3×10^{-4} cm^2/V at electric fields higher than 10^6 V/cm (Figure 3). Post functionalized compounds **3c**, **3f** and **3h** showed hole motilities similar to those of compound **3a** at the same electric field. This result indicated the absence of significant effects of post functionalization on hole mobility's of the studied derivatives. The tested compounds were characterized

by dispersive hole transport, as was evident from the shapes of their photocurrent transients (Figure S7). It was not possible to obtain transit times (required for calculations of charge mobility) from photocurrent transients for the other compounds, apparently due to the strong charge-transport dispersing which is typical for good emitters.[39] For the same reasons, transit times for electrons were also not detected in the corresponding photocurrent transients.

Electroluminescence

Taking into account that compounds **3a**, **3c**, **3f** and **3h** are characterized by relatively high PLQYs in solid-state and that they are capable of transporting charges, electroluminescent properties of the non-doped light-emitting layers of these selected compounds were further tested in OLEDs with the structure ITO/MoO_3(1 nm)/NPB (30 nm)/**3a**, **3c**, **3f** or **3h** (18 nm)/BPhen (33 nm)/LiF(0.5 nm)/Al. The layers of molybdenum trioxide (MoO_3) and lithium fluoride (LiF) were used as hole- and electron-injection layers, and the layers of *N*,*N*′-di(1-naphthyl)-*N*,*N*′-diphenyl-(1,1′-biphenyl)-4,4′-diamine (NPB) and bathophenanthroline (BPhen) were employed as hole- and electron-transporting layers, respectively. As are result, energy barriers which might prevent charge-injection into the light-emitting layers were absent in the designed OLED structures (Figure 4a). In addition, the layers of NPB and BPhen acted as electron- and hole-blocking layers due to the LUMO-LUMO energy barrier between NPB and light-emitting layers and the HOMO-HOMO energy barrier between BPhen and light-emitting layers, respectively (Figure 4a). Thus, recombination of charge pairs was anticipated within the light-emitting layers of **3a**, **3c**, **3f** or **3h**. This expectation was in good agreement with EL spectra of OLEDs based on **3a**, **3c**, **3f** or **3h** (Figure 4b). The similar EL spectra with the intensity maxima at 474 nm were observed for all the fabricated devices. Stable EL spectra under different electrical excitations were observed for the devices, showing that the recombination zone was not shifted to the charge-transporting layers under high electric fields partly due to the good charge-blocking properties of NPB and BPhen (Figure S6). EL spectra of devices **3a**, **3c**, **3f** and **3h**, being only slightly different due to the different excitations used, i.e. optical and electrical (Figure 1b, Figure 4b), were in good agreement with PL spectra of the corresponding films. CIE coordinates of the fabricated devices corresponded with blue color (Figure S9, Table 3).

By tenfold increase in maximum brightness was observed for the device, based on compound **3f** containing OCH_3 group in comparison to that of device based on non-substituted emitter **3a** (Figure 4c). To understand why tenfold increase in maximum brightness was observed for the device, based on compound **3f** containing methoxy group in comparison to that of device based on non-substituted emitter 3a (Figure 4c), we plotted brightness vs. current density for the fabricated devices (Figure S10). These dependences were well linearly fitted with the slope

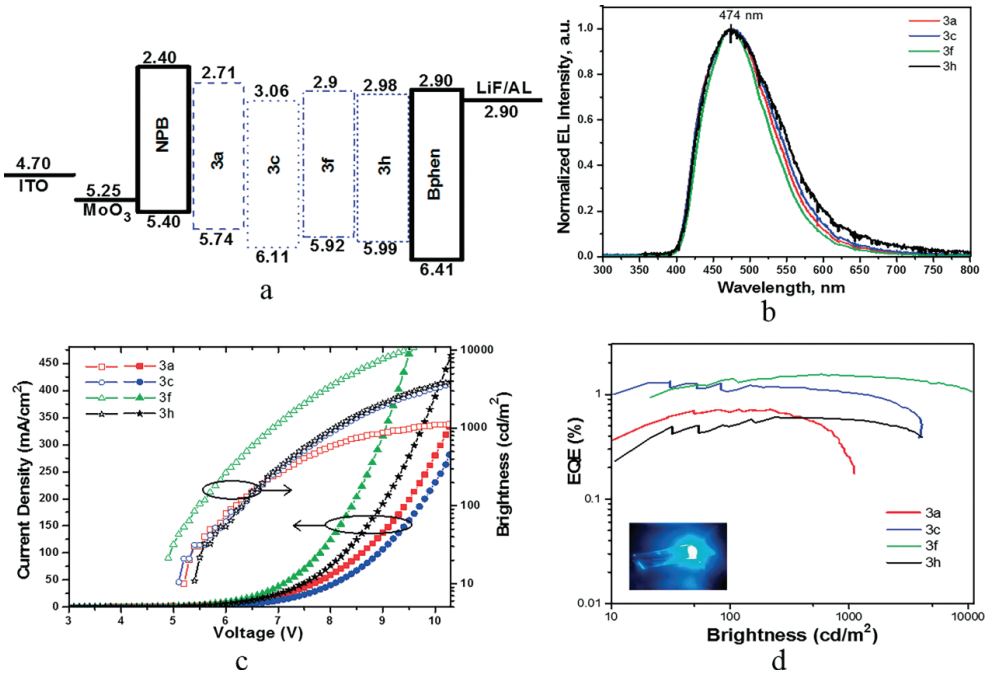

Figure 4. Equilibrium energy diagram (a), EL spectra recorded at 7 V (b), characteristics of current density and brightness vs. applied voltages (c) and dependences of EQEs vs. brightness (d) of OLEDs. The inset is photo of device 3f.

Table 3. Fabricated OLED device for **3a**, **3c**, **3f and 3h**.

Device	V_{on} [V]	L_{max} [cd/m^2]	L at 9 V [cd/m^2]	PE_{max}[a] [lm/W]	CE_{max}[a] [cd/A]	EQE_{max} [%]	CIE1931 coordinates (x, y) at 10V
3a: ITO/MoO3/NPB/3a/TPBi/LiF/Al	5.2	1100	900	0.8	1.9	0.8	(0.194, 0.256)
3c: ITO/MoO3/NPB/3c/TPBi/LiF/Al	5.1	4100	2100	1.2	1.9	1.2	(0.185, 0.244)
3f: ITO/MoO3/NPB/3f/TPBi/LiF/Al	4.9	11300	8300	1.6	1.9	1.6	(0.179, 0.246)
3h: ITO/MoO3/NPB/3h/TPBi/LiF/Al	5.4	4100	2200	0.6	0.7	0.6	(0.201, 0.267)

[a] **PE_{max}** and **CE_{max}** are maximum power and current efficiencies, respectively.

of **1** for all the devices at low brightness demonstrating that their electroluminescence resulted from singlet exciton recombination.[40] In case of device **f**, the liner dependence of brightness vs. current density was observed at high current density (Figure R1). This observation can be explained by the perfect charge balance and/or negligible quenching of excitons at broad range of electric fields in light emitting layer **3f**. In contrast, brightness of device **a** based on light-emitting layer **3a** is apparently limited by charge disbalance and/or exciton quenching at high electric fields (Figure S10).

In contrast to high roll-off efficiency of blue phosphorescent OLEDs which suffered from formation of "hot excitons" due to the presence of long-lived triplet excitons,[41] the fabricated blue fluorescent device **3f** showed low roll-off efficiency (Figure 4d). Its external quantum efficiency (EQE) at very high brightness (L) of 10000 cd/m^2 for blue OLEDs exhibited a slight drop in comparison to its maximum EQE of 1.6 % (Figure 4d). Better OLED performances of devices based on **3c** and **3f**, in comparison with that of the device based on **3a**, were mainly related to higher PLQY values of the films of **3c** and **3f** in comparison with that of the film of **3a**. In addition, differences between charge-injection and charge-transporting properties of compounds **3a**, **3c**, **3f** and **3h** should also play important roles. The differences between current density vs. applied voltages characteristics were observed for the studied devices (Figure 4c). Slightly different turn-on voltages ($\boldsymbol{V_{on}}$ = 4.9–5.4V) were obtained for the fabricated devices (Table 3). For the device based on **3f**, the film of which showed PLQY of 59 %, maximum EQE was two times lower than its theoretical maximum (4.4 %) estimated according to the well-known relationship $\eta_{ext} = (\gamma \times \eta_{ST} \times PLQY) \times \eta out$ using the charge balance factor $\gamma = 1$ and the fraction of radiative excitons $\eta_{ST} = 0.25$ for simple fluorescent emitters.[41] Therefore, further improvement of EQE of device based on **3f** can be expected. Nevertheless, the performed electroluminescent investigations not only testify the potential of the derivatives of THDP and PI in blue fluorescent OLEDs, but also demonstrate the requirements of their modifications through smart molecule design.

Theoretical Calculations

To estimate the differences between the geometric and optical properties, quantum-chemical calculations were performed by density functional theory (DFT) and time-dependent density functional theory (TD-DFT) at the B3LYP/6-31G(d) level. The calculated highest occupied molecular orbital (HOMO), lowest unoccupied molecular orbital (LUMO), oscillator strength (f), excited state energies and DEST are depicted in Figure S1 and Table S2. The HOMO was mainly localized in PI units and extended to phenyl parts of BTHDP core, there by suggesting that PI acts as an acceptor. The LUMO was fully occupied on the BTHDP donor unit and partially extended to the imidazole parts of PI units, which suggested that the nature of the substitution could also influence the optical properties.

For example, a slightly distinct trend was observed in **3g** and **3i**; LUMO was fully localized only on *N*-phenyl parts of PI core owing to the strong CN and NO_2 acceptors at the *para* position. Due to this, the HOMO was completely isolated and widely distributed to PI, and the THDP core resulted in a small overlap of HOMO and LUMO. This led to a small calculate lowest singlet–triplet gap (ΔE_{ST}) values of 0.33 and 0.03 eV, oscillator strength (f) values of 0.034 and 0.008 for **3g** and **3i** respectively. Hence, the increased charge transfer (CT) character with red-shifted properties can be observed. While the other emitters displayed almost similar singlet and triplet energies, large ΔE_{ST} and increased f, with completely overlapped HOMO and LUMO levels, suggest a probable increase in PLQYs. Furthermore, the calculated HOMO levels were in the range of 5.03–5.18 eV, while the LUMO levels were in the range of 1.42–1.50 eV, which gave almost similar energy gap (Eg) of 3.60 eV. Deeper HOMO values of –5.30, –5.33 eV and LUMO values of –1.94, –2.77 eV were observed for **3g** and **3i** respectively due to the acceptor's strength of CN and NO_2 functionalities. The calculated optical parameters are tabulate in Table S2.

Conclusions

Ten new fluorescent derivatives of tetrahydrodibenzophenanthridine and phenanthroimidazole were designed, synthesized and characterized as emitters for blue organic light-emitting diodes. Toluene solutions of the compounds exhibited a high photoluminescence quantum yield up to 93 %. For the films, photoluminescence quantum yields up to 59 % were observed. The best blue OLED exhibited brightness exceeding 10000 cd/m^2 and a relatively low roll-off efficiency. The best photoluminescence and electroluminescence performances were observed for the compound containing methoxy substituents. We performed DFT calculations and observed the lowest singlet–triplet gap (ΔE_{ST}) values of 0.33 and 0.03 eV, oscillator strength (f) values of 0.034 and 0.008 for CN and NO_2 derivatives. Interestingly, the compound **3g** and **3i** values were HOMO levels, and they were in the range of 5.03–5.18 eV, while the LUMO levels were in the range of 1.42–1.50 eV, which offered an almost similar energy gap Eg of 3.60 eV. The deeper HOMO values were found to be –5.30, –5.33 eV while the LUMO values were –1.94, –2.77 eV.

Experimental Section

General Information: All organic chemicals and solvents were purchased from Sigma-Aldrich, TCI, SD Fine, and AVRA and were used without further purification. NMR spectra were taken on Bruker 400 MHz using $CDCl_3$ as the solvent with tetramethylsilane as an internal standard. Melting points were measured on a microprocessor-based melting point apparatus and were not corrected. HRMS values were obtained on a Jeol GC Mate II GC-mass spectrometer. FTIR spectra of the synthesized organic compounds were recorded using a Jasco-4100 spectrometer instrument. Ultraviolet–visible spectra were recorded using a Hitachi U-2910 spectrophotometer. Fluorescence spectra in solution and solid state were measured using a Hitachi F7000 fluorescence spectrometer.

Photoluminescence (PL) spectra of 10^{-5} M solutions and of solid films of the compounds were recorded using Edinburgh Instrument FLS980 Fluorescence Spectrometer. For recording the UV/Vis and PL spectra, thin solid films were prepared by the spin-coating technique utilizing SPS-Europe Spin150 Spin processor using 1 mg/mL solutions of the compounds in chloroform on the pre-cleaned quartz substrates. The PL spectra were recorded at a low temperature (77 K). Fluorescence quantum yields (ΦF_1) of the solutions and of the solid films were estimated using an integrated sphere. Edinburgh Instruments FLS980 spectrometer with Pico Quant LDH-D-C-375 laser (wavelength 374 nm) as the excitation source was utilized for photoluminescence decay curves. Differential scanning calorimetry (DSC) measurements were carried out in a nitrogen atmosphere with a DSC TA Instruments Q2000 thermal analyser at a heating rate of 10 °C/min. The sample (approximately 2–3 mg) was placed in a closed aluminum pan. An empty pan was used as a reference. Electrochemical measurements were performed with an Autolab M101 potentiostat. Standard, three electrode setup consisting of platinum wire working electrode, platinum wire counter electrode and silver wire quasi-reference electrode calibrated vs. ferrocene/ferrocenium redox couple prior to each experiment was used. All electrochemical experiments were conducted in electrolyte: 0.1 M solution of Tetrabutylammoniumhexafluorophosphate (Bu4NPF6) (TCI) in dichloromethane (Chromasolv, HPLC grade). Solutions were degassed with argon prior to experiments and kept in an inert atmosphere during measurements. Onset of oxidation was used for calculation of ionization potential (IP^{CV}) of compounds. While, onset of reduction was used for calculation of electron affinity (EA^{CV}) of compounds. The ionization potential ($Ip^{(PE)}$) of the solid state sample was measured by photoelectron emission spectrometry in air as described before in Ref.[2] Indium tin oxide (ITO)/thick layer of compounds/Al were fabricated by depositing organic layers under vacuum of 2×10^{-6} mBar. The charge carrier mobility (μ) measurements of vacuum deposited layer were carried out by the time of flight method (TOF). The TOF experimental setup consisted of a pulsed Nd:YAG laser (EKSPLA NL300, a wavelength of 355 nm, pulse duration 3–6 ns), a Keithley 6517B electrometer, a Tektronix TDS 3052C oscilloscope, and was as described. The transit time (t_{tr}) with the applied bias (V) indicated the passage of charges through the entire thickness (d) of the samples. Hole mobility was calculated as $\mu = d^2/U{\cdot}tr$. OLEDs were prepared by vacuum deposition of organic and metal layers onto pre-cleaned ITO coated glass substrate under pressure lower than 2×10^{-6} mBar. Keithley 6517B electrometer, calibrated photodiode and Keithley 2400C source meter were used for recording current density via voltage and luminance via voltage characteristics.

Synthesis of 5-[4-(4,4,5,5-Tetramethyl-1,3,2-dioxaborolan-2-yl)phenyl]-7,8,13,14-tetrahydrodibenzo[a,i]phenanthridine (1): A mixture of 4-(4,4,5,5-tetramethyl-1,3,2-dioxaborolan-2-yl)benzaldehyde (10 mmol) and ammonium acetate (15 mmol) was taken in a 100 mL conical flask containing 10 mL of absolute ethanol at room temperature, sealed and warmed using water bath 15 min until the dissolution of the solid contents. After bringing the reaction mixture to room temperature, 2-teralone (20 mmol) was added, sealed and the mixture was warmed for 5 min and the reaction mixture was kept aside for 24 h in an open air. After the completion of the reaction was monitored by TLC. The resulting product was purified by the column chromatography over silica gel (60–120 mesh) using *n*-hexane and ethyl acetate mixture (9:1) as eluent to give the compound **(1)**. Thus obtained solid was further purified by recrystallizing in 1:1 ethanol and tetrahydrofuran mixture to afford compound **(1)** 65 % as a yellow solid.[42]

Synthesis of 2-(4-Bromophenyl)-1-phenyl-1*H*-phenanthro-[9,10-*d*]imidazole (PI) and Their Derivatives (2a–j): A mixture of 9,10-phenanthrenequinone (10.0 mmol), aniline derivatives (10.0 mmol), 4-Bromobenzaldehyde (10.0 mmol), ammonium acetate (15.0 mmol), and acetic acid (15 mL) was refluxed for 24 h. After that, the mixture was cooled to room temperature, and then the crude product was extract with ethyl acetate (3X30 mL) and finally dried with sodium sulfate. It was then purified by chromatography using hexane/ethyl acetate (9:1) as an eluent to obtain the product as white powder (2a–**j**). The characterization of compounds **2a–j** were matched with previous reported work.[43] Quantitative yield: 75–90 %.

Synthesis of 5-[4′-(1-Phenyl-1*H*-phenanthro[9,10-*d*]imidazol-2-yl)-(1,1′-biphenyl)-4-yl]- 7,8,13,14-tetrahydrodibenzo[a,i]phenanthridine and Their Derivatives (3a–j): A mixture of compound **1** (0.250 g, 6.2 mmol), compound **2a–j** (6.82 mmol), $Pd(PPh_3)_4$ (72 mg, 0.062 mmol) and Cs_2CO_3 (0.404 g, 12.4 mmol) in dioxane/H_2O (4:1) 5 mL was stirred under nitrogen at 80 °C for 24 h. After cooling to room temperature, the reaction mixture was extracted with dichloromethane, and the mixture was further purified by column chromatography (8:2) to obtain a yellow solid 3a–**j** (Yield: 60–78 %).[44]

Synthesis of 5-[4-(4,4,5,5-Tetramethyl-1,3,2-dioxaborolan-2-yl)phenyl]-7,8,13,14-tetrahydrodibenzo[a,i]phenanthridine (1): Yellow solid; (Yield 62 %); Melting point: 302–304 °C; FTIR (KBr cm^{-1}): 3323, 3070, 2966, 2839, 1606, 1548, 1483, 1425, 1402, 1342, 1259, 1165, 1103, 1043, 1016, 945, 891, 840, 804, 740; ^{1}H NMR (400 MHz, $CDCl_3$) TM ppm: 1.36 (s, 12H, CH_2), 2.78–2.75 (t, 2H, J = 8Hz, CH_2), 2.96–2.93 (m, 2H, CH_2), 3.15–3.06 (m, 4H, CH_2), 6.88–6.87 (d, 2H, J = 4Hz, ArCH), 7.12–7.08 (m, 1H, ArCH), 7.35–7.22 (m, 4H, ArCH), 7.46–7.44 (d, 2H, J = 8Hz, ArCH), 7.51–7.49 (d, 1H, J = 8Hz, ArCH), 7.78–7.76 (d, 2H, J = 8Hz, ArCH), ^{13}C NMR {^{1}H} (100 MHz, $CDCl_3$)TM ppm: 24.9 (6XCH), 29.2 (CH), 29.4 (CH), 29.5 (CH), 30.9 (CH), 33.1 (CH), 83.8 (C), 125.8 (C), 126.0 (C), 126.8 (C), 127.0 (C), 127.5 (C), 127.6 (C), 127.8 (C), 128.7 (C), 128.9 (C), 129.2 (C), 129.4 (C), 129.7 (C), 132.8 (C), 133.0 (C), 134.7 (C), 138.6 (C), 139.7 (C), 144.8 (C), 145.6 (C), 153.7 (C), 158.1 (C); HRMS (EI-ion trap) for $C_{33}H_{32}BNO_2$ calculated [M$^+$] m/z 485.2526, observed mass: 485.2523.

5-[4′-(1-Phenyl-1*H*-phenanthro[9,10-*d*]imidazol-2-yl)-(1,1′-biphenyl)-4-yl]-7,8,13,14-tetrahydrodibenzo[a,i]phenanthridine(3a): Yellow solid; (Yield 78 %); Melting point: 336–338 °C; FTIR (KBr cm^{-1}): 2935, 2845, 1548, 1452, 1392, 1234, 1145, 1001, 941, 827, 746, 698, 617; ^{1}H NMR (400 MHz, $CDCl_3$) TM ppm: 2.81–2.78 (t, 2H, J = 6.8Hz, CH_2), 2.98–2.95 (t, 2H, J = 8 Hz, CH_2), 3.17–3.09 (m, 4H, CH_2), 6.93–6.90 (t, 1H, J = 8 Hz, ArCH), 7.00–6.98 (d, 1H, J = 8 Hz, ArCH), 7.16–7.12 (t, 1H, J = 8 Hz, ArCH), 7.20–7.18 (d, 1H, J = 8 Hz, ArCH), 7.37–7.25 (m, 7H, ArCH), 7.58–7.49 (m, 10H, ArCH), 7.67–7.63 (t, 6H, J = 8 Hz, ArCH), 7.77–7.73 (t, 1H, J = 8 Hz, ArCH), 8.72–8.70 (d, 1H, J = 8 Hz, ArCH), 8.79–8.76 (d, 1H, J = 8 Hz, ArCH), 8.91–8.89

(d, 1H, *J* = 8 Hz, ArCH): ^{13}C NMR {^{1}H} (400 MHz, $CDCl_3$)^{TM} ppm: 29.2 (CH), 29.4 (CH), 29.5 (CH), 33.1 (CH), 120.8 (C), 122.8 (C),123.0 (C), 123.1 (C), 124.1 (C), 124.8 (C), 125.6 (C), 125.7 (C), 126.1 (C), 126.2 (C), 126.7 (4XC), 126.9 (C), 127.1 (C), 127.2 (C), 127.3 (C), 127.5 (4XC), 127.7 (C), 127.8 (C), 128.2 (C), 128.7 (C), 128.9 (4XC), 129.1 (C), 129.3 (C), 129.4 (C), 129.6 (2XC), 129.8 (C), 130.2 (2XC), 130.3 (C), 137.5 (C), 138.7 (C), 138.8 (C), 139.5 (C), 139.6 (C), 141.0 (C), 141.3 (C), 145.8 (C), 150.6 (C), 153.3 (C), 158.2 (C); HRMS (EI-ion trap) for $C_{54}H_{37}N_3$ calculated [M$^+$] *m/z*: 727.2987, observed mass: 727.2985.

5-{4′-[1-(*p*-Tolyl)-1*H*-phenanthro[9,10-*d*]imidazol-2-yl]-(1,1′-biphenyl)-4-yl}-7,8,13,14-tetrahydrodibenzo[a,i]phenanthridine(3b): Yellow solid; (Yield 74 %); Melting point: 308–310 °C; FTIR (KBr cm-1): 3032, 2954, 2926, 2845, 1776, 1608, 1518, 1452, 1390, 1232, 1159, 1033, 950, 825, 748, 721, 619; 1H NMR (400 MHz, $CDCl_3$) TM ppm: 2.55 (s, 3H, CH_3), 2.80–2.79 (m, 2H, CH_2), 2.98–2.94 (m, 2H, CH_2), 3.17–3.09 (m, 4H, CH_2), 7.05–6.89 (m, 2H, ArCH), 7.17–7.12 (m, 1H, ArCH), 7.45–7.22 (m, 12H, ArCH), 7.62- 7.49 (m, 9H, ArCH), 7.69–7.65 (t, 2H, *J* = 8 Hz, ArCH), 7.76–7.72 (t, 1H, *J* = 8 Hz, ArCH), 8.71–8.69 (d, 1H, *J* = 8 Hz, ArCH), 8.77–8.75 (d, 1H, *J* = 8 Hz, ArCH), 8.90–8.88 (d, 1H, *J* = 8 Hz, ArCH); ^{13}C NMR {^{1}H} (400 MHz, $CDCl_3$)^{TM} ppm: 21.5 (CH), 29.2 (CH), 29.4 (CH), 29.5 (CH), 33.1 (CH), 119.9 (C), 120.9 (C), 122.7 (C), 123.1 (C), 124.0 (C), 124.8 (C), 125.5 (C), 125.7 (C), 125.8 (C), 126.0 (C), 126.2 (C), 126.7 (2XC), 126.9 (C), 127.0 (C), 127.0 (C), 127.2 (C), 127.6 (2XC), 127.7 (C), 127.8 (C), 128.2 (C), 128.3 (2xC), 128.7 (C), 128.8 (C), 128.9 (C), 129.2 (2XC), 129.5 (C), 129.6 (2XC), 130.2 (C), 130.3 (C), 130.8 (C), 132.9 (C), 133.0 (C), 136.1 (C), 137.4 (C), 138.7 (C), 139.5 (C), 139.6 (C), 139.9 (C), 140.1 (C), 141.9 (C), 141.3 (C), 145.8 (C), 150.6 (C), 153.3 (C), 158.2 (C); HRMS (EI-ion trap) for $C_{55}H_{39}N_3$ calculated [M$^+$] *m/z*: 741.3144, observed mass: 741.3141.

5-{4′-[1-(4-Fluorophenyl)-1*H*-phenanthro[9,10-*d*]imidazol-2-yl]-(1,1′-biphenyl)-4-yl}-7,8,13,14-tetrahydrodibenzo[a,i]phenanthridine(3c): Yellow solid; (Yield 69 %); Melting point: 354–356 °C; FTIR (KBr cm^{-1}): 3061, 2954, 2837, 1508, 1450, 1388, 1219, 1149, 1001, 948, 831, 748, 723, 667, 617; ^{1}H NMR (400 MHz, $CDCl_3$) ^{TM} ppm: 2.81–2.78 (t, 2H, *J* = 8 Hz, CH_2), 2.98–2.94 (m, 2H, CH_2), 3.17–3.09 (m, 4H, CH_2), 6.93–6.90 (t, 1H, *J* = 8 Hz, ArCH), 7.00–6.98 (d, 1H, *J* = 8 Hz, ArCH), 7.16–7.12 (t, 1H, *J* = 8 Hz, ArCH), 7.21–7.19 (d, 1H, *J* = 8 Hz, ArCH), 7.27–7.25 (d, 2H, *J* = 8 Hz, ArCH), 7.37–7.29 (m, 7H, ArCH), 7.59–7.51 (m, 10H, ArCH), 7.68–7.63 (m, 3H, ArCH), 7.77–7.73 (t, 1H, *J* = 8 Hz, ArCH), 8.72–8.70 (d, 1H, *J* = 8 Hz, ArCH), 8.79–8.77 (d, 1H, *J* = 8 Hz, ArCH), 8.89–8.87 (d, 1H, *J* = 8 Hz, ArCH); ^{13}C NMR {^{1}H} (400 MHz, $CDCl_3$)^{TM} ppm: 29.2 (CH), 29.4 (CH), 29.5 (CH), 33.1 (CH), 117.2 (C), 117.4 (C), 120.6 (C), 122.8 (C), 122.9 (C), 123.1 (C), 124.2 (C), 125.0 (C), 125.7 (C), 126.0 (C), 126.3 (C), 126.8 (C), 126.9 (4xC), 127.1 (C), 127.1 (C), 127.3 (C), 127.6 (C), 127.7 (4XC), 127.9 (C), 128.2 (C), 128.3 (C), 128.7 (C), 128.9 (4XC), 129.1 (C), 129.3 (C), 129.7 (C), 130.4 (C), 130.9 (C), 131.0 (C), 132.9 (C), 133.0 (C), 134.8 (C), 137.5 (C), 138.7 (C), 139.4 (C), 139.7 (C), 141.2 (C), 141.5 (C), 145.8 (C), 150.76 (C), 153.2 (C), 158.2 (C); HRMS (EI-ion trap) for $C_{54}H_{36}FN_3$ calculated [M$^+$] *m/z*: 745.2893, observed mass: 745.2890.

5-{4′-[1-(4-Chlorophenyl)-1*H*-phenanthro[9,10-*d*]imidazol-2-yl]-(1,1′-biphenyl)-4-yl}-7,8,13,14-tetrahydrodibenzo[a,i]phenanthridine(3d): Yellow solid; (Yield 64 %); Melting point: 330–332 °C; FTIR (KBr cm^{-1}): 3059, 2945, 2845, 1608, 1492, 1396, 1271, 1232, 1166, 1002, 948, 833, 748, 696, 617; ^{1}H NMR (400 MHz, $CDCl_3$) ^{TM} ppm: 2.81–2.73 (m, 2H, CH_2), 2.98 –2.93 (m, 2H, CH_2), 3.17–3.08 (m, 4H, CH_2), 6.70–6.68 (d, 1H, *J* = 8 Hz, ArCH), 7.00–6.87 (m, 4H, ArCH), 7.16–7.08 (m, 1H, ArCH), 7.37- 7.21 (m, 2H, ArCH), 7.68–7.49 (m, 10H, ArCH), 7.77–7.73 (t, 1H, *J* = 8 Hz, ArCH), 8.89–8.70 (m, 2H, ArCH); ^{13}C NMR {^{1}H} (400 MHz, $CDCl_3$)^{TM} ppm: 29.2 (CH), 29.4 (CH), 29.5 (CH), 30.9 (CH), 33.1 (CH), 115.8 (C), 120.6 (C), 122.8 (C), 123.1 (C), 124.2 (C), 125.0 (C), 125.6 (C), 125.7 (C), 126.0 (C), 126.4 (4XC), 126.8 (C), 126.9 (C), 126.9 (C), 127.1 (C), 127.4 (4XC), 127.6 (C), 127.7 (C), 127.8 (C), 127.9 (C), 128.0 (C), 128.3 (C), 128.7 (4XC), 129.3 (C), 129.5 (C), 129.7 (C), 130.4 (C), 130.4 (C), 130.5 (C), 131.1 (C), 133.0 (C), 135.8 (C), 138.7(C), 139.6 (C), 141.2 (C), 141.4 (C), 145.8 (C), 150.6 (C), 153.2 (C), 157.9 (C), 158.2 (C); HRMS (EI-ion trap) for $C_{23}H_{18}ClN_2$ calculated [M$^+$] *m/z*: 761.2598, observed mass: 761.2591.

5-{4′-[1-(3,5-Dimethylphenyl)-1*H*-phenanthro[9,10-*d*]imidazol-2-yl]-(1,1′-biphenyl)-4-yl}-7,8,13,14-tetrahydrodibenzo[a,i]-phenanthridine(3e): Yellow solid; (Yield 67 %); Melting point: 318–320 °C; FTIR (KBr cm^{-1}): 3018, 2943, 2839, 1608, 1469, 1392, 1145, 1001, 947, 831, 748, 725, 619; ^{1}H NMR (400 MHz, $CDCl_3$) ^{TM} ppm: 2.43 (s, 6H, CH_3), 2.82–2.79 (t, 2H, *J* = 8 Hz, CH_2), 2.99–2.95 (t, 2H, *J* = 8 Hz, CH_2), 3.18–3.10 (m, 4H, CH_2), 6.94–6.90 (t, 1H, *J* = 8 Hz, ArCH), 7.01–6.99 (d, 1H, *J* = 8 Hz, ArCH), 7.22–7.13 (m, 5H, ArCH), 7.33–7.26 (m, 11H, ArCH), 7.38–7.34 (t, 1H, *J* = 8 Hz, ArCH), 7.54–7.50 (m, 5H, ArCH), 7.60–7.58 (d, 4H, *J* = 8 Hz, ArCH), 7.67–7.63 (t, 1H, *J* = 8 Hz, ArCH), 7.75–7.73 (d, 3H, *J* = 8 Hz, ArCH), 8.72–8.70 (d, 1H, *J* = 8 Hz, ArCH), 8.78–7.76 (d, 1H, *J* = 8 Hz, ArCH), 8.90–8.88 (d, 2H, *J* = 8 Hz, ArCH); ^{13}C NMR {^{1}H} (400 MHz, $CDCl_3$)^{TM} ppm: 21.1 (CH), 29.2 (CH), 29.5 (CH), 29.6 (CH),33.3 (2XCH), 115.8 (C), 125.8 (C), 126.0 (C), 126.1 (C), 126.5 (4XC), 126.6 (C), 126.9 (C), 126.9 (C), 127.1 (C), 127.4 (4XC), 127.5 (C), 127.7 (C), 127.9 (C), 128.1 (C), 128.2 (4XC), 128.7 (C), 128.9 (C), 129.0 (C), 129.5 (4XC), 129.6 (C), 129.7 (C), 133.0 (C), 133.1 (2XC), 134.6 (C), 137.0 (C), 138.2 (C), 138.7 (C), 138.8 (2XC), 139.6 (C), 139.7 (C), 140.2 (C), 141.2 (C), 145.8 (C), 146.4 (C), 153.4 (C), 158.2 (C); HRMS (EI-ion trap) for $C_{56}H_{41}N_3$ calculated [M$^+$] *m/z*: 755.3300, observed mass: 755.3298.

5-{4′-[1-(4-Methoxyphenyl)-1*H*-phenanthro[9,10-*d*]imidazol-2-yl]-(1,1′-biphenyl)-4-yl}-7,8,13,14-tetrahydrodibenzo[a,i]phenanthridine(3f): Yellow solid; (Yield 66 %); Melting point: 358–360 °C; FTIR (KBr cm^{-1}): 2960, 2829, 1608, 1508, 1450, 1394, 1290, 1244, 1166, 1107, 1024, 948, 831, 746, 725, 617; ^{1}H NMR (400 MHz, $CDCl_3$) ^{TM} ppm: 2.82–2.78 (t, 2H, *J* = 8 Hz, CH_2), 2.98–2.95 (t, 2H, *J* = 8 Hz, CH_2), 3.18–3.09 (m, 4H, CH_2), 3.97 (s, 3H, OCH_3), 6.94–6.90 (t, 1H, *J* = 8 Hz, ArCH), 7.00–6.99 (d, 1H, *J* = 4 Hz, ArCH), 7.16–7.10 (m, 3H, ArCH), 7.38–7.26 (m, 14H, ArCH), 7.60–7.45 (m, 10H, ArCH), 7.77–7.64 (m, 4H, ArCH), 8.72–8.70 (d, 1H, *J* = 8 Hz, ArCH), 8.79–8.77 (d, 1H, *J* = 8 Hz, ArCH), 8.90–8.88 (d, 1H, *J* = 8 Hz, ArCH); ^{13}C NMR {^{1}H} (400 MHz, $CDCl_3$)^{TM} ppm: 29.2 (CH), 29.5 (CH), 29.6 (CH), 33.1 (CH), 55.4 (2XCH), 114.3 (C), 115.6 (C), 125.7 (C), 125.7 (C), 126.0 (C), 126.6 (C), 126.6 (C), 126.9 (4XC), 127.0 (C), 127.4 (C), 127.6 (4XC), 127.7 (C), 127.8 (C), 128.2 (C), 128.4 (4xC), 128.7 (C), 128.9 (C), 129.6 (C), 129.6 (2XC), 129.7 (C), 129.9 (C), 130.3 (C), 130.7 (2XC), 131.2 (C), 131.3 (C), 132.9 (C), 133.5 (C), 134.5 (C), 138.3 (C), 138.7 (C), 138.7 (C), 139.7 (C), 140.3 (C), 141.2 (C), 145.8 (C), 146.8 (C), 153.4 (C), 158.2 (C), 159.2 (C); HRMS (EI-ion trap) for $C_{55}H_{39}N_3O$ calculated [M$^+$] *m/z*: 757.3093, observed mass: 757.3090.

4-{2-[4′-(7,8,13,14-Tetrahydrodibenzo[a,i]phenanthridin-5-yl)-(1,1′-biphenyl)-4-yl]-1*H*-phenanthro[9,10-*d*]imidazol-1-yl}-benzonitrile(3g): Yellow solid; (Yield 72 %); Melting point: 328–330 °C; FTIR (KBr cm^{-1}): 2978, 1604, 1508, 1452, 1396, 1253, 1166, 1118, 1004, 950, 831, 748, 725, 617; ^{1}H NMR (400 MHz, $CDCl_3$) ^{TM} ppm: 2.81–2.78 (t, 2H, *J* = 8 Hz, CH_2), 2.98–2.95 (t, 2H, *J* = 8 Hz, CH_2), 3.17–3.09 (m, 4H, CH_2), 6.94–6.90 (t, 1H, *J* = 8 Hz, ArCH), 7.00–6.98 (d, 1H, *J* = 8 Hz, ArCH), 7.26–7.10 (m, 2H, ArCH), 7.37–7.25 (m, 7H, ArCH), 7.60–7.51 (m, 10H, ArCH), 7.70–7.66 (m, 3H, ArCH), 7.78–7.74 (t, 1H, *J* = 8 Hz, ArCH), 7.93–7.92 (d, 2H, *J* = 4 Hz, ArCH), 8.72–8.70 (d, 1H, *J* = 8 Hz, ArCH), 8.80–8.78 (d, 1H, *J* = 8 Hz, ArCH), 8.88–8.86 (d, 1H, *J* = 8 Hz, ArCH); ^{13}C NMR {^{1}H} (400 MHz, $CDCl_3$)^{TM} ppm: 29.2 (CH), 29.4 (CH), 29.5 (CH), 33.1 (CH), 113.9 (C), 117.7 (C), 120.4

(C), 122.4 (C), 122.8 (C), 123.1 (C), 124.4 (C), 125.2 (C), 125.7 (C), 126.0 (C), 126.0 (4XC), 126.5 (C), 126.9 (C), 127.0 (C), 127.1 (C), 127.5 (4XC), 127.6 (C), 127.7 (C), 127.9 (C), 128.4 (C), 128.6 (C), 128.7 (4XC), 128.9 (C), 129.4 (C), 129.6 (C), 129.8 (C), 130.2 (C), 130.4 (C), 132.9 (C), 133.0 (C), 134.0 (C), 138.0 (C), 138.7 (C), 139.1 (C), 139.6 (C), 141.6 (C), 142.8 (C), 145.8 (C), 150.5 (C), 153.2 (C), 158.2 (C); HRMS (EI-ion trap) for $C_{55}H_{36}N_4$ calculated [M$^+$] *m/z*: 752.2940, observed mass: 752.2938.

5-{4′-[1-(3,5-Dimethoxyphenyl)-1*H*-phenanthro[9,10-*d*]imidazol-2-yl]-(1,1′-biphenyl)-4-yl}-7,8,13,14-tetrahydrodibenzo-[a,*i*]phenanthridine(3h): Yellow solid; (Yield 60 %); Melting point: 278–280 °C; FTIR (KBr cm^{-1}): 2949, 1724, 1593, 1452, 1330, 1236, 1203, 1155, 1041, 999, 945, 831, 746, 725, 617; ^{1}H NMR (400 MHz, $CDCl_3$) ™ ppm: 2.81–2.78 (t, 2H, *J* = 6 Hz, CH_2), 2.98–2.95 (t, 2H, *J* = 6 Hz, CH_2), 3.17–3.09 (m, 4H, CH_2), 3.80 (s, 6H, OCH_3), 6.72–6.71 (d, 3H, *J* = 4 Hz, ArCH), 6.94–6.90 (t, 1H, *J* = 8 Hz, ArCH), 7.01–6.99 (d, 1H, *J* = 8 Hz, ArCH), 7.16–7.13 (t, 1H, *J* = 8 Hz, ArCH), 7.37–7.25 (m, 9H, ArCH), 7.60–7.52 (m, 9H, ArCH), 7.67–7.63 (t, 1H, *J* = 8 Hz, ArCH), 7.78–7.72 (m, 3H, ArCH), 8.72–8.70 (d, 1H, *J* = 8 Hz, ArCH), 8.78–8.76 (d, 1H, *J* = 8 Hz, ArCH), 8.89–8.87 (d, 1H, *J* = 8 Hz, ArCH); ^{13}C NMR {^{1}H} (400 MHz, $CDCl_3$)™ ppm: 29.2 (CH), 29.5 (CH), 29.6 (CH), 33.1 (CH), 55.8 (2XCH), 102.0 (C), 102.3 (C), 107.3 (C), 121.1 (C), 122.8 (C), 122.9 (C), 123.1 (C), 124.9 (C), 125.6 (C), 125.8 (C), 126.1 (4XC), 126.4 (C), 126.8 (C), 126.9 (C), 127.1 (C), 127.3 (C), 127.6 (2XC), 127.7 (C), 127.9 (C), 128.1 (C), 128.3 (4XC), 128.9 (C), 129.2 (C), 129.3 (2XC), 129.4 (C), 129.7 (C), 130.3 (2XC), 132.9 (C), 133.0 (C), 138.7 (C), 139.6 (C), 139.7 (C), 140.3 (2XC), 141.0 (C), 141.3 (C), 145.8 (C), 150.3 (C), 153.3 (C), 158.2 (C), 161.8 (C); HRMS (EI-ion trap) for $C_{56}H_{41}N_3O_2$ calculated [M$^+$] *m/z*: 787.3199, observed mass: 787.3196.

5-{4′-[1-(4-Nitrophenyl)-1*H*-phenanthro[9,10-*d*]imidazol-2-yl]-(1,1′-biphenyl)-4-yl}-7,8,13,14-tetrahydrodibenzo[a,*i*]phenanthridine (3i): Yellow solid; (Yield 68 %); Melting point: 268–270 °C; FTIR (KBr cm^{-1}): 2954, 1612, 1479, 1394, 1232, 1118, 1001, 948, 831, 750, 725, 617; ^{1}H NMR (400 MHz, $CDCl_3$) ™ ppm: 2.82–2.79 (t, 2H, *J* = 8 Hz, CH_2), 2.99–2.96 (m, 2H, CH_2), 3.19–3.10 (m, 4H, CH_2), 6.95–6.91 (t, 1H, *J* = 8 Hz, ArCH), 7.01–7.00 (d, 1H, *J* = 8 Hz, ArCH), 7.18–7.11 (m, 2H, ArCH), 7.38–7.28 (m, 5H, ArCH), 7.61–7.52 (m, 10H, ArCH), 7.71–7.68 (m, 3H, ArCH), 7.79–7.75 (m, 10H, ArCH), 7.94–7.93 (d, 2H, *J* = 4 Hz, ArCH), 8.73–8.71 (d, 1H, *J* = 8 Hz, ArCH), 8.81–8.79 (d, 1H, *J* = 8 Hz, ArCH), 8.89–8.87 (d, 1H, *J* = 8 Hz, ArCH); ^{13}C NMR {^{1}H} (400 MHz, $CDCl_3$)™ ppm: 29.2 (CH), 29.5 (CH), 29.6 (CH), 33.2 (CH), 113.9 (C), 117.7 (C), 120.4 (C), 122.4 (C), 122.8 (C), 123.2 (C), 124.4 (C), 125.3 (C), 125.7 (C), 126.0 (C), 126.1 (2xC), 126.5 (C), 126.9 (2xC), 127.0 (2xC), 127.1 (C), 127.5 (C), 127.6 (2xC), 127.7 (C), 127.8 (C), 127.9 (C), 128.4 (2xC), 128.6 (C), 128.7 (2xC), 128.9 (2xC), 129.5 (C), 129.7 (C), 129.8 (2xC), 130.3 (C), 130.4 (C), 132.9 (C), 133.0 (C), 134.0 (C), 138.0 (C), 138.7 (C), 139.2 (C), 139.7 (C), 141.6 (C), 142.8 (C), 145.8 (C), 150.5 (C), 153.2 (C), 158.2 (C); HRMS (EI-ion trap) for $C_{54}H_{36}N_4O_2$ calculated [M$^+$] *m/z*: 772.2838, observed mass: 772.2838.

5-{4′-[1-(Pyridin-2-yl)-1*H*-phenanthro[9,10-*d*]imidazol-2-yl]-(1,1′-biphenyl)-4-yl}-7,8,13,14-tetrahydrodibenzo[a,*i*]phenanthridine (3j): Yellow solid; (Yield 65 %); Melting point: 280–282 °C; FTIR (KBr cm^{-1}): 3039, 2949, 2835, 1707, 1610, 1550, 1481, 1396, 1232, 1116, 1001, 945, 831, 748, 721, 694, 617; ^{1}H NMR (400 MHz, $CDCl_3$) ™ ppm: 2.92–2.89 (t, 2H, *J* = 8 Hz), 3.08–3.05 (t, 2H, *J* = 6 Hz), 3.27–3.25 (t, 2H, *J* = 8 Hz), 3.42–3.39 (t, 2H, *J* = 8 Hz), 7.02–6.87 (m, 2H, ArCH), 7.17–7.14 (t, 3H, *J* = 6 Hz, ArCH), 7.51–7.29 (m, 19H, ArCH), 7.60–7.58 (d, 1H, *J* = 8 Hz, ArCH); ^{13}C NMR {^{1}H} (400 MHz, $CDCl_3$)™ ppm: 27.1 (CH), 27.8 (CH), 27.9 (CH), 30.6 (CH), 110.3 (C), 113.1 (C), 117.9 (C), 118.7 (C), 120.9 (C), 124.8 (C), 126.2 (C), 126.8 (C), 127.4 (2XC), 127.6 (C), 127.8 (C), 128.1 (C), 128.1 (C), 128.2 (C), 128.6 (C), 128.8 (C), 128.9 (C), 129.1 (C), 129.3 (C), 129.4 (C), 129.8 (C), 130.0 (C), 130.1 (C), 130.1 (C), 130.4 (C), 130.6 (C), 120.6 (C), 130.7 (C), 130.9 (C), 131.3 (C), 131.8 (C), 131.8 (C), 132.7 (C), 133.5 (C), 137.5 (C), 138.2 (C), 138.6 (C), 141.9 (C), 143.7 (C), 143.3 (C), 144.3 (C), 144.9 (C), 153.2 (C), 156.7 (C), 160.3 (C), 160.7 (C), 161.2 (C), 161.6 (C); HRMS (EI-ion trap) for $C_{53}H_{36}N_4$ calculated [M$^+$] *m/z*: 728.2940, observed mass: 728.2938.

Acknowledgments

The authors thanks to VIT for giving Research associate fellowship (Ref: VIT/HR/2017/5069). The authors thank to Dr. R. Srinivasan, SSL-VIT for language editing. This work was supported by the project of scientific co-operation program between Latvia, Lithuania and Taiwan "Polymeric Emitters with Controllable Thermally Activated Delayed Fluorescence for Solution-processable OLEDs" (grant No. P-LLT-19-14).

Keywords: Phenananthridines · Phenanthroimidazoles · Blue luminophore · Electrochemistry · Solvatochromism

[1] G. M. Farinola, R. Ragni, *Chem. Soc. Rev.* **2011**, *40*, 3467–3482.
[2] a) H. Ulla, B. Garudachari, M. N. Satyanarayan, G. Umesh, A. M. Isloor, *Optical Mater.* **2014**, *36*, 704–711; b) J.-H. Lee, S. H. Cheng, S. J. Yoo, H. Shin, J. H. Chang, C. I. Wu, K. T. Wong, J. J. Kim, *Adv. Funct. Mater.* **2015**, *25*, 342–342.
[3] a) Q. Wang, I. W. H. Oswald, X. Yang, G. Zhou, H. Jia, Q. Qiao, Y. Chen, J. Hoshikawa-Halbert, B. E. Gnade, *Adv. Mater.* **2014**, *26*, 8107–8113; b) C. Tang, R. Bi, Y. Tao, F. Wang, X. Cao, S. Wang, T. Jiang, C. Zhong, H. Zhang, W. Huang, *Chem. Commun.* **2015**, *51*, 1650–1653.
[4] a) M. A. Baldo, M. E. Thompson, S. R. Forrest, *Nature* **2000**, *403*, 750–753; b) H. Nakanotani, T. Higuchi, T. Furukawa, K. Masui, K. Morimoto, M. Numata, H. Tanaka, Y. Sagara, T. Yasuda, C. Adachi, *Nat. Commun.* **2014**, *5*, 4016.
[5] J. Tagare, S. Vaidyanathan, *J. Mater. Chem. C* **2018**, *6*, 10138–10173.
[6] M. A. Baldo, D. F. O'Brien, Y. You, A. Shoustikov, S. Sibley, M. E. Thompson, S. R. Forrest, *Nature* **1998**, *395*, 151–154.
[7] T. W. Lee, T. Noh, H. W. Shin, O. Kwon, J. J. Park, B. K. Choi, M. S. Kim, D. W. Shin, Y. R. Kim, *Adv. Funct. Mater.* **2009**, *19*, 1625–1630.
[8] M. A. Baldo, C. Adachi, S. R. Forrest, *Phys. Rev. B* **2000**, *62*, 10967–10977.
[9] a) Q. Zhang, J. Li, K. Shizu, S. Huang, S. Hirata, H. Miyazaki, C. Adachi, *J. Am. Chem. Soc.* **2012**, *134*, 14706–14709; b) H. Kaji, H. Suzuki, T. Fukushima, K. Shizu, K. Suzuki, S. Kubo, T. Komino, H. Oiwa, F. Suzuki, A. Wakamiya, Y. Murata, C. Adachi, *Nat. Commun.* **2015**, *6*, 8476; c) Y. Zhao, J. Chen, D. Ma, *Appl. Phys. Letters.* **2011**, *99*, 163303.
[10] a) J. Yang, J. Huang, Q. Li, Z. Li, *J. Mater. Chem. C* **2016**, *4*, 2663–2684; b) S. Y. Lee, C. Adachi, T. Yasuda, *Adv. Mater.* **2016**, *28*, 4626–4631; c) D. R. Lee, B. S. Kim, C. W. Lee, Y. Im, K. S. Yook, S. H. Hwang, J. Y. Lee, *ACS Appl. Mater. Interfaces* **2015**, *7*, 9625–9629; d) R. Kumar Konidena, K. R. Justin Thomas, D. Kumar Dubey, S. Sahoo, J. H. Jou, *Chem. Commun.* **2017**, *53*, 11802–11805.
[11] a) J. Tagare, H. Ulla, M. N. Satyanarayan, S. Vaidyanathan, *J. Photochem. Photobiol. A* **2018**, *353*, 53–64; b) W. C. Chen, Y. Yuan, S. F. Ni, Q. X. Tong, F. L. Wong, C. S. Lee, *Chem. Sc.*, **2017**, *8*, 3599–3608.
[12] a) B. Wang, X. Lv, J. Tan, Q. Zhang, Z. Huang, W. Yi, L. Wang, *J. Mater. Chem. C* **2016**, *4*, 8473–8482; b) C. Li, S. Wang, W. Chen, J. Wei, G. Yang, K. Ye, Y. Liu, Y. Wang, *Chem. Commun.* **2015**, *51*, 10632–10635.
[13] W. C. Chen, Y. Yuan, S. F. Ni, Z. L. Zhu, J. Zhang, Z. Q. Jiang, *ACS applied materials & interfaces*, **2017**, *9*, 7331–7338.
[14] J. Zhao, B. Liu, Z. Wang, Q. Tong, X. Du, C. Zheng, H. Lin, S. Tao, X. Zhang, *ACS Appl. Mater. Interfaces* **2018**, *10*, 9629–9637.
[15] A. Ivanauskaite, R. Lygaitis, S. Raisys, K. Kazlauskas, G. Kreiza, D. Volyniuk, D. Gudeika, S. Jursenas, J. V. Grazulevicius, *Phys. Chem. Chem. Phys.* **2017**, *19*, 16737–16748.
[16] Y. Zhang, J. H. Wang, G. Han, F. Lu, Q. X. Tong, *RSC Adv.* **2016**, *6*, 70800–70809.

[17] Z. L. Zhu, M. Chen, W. C. Chen, S. F. Ni, Y. Y. Peng, C. Zhang, Q. X. Tong, F. Lu, C. S. Lee, *Org. Electron.* **2016**, *38*, 323–329.
[18] a) Y. Kijima, N. Asai, S. I. Tamura, *Japanese. J. Appl. Phys.* **1999**, *38*, 5274–5277; b) D. F. O'Brien, M. A. Baldo, M. E. Thompson, S. R. Forrest, *Appl. Phys. Lett.* **1999**, *74*, 442–444; c) S. Naka, H. Okada, H. Onnagawa, T. Tsutsui, *Appl. Phys. Lett.* **2000**, *76*, 197–199; d) F. Wang, J. Hu, X. Cao, T. Yang, Y. Tao, L. Mei, X. Zhang, W. Huang, *J. Mater. Chem. C* **2015**, *3*, 5533–5540.
[19] M. Y. Lai, C. H. Chen, W. S. Huang, J. T. Lin, T. H. Ke, L. Y. Chen, M. H. Tsai, C. C. Wu, *Angew. Chem. Int. Ed.* **2008**, *47*, 581–585; *Angew. Chem.* **2008**, *120*, 591.
[20] W. C. Chen, Y. Yuan, Y. Xiong, A. L. Rogach, Q. X. Tong, C. S. Lee, *ACS Appl. Mater. Interfaces* **2017**, *9*, 26268–26278.
[21] U. Balijapalli, S. Manickam, K. Thirumoorthy, K. Natesan Sundaramurthy, K. I. Sathiyanarayanan, *J. Org. Chem.* **2019**, *84*, 11513.
[22] Z. Wang, P. Lu, S. Chen, Z. Gao, F. Shen, W. Zhang, Y. Xu, H. S. Kwok, Y. Ma, *J. Mater. Chem.* **2011**, *21*, 5451–5456.
[23] a) S. Zhuang, R. Shangguan, J. Jin, G. Tu, L. Wang, J. Chen, D. Ma, X. Zhu, *Org. Electron.* **2012**, *13*, 3050–3059; b) C. J. Kuo, T. Y. Li, C. C. Lien, C. H. Liu, F. I. Wu, M. J. Huang, *J. Mater. Chem.* **2009**, *19*, 1865–1871.
[24] Z. Wang, X. Li, K. Xue, H. Li, X. Zhang, Y. Liu, Z. Yu, P. Lu, P. Chen, *J. Mater. Chem. C* **2016**, *4*, 1886–1894.
[25] R. J. Holmes, S. R. Forrest, Y. J. Tung, R. C. Kwong, J. J. Brown, S. Garon, M. E. Thompson, *Appl. Phys. Lett.* **2003**, *82*, 2422–2424.
[26] J. W. Kang, D. S. Lee, H. D. Park, Y. S. Park, J. W. Kim, W. I. Jeong, K. M. Yoo, K. Go, S. H. Kim, J. J. Kim, *J. Mater. Chem.* **2007**, *17*, 3714–3719.
[27] K. Natesan Sundaramurthy, K. Sathiyanarayanan, P. Aravindan, *Bull. Korean Chem. Soc.* **2009**, *30*, 2555.
[28] U. Balijapalli, S. Udayadasan, E. Shanmugam, K. I. Sathiyanarayanan, *Dyes Pigm.* **2016**, *130*, 233–244.
[29] W. Qin, Z. Yang, Y. Jiang, J. W. Y. Lam, G. Liang, H. S. Kwok, B. Z. Tang, *Chem. Mater.* **2015**, *27*, 3892–3901.
[30] M. Venkatesan, K. I. Sathiyanarayanan, *Sensors Actuators B* **2018**, *267*, 373–380.
[31] See ref.[15].
[32] E. Miyamoto, Y. Yamaguchi, M. Yokoyama, *Denshi Shashin Gakkaishi (Electrophotography)* **1989**, *28*, 364–370.
[33] Z. R. Grabowski, K. Rotkiewicz, W. Rettig, *Chem. Rev.* **2003**, *103*, 3899–4032.
[34] M. Liu, Y. Liang, P. Chen, D. Chen, K. Liu, Y. Li, S. Liu, X. Gong, F. Huang, S. J. Su, Y. Cao, *J. Mater. Chem. A* **2014**, *2*, 321–325.
[35] V. Mimaite, J. V. Grazulevicius, R. Laurinaviciute, D. Volyniuk, V. Jankauskas, G. Sini, *J. Mater. Chem. C* **2015**, *3*, 11660–11674.
[36] I. Hladka, D. Volyniuk, O. Bezvikonnyi, V. Kinzhybalo, T. J. Bednarchuk, Y. Danyliv, R. Lytvyn, A. Lazauskas, J. V. Grazulevicius, *J. Mater. Chem. C* **2018**, *6*, 13179–13189.
[37] a) N. C. Greenham, R. H. Friend, D. D. C. Bradley, *Adv. Mater.* **1994**, *6*, 491–494; b) N. A. Kukhta, D. Volyniuk, L. Peciulyte, J. Ostrauskaite, G. Juska, J. V. Grazulevicius, *Dyes Pigm.* **2015**, *117*, 122–132.
[38] N. C. Giebink, B. W. D'Andrade, M. S. Weaver, P. B. Mackenzie, J. J. Brown, M. E. Thompson, S. R. Forrest, *J. Appl. Phys.* **2008**, *103*, 044509.
[39] J. Lee, C. Jeong, T. Batagoda, C. Coburn, M. E. Thompson, S. R. Forrest, *Nat. Commun.* **2017**, *8*, 15566.
[40] B. Liu, Z.-W. Yu, D. He, Z.-L. Zhu, J. Zheng, Y.-D. Yu, W.-F. Xie, Q.-X. Tong, C.-S. Lee, *J. Mater. Chem. C* **2017**, *5*, 5402–5410.
[41] a) T. Tsutsui, *MRS Bull.* **1997**, *22*, 39–45; b) C. A. Amorim, M. R. Cavallari, G. Santos, F. J. Fonseca, A. M. Andrade, S. Mergulhão, *J. Non-Cryst. Solids* **2012**, *358*, 484–491.
[42] U. Balijapalli, S. Manickam, M. D. Thiyagarajan, K. I. Sathiyanarayanan, *RSC Adv.* **2016**, *6*, 58549–58560.
[43] N. Zhou, S. Wang, Y. Xiao, X. Li, *Chem. Asian J.* **2018**, *13*, 81–88.
[44] Y. Tan, Z. Zhao, L. Shang, Y. Liu, C. Wei, J. Li, H. Wei, Z. Liu, Z. Bian, C. Huang, *J. Mater. Chem. C* **2017**, *5*, 11901–11909.

Received: November 21, 2019

molecules

MDPI

Article

Towards blue AIE/AIEE: Synthesis and Applications in OLEDs of Tetra-/Triphenylethenyl Substituted 9,9-Dimethylacridine Derivatives

Monika Cekaviciute [1], Aina Petrauskaite [1], Sohrab Nasiri [1], Jurate Simokaitiene [1], Dmytro Volyniuk [1], Galyna Sych [1], Ruta Budreckiene [2] and Juozas Vidas Grazulevicius [1,*]

[1] Department of Polymer Chemistry and Technology, Kaunas University of Technology, Radvilenu rd. 19, LT-50254 Kaunas, Lithuania

[2] Department of Biochemistry, Lithuanian University of Health Sciences, A. Mickeviciaus st. 9, LT-44307 Kaunas, Lithuania

* Correspondence: juozas.grazulevicius@ktu.lt; Tel.: +370-699-409-64

Academic Editor: Christopher Pigge
Received: 13 December 2019; Accepted: 21 January 2020; Published: 21 January 2020

Abstract: Aiming to design blue fluorescent emitters with high photoluminescence quantum yields in solid-state, nitrogen-containing heteroaromatic 9,9-dimethylacridine was refined by tetraphenylethene and triphenylethene. Six tetra-/triphenylethene-substituted 9,9-dimethylacridines were synthesized by the Buchwald-Hartwig method with relatively high yields. Showing effects of substitution patterns, all emitters demonstrated high fluorescence quantum yields of 26–53% in non-doped films and 52–88% in doped films due to the aggregation induced/enhanced emission (AIE/AIEE) phenomena. In solid-state, the emitters emitted blue (451–481 nm) without doping and deep-blue (438–445 nm) with doping while greenish-yellow emission was detected for two compounds with additionally attached cyano-groups. The ionization potentials of the derivatives were found to be in the relatively wide range of 5.43–5.81 eV since cyano-groups were used in their design. Possible applications of the emitters were demonstrated in non-doped and doped organic light-emitting diodes with up to 2.3 % external quantum efficiencies for simple fluorescent devices. In the best case, deep-blue electroluminescence with chromaticity coordinates of (0.16, 0.10) was close to blue color standard (0.14, 0.08) of the National Television System Committee.

Keywords: tetra-/triphenylethene; acridan; aggregation induced emission enhancement; electroluminescence.

1. Introduction

Organic fluorophores emitting prompt blue fluorescence are required by industry since they are characterized by many advantages including high photoluminescence quantum yield (PLQY), fast fluorescent decays (in ns range, which are of interest not only for displays but also for visible light communications), good blue color purity, chromaticity coordinates which meet the National Television System Committee requirements, etc. [1–4]. Despite lower theoretical maximum of internal quantum efficiency (25%) of singlet emission based electroluminescent devices in comparison to that of phosphorescent [5] and thermally activated delayed fluorescence (TADF) [6] based devices, blue fluorescent emitters are used in commercial organic light-emitting diodes (OLEDs) of display and lighting technologies [7]. Such interest in blue fluorescence is mainly explained by its higher stability under electrical excitation, than that of mentioned blue phosphorescent and TADF emitters, the stability of which is fundamentally limited due to the

presence of "hot" exciton forming long-lived triplet excitons [8,9]. Blue fluorescent emitters can be used for a novel energy-saving variety of OLEDs called hyper-fluorescent OLEDs, which are based on energy transfer from the TADF host to the fluorescent emitter in the light-emitting layer [10]. PLQY of OLED emitters (light-emitting layers) has to be close to 100%, which is not a simple task since aggregation-induced quenching is a common property of organic fluorophores [11–13]. To increase PLQY of emitters in solid state, one of the most promising molecular design strategies is introduction of moieties, prompting aggregation-induced emission (AIE) or aggregation induced emission enhancement (AIEE). Tetraphenylethene and triphenylethene are such moieties which usually give significant rise of PLQYs in solid state of many fluorophores including OLED emitters [14,15]. Notably, materials exhibiting AIE or AIEE phenomena are established as multifunctional materials. They are useful not only for OLEDs but also for chemical sensing, for detection of stimuli responses, bio and surface visualizations etc. [16].

Compounds based on carbazole [17–19] or triphenylamine [20,21] moieties substituted by tetraphenylethene and/or triphenylethene units were previously reported to show AIE or AIEE effects. Due to the specific linkage topology, some of them displayed blue/sky-blue fluorescence [22,23]. In addition to carbazole and triphenylamine, nitrogen-containing heteroaromatic acridan derivatives are also well established in OLED technology, some of them as blue emitters. It is expected that tetra-/triphenylethenyl substituted acridanes can exhibit high PLQYs in solid-state. We aimed to check this expectation in the current work. Deep-blue fluorescent OLEDs were recently developed achieving theoretical limit of EQEs (5%) [24]. Such high efficiencies of fluorescent OLEDs were explained by usage of novel emitters with *tert*-butyl substituents which inhibit dimer formation and crystallization-induced emission reduction. It was therefore of interest to use *tert*-butyl-substituted acridan moiety in the design of our emitters with potential ability of aggregation induced/enhanced emission. In the design of new materials for OLEDs, not only high luminescence efficiency but also proper HOMO and LUMO energy levels are of great importance to ensure efficient hole/electron injection under external electric fields [25]. Both acridan and tetra-/triphenylethenyl are electron-donating units and compounds containing these moieties are expected to have low ionization potentials. To control ionization potentials of acridan derivatives, electron-accepting cyano substituents were introduced.

In this work, we report on the design and synthesis of new acridan-based emitters containing tetra-/triphenylethene units. Photophysical, thermal, electrochemical, and electroluminescent properties of the synthesized compounds were investigated to demonstrate the effect of different substitutions.

2. Results and Discussion

2.1. Synthesis

The synthetic route towards the targeted 9,9-dimethylacridine derivatives is shown in Scheme 1. Compounds **1–6** were synthesized by a one-step procedure, i.e., by the Buchwald-Hartwig method [26,27] in the presence of palladium complex. The synthesized compounds were identified by mass-, IR- and ^{1}H, ^{13}C NMR spectrometries.

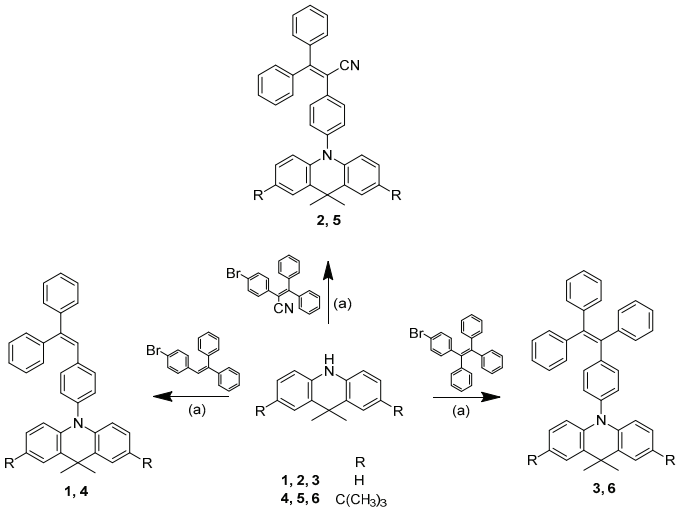

Scheme 1. Syntheses scheme of compounds **1–6**. (**a**) NaO*t*-Bu, $Pd(OAc)_3$, P(*t*-Bu)$_3$, anhydrous toluene, reflux.

2.2. Thermal Properties

The thermal characterization of the compounds was performed by DSC and TGA under nitrogen atmosphere (Figure 1). The thermal characteristics are summarized in Table 1. All the synthesized compounds (**1–6**) showed one-step thermal degradation with moderately high thermal stability (Figure 1b). The temperatures of five percent weight loss (T_d) were in the range of 294–327 °C, as confirmed by TGA with the heating rate of 20 °C/min. T_d of compounds containing no *tert*-butyl groups (**1–3**) were found to be lower than those of the respective *tert*-butyl substituted compounds (**4–6**). Compounds **3** and **6** containing tetraphenylethenyl moieties exhibited higher T_d values than compounds **1** and **4** containing triphenylethenyl units. All the synthesized compounds could be used for the formation of the layers using a vacuum evaporation.

All the compounds were obtained as crystalline substances. Compounds **1–6** showed melting temperatures (T_m) which in the range from 192 to 290 °C (Figure 1a, S1). Melting points of *tert*-butyl substituted compounds (**4–6**) were found to be higher than those of the respective compounds without such substituents (**1–3**). Triphenylethenyl-substituted compounds **1** and **4** possess considerably lower melting points as compared to compounds substituted by tetraphenylethenyl units (**3** and **6**) [28]. Introduction of larger substituents such as cyano-group (compounds **2**,**5**) and phenyl (compounds **3**,**6**) fragments instead of hydrogen (compounds **1**,**4**) in the ethylene unit highly increased the T_m and T_d values of compounds (Table 1). Moreover, the introduction of bulky *tert*-butyl groups apparently affects the crystal packing between adjacent molecules and conformational arrangements of acridan units that resulted in increased T_m values for compounds **4–6**, with respect to non-substituted compounds **1–3** [29,30]. The attachment of *tert*-butyl substituents seems to make structures even more bulky and rigid which presumably leads to the enhanced T_m of compounds **4–6** as well as to their tendency to crystallize from liquid phase [30]. Compounds **4** and **5** also showed polymorphism (Figure 1a). Their samples exhibited two endothermal melting peaks in the first DSC heating scans (Table 1). When the melt samples of compounds **1–3** and **6** were cooled down during DSC experiments, they formed molecular glasses with glass transition temperatures (T_g) in the range of 55–105 °C. Molecular glasses of compounds **2** and **6** were not morphologically stable; they tended to crystallize on further heating. Molecular glasses of compounds **1** and **3** did not show inclination to crystallization in DSC experiments. Compound **1** containing triphenylethenyl moiety showed

considerably lower T_g (by 27 °C) than its analogous compound **3** containing tetraphenylethenyl species. Such observation can be explained by higher molecular weight and stronger intermolecular interactions of compound **3** in the glassy state [15]. Compounds **4** and **5** did not show ability of glass-formation. Exothermal crystallization signals were observed at 160 and 248, 278 °C for **4** and **5**, respectively.

Table 1. Thermal characteristics of compounds **1–6**.

Compound	T_{cr}, °C	T_g**, °C	T_m, °C	T_d, °C
1	-	55	192	294
2	150 **	79	225	318
3	-	82	250	308
4	160 *	-	188, 199	309
5	248 *, 278 **	-	278, 290	322
6	157 **, 192 **	105	266	327

Crystallization temperature (T_{cr}), glass transition temperatures (T_g) and melting points (T_m) were measured by DSC (heating rate of 10 °C/min under nitrogen atmosphere). * - cooling DSC scan, ** - second DSC heating scan. 5% weight loss temperatures (T_d) were estimated by TGA (heating rate of 20 °C/min under nitrogen atmosphere).

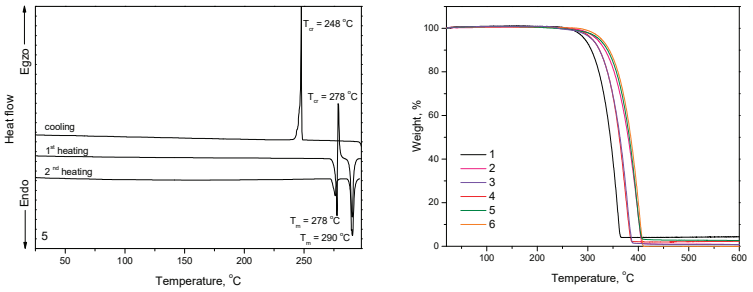

(**a**) (**b**)

Figure 1. (**a**) DSC curves of compound **5** (scan rate of 10 °C/min. N_2 atmosphere) and (**b**) TGA curves of compounds **1–6** (scan rate of 20 °C/min. N_2 atmosphere).

2.3. Theoretical Calculations.

Theoretical quantum calculations based on DFT/B3LYP/6-31* using Spartan '14 package software were carried out to understand photophysical and electrochemical properties of target compounds. The overall optimized geometries and distribution of highest occupied molecular (HOMO) and lowest unoccupied molecular orbitals (LUMO) for the ground state of compounds **1–6** are illustrated in Figure 2. All compounds along the series adopt highly twisted non-planar configurations, preferable for the active rotations of phenyl rings in the solutions, and are restricted in the solid state. The HOMO of all the compounds **1–6** was found to be similar and localized mainly on the acridan unit and slightly on the connected phenyl ring. Meanwhile the LUMO mainly located on twisted tri- or tetraphenyl ethylene units. Such a HOMO–LUMO separation can be explain by close to perpendicular molecular geometries with dihedral angles between acridan electron-donating fragment and tri- or tetraphenyl frament of 85–88°. Moreover, HOMO–LUMO separation imparts the luminogens with intramolecular charge-transfer characteristics confirmed by experimental photophysical measurements described below (Figure 2). The theoretically calculated HOMO energies were found to be in the range from 4.7 eV to 4.9 eV while the LUMO energies varied from

1.3 eV up to 2.1 eV (Table 2). Due to the presence of additional electron-donating di-*tert*-butyl groups the HOMO energies of compounds 4–6 were found to be slightly lower in respect to the corresponding non-substituted acridan-based compounds **1**–**3**. The same tendency was observed for the LUMO energies of compounds. The theoretically calculated energy gaps varied in the range of 2.7–3.6 eV with the highest values for the compounds with tri- and tetraphenyl ethene fragments (3.3 eV and 3.4 eV) (Table 2). Due to the presence of electron-withdrawing cyano-group compounds **2** and **5** exhibited lower energy gap values of 2.8 and 2.7 eV, respectively (Table 2).

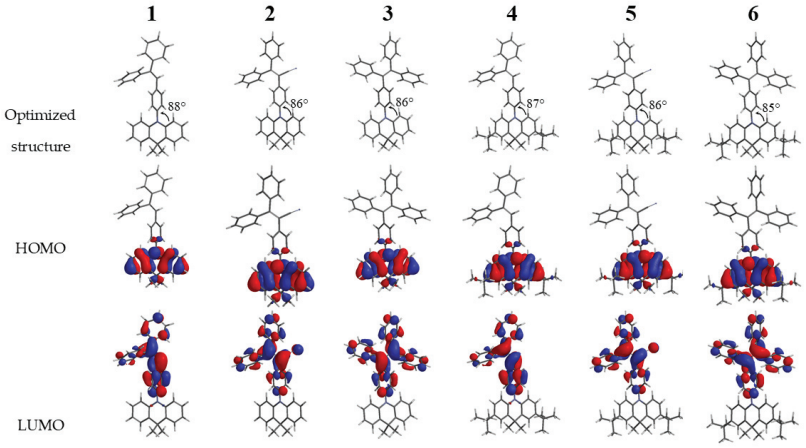

Figure 2. Spatial highest occupied molecular orbitals (HOMO) and lowest unoccupied molecular orbitals (LUMO) distributions for compounds **1**–**6** (DFT/B3LYP/6–31*).

2.4. Electrochemical and Photoelectrical Properties.

Electrochemical properties of the compounds were studied by cyclic voltammetry (CV). The ionization potential values (IP_{CV}) were determined from the values of the first onset oxidation potential with respect to ferrocene (Figures 3a and S2). The IP_{CV} values of synthesized compounds ranged from 5.40 to 5.63 eV (Table 2). Ionization potentials of vacuum deposited films (IP_{EP}) of compounds **1**–**6** were also determined by electron photoemission method in air (Figure 3b). The IP_{EP} values of **1**–**6** ranged from 5.43 to 5.81 eV. The ionization potential values of *tert*-butyl substituted compounds **4**–**6** were found to be lower than those of compounds containing no *tert*-butyl groups (**1**–**3**) due to the slight donating effect of these groups. IP values of compounds **2** and **5** are higher than those of the rest compounds due to the accepting properties of the cyano-group.

Table 2. Electrochemical, photoelectrical, and optical characteristics of compounds **1–6**.

Compound	E_g^{opt}, eV	E_{onset}, V	IP_{CV}, eV	IP_{EP}, eV	EA_{EP}, eV	HOMO, eV	LUMO, eV	$E_{g,\,theor}$
1	3.07	0.79	5.59	5.70	2.63	−4.8	−1.5	3.3
2	2.66	0.83	5.63	5.81	3.15	−4.9	−2.1	2.8
3	2.86	0.74	5.54	5.66	2.80	−4.8	−1.4	3.4
4	2.67	0.60	5.40	5.50	2.83	−4.7	−1.4	3.3
5	2.57	0.66	5.46	5.63	3.06	−4.7	−2.0	2.7
6	2.61	0.60	5.40	5.43	2.82	−4.7	−1.3	3.4

The onset oxidation potentials (E_{onset}) versus Fc measured by CV from the first redox cycle. The optical band gap (E_g^{opt}) estimated from the edges of absorption spectra of solid samples ($E_g^{opt} = 1240/\lambda_{onset}$). Ionization potentials (IP_{EP}) measured by photoelectron emission in air method. Ionization potentials (IP_{CV}) measured by CV: $IP_{CV}=4.8+E_{onset}$ [31]. Electron affinities calculated using equation $EA_{EP} = IP_{EP} - E_g^{opt}$. HOMO/LUMO -energies of highest occupied and lowest unoccupied molecular orbitals. $E_{g,\,theor}$ = HOMO-LUMO

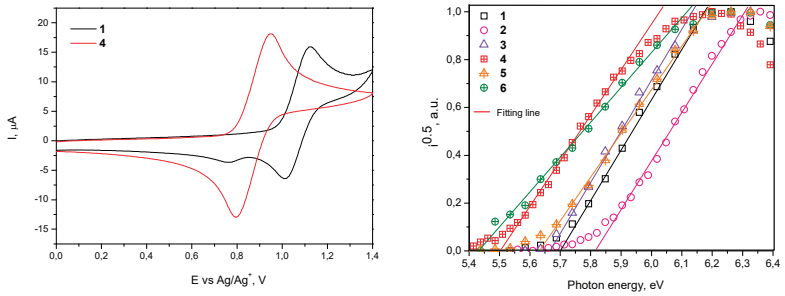

(**a**) (**b**)

Figure 3. (**a**) First cyclic voltammetry (CV) cycle curves of dilute solutions of compounds **1** and **4** in dichloromethane (room temperature) recorded at sweep rate of 0.1 V/s and (**b**) photoelectron emission spectra of solid films of compounds **1–6**.

2.5. Photophysical Properties

To investigate electronic structures of differently substituted compounds **1–6** in the ground state, absorption spectra of their dilute toluene and THF solutions were recorded (Figure 4). The wavelengths of absorption spectra maxima of the solutions of compounds **1–6** were not particularly sensitive to the solvents used and were observed at ca. 290 nm. The position of this UV band is close to that of acridan (Figure 4a). This observation shows that the low energy bands of compounds **1–6** can be mainly attributed to the local acridan transitions. The shoulders (maxima) at ca. 310–320 nm are attributed to the influence of tetra-/triphenylethenyl moieties. Weak lower-energy absorption bands in the range of 350–450 nm are apparently related to intermolecular charge transfer (ICT) between acridan and tetra-/triphenylethenyl moieties (Figure 4a, inset). This observation can apparently be explained by HOMO–LUMO separation of the compounds due to their twisted molecular structures (Figure 2). Compounds **2** and **5** displayed the most red-shifted ICT bands due to the presence of relatively strong electron-acceptors, i.e., cyano groups. UV absorption spectra of vacuum-deposited films of **1–6** replicated the spectra of the corresponding solutions well (Figure 4b). Slightly shifted low energy edges of UV absorption spectra of vacuum-deposited films in comparison to those of solutions can be explained either by stronger ICT of **1–6** in solid-state or by aggregation effects.

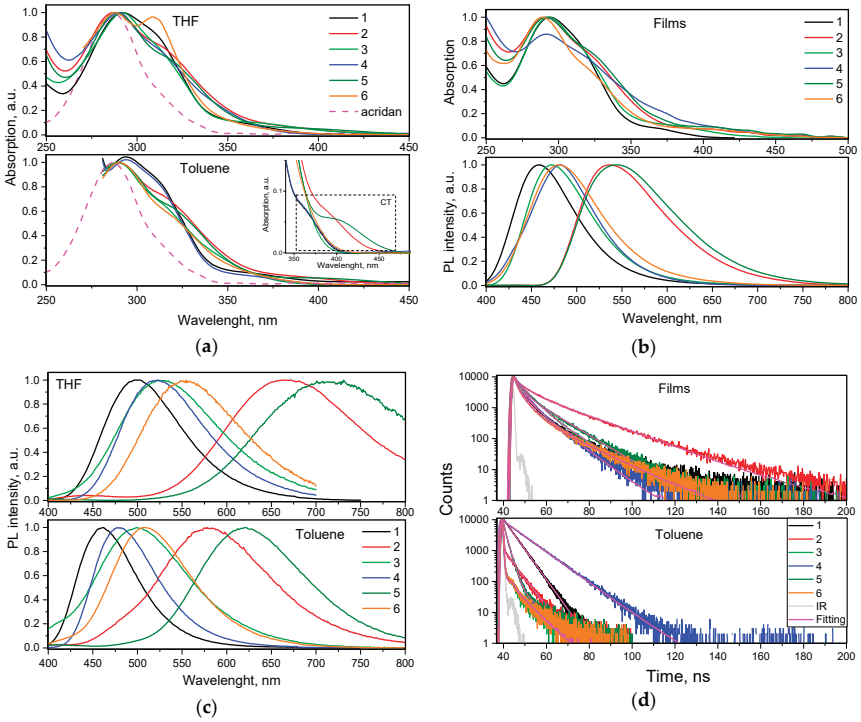

Figure 4. (**a**) UV-vis absorption spectra of THF and toluene solutions of compounds **1–6** in (10^{-5} M). The low-energy ICT absorption bands of the solutions in toluene are zoomed in the inset. (**b**) UV-vis absorption and PL spectra of the films of **1–6**. (**c**) Steady-state PL spectra of THF and toluene solutions of compounds **1–6**. (**d**) PL decays of solid samples and toluene solutions of **1–6** recorded at excitation wavelength 374 nm.

Because of ICT, PL spectra of compounds **1–6** were found to be sensitive to polarity of the media. Thus, PL spectra of THF solutions of compounds **2** and **5** were significantly red-shifted in comparison to their toluene solutions (Figure 4c). Weak red-shifts were also observed for compounds **1**, **3**, **4**, and **6**, containing no cyano groups, induced by the molecular twisting. The introduction of additional phenyl group into phenylethenyl moieties resulted in red-shifts of the fluorescence spectra (cf. the spectra of **3** and **6** with those of **1** and **4**). PL spectra of solid films of compounds **1–6** were found to be similar to PL spectra of the corresponding toluene solutions apparently because low dielectric constants of the solid samples (close to that of toluene). Blue-shifted emission of the solid films of compounds **1–6** with respect to that of THF solutions may be explained by the influence of relaxation of local exited (LE) states. This assumption is in agreement with double exponential photoluminescence decays of the films of **1–6** that can be related to overlapping of relaxation of LE and ICT states (Figure 4d, Figure S3). Solid films of compounds **1**, **3**, **4**, and **6** emitted in the blue region with PL spectra peaked at 458–482 nm (Figure 4b). However, yellowish-green emission was observed for the films of compounds **2** and **5** due to the presence of cyano groups. PL decays of **1–6** were observed in ns-range that prove simple fluorescent nature of emission (Figure 4d). Faster fluorescence transients mostly with mono exponential fitting were observed for the solutions of compounds **1–6** relative to those of solid samples.

Table 3. Photophysical characteristics of compounds **1–6.**

Compound	Toluene			THF		Non-doped film			Doped film	
	λ_{abs}^{max}, nm	λ_{PL}^{max}, nm	PLQY, %	λ_{abs}^{max}, nm	λ_{PL}^{max}, nm	λ_{abs}^{max}, nm	λ_{PL}^{max}, nm	PLQY, %	λ_{PL}^{max}, nm	PLQY, %
1	294	460	32	292	499	290	451	51	438	72
2	289	578	1	287	665	290	481	53	522	88
3	289	499	< 1	289	527	288	452	44	442	71
4	294	477	39	290	522	290	464	40	440	52
5	290	622	2	288	715	289	531	26	550	38
6	290	508	1	289	553	288	475	53	445	83

λ_{abs}^{max} — the wavelength of absorption maximum. λ_{PL}^{max} — the wavelength of emission maximum (λ_{ex} = 310 nm). The PL spectra of doped solid films **1–6**: mCP are shown in Figure S4.

Fluorescence quantum yields (PLQY) of dilute solutions in toluene and of non-doped and doped films of the compounds **1–6** are given in Table 3. The films of all the studied compounds exhibited considerably higher PLQY than the corresponding dilute solutions. This observation indicates aggregation induced emission (AIE) for compounds **2**, **3**, **5**, and **6**, with practically absent emission of solutions, and aggregation induce emission enhancement (AIEE) for compounds **1** and **4** with relatively strong emission of the solution in toluene (PLQYs of 32 and 39%). Since non-radiative rates of toluene solutions of compounds **1** and **4** were much lower than those of toluene solutions of other compounds (Table S1), different PLQY values were obtained for compounds 1–6. PLQY values (26–53%) of non-doped films of the compounds were still much below unity apparently because of intermolecular quenching which may be partly overcome by appropriate hosting [32]. Indeed, using 1,3-bis(N-carbazolyl)benzene (mCP) as the host, the doped films with 10% wt. of the guest showed improved PLQY reaching 88% in case of compound **2** doped in mCP due to its lowest non-radiative rate in comparison to that of other compounds (Table S1). This finding highlights potential of the compounds for the application in OLEDs.

To investigate AIE/AIEE of **1–6**, PL spectra of their dispersions in the THF-water mixtures with various water fractions (f_w) were recorded (Figures 5a, 5b, S5). Being insoluble in water, emissive aggregates of **1–6** were formed at the certain concentration of water highlighting AIE/AIEE phenomena. Relative dependences of intensities and wavelengths of PL peaks of compounds **1–6** versus water fractions are shown in Figures 4c and 4d respectively. With the increase in water fraction in THF-water mixture, emission intensity of the dispersion of compound **1** constantly decreased and PL maximum wavelength red-shifted until the aggregates were formed (Figures 4c, 4d). These effects were caused by increasing polarity of the THF-water mixtures to which ICT fluorescence is very sensitive. The further increase of f_w lead to the increase of emission intensity and blue shifts of PL spectra due to the increasing amount of aggregates. The similar regularities were observed for the compounds **2–4**, **6** and were in good agreement with those reported for many other AIE/AIEE compounds [33–35]. However, slightly different behavior was observed for compound **5** (Figure 5b). The dispersion of compound **5** showed maximum emission intensity and higher blue shift at f_w = 70%. The further increase of f_w induced decrease of PL intensity and PL red-shift (Figures 4c, 4d). Similar observation was previously detected for compounds with AIE/AIEE effects, although the reason for this is not clear yet [36–38]. To our opinion, this observation can apparently be explained by structural modification of aggregates, when their sizes were further increased.

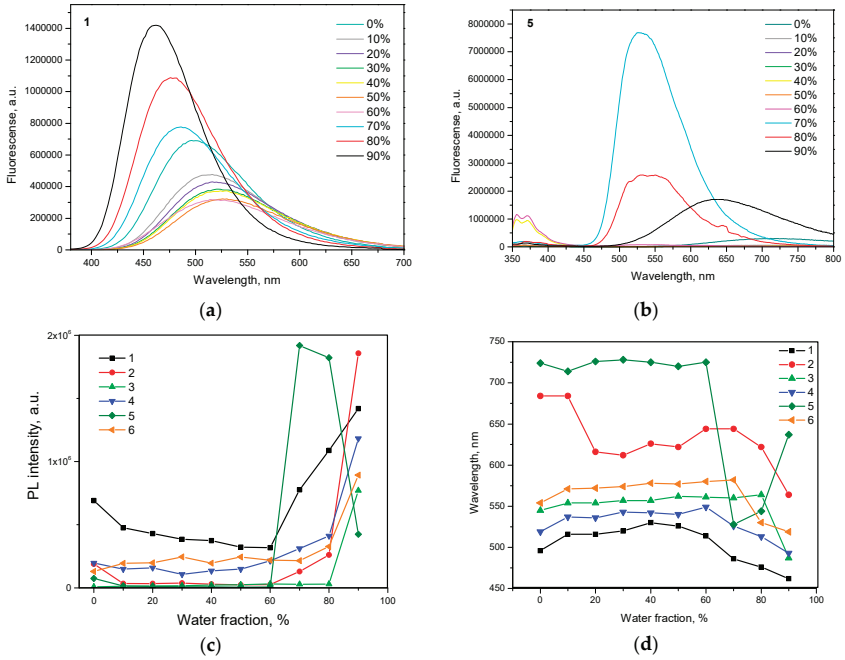

Figure 5. Emission spectra of compounds (**a**) **1** and (**b**) **5** in THF/water mixtures (0–90%). Plots of (**c**) maximum emission intensity and (**d**) wavelength versus water fraction for the dispersions of compounds **1–6** in the mixtures of THF and water.

2.6. Electroluminescent Properties

Since compounds **1–6** showed high PLQYs in solid-state, they were tested as emitters for non-doped fluorescent OLEDs. Taking into account the values of ionization potentials and electron affinities obtained for vacuum-deposited films of compounds **1–6**, their electroluminescent properties were studied using device structure: ITO/MoO_3 (0.5 nm)/NPB (35 nm)/mCP (7 nm)/ light-emitting layer (20 nm)/TSPO1 (7 nm)/TPBi (30 nm)/LiF (0.5 nm)/Al. Non-doped light-emitting layers of compounds **1–6** were used in devices **1N–6N**, respectively. The layers of MoO_3, NPB, mCP, TSPO1, TPBi, and LiF were used as hole-injecting layer, hole transporting layer, exciton blocking layer, hole/exciton blocking layer, electron transporting layer, and electron-injecting layer, respectively. According to an equilibrium energy diagram of the devices that demonstrates absence of big energy barriers for transported charges under applied external voltages (Figure S6), both holes and electrons were effectively injected to light-emitting layers. Light-emitting recombination of the formed excitons occurred within light-emitting layers. Thus is evident from the shapes of electroluminescence (EL) spectra of devices **1N–6N** that were very similar to the shapes of PL spectra of vacuum-deposited films **1–6**, respectively (Figure 6a). EL spectra of devices **1N–6N** were found to be similar under different applied voltages proving the main contribution of emitters **1–6** in electroluminescence (Figure S7). Blue EL with close CIE coordinates (x from 0.15 to 0.17 and y from 0.13 to 0.25) was observed for devices **1N**, **3N**, **4N**, and **6N** based on acridan and tetra-/triphenylethenyl-based emitters **1**, **3**, **4**, and **6**, containing no cyano groups (Table 4). As seen in Table S2, the device 1N is characterized by the most blue-shifted electroluminescence with CIE color coordinates (0.15, 0.13) in comparison to that of previously published devices based on tetra(tri)phenylethene-substituted carbazole or triphenylamine OLED emitters. Meanwhile, OLEDs with the emitting layers of compounds **2** and **5**

demonstrated yellow EL with CIE of (0.34, 0.56) and (0.41, 0.53) for devices **2N** and **5N** similarly to PL of vacuum-deposited films (Figure 3).

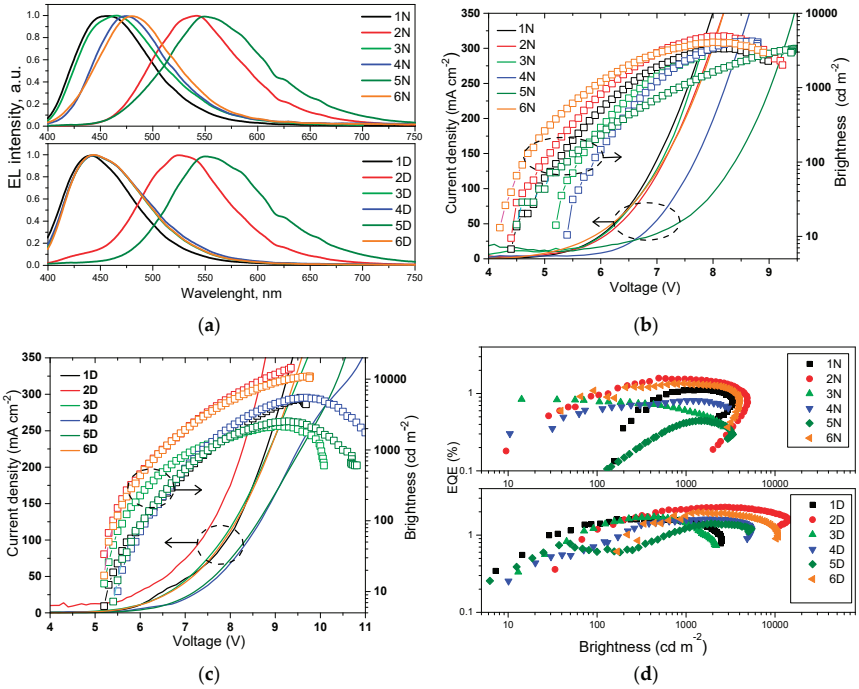

Figure 6. (**a**) Electroluminescence (EL) spectra, (**b**,**c**) current density-voltage-brightness and (**d**) external quantum efficiency-brightness characteristics of non-doped (**1N–6N**) and doped (**1D–6D**) organic light-emitting diodes (OLEDs).

Brightness exceeded of 1000 cd/m² for all non-doped devices **1N–6N**. It reached maximum value of 4940 cd/m² in case of device **2N**. EL spectrum of this device was closest to the sensitivity of human eye. In addition, the film of emitter **2** was characterized by high PLQY of 53% (Table 3). Turn on voltages of devices **1N–6N** were observed in the range of 4.2–5.4 V demonstrating satisfactory charge-injecting and charge-transporting properties of the devices. Maximum external quantum efficiencies (EQE) of devices **1N–6N** were roughly proportional to PLQY values of the non-doped films of the corresponding emitters. (Figure 6d, Table 4). These EQEs are close to those of blue/green devices based on carbazole/triphenylamine and tetra-/triphenylethenyl-containing derivatives [22,39]. The highest EQE of 1.59% was obtained for device **2N**. This value is lower than 2.65%, which is theoretical maximum of EQE for device with fluorescent emitter having PLQY of 53%. Theoretical EQE for device **2N** was calculated by formula $\eta_{ext}=\gamma\times\phi_{PL}\times\chi\times\eta_{out}$ using the charge-balance factor $\gamma = 1$, the efficiency of exciton production $\chi = 0.25$ (as for fluorescent emitter), the outcoupling efficiency $\eta_{out} = 0.2$, and $\phi_{PL} = 0.53$ for the film of compound **2**. Apparently, the charge-balance factor of the studied devices is lower than unity. This presumption can be supported by poor charge-transporting properties of the emitters **1–6**. We tried to measure charge mobilities in vacuum-deposited films of compounds **1–6** by the time of flight (TOF) method, however, the transit times were not observed possibly because of the fast relaxation of charges in their layers (Figure S8). TOF measurements roughly demonstrated the charge transporting "problems" of the non-doped films of compounds **1–6**. Therefore, usage of appropriate hosts was essential. The commonly used host mCP was chosen for

the fabrication of doped OLEDs exploiting the same device structure as for non-doped devices. In doped devices **1D–6D**, light-emitting layers **1–6** (10 wt.%) doped in mCP were used. Selection of the host was based not only on its appropriate HOMO/LUMO energy levels but also on high PLQYs of the films of **1–6** (10 wt.%) doped in mCP, which ranged from 38 to 88%. Usage of the host allowed the increase of PLQY of compounds **1–6** in solid-state, apparently, due to the decrease of intermolecular interactions (restrictions of π–π* stacking) between neighboring molecules. PL spectra of the doped films were slightly blue-shifted in comparison to PL spectra of the corresponding non-doped films. Polarity and aggregation effects (Figures 3 and S12) can explain this observation. EL spectra of doped devices **1D–6D** were in good agreement with PL spectra of light-emitting layers **1–6**: mCP (Figure S4). The shapes of EL spectra of the doped devices were the practically same under different external voltages (Figure S7). CIE coordinates of the doped devices **1D–6D** were slightly shifted to deeper blue region in comparison to those of non-doped devices **1N–6N** (Table 4).

Table 4. The electroluminescent parameters of non-doped **1N–6N** and doped **1D–6D** devices.

Device	Turn on Voltage (V)	Maximum Brightness (cd/m²)	Maximum Current Efficiency (cd/A)	Maximum Power Efficiency (lm/W)	Maximum External Quantum Efficiency (%)	EL peak (nm)	CIE coordinates (x, y)
Non-doped devices 1N–6N							
1N	4.4	3350	2.23	1.07	1.10	456	0.15, 0.13
2N	4.4	4940	2.90	1.60	1.59	540	0.34, 0.56
3N	5.2	2630	2.83	1.78	0.86	465	0.16, 0.16
4N	5.4	4200	1.10	0.51	0.82	475	0.15, 0.22
5N	4.5	3360	1.30	0.53	0.45	550	0.41, 0.53
6N	4.2	4090	1.55	0.89	1.35	480	0.17, 0.25
Doped devices 1D–6D							
1D	5.2	5460	2.48	1.18	1.63	439	0.16, 0.10
2D	5.2	14400	4.67	2.13	2.32	525	0.28, 0.49
3D	5.2	2180	2.11	1.06	1.72	444	0.17, 0.16
4D	5.5	5460	3.10	1.29	1.62	444	0.16, 0.12
5D	5.4	2540	1.65	0.64	1.42	550	0.43, 0.53
6D	5.2	10900	1.95	0.94	1.93	444	0.16, 0.12

As it was expected, maximum EQEs of all the doped devices (1D–6D) were improved in comparison to those of non-doped ones mainly due to the incensed PLQYs of the emitters dispersed in host and due to the satisfactory charge-transporting properties of mCP (Table 4) [40]. The highest maximum EQE of 2.32% was also obtained for device **2D** based on compound **2**, which showed the highest PLQY of 88% when dispersed in mCP. However, charge-injection properties of the doped devices were not improved. This is evident taking into account the higher turn on voltages of devices **1D–6D** compared to those of devices **1N–6N**. This observation can be attributed to induced energy barrier in the device structure by relatively deep HOMO of mCP. Nevertheless, it is demonstrated that compounds **1–6** can be used as fluorescent emitters in doped OLEDs. When appropriate host exhibiting thermally activated delayed fluorescence (TADF) is available, it is worth testing compounds **1–6** as fluorescent emitters in three component systems of **1–6**: TADF host:host for increasing efficiencies of **1–6**-based OLEDs, keeping in mind that exciton production probability $\chi = 1$ for TADF based systems [10]. In addition, compounds **1–6** are potential candidates for sensing applications since they exhibit different emission intensities in liquids and solids.

3. Materials

All the required chemicals, i.e., 2-(4-bromophenyl)-1,1-diphenylethenylene, 2-(4-bromophenyl)-1,2,2-triphenylethenylene, solution of tri-*tert*-butylphosphine in toluene (1.00 M), sodium *tert*-butoxide, and palladium acetate were obtained from Sigma-Aldrich and used as received. 9,9-

Dimethylacridine and 2,7-di-*tert*-butyl-9,9-dimethylacridine were purchased from Center for Physical Sciences and Technology, Lithuania. 2-(4-Bromophenyl)-2-cyano-1,1-diphenylethylene (Mp = 158–160 °C) was obtained according to the previously described procedure [41].

10-(4-(2,2-Diphenylethenyl)phenyl)-9,9-dimethylacridine (**1**). 9,9-Dimethylacridine (0.70 g, 4.78 mmol) and 2-(4-bromophenyl)-1,1-diphenylethylene (1.34 g, 5.74 mmol) were dissolved in anhydrous toluene (10 ml) under Ar. Sodium *tert*-butoxide (0.64 g, 9.56 mmol), palladium acetate (0.02 g, 0.09 mmol), and a solution of tri-*tert*-butylphosphine in toluene (1.00 M, 0.02 ml, 0.09 mmol) were added to the solution and the reaction mixture was refluxed for 12 h. When the reaction was finished (TLC control), the mixture was cooled down to the room temperature and extracted with ethyl acetate. The organic extract was washed with water and dried (Na_2SO_4). Then, the solvent was evaporated under vacuum. The product was purified by silica gel column chromatography using hexane as an eluent. White crystals were obtained after recrystallization from hexane with the yield of 72% (1.11 g). Mp = 188–191 °C. MS (ES^+), *m*/*z* = 463 $[M]^+$. ^1H NMR (400 MHz, $CDCl_3$) δ (ppm): 1.57 (s, 6H), 6.19 (d, *J* = 8.1 Hz, 2H), 6.82 (t, *J* = 7.3 Hz, 2H), 6.88 (t, *J* = 7.6 Hz, 2H), 6.98-7.02 (m, 3H), 7.17 (d, *J* = 8.3 Hz, 2H), 7.19-7.22 (m, 2H), 7.23-7.32 (m, 8H), 7.34 (d, *J* = 6.8 Hz, 2H). ^{13}C NMR (100 MHz, $CDCl_3$) δ (ppm): 31.1, 35.9, 114.1, 120.5, 125.1, 126.3, 127.2, 127.6, 127.7, 127.8, 128.3, 128.8, 130.1, 130.3, 130.8, 131.9, 137.4, 139.4, 140.1, 140.9, 143.2, 143.7. IR ν_{max} (KBr): 3054, 3028 (C–H, Ar); 2958 (C–H); 1587 (C_6H_5-); 1471, 1446 (–CH_3); 1321 (Ph–CH_3); 1267 (C–N–, Ar); 923, 751 (C=C–H); 698 (CH=CH).

10-(4-(1-Cyano-2,2-diphenylethenyl)phenyl)-9,9-dimethylacridine (**2**). Compound **2** was prepared by a similar procedure to compound **1**, using 9,9-dimethylacridine (0.40 g, 4.78 mmol), 2-(4-bromophenyl)-2-cyano-1,1-diphenylethylene (0.83 g, 5.74 mmol), sodium *tret*-butoxide (0.37 g, 9.56 mmol), palladium acetate (0.01 g, 0.09 mmol), and a solution of tri-*tert*-butylphosphine in toluene (1.00 M, 0.01 ml, 0.09 mmol). Light yellow crystals were obtained after recrystallization from hexane with the yield of 83 % (0.77 g). Mp = 219–222 °C. MS (ES^+), *m*/*z* = 488 $[M]^+$. ^1H NMR (400 MHz, $CDCl_3$) δ (ppm): 1.59 (s, 6H), 6.14 (d, *J* = 7.9 Hz, 2H), 6.86 (t, *J* = 7.3 Hz, 2H), 6.89–6.95 (m, 2H), 7.01 (d, *J* = 7.2 Hz, 2H), 7.11 (d, *J* = 8.2 Hz, 2H), 7.14–7.23 (m, 2H), 7.32–7.45 (m, 10H). ^{13}C NMR (100 MHz, $CDCl_3$) δ (ppm): 31.2, 35.9, 110.7, 113.9, 119.9, 120.8, 125.3, 126.4, 128.3, 128.6, 129.4, 130.0, 130.1, 130.2, 130.9, 131.5, 132.3, 135.1, 138.9, 139.9, 140.6, 141.1, 158.9. IR ν_{max} (KBr): 3050, 3032 (C–H, Ar); 2975, 2957 (C–H); 2208 (–C≡N); 1588, 1506 (C_6H_5–); 1472, 1445 (–CH_3); 1324 (Ph–CH_3); 1270 (C–N–, Ar); 1110 (–C–N–); 922, 748 (C=C–H); 704 (CH=CH).

10-(4-(1,2,2-Triphenylethenyl)phenyl)-9,9-dimethylacridine (**3**). Compound **3** was prepared by the similar procedure as compound **1**, using 9,9-dimethylacridine (0.40 g, 4.78 mmol), 2-(4-bromophenyl)-1,1,2-triphenylethylene (0.94 g, 5.74 mmol), sodium *tret*-butoxide (0.37 g, 9.56 mmol), palladium acetate (0.01 g, 0.09 mmol), and a solution of tri-*tert*-butylphosphine in toluene (1.00 M, 0.01 ml, 0.09 mmol). White crystals were obtained after recrystallization from hexane with the yield of 68% (0.70 g). Mp = 245–248 °C. MS (ES^+), *m*/*z* = 539 $[M]^+$. ^1H NMR (400 MHz, $CDCl_3$) δ (ppm): 1.66 (s, 6H), 6.25 (d, *J* = 8.1 Hz, 2H), 6.93 (t, *J* = 7.4 Hz, 2H), 7.01 (t, *J* = 7.7 Hz, 2H), 7.07 (d, *J* = 8.2 Hz, 2H), 7.10–7.20 (m, 15H), 7.30 (d, *J* = 8.2 Hz, 2H), 7.45 (d, *J* = 7.6 Hz, 2H). ^{13}C NMR (100 MHz, $CDCl_3$) δ (ppm): 31.3, 36.1, 114.1, 120.6, 125.3, 126.4, 126.8, 126.9, 127.8, 127.9, 128.0, 130.1, 130.6, 131.4, 131.6, 133.8, 139.2, 140.5, 140.9, 142.1, 143.1, 143.3, 143.7, 144.1. IR ν_{max} (KBr): 3052, 3024 (C–H, Ar); 2948 (C–H); 1590, 1508 (C_6H_5–); 1475, 1441 (–CH_3); 1324 (Ph–CH_3); 1270 (C–N–, Ar); 921, 748 (C=C–H); 694 (CH=CH).

*2,7-Di-*tert*-butyl-10-(4-(2,2-diphenylethenyl)phenyl)-9,9-dimethylacridine* (**4**). Compound **4** was prepared by the similar procedure as compound **1**, using 2,7-di-*tert*-butyl-9,9-dimethylacridine (0.70 g, 3.11 mmol), 2-(4-bromophenyl)-1,1-diphenylethylene (0.88 g, 3.74 mmol), sodium *tret*-butoxide (0.42 g, 6.22 mmol), palladium acetate (0.01 g, 0.06 mmol), and a solution of tri-*tert*-butylphosphine in toluene (1.00 M, 0.01 ml, 0.06 mmol). Light yellow crystals were obtained after recrystallization from hexane with the yield of 89% (1.12 g). Mp = 192–196 °C. MS (ES^+), *m*/*z* = 576 $[M]^+$. ^1H NMR (400 MHz, $CDCl_3$) δ (ppm): 1.22 (s, 18H), 1.60 (s, 6H), 6.02–6.16 (m, 2H), 6.89 (d, *J* = 8.0 Hz, 2H), 6.93–7.03 (m, 3H), 7.10–7.16 (m, 2H), 7.17–7.21 (m, 2H), 7.22–7.32 (m, 8H), 7.36 (s, 2H). ^{13}C NMR (100 MHz, $CDCl_3$) δ (ppm): 29.8, 31.6, 34.2, 36.4, 113.3, 122.1, 123.0, 127.4, 127.6, 127.7, 127.8, 128.3, 128.8, 130.4, 130.9, 131.9, 137.2, 140.1, 143.3, 143.5. IR ν_{max} (KBr): 3081, 3050 (C–H, Ar); 2949, 2901 (C–H); 1603, 1506

(C_6H_5–); 1490 (–CH_3); 1410, 1361 ((CH_3)$_3$C–); 1330 (Ph–CH_3); 1265 (C–N–, Ar); 890, 817, 763 (C=C–H); 696 (CH=CH).

2,7-Di-tert-*butyl-10-(4-(1-cyano-2,2-diphenylethenyl)phenyl)-9,9-dimethylacridine* (**5**). Compound **5** was prepared by the similar procedure to compound **1**, using 2,7-di-*tert*-butyl-9,9-dimethylacridine (0.40 g, 2.85 mmol), 2-(4-bromophenyl)-2-cyano-1,1-diphenylethylene (0.49 g, 3.41 mmol), sodium *tert*-butoxide (0.22 g, 5.69 mmol), palladium acetate (0.01 g, 0.06 mmol), and a solution of tri-*tert*-butylphosphine in toluene (1.00 M, 0.01 ml, 0.06 mmol). The product was purified by silica gel column chromatography using an eluent mixture of THF and hexane in the volume ratio of 1:50. Yellow crystals were obtained after recrystallization from the eluent mixture of solvents with the yield of 85% (0.64 g). Mp = 272–275 °C. MS (ES^+), *m*/*z* = 600 $[M]^+$. ^{1}H NMR (400 MHz, $CDCl_3$) δ (ppm): 1.24 (s, 18H), 1.61 (s, 6H), 5.98–6.13 (m, 2H), 6.93 (d, *J* = 8.0 Hz, 2H), 6.99 (d, *J* = 9.8 Hz, 2H), 7.10 (d, *J* = 7.2 Hz, 2H), 7.14–7.22 (m, 4H), 7.34–7.47 (m, 8H). ^{13}C NMR (100 MHz, $CDCl_3$) δ (ppm): 29.9, 31.7, 34.2, 36.4, 110.8, 113.6, 120.0, 123.1, 128.3, 128.6, 129.4, 130.0, 130.2, 130.9, 131.7, 132.2, 134.8, 138.9, 140.1, 158.8. IR ν_{max} (KBr): 3054, 3037 (C–H, Ar); 2957, 2901 (C–H); 2206 (–C≡N); 1639 (C=C, Ar); 1601, 1506 (C_6H_5–); 1489 (–CH_3); 1410, 1361 ((CH_3)$_3$C–); 1328 (Ph–CH_3); 1267 (C–N–, Ar); 887, 809, 745 (C=C–H); 699 (CH=CH).

2,7-Di-tert-*butyl-10-(4-(1,2,2-triphenylethenyl)phenyl)-9,9-dimethylacridine* (**6**). Compound **6** was prepared by the similar procedure as compound **1**, using 2,7-di-*tert*-butyl-9,9-dimethylacridine (0.40 g, 3.11 mmol), 1-(4-bromophenyl)-1,2,2-triphenylethylene (0.61 g, 3.73 mmol), sodium *tert*-butoxide (0.24 g, 6.22 mmol), palladium acetate (0.01 g, 0.06 mmol), and a solution of tri-*tert*-butylphosphine in toluene (1.00 M, 0.01 ml, 0.06 mmol). White crystals were obtained after recrystallization from hexane with the yield of 77% (0.62 g). Mp = 261–263 °C. MS (ES^+), *m*/*z* = 652 $[M]^+$. ^{1}H NMR (400 MHz, $CDCl_3$) δ (ppm): 1.24 (s, 18H), 1.60 (s, 6H), 5.98–6.13 (m, 2H), 6.92 (d, *J* = 8.4 Hz, 2H), 6.96 (d, *J* = 8.0 Hz, 2H), 7.00–7.11 (m, 15H), 7.15–7.19 (m, 2H), 7.37 (s, 2H). ^{13}C NMR (100 MHz, $CDCl_3$) δ (ppm): 25.1, 31.6, 34.2, 36.7, 113.3, 122.3, 122.9, 126.6, 126.7, 126.8, 127.6, 127.8, 127.9, 129.5, 130.6, 131.4, 131.5, 133.6, 139.5, 140.5, 141.9, 143.1, 143.3, 143.7, 143.8. IR ν_{max} (KBr): 3054, 3039 (C–H, Ar); 2953, 2896 (C–H); 1603, 1509 (C_6H_5–); 1493, 1443 (–CH_3); 1412, 1362 ((CH_3)$_3$C–); 1336 (Ph–CH_3); 1267 (C–N–, Ar); 890, 808, 744 (C=C–H); 696 (CH=CH).

Devices were fabricated using the synthesized materials as AIE/AIEE emitters and commercially available molybdenum trioxide (MoO_3), N,N′-di(1-naphthyl)-N,N′-diphenyl-(1,1′-biphenyl)-4,4′-diamine (NPB), 1,3-bis(N-carbazolyl)benzene (mCP), diphenyl[4-(triphenylsilyl)phenyl]phosphine oxide (TSPO1), 2,2′,2′′-(1,3,5-benzinetriyl)-tris(1-phenyl-1-H-benzimidazole) (TPBi), fluorolithium (LiF) as additional functional layers.

4. Conclusions

We synthesized and characterized six tetra-/triphenylethene-substituted 9,9-dimethylacridine derivatives, which exhibited aggregation induced emission (enhancement) allowing achieving high fluorescence quantum yields of 26–53% for non-doped and 52–88% for doped films. Cyano-substitution resulted in increase of ionization potentials of the derivatives and lead to significant red-shifts of emission. Non-doped and doped films of four tetra-/triphenylethene-substituted 9,9-dimethylacridine derivatives were characterized by blue (451–481 nm) and deep-blue (438–445 nm) fluorescence in respectively. Utilizing the synthesized compounds in organic light-emitting diodes, deep-blue electroluminesce with chromaticity coordinates of (0.16, 0.10), close to the blue color standard (0.14, 0.08) of the National Television System Committee, were obtained. The devices exhibited external quantum efficiencies up to 2.3%.

Supplementary Materials: The following are available online at www.mdpi.com/xxx/s1, Methods and Instrumentation, Figure S1: DSC curves for powder of compounds **1**–**6**, Figure S2: First CV cycle curves of compounds **1**–**6**, Figure S3: PL decays of compounds **1**–**6** in (**a**) toluene and (**b**) THF solutions and in (**c**) non-doped and (**d**) doped films, Figure S4: Normalized PL spectra of doped solid films **1**–**6**:mCP (excitation wavelength was 330 nm), Figure S5: Emission spectra of compounds **1**–**6** in THF/water mixtures (0–90%) and plot of maximum emission intensity and wavelength of compounds **1**–**6** versus water fraction, Figure S6: The structure of the non-doped and doped devices, Figure S7: TOF transients of compounds **2**, **5** and **6**.

Author Contributions: J.S., M.C. and R.B. designed the structures and synthetic routes; M.C. and A.P. performed the synthesis and identification; J.S., S.N and D.V. performed characterization of the compounds; GS performed theoretical investigations; J.S., J.V.G., D.V. and R.B. analyzed and discussed the data; all the authors contributed to writing of the manuscript. All authors have read and agreed to the published version of the manuscript.

Funding: This research was funded by European Union's Horizon 2020 research and innovation programme under the Marie Skłodowska-Curie Research and Innovation Staff Exchange (RISE) scheme (grant agreement No 823720).

Conflicts of Interest: The authors declare no conflict of interest.

References

1. Kim, H.-G.; Shin, H.; Ha, Y.H.; Kim, R.; Kwon, S.-K.; Kim, Y.-H.; Kim, J.-J. Triplet harvesting by a fluorescent emitter using a phosphorescent sensitizer for blue organic-light-emitting diodes. *ACS Appl. Mater. Interfaces* **2019**, *11*, 1, 26–30.
2. Wen, S.-W.; Lee, M.-T.; Chen, C.H. Recent development of blue fluorescent OLED materials and devices. *J. Display Technol.* **2005**, *1*, 1, 90–99.
3. Volyniuk, D.; Cherpak, V.; Stakhira, P.; Minaev, B.; Baryshnikov, G.; Chapran, M.; Tomkeviciene, A.; Keruckas, J.; Grazulevicius, J.V.; Highly efficient blue organic light-emitting diodes based on intermolecular triplet–singlet energy transfer. *J. Phys. Chem. C.* **2013**, *117*, 44, 22538–22544.
4. Takita, Y.; Takeda, K.; Hashimoto, N.; Nomura, S.; Suzuki, T.; Nakashima, H.; Uesaka, S.; Seo, S.; Yamazaki, S. Highly efficient deep-blue fluorescent dopant for achieving low-power OLED display satisfying BT.2020 chromaticity. *J Soc Inf Disp.* **2018**, *26*, 2, 55–63.
5. Adachi, C.; Baldo, M.A.; Thompson, M. E.; Forrest, S. R.; Nearly 100% internal phosphorescence efficiency in an organic light-emitting device. *J. Appl. Phys.* **2001**, *90*, 5048–5051.
6. Uoyama, H.; Goushi, K.; Shizu, K.; Nomura, H.; Adachi, C. Highly efficient organic light-emitting diodes from delayed fluorescence. *Nature* **2012**, *492*, 234–238.
7. Chen, B.; Liu, B.; Zeng, J.; Nie, H.; Xiong, Y.; Zou, J.; Ning, H.; Wang, Z.; Zhao, Z.; Tang, B.Z. Efficient bipolar blue AIEgens for high-performance nondoped blue OLEDs and hybrid white OLEDs. *Adv. Funct. Mater.* **2018**, *28*, 1803369.
8. Lee, J.; Jeong, C.; Batagoda, T.; Coburn, C.; Thompson, M.E.; Forrest, S.R. Hot excited state management for long-lived blue phosphorescent organic light-emitting diodes. *Nat. Commun.* **2017**, *8*, 15566.
9. Giebink, N.C.; D'Andrade, B.W.; Weaver, M.S.; Mackenzie, P.B.; Brown, J.J; Thompson, M.E.; Forrest, S.R. Intrinsic luminance loss in phosphorescent small-molecule organic light emitting devices due to bimolecular annihilation reactions. *J. Appl. Phys.* **2008**, *103*, 044509.
10. Nakanotani, H.; Higuchi, T.; Furukawa, T.; Masui, K.; Morimoto, K.; Numata, M.; Tanaka, H.; Sugara, Y.; Yasuda, T.; Adachi, C. High-efficiency organic light-emitting diodes with fluorescent emitters. *Nat. Commun.* **2014**, *5*, 4016.
11. Chen, C.-T. Evolution of Red Organic Light-Emitting Diodes: Materials and Devices. *Chem. Mater.* **2004**, *16*, 4389–4400.
12. Reig, M.; Gozálveza, C.; Bujaldóna, R.; Bagdziunas. G.; Ivaniuk, K.; Kostiv, N.; Volyniuk, D.; Grazulevicius, J.V.; Velasco, D. Easy accessible blue luminescent carbazole-based materials for organic light-emitting diodes. *Dyes Pigm.* **2017**, *137*, 24–35.
13. Shih, P.-I.; Chiang, C.-L.; Dixit, A.K.; Chen, C.-K.; Yuan, M.-C.; Lee, R.-Y.; Chen, C.-T.; Diau, E.W.-G.; Shu, C.-F. Novel carbazole/fluorene hybrids: host materials for blue phosphorescent OLEDs. *Org. Lett.* **2006**, *8*, 2799–2802.
14. Hong, Y.; Lam, J.W.Y.; Tang, B.Z. Aggregation-induced emission: phenomenon, mechanism and applications. *Chem. Commun.* **2009**, *0*, 4332–4353.
15. Tomkeviciene, A.; Sutaite, J.; Volyniuk, D.; Kostiv, N.; Simkus, G.; Mimaite, V.; Grazulevicius, J.V. Aggregation-induced emission enhancement in charge-transporting derivatives of carbazole and tetra(tri)phenylethylene. *Dyes Pigm.* **2017**, *140*, 363–374.
16. Mei, J.; Leung, N.L.C.; Kwok, R.T.K.; Lam, J.W.Y.; Tang, B.Z. Aggregation-induced emission: together we shine, united we soar! *Chem. Rev.* **2015**, *115*, 21, 11718–11940.
17. Maity, S.; Aich, K.; Prodhan, C.; Chaudhuri, K.; Pramanik, A.K.; Das, S.; Ganguly, J. Solvent-dependent nanostructures based on active π-aggregation induced emission enhancement of new carbazole derivatives of triphenylacrylonitrile. *Chem. Eur. J.* **2019**, *25*, 4856–4863.

18. Yingying, Z.; Zhiwen, Y.; Jihua, T.; Zhipeng, Q.; Yuanyou, M.; Jia, H.; Qingdan, Y.; Shaomin, J.; Ning, C.; Yanping, H. Synthesis, aggregation-induced emission (AIE) and electroluminescence of carbazole-benzoyl substituted tetraphenylethylene derivatives. *Dyes Pigm.* **2020**, *173*, 107898.
19. Lo, D.; Chang, C-H.; Krucaite, G.; Volyniuk, D.; Grazulevicius, J.V.; Grigalevicius, S. Sky-blue aggregation-induced emission molecules for non-doped organic light-emitting diodes. *J Mater. Chem. C* **2017**, *5*, 6054–6060.
20. Wang, X.; Wang, Y.; Zhan, Y.; Yang, P.; Zhang, X.; Xu, Y. Piezofluorochromism of triphenylamine-based triphenylacrylonitrile derivative with intramolecular charge transfer and aggregation-induced emission characteristics. *Tetrahedron Lett.* **2018**, *59*, 2057–2061.
21. Lin, H.-T.; Huang, C.-L.; Liou, G.-S. Design, synthesis, and electrofluorochromism of new triphenylamine derivatives with AIE-active pendent groups. *ACS Appl. Mater. Interfaces* **2019**, *11*, 11684−11690.
22. Zhao, Z.; Chan, C.Y.K.; Chen, S.; Deng, C.; Lam, J.W.Y.; Jim, C.K.W.; Hong, Y.; Lu, P.; Chang, Z.; Chen, X.; Lu, P.; Kwok, H.S.; Qiu, H.; Tang, B.Z. Using tetraphenylethene and carbazole to create efficient luminophores with aggregation-induced emission, high thermal stability, and good hole-transporting property. *J. Mater. Chem.* **2012**, *22*, 4527−4534.
23. Nasiri, S.; Cekaviciute, M.; Simokaitiene, J.; Petrauskaite, A.; Volyniuk, D.; Andruleviciene, V.; Bezvikonnyi, O.; Grazulevicius, J.V. Carbazole derivatives containing one or two tetra-/triphenylethenyl units as efficient hole-transporting OLED emitters. *Dyes Pigm.* **2019**, *168*, 93–102.
24. Pan, S.; Liu, K.; Ye, Y.; Gao, X.; Tang, Z.; Ye, Z.; Yu, N.; Guo, K.; Wei, B. Decrease of intermolecular interactions for less-doped efficient deep blue monomer light-emitting diodes. *Org. Electron.* **2019**, https://doi.org/10.1016/j.orgel.2019.105577.
25. Bujak, P.; Kulszewicz-Bajer, I.; Zagorska, M.; Maurel, V.; Wielgus, I.; Pron, A. Polymers for electronics and spintronics. *Chem. Soc. Rev.* **2013**, *42*, 8895–8999.
26. Hartwig, J.F. Palladium-catalyzed amination of aryl halides: mechanism and rational catalyst design. *Synlett* **1997**, *4*, 329–340.
27. Mitra, S.; Darira, H.; Chattopadhyay, P. Efficient synthesis of imidazole-fused benzodiazepines using palladium-catalyzed intramolecular C-N bond formation reaction. *Synthesis* **2013**, *45*, 85–92.
28. Sych, G.; Simokaitiene, J.; Bezvikonnyi, O.; Tsiko, U, Volyniuk, D.; Gudeika, D.; Grazulevicius, J.V. Exciplex-enhanced singlet emission efficiency of nondoped organic light emitting diodes based on derivatives of tetrafluorophenylcarbazole and tri/tetraphenylethylene exhibiting aggregation-induced emission enhancement. *J. Phys. Chem. C* **2018**, *122*, 26, 14827–14837.
29. Hladka, I; Volyniuk, D.; Bezvikonnyi, O.; Kinzhybalo, Bednarchuk, T. J.; Danyliv, Y.; Lytvyn, R.; Lazauskas, A.; Grazulevicius, J. V. Polymorphism of derivatives of tert-butyl substituted acridan and perfluorobiphenyl as sky-blue OLED emitters exhibiting aggregation induced thermally activated delayed fluorescence. *J. Mater. Chem. C* **2018**, *1*, 13179-13189.
30. Keruckas, J.; Volyniuk, D.; Simokaitiene, J.; Narbutaitis, E.; Lazauskas, A.; Lee, P.-H.; Chiu, T.-L.; Lin, C.-F.; rsenyan, P.; Lee, J.-H.; Grazulevicius, J.V. Methoxy- and *tert*-butyl-substituted *meta*-bis(*N*-carbazolyl)phenylenes as hosts for organic light-emitting diodes. *Org. Electron.* **2019**, *73*, 317–326.
31. Kaafanari, B.L.; El-Ballouli, A.O.; Trattnig, R.; Fonari, A.; Sax, S.; Wex, B.; Risko, C.; Khnayzer, R.S.; Barlow, Z.; Patra, D.; Timofeeva, T.V.; List, E.J.W.; Bredas, J.-L.; Marder, S.R. Bis(carbazolyl) derivatives of pyrene and tetrahydropyrene: synthesis, structures, optical properties, electrochemistry, and electroluminescence. *J. Mater. Chem. C* **2013**, *1*, 1638–1650.
32. Tomkeviciene, A.; Matulaitis, T.; Guzauskas, M.; Andruleviciene, V.; Volyniuk, D.; Grazulevicius, J.V. Thianthrene and acridan-substituted benzophenone or diphenylsulfone: Effect of triplet harvesting via TADF and phosphorescence on efficiency of all-organic OLEDs. *Org. Electron.* **2019**, *70*, 227–239.
33. Huo, J.; Wang, H.; Li, S.; Shi, H.; Tang, Y.; Tang, B.Z. Designand development of highly efficient light-emitting layersin OLEDs with dimesitylboranes: an updated review. *Chem. Rec.* **2019**, *19*, 1–15.
34. *Principles and Applications of Aggregation Induced Emission*, Editors: Tang, Y., Tang, B.Z.; Springer Nature: Switzerland AG, 2019; pp. 514.
35. Tan, X.-F.; Wang, P.-P.; Lu, L.; Bezvikonnyi, O.; Volyniuk, D.; Grazulevicius, J.V.; Zhao, Q.-H. Comparative study of multi-functional luminogens with 1,3,5-triazine as the core and phenothiazine or phenoxy donors as the peripheral moieties for non-doped/doped fluorescent and red phosphorescent OLEDs. *Dyes Pigm.* **2020**, *173*, 107793.

36. Han, T.; Hong, Y.; Xie, N.; Chen, S.; Zhao, N.; Zhao, E.; Lam, J.W.Y.; Sung, H.H.Y.; Dong, Y.; Tong, B.; Tang. B.Z. Defect-sensitive crystals based on diaminomaleonitrilefunctionalized Schiff base with aggregation-enhanced emission. *J. Mater. Chem. C*, **2013**, *1*, 7314.
37. Zhang, X.; Chi, Z.; Xu, B.; Chen, C.; Zhou, X.; Zhang, Y.; Liu, S.; Xu. J. End-group effects of piezofluorochromic aggregation-induced enhanced emission compounds containing distyrylanthracene. *J. Mater. Chem.*, **2012**, *22*, 18505.
38. Yang, Z.; Chi, Z.; Xu, B.; Li, H.; Zhang, X.; Li, X.; Liu, S.; Zhang. Y.; Xu. J. High-Tg carbazole derivatives as a new class of aggregation-induced emission enhancement materials. *J. Mater. Chem.*, **2010**, *20*, 7352.
39. Liu, Y.; Chen, S.; Lam, J.W.Y.; Lu, P.; Kwok, R.T.K.; Mahtab, F.; Kwok, H.S.; Tang, B.Z. Tuning the electronic nature of aggregation-induced emission luminogens with enhanced hole-transporting property. *Chem. Mater.* **2011**, *23*, 2536–2544.
40. Wu, M.-F.; Yeh, S.-J.; Chen, C.-T.; Murayama, H.; Tsuboi, T.; Li, W.-S.; Chao, I.; Liu, S.-W.; Wang, J.-K. The quest for high-performance host materials for electrophosphorescent blue dopants. *Adv. Funct. Mater.* **2007**, *17*, 1887–1895.
41. Yuan, W.Z.; Tan, Y.; Gong, Y.; Lu, P.; Lam, J.W.Y.; Shen, X.Y.; Feng, C.; Sung, H.H-Y.; Lu, Y.; Williams, I.D.; Sun, J.Z.; Zhang, Y.; Tang, B.Z. Synergy between twisted conformation and effective intermolecular interactions: strategy for efficient mechanochromic luminogens with high contrast. *Adv. Mater.* **2013**, *25*, 2837–2843.

Sample Availability: Samples of the compounds **1–6** are available from the authors.

Chemical Engineering Journal 401 (2020) 125962

Contents lists available at ScienceDirect

Chemical Engineering Journal

journal homepage: www.elsevier.com/locate/cej

Multifunctional asymmetric D-A-D' compounds: Mechanochromic luminescence, thermally activated delayed fluorescence and aggregation enhanced emission

Ramin Pashazadeh[a], Galyna Sych[a], Sohrab Nasiri[a], Karolis Leitonas[a], Algirdas Lazauskas[b], Dmytro Volyniuk[a], Peter J. Skabara[c], Juozas Vidas Grazulevicius[a,*]

[a] Department of Polymer Chemistry and Technology, Kaunas University of Technology, Radvilenu Rd. 19, LT-50254 Kaunas, Lithuania
[b] Institute of Materials Science, Kaunas University of Technology, K. Baršausko St. 59, LT51423 Kaunas, Lithuania
[c] WestCHEM, School of Chemistry, University of Glasgow, Glasgow G12 8QQ, UK

HIGHLIGHTS

- Donor-acceptor-donor* emitters exhibiting TADF, AIEE, and stimuli sensitive emission.
- Reversible emission colour changes under grinding or fuming.
- Doped OLEDs with maximum external quantum efficiency up to 10.5%.
- Non-doped devices with the different colours of electroluminescence.

GRAPHICAL ABSTRACT

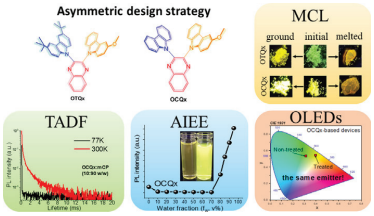

ARTICLE INFO

Keywords:
Thermally activated delayed fluorescence
Mechanoluminescence
Aggregation induced emission enhancement
Asymmetric donor-acceptor
Organic light-emitting diodes

ABSTRACT

Herein, we report synthesis and properties of new multifunctional materials, containing quinoxaline as an acceptor core and differently substituted carbazole moieties as the donors within unsymmetrical D-A-D' type structures. The compounds exhibit thermally activated delayed fluorescence, luminescence variation in response to external stresses (from green to orange) and emission enhancement in the aggregated state. The effect of substitutions on the different properties is discussed. The investigation suggests that the strength of the donor determines the optical properties of unsymmetrical bipolar emitters. Density functional theory calculations revealed that in the ground and the excited state, electrons of the highest occupied molecular orbitals (HOMOs) are mainly localized on the stronger donor. Mechanochromism studies demonstrated that the bulky *tert*-butyl groups attached to the carbazole moiety give rise to a hypsochromic effect. It is also associated with the strong reversible colour contrast, in the range of 524–583 nm, in response to external stresses. Using the synthesized compound as an emitter in organic light emitting diode, maximum external quantum efficiency of 10.5% and luminance of 48800 cd.cm^{-2} were observed.

1. Introduction

Multifunctional compounds with capability to demonstrate more than one functionality represent one of the most intriguing classes of materials [1–3]. Purely organic luminescent materials, in comparison to metal complexes, have been of particular interest due to their relatively low cost and high diversity in terms of structural design and physical properties [4]. Recently, there has been a surge of interest in three

* Corresponding author.
E-mail address: juozas.grazulevicius@ktu.lt (J.V. Grazulevicius).

https://doi.org/10.1016/j.cej.2020.125962
Received 8 April 2020; Received in revised form 3 June 2020; Accepted 17 June 2020
Available online 20 June 2020

kinds of luminescent materials that exhibit thermally activated delayed fluorescence (TADF), aggregation induced emission (AIE) and mechanochromic luminescence (MCL). Donor-acceptor (D-A) compounds with strong intramolecular charge transfer (ICT) exhibiting TADF have become desirable synthetic targets in the area of organic light emitting diodes. TADF materials afford to harvest both 75% of non-emissive triplets as well as 25% of emissive singlet excitons via reverse intersystem crossing (rISC) to achieve 100% internal quantum efficiency of OLEDs [4–8]. Negligible singlet-triplet energy splitting (ΔE_{ST}) enabling rISC and high solid-state photoluminescence quantum yields (PLQY) are the main requirements for effective TADF emitters. A D-A/ D-A-D design strategy with different configurations leads to the small HOMO-LUMO overlap, and thus, desirable small ΔE_{ST} enabling effective TADF. Nevertheless, most conventional luminophores with desirable separation of HOMO-LUMO experience low solid state PLQY. Much effort has been devoted for the design of organic conjugates which exhibit aggregation induced emission enhancement (AIEE). The restriction of intramolecular motions and prevention of intermolecular π-π stacking of AIEE-active compounds led to the intense solid-state emission [9,10]. TADF and AIEE-active compounds have been widely used for the fabrication of efficient non-doped OLEDs [11].

Over the past two decades, there has been considerable activity in the studies of organic materials that change their luminescence wavelengths in response to external changes in the immediate environment [12–14]. MCL materials are associated with the variety of applications such as sensors, security inks, disease detectors [15]. Typically, in MCL materials, the molecular packing mode is affected by mechanical stress and this causes a change in the absorption and emission characteristics of the material and therefore a variation of emission colour [12]. Despite numerous studies, the principle design of MCL compounds is not yet clear.

Organic compounds exhibiting MCL, TADF and AIEE can endow a variety of multifunctional applications in science and industry [16–18].

Inspired by our recent studies on the synthesis of symmetrical quinoxaline-based compounds, which demonstrated TADF, MCL and/or room temperature phosphorescence [19,20], with the aim to investigate the influence of the chemical modification on the properties of quinoxaline derivatives, new asymmetric D-A-D' compounds were designed (Scheme 1).

Asymmetric TADF molecules are relatively rare. Nevertheless, they remaining as a hot topic for scientific community during last years [18,21–28]. Alteration of the weaker electron-donor (carbazole or di-*tert*-butyl carbazole) in the D-A-D' asymmetric structures afford to change the intermolecular interactions and photophysical properties of the solid samples, retaining small ΔE_{ST} and stable TADF due to the strong ICT between the stronger electron-donor 3-methoxycarbazole and quinoxaline electron-acceptor. Most recently, our group reported asymmetric TADF molecules without any bridge between the donor and acceptor units, based on benzonitrile as the acceptor [29]. Herein, we document the design, synthesis and investigation of new unsymmetrical D–A–D' derivatives in which differently substituted carbazole donor moieties are directly linked to the quinoxaline unit (Scheme 1). In parallel, the effect of the attachment of *tert*-butyl and methoxy substituents to carbazole unit at its 3- or 3,6-positions on the photophysical, electrochemical and thermal properties of the compounds was investigated. The developed compounds were used as emitters in doped and non-doped OLEDs. Electroluminescence colour of the devices could be affected by appropriate treatment due to the MCL.

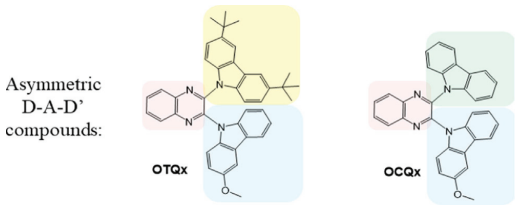

Scheme 1. Chemical structures of asymmetric D-A-D' compounds.

2. Results

2.1. Molecular design, synthesis

The D-A-D' design strategy was chosen for the synthesis of new multifunctional AIEE- MCL- and TADF-active compounds. Asymmetric D-A-D' compounds with different molecular configurations allow to achieve diverse optical properties. 3-Methoxy carbazole moiety was selected as the stronger electron donor which, in combination with electron-deficient quinoxaline, ensured negligible ΔE_{ST} and profound TADF. Meanwhile, carbazole and di-*tert*-butyl carbazole moieties played the role of weaker electron-donor fragments which allowed to tune the photophysical characteristics of the solid samples. D/D' were covalently linked to the quinoxaline moiety similarly as it was done in earlier reported compounds [19]. In this case, the direct D-A-D' linkage caused the rigidification of the sterically hindered electron-donors and enabled high dihedral angle between D/D' and A which also assured small ΔE_{ST} and relatively high PLQY. In addition, twisted asymmetric molecular configurations allowed to reduce the π–π interactions enabling AIEE [21].

One-pot low-cost synthesis of luminogens OCQx and OTQx was conducted according to the procedure described in the Supporting information (Scheme S1 and S2 in SI). The synthetic route included formation of the carbazolyl/di-*tert*-butyl carbazolyl nucleophiles upon treatment with a Na-O*t*Bu base in the first stage. The subsequent nucleophilic attack occurred on the 2, 3- positions of dichloroquinoxaline which resulted in the formation of monosubstituted intermediate compounds 1 and 2. The further nucleophilic aromatic reaction (S_NAr) between 1/ 2 and previously prepared 3-methoxy carbazolyl nucleophile afforded target compounds OCQx and OTQx in medium yields. The structures and purity of these compounds were confirmed by NMR spectroscopy and mass spectrometry (Supporting information).

2.2. Photophysical properties

Absorption and emission spectra of the solutions and films of compounds OCQx and OTQx are shown in Fig. 1. The photophysical data are summarized in Table 1. Absorption spectra of the compounds depict π-π* transitions of the aromatic rings at ca. 240 and 290 nm, and n-π* transitions of locally excited carbazolyl fragments at ca. 330 nm and 347 nm [30]. To obtain an insight into the electron distribution of the asymmetric D-A-D' molecules (OCQx and OTQx), density functional theory (DFT) calculations were performed at the b3LYP/6-31 g level. The lowest energy absorption band (at ca. 420 nm) is attributed to the $S_0 \rightarrow S_1$ and $S_0 \rightarrow S_2$ transitions, as confirmed by the theoretically calculated absorption spectra of both the compounds (Fig. S1a, b). The $S_0 \rightarrow S_1$ and $S_0 \rightarrow S_2$ electronic transitions are assigned to the H-1/H → L transitions (Table S1). The respective highest occupied and lowest unoccupied natural transition orbitals (HONTO/LUNTO) of the vertical $S_0 \rightarrow S_1$ and $S_0 \rightarrow S_2$ transitions are depicted in Fig. S1c. The $S_0 \rightarrow S_1$ is characterized by the main charge transfer from methoxy-carbazole to quinoxaline unit with the oscillator strength values of 0.0617 and 0.0569 for OCQx and OTQx, respectively. Meanwhile, in the $S_0 \rightarrow S_2$ excitation, the ICT from weaker electron-donor (carbazole/di-*tert*-butyl carbazole) to quinoxaline acceptor dominated (Fig. S1c). For deeper understanding and comparison, the excited state optimization was performed for the asymmetrical D-A-D' and previously published symmetrical D-A-D type compounds (CzQx, tCzQx, OCQx) [19]. The calculations revealed that at excited state LUMOs of both asymmetrical and symmetrical molecules are mainly distributed on quinoxaline unit (Fig. 2, Fig. S2 and S3). In the symmetrical structures the HOMOs are

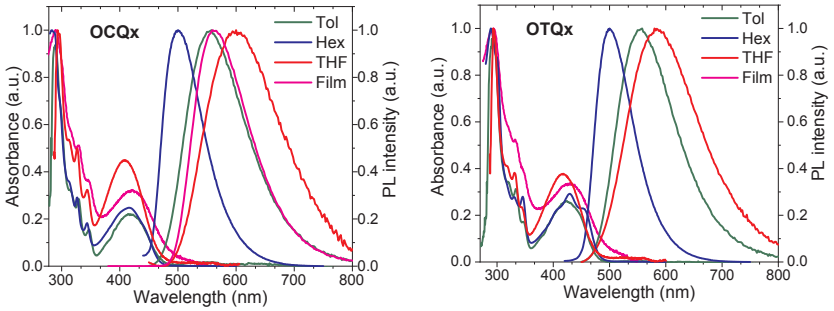

Fig. 1. Absorption and photoluminescence spectra of thin films and solutions of OCQx and OTQx in the solvents of various polarities.

mainly localized on both donors and slightly on the acceptor unit (Fig. S2).

As shown in Fig. 2 and Fig. S3, in the ground and excited states (both S_1 and T_1) of the unsymmetrical structures, the HOMOs are mainly localized on the stronger electron-donating unit, 3-methoxycarbazole. The bigger the difference in electron-donating ability of the donors, the more expressed is the localization of the HOMO on the stronger donor. Consequently, we can state that the ICT occurs mainly between 3-methoxy carbazole and quinoxalin and corresponds to the dominative H → L transition (Table S2). Based on this presumption, the similar photophysical properties could be expected for OCQx and OTQx, due to the presence of the 3-methoxycarbazole unit in both structures. However, the photophysical properties in the solid state can be different due to differences in morphology. The optical band gaps obtained from the onset of the lowest absorption energy band of the toluene solutions were found to be similar for both the compounds, i.e., 2.61 eV for OCQx and 2.59 eV for OTQx (Table 1). By increasing the solvent polarity, PL spectra of the solutions of both OCQx and OTQx bathochromically shifted from green for the hexane solutions up to orange for the THF solutions. The solutions of the compounds in hexane and toluene solvents demonstrated the similar PL spectra with the maxima located at 500 nm and 553/554 nm, respectively. Nevertheless, compound OCQx demonstrated stronger solvatochromism with respect to its counterpart OTQx. Apparently, the dipole moment of the excited state of OCQx is higher relative to that of the excited state of OTQx.

2.2.1. Characterisation of thermally activated delayed fluorescence

The energies of the first excited singlet and triplet states were estimated from the onset of photoluminescence (PL) and phosphorescence (PH) spectra recorded for the films of compounds doped in mCP (10% w/w) at 77 K (Fig. S4). As depicted in Table 1, negligible singlet–triplet energy splitting of ~0.1 eV was observed for both OCQx and OTQx, which can be evidence to support a fast reverse intersystem crossing (rISC) and, subsequently, delayed fluorescence (DF). The experimentally obtained S_1 energies were close to the values obtained by quantum chemical calculations, $S_1 \approx$ 2.60 eV for OCQx and OTQx (Table S3). However, the theoretical values of energy of T_1 states (2.26 eV and 2.28 eV) were lower than experimental values and led to a larger gap between the singlet and the triplet states (ca. 0.30 eV). The discrepancy of the ΔE_{ST} values obtained by chemical quantum calculations (calculated for compounds in vacuum) and experimental ones (obtained for the films of the solid solutions of the compounds in mCP host) can be explained by the different environment which can lead to the diverse intermolecular interactions. Due to small ΔE_{ST}, several technical measurements were employed to investigate the possibility of DF and its mechanism. Measurements of PL intensity of air-equilibrated and degassed doped films (in mCP as a host), were employed to investigate the contribution of triplets in the emission profile (Fig. S5). The results showed enhancement of PLQY from 19% to 23% for the film containing OCQx and from 17% to 38% for the film containing OTQx. Meanwhile, the DF characteristics of the compounds were investigated by monitoring transient PL decays of the compounds molecularly dispersed in mCP at varying temperatures from 77 K to 300 K (Fig. S6). With the increase of temperature, an increase in emission intensity was recorded. This observation can be assigned to an increase in rISC efficiency and larger contribution of delayed fluorescence. To further clarify the origin of delayed fluorescence, the DF intensity of the compounds was studied as a function of varying laser power at room temperature (Fig. S7). The resulting linear plot demonstrated a slope close to 1, which confirmed the TADF nature of the emission. The increasing laser power resulted not only in the increase of the intensity of emission, but also in the broadening of the PL spectra (Fig. S7).

2.2.2. Aggregation induced emission enhancement

AIEE for OCQx and OTQx was assessed by measuring the PL intensity of the dispersions of the compounds in water/THF mixtures with the different water fractions (f_w). As depicted in Fig. 3, the solutions of the compounds in pure THF demonstrated very weak PL. After deoxygenation of as prepared THF solutions of OCQx and OTQx, their emission intensities did not increase and PL decays were found to be in the nanosecond range (Fig. S8). This observation means that the solutions of compounds OCQx and OTQx in THF were not characterized by triplet harvesting, thus TADF properties were not observed. By adding water into THF solutions, the polarity of the solvent mixture was

Table 1
Photophysical properties of OCQx and OTQx.

Sample	Abs[a] (nm)	PL[b] (nm)					S_1/T_1[c] (eV)	ΔE_{ST}[d] (eV)	τ_1/τ_2[e] (ns/μs)	PLQY[f] (air/deg)	PLQY[g] (air/deg)
		Hex	Tol	THF	mCP	film					
OCQx	289, 328, 346	500	554	601	546	563	2.60/2.51	0.10	4.3/1340	0.19/0.23	0.17/0.24
OTQx	291, 333, 347	500	553	584	539	567	2.61/2.55	0.06	4.9/1422	0.17/0.38	0.25/0.51

a) Absorption maxima for solutions in toluene at RT; b) emission maxima in different solvents, films and 1,3-bis(*N*-carbazolyl)benzene (mCP 10% w/w); c) singlet–triplet energies of the molecular dispersions in mCP 10% (w/w); d) singlet–triplet energy gap; e) PL lifetimes of compounds blended in mCP at RT; Absolute PL quantum yield (PLQY) measured in air and degassed at RT in f) mCP and g) tris(4-carbazoyl-9-ylphenyl)amine (TCTA 10% w/w) hosts.

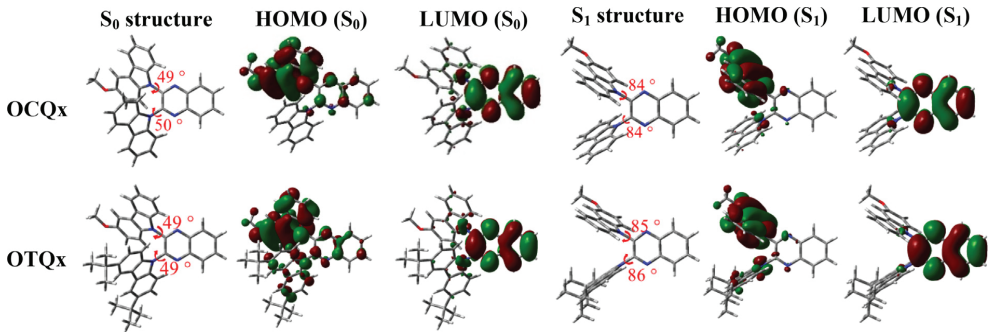

Fig. 2. Optimised geometries and calculated HOMO, LUMO distributions of OCQx and OTQx in the ground and excited S_1 states, obtained using density functional theory (DFT) at the B3LYP/6-31G level.

gradually increased, which resulted in bathochromic shifts accompanied by some decrease of PL intensity. The compounds began to aggregate in a specific ratio of THF/water, and the aggregation point depended on the presence of alkyl groups in their structures. In the case of OTQx, aggregation occurred at lower fraction of water than in the case of OCQx due to the presence of *tert*-butyl groups in its structure.

The maximum emission intensity for the solution of OTQx in THF (0% of water) was observed at 583 nm while for the f_w = 60% the emission wavelength changed to 614 nm. When water fraction exceeded 60%, the emission shifted towards the blue region and the PL intensity increased, which indicated aggregation process. Fig. 3 shows the effect of the polarity of the media on the width of the PL spectra. Compound OTQx at 60% water fraction exhibited the highest full width at half maximum (FWHM) of 195 nm, indicating the strongest intramolecular charge transfer effect in the polar environment. On the contrary, the FWHM of OTQx significantly decreased to 121 nm, at water fraction of 95%.

Fig. 3c, d illustrates the effect of water fraction on the wavelength and intensity of emission of OCQx. Compound OCQx showed the similar AIEE properties, except the fact that AIEE occurred at f_w = 70%. When the water fraction increased from 0 to 70%, its PL intensity decreased. In addition, bathochromic shifts and an increase of FWHM were observed. The further increase in the water fraction above 70%, resulted in an increase of fluorescence intensity, hypsochromic shifts

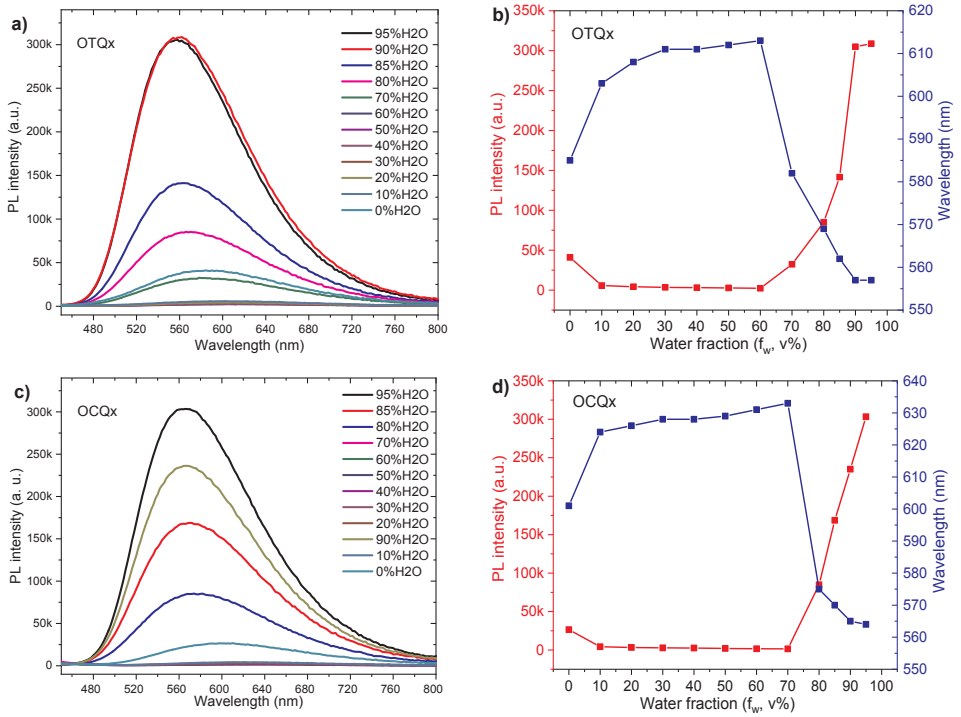

Fig. 3. Fluorescence spectra of the dispersions of a) OTQx and c) OCQx in the mixtures of THF and water with different values of water fraction. Effect of water fraction on PL intensity and wavelength of the dispersions of b) OTQx and d) OCQx.

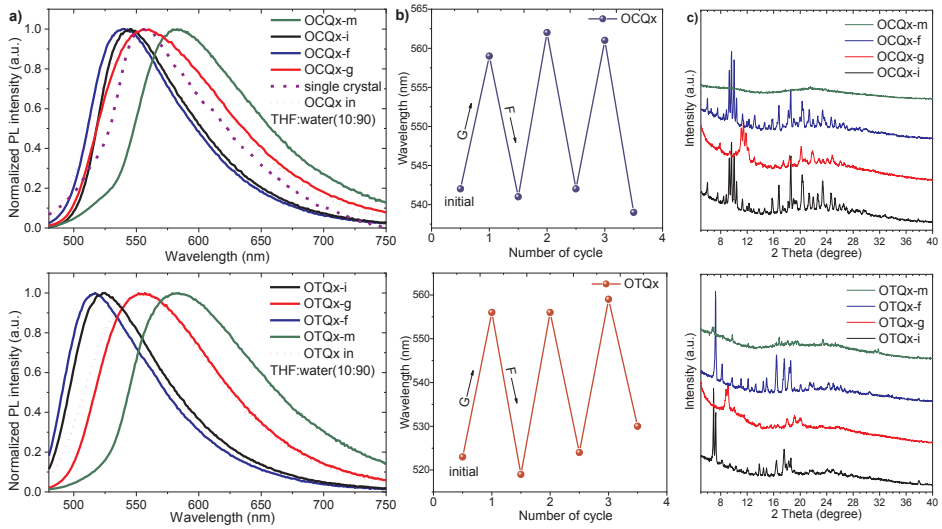

Fig. 4. a) Effects of external stimuli on PL spectra of OCQx and OTQx; b) PL maxima after the different numbers of grinding (G)/fuming (F) cycles. c) Powder X-ray diffractograms of OTQx and OCQx being in their different states. (i - initial (as-prepared), g - ground, f – fumed and m – melted).

and narrower peaks due to AIEE. The observation of AIEE can be explained by the restriction of vibrations of the donor and acceptor moieties of the molecules in the solid state. Maintaining of the certain distances between adjacent molecules diminished π-π stacking and quenching of emission. These results illustrate the effect of the polar environment on the PL intensity as well as on the width of the emission band and its energy.

According to the literature [31], AIEE properties can be related to the MCL properties. It is worth to note that PL spectra of the dispersions of OTQx and OCQx in THF/water (10:90) mixtures are very similar to the corresponding PL spectra of their ground forms (Fig. 4a). The structure as well as emission properties including TADF of the formed aggregates of OTQx and OCQx in water/THF mixtures may be similar to those of ground forms of OTQx and OCQx (see descriptions in next section). However, additional experiments are required to prove this assumption.

2.2.3. *Mechanochromic luminescence*

Possibilities of tuning the emission colour upon application of external stimuli were studied. As it was mentioned above, OTQx contains stronger electron-donating units in its structure in comparison with OCQx. Typically, compounds with stronger donors in the as-prepared state exhibit longer wavelengths of emission than compounds containing weaker donors [31]. It was found that OTQx and OCQx in the pristine forms (OTQx-i and OCQx-i) emitted in the green-yellow region of the spectrum with the maxima located at 524 nm and 544 nm, respectively. Fig. S9 and Table S4 contain the corresponding CIE colour coordinates of emissions of the compounds being in the different solid states. In the solid state the emission largely depends on the intermolecular interactions and on the distance between the adjacent molecules. Apparently, the bulky *tert*-butyl groups decrease the extent of π-π stacking among the adjacent molecules which results in a hypsochromic shift of the solid sample of OTQx.

Upon applying of external stresses compound OTQx showed three colours of emission in its different states (pristine, ground, molten) which varied from green to orange (Fig. 4, Table S4, Fig. S9). The pristine form (OTQx-i) demonstrated green emission peaked at 524 nm, which red-shifted to 555 nm after grinding by a spatula. Powder X-ray diffraction (XRD) analysis was employed to further investigate the microstructure and morphology of the compounds in their different states. Degrees of crystallinity of as-prepared, ground, fumed and melted OTQx samples were found to be 51.4, 42.6, 55.6 and 26.9%, respectively. The similar tendency was observed for OCQx-i, OCQx-g, OCQx-f and OCQx-m with the degrees of crystallinity of 60.7, 47.1, 62.7 and 29.3%, respectively. Upon grinding of the crystalline form of the initial powder the molecular packing rearranged, the peaks disappeared, and a new packing motif was formed (Fig. 4c). This result was evidenced by the appearance of new peaks in X-ray diffractogram of the ground samples. The observation of new well-ordered packing motif in the ground form can be explained by strong intermolecular interaction. The pristine green emission colour reappeared with fumigation of the ground form through exposing it to vapor of methylene chloride for 5 min. In this process, the vapor of solvent becomes occluded into the unit cell and expands it, which results in the change of molecular assembly. After fuming (OTQx-f), the emission centered at 517 nm, i.e. was blue-shifted in comparison with the emission of the initial form. For these compounds, mechanochromism was observed either due to alteration of the twist angles between the donor and acceptor units or due to the variation of the molecular packing.

The powder XRD analysis confirmed that observation of shorter emission wavelength for OTQx-f, can be ascribed to the formation of a new orientation in molecular packing. Heating of the initial form above the melting point (OTQx-m) resulted in a large bathochromic shift up to 59 nm (emission centered at 583 nm), accompanied by broadening of the PL spectrum. The PL spectrum of the neat film (OTQx-film) was red-shifted relative to that of its ground form, while the values of FWHM were comparable (ca. 110 nm) (Table S4). This observation is an indication of closer distances and stronger intermolecular interaction in the neat film.

OCQx also exhibited colour tuning in response to external stimuli. The initial yellow emitting solid form of OCQx with a PL maximum at 544 nm changed to PL maximum of 559 nm after grinding the sample by a spatula. XRD showed new peaks developed after grinding, which implied a new molecular orientation or packing and the potential to develop a well-ordered crystalline structure. The original fluorescence colour of as-prepared powders could be nearly recovered by fuming of

ground powders in DCM vapors during three grinding-fuming cycles. This observation indicates the reversible mechanochromism of OCQx and OTQx (Fig. 4b). The different reversibility results observed for OTQx can be ascribed to the presence of *tert*-butyl groups attached to carbazole moiety in OTQx, which leads to the different distances between the neighboring molecules, different packing forms and, consequently, varying intermolecular interaction in the different states.

The single crystal X-ray analysis of the sample of OCQx prepared by slow evaporation of hexane/acetone solution revealed that the dihedral angles between quinoxaline and carbazole or 3-methoxy carbazole units were of 50° and 54°, respectively (Fig. S10). Compound OCQx experienced only week C–H···π intermolecular interactions in the single crystal structure. The distances of C–H···π interactions were found to be 2.839 Å, 2.797 Å, 3.014 Å and 3.192 Å. Interestingly, the emission peak wavelength of single crystal observed at 557 nm is identical to the PL peak wavelength of the ground sample. This observation suggests that molecules in ground state experience similar to the single crystal conformation and intermolecular interactions. Through fumigation, when the ground form was reverted to the as-prepared state, the PL maximum blue-shifted relative to that of the initial form and appeared at 539 nm. The fumed and initial form showed the similar XRD peaks as well as similar FWHM values of 84 and 86 nm for the initial and fumed forms, respectively. These observations reflect that the blue shift of emission of the fumed form was apparently not because of a variation in the molecular orientation nor tuning of twist angle. It could occur because of the longer distance between neighboring molecules and, subsequently, reduced extent of intermolecular interactions. Upon melting, the PL spectrum was shifted to orange region and peaked at 582 nm. The neat film of OCQx showed emission peaking at 562 nm and a FWHM of 113 nm which was close to that of the film of OTQx.

The PL decays analysis demonstrate different PL character of compounds OTQx and OCQx being in the different solid states (Fig. S11 and S12, Table S5). Compound OCQx exhibited TADF being in all studied solid states, while compound OTQx demonstrated prompt fluorescence in the initial and fumed solid states and TADF in the ground and melted solid states. It is worth to note that switch-on/switch-off TADF observed for compound OTQx is rather rare in the literature and may suggest its unique application in security field, for example.

2.3. Electrochemical and thermal properties

The effects of the substitutions on the carbazole unit were observed by electrochemical and thermal studies (Table 2). The electrochemical properties of the compounds were assessed by cyclic voltammetry in CH_2Cl_2 solution (Fig. S13). Both the compounds demonstrated reversible oxidation and reduction processes, which is an indication of electrochemical stability. The estimated electron affinities values for both molecules were nearly identical, due to the common electron-withdrawing unit, quinoxaline, in their structures. On the contrary, the estimated ionization potential values were found to differ by 0.1 eV. Compound OTQx, exhibited slightly lower ionisation energy value of 5.48 eV relative to that of OCQx (5.58 eV). This observation suggests that the oxidation of OTQx requires less energy than that of OCQx, which can be attributed to stronger electron donation ability of the donor moieties of OTQx.

Photoelectron emission spectroscopy (PES) was employed to identify the ionisation energy (IE) of the compounds in the solid state (Table 2). The IEs values were found to be 5.63 and 5.74 eV for OTQx and OCQx, respectively. The ionisation energies demonstrate that OTQx tend to oxidize at lower energies, due to the presence of the stronger electron donors in its structure. By comparing the IE values estimated by CV and PES, it can be seen that in the solid state removing of an electron requires more energy than in solution. is more difficult than in solution state. This observation can be attributed to the stronger intermolecular interactions in the solid state.

Thermogravimetric analysis (TGA) and differential scanning calorimetry (DSC) were used to estimate the thermal stability and the temperatures of morphological transitions of the compounds (Fig. S14, S15). The results showed that by attaching *t*-Bu groups to the carbazole moiety the decomposition temperature and glass transition temperature were raised. Thus, 5% mass loss temperature of 329 °C was observed for OTQx. It is by 10°higher than that of OCQx. OTQx, possessing heavier fragments in its structure, requires a higher energy to convert the solid state into a liquid one. It exhibited higher T_g of 111°C. The melting points of the compounds were found to be close, indicating comparable intermolecular interactions in the crystalline state.

2.4. Electroluminescence

To examine electroluminescencent (EL) properties of OTQx and OCQx, doped and non-doped OLEDs were fabricated, having device structures: ITO/MoO_3(0.5 nm)/NPB (35 nm)/OTQx or OCQx (10 wt %):TCTA (20 nm)/TSPO1 (7 nm)/TPBi (30 nm)/LiF (0.5 nm)/Al. OLEDs with the light-emitting layer consisting of OTQx or OCQx as the TADF emitter and TCTA as the host respectively are named as devices A and B. The charge/exciton recombination zones were located within the light-emitting layer of the devices A and B owing to the additional layers of hole-injecting (molybdenum trioxide (MoO_3)), hole transporting (*N,N′*-di(1-naphthyl)-*N,N′*-diphenyl-(1,1′-biphenyl)-4,4′-diamine (NPB)), hole/exciton blocking (diphenyl[4-(triphenylsilyl)phenyl] phosphine oxide (TSPO1)), electron transporting (2,2′,2″-(1,3,5-benzinetriyl)-tris(1-phenyl-1-H-benzimidazole) (TPBi)), and electron-injecting fluorolithium (LiF) (Fig. 5a). EL spectra of devices A (λ_{max} = 544 nm) and B (λ_{max} = 535 nm) are very similar to the PL spectra of the layers of OTQx (10%):TCTA (λ_{max} = 553 nm) and OCQx (10%):TCTA (λ_{max} = 545 nm) respectively (Fig. 5b).

EL spectrum of OTQx-based device is slightly red-shifted in comparison to EL spectrum of OCQx-based device, suggesting a stronger intermolecular interactions and closer packing for the OTQx:TCTA. Yellowish-green and green electroluminescence with CIE colour coordinates of (0.374, 0.572) and (0.338, 0.556) and with high maximum brightness of 48,800 and 41500 cd/m^2 and were observed for devices A and B, respectively (Fig. 5b-d, Fig. 6a). Good colour stability of electroluminescence of devices A and B was obtained under different applied voltages owing efficient host–guest energy transfer (Fig. 5b). Since EL spectra did not contain bands in the blue spectral region, there was not evidence of emission of the host TCTA and/or charge-transporting materials NPB and TPBi. The further analysis of EL spectra of devices A and B showed that the spectra can not be well fitted (since R^2 was 0.9699 or 0.9724, respectively) by Gaussian single peak fitting

Table 2
Electrochemical and thermal characteristics of OCQx and OTQx.

Sample	IP[a] (eV)	EA[a] (eV)	E_g[b] (eV)	IE[c] (eV)	EA[d] (eV)	E_g[e] (eV)	$T_m/T_d/T_g$[f] (°C)
OCQx	5.58	3.03	2.61	5.74	3.25	2.49	195/319/98
OTQx	5.48	3.02	2.59	5.63	3.18	2.45	194/329/111

a) Estimated by cyclic voltammetry for solutions in CH_2Cl_2; b) estimated from the absorption onset of the solution of the compound in toluene; c) estimated by PES of a solid film; d) EA = IP- E_g; e) estimated from the absorption onset of a solid film; f) melting point (T_m), glass transition (T_g) and decomposition (T_d) temperatures determined by DSC and TGA measurements.

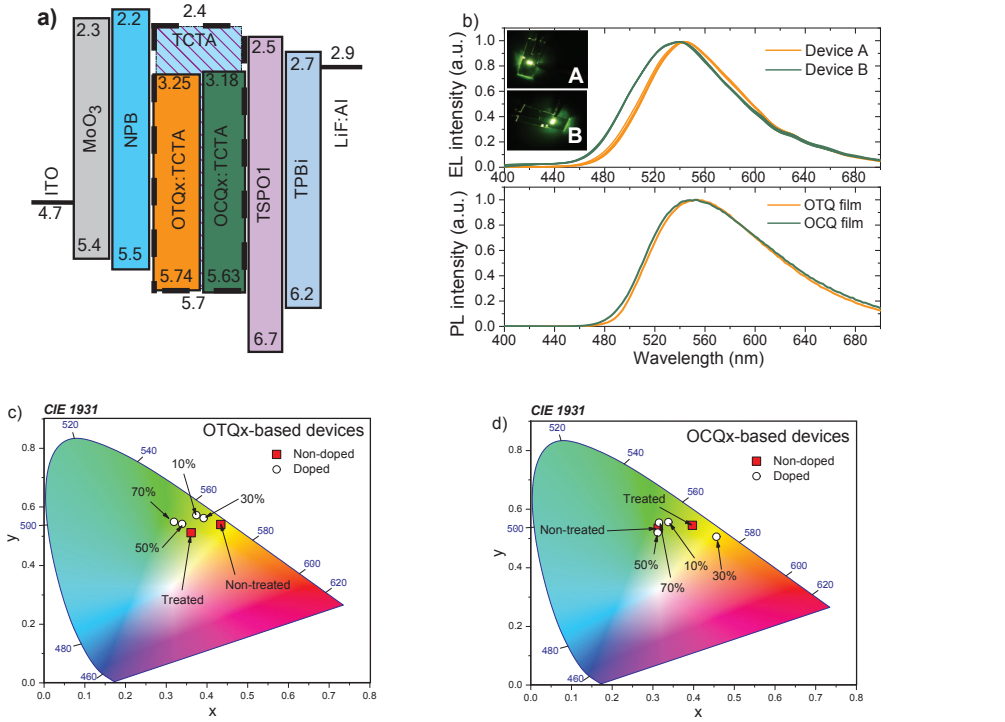

Fig. 5. a) Equilibrium energy diagram of devices A and B; b) EL spectra at voltages ranging from 6 to 11 V with the step of 1 V and PL spectra of light-emitting layers of OTQx(10%):TCTA and OCQx(10%):TCTA; c) and d) CIE 1931 colour diagrams for OTQx and OCQx-based OLEDs. The percentages show concentration of emitters OTQx or OCQx in TCTA host.

(Fig. S16). The perfect fitting (R^2 was 0.9998 or 0.9997, respectively) of EL spectra was obtained only by three peaks fitting (Fig. S16). This observation suggests that EL spectra of OTQx and OCQx-based devices resulted from multipeak emission which is in good agreement with mechanochromic luminescence properties of compounds OTQx and OCQx. Apparently, the different aggregates of OTQx and OCQx can be formed under vacuum deposition even of hosted light-emitting layers of devices A and B. Such result (aggregation effects of TADF emitters OTQx and OCQx on their EL properties) is also in agreement with our previous study on hosting and aggregation effects of TADF emitter [33]. Overlapping of different emissions of such aggregates affected EL spectra of the devices. The above assumptions can be supported by inconstant shifts of the maximum of EL spectra and of the corresponding CIE coordinates of the doped devices with the different concentration of emitters OTQx or OCQx when their concentration was constantly increased from 10 to 100% (Fig. 5c, d, Table 3).

Maximum current and power efficiencies of 33.6/15.8 cd/A and 21/8.4 lm/W were obtained for devices A/B, respectively (Fig. 6b, S17, Table 3). Devices A and B exhibited maximum EQE_{max} of 10.50 and 4.95% respectively which is in good agreement with the PLQYs of the layers of OTQx (10 wt%):TCTA and OCQx (10 wt%):TCTA (51 and 24%, respectively) (Fig. 6b, Table 3).

Maximum EQE_{max} values were achieved at high brightness (ca. 4200 cd/m^2 for device A and ca.2200 cd/m^2 for device B) which mainly were related to charge balance within light-emitting layers at higher electric fields than turn-on voltages. At brightness of 10000 cd/m^2, EQE

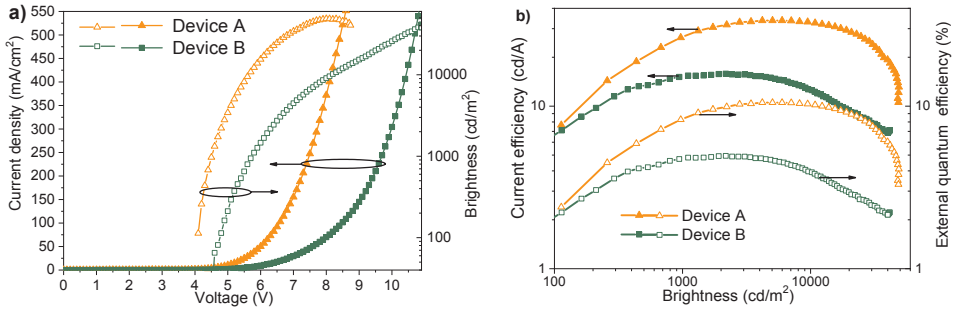

Fig. 6. a) current density and brightness *versus* voltage; b) current and external quantum efficiencies *versus* brightness for devices A and B.

Table 3
Output parameters of OLEDs A and B.

Device		EL peak (nm)	Turn on Voltage (V)	Maximum Brightness (cd/m^2)	Maximum Current Efficiency (cd/A)	Maximum Power Efficiency (lm/W)	Maximum External Quantum Efficiency (%)	CIE coordinates (X, Y)
OTQx	non-doped	555	4.21	9661	2.19	1.23	0.71	(0.434, 0.540)
	non-doped treated*	544	8.29	5725	2.42	0.66	0.77	(0.361, 0.512)
	70%	534	4.89	5412	3.04	1.59	0.91	(0.319, 0.549)
	50%	540	4.17	2937	3.96	2.59	1.23	(0.339, 0.542)
	30%	547	4.90	44,888	13.38	5.68	4.05	(0.392, 0.562)
	10% (Device A)	544	4.08	48,809	33.64	21.08	10.53	(0.374, 0.572)
OCQx	non-doped	530	4.43	2577	1.48	0.85	0.48	(0.313, 0.535)
	non-doped treated*	548	8.18	7241	2.03	0.52	0.64	(0.397, 0.545)
	70%	531	4.12	3008	1.66	1.04	0.52	(0.315, 0.554)
	50%	533	4.20	2543	1.18	0.74	0.59	(0.312, 0.520)
	30%	568	4.19	20,918	6.23	3.09	2.31	(0.456, 0.506)
	10% (Device B)	535	4.49	41,488	15.83	8.36	4.95	(0.338, 0.556)

*The non-doped emitter treated with the toluene vapour at 120 °C for 20 min.

values of devices A and B only slightly dropped exhibiting small efficiency roll-offs of ca. 3 and 21%. EQE_{max} values dramatically decreased with increasing the concentration of guests (OTQx or OCQx) in the light-emitting layers (Fig. S17, Table 3). This observation can apparently be attributed to both decrease of PLQYs because of aggregation-caused quenching and charge dis-balance at high concentration of the dopant. Non-doped OTQx- and OCQx-based devices were characterized by EQE_{max} of 0.71 and 0.48%, respectively (Table 3). Such efficiencies (close to 1%) are similar to EQEs of recently published MCL emitter-based OLEDs which demonstrated emission colour changes due to the treatments of light-emitting layers [32,33]. Interestingly, the blue shift of EL spectra and increase of EQE_{max} were observed when light-emitting layers of non-doped devices were treated by vapor of toluene (Fig. S18, Table 3). Thus, such treatment of light-emitting layers allowed to switch yellow electroluminescence with CIE colour coordinates (0.434, 0.540) or (0.313, 0.535) for non-doped OTQx- and OCQx-based devices to green electroluminescence with CIE colour coordinates (0.361, 0.512) or (0.397, 0.545), respectively (Fig. 5c, d). This observation indicates that OLED efficiency can be improved and the emission colour can be modified when mechanochromic luminophores are used in the device structures.

3. Conclusions

We have synthesized unsymmetrical carbazole-quinoxaline-carbazole' derivatives as new multifunctional materials. The materials exhibited thermally activated delayed fluorescence, reversible mechanochromic luminescence and aggregation induced emission enhancement. The effect of the donor moieties and of the different substitution pattern on the properties is discussed. Photophysical and electrochemical studies of the compounds revealed that the compound containing unsubstituted carbazole unit possesses stronger dipole moment and stronger intermolecular interactions, in comparison with its counterpart. The attachment of *tert*-butyl substituents to one carbazole unit yielded more efficient thermally activated delayed fluorescence, increased thermal stability and stronger mechanoluminescence. By choosing appropriate hosts, a photoluminescence quantum yield exceeding 50% for OTQx was observed in the solid-state for one compound. Under external stimulus, the changes of emission in a wide spectral range (from 524 to 583 nm) was detected for the compounds. The best fabricated organic light emitting diode showed maximum external quantum efficiency (EQE) of 10.5%, turn-on voltage up to 4 V, maximum brightness of 48 800 cd/m^2 and maximum current efficiency of 33.6 cd/A.

Declaration of Competing Interest

The authors declare that they have no known competing financial interests or personal relationships that could have appeared to influence the work reported in this paper.

Acknowledgements

The financial support from the European Social Fund (project No 09.3.3-LMT-K-712-01-0140) under grant agreement with the Research Council of Lithuania (LMTLT) is gratefully acknowledged.

Appendix A. Supplementary data

Supplementary data to this article can be found online at https://doi.org/10.1016/j.cej.2020.125962.

References

[1] K.K. Neena, P. Sudhakar, K. Dipak, P. Thilagar, Diarylboryl-phenothiazine based multifunctional molecular siblings, Chem. Commun. 53 (2017) 3641–3644. doi: 10.1039/c6cc09717k.
[2] A. Lendlein, R.S. Trask, Multifunctional materials: concepts, function-structure relationships, knowledge-based design, translational materials research, Multifunct. Mater. 1 (2018) 010201, , https://doi.org/10.1088/2399-7532/aada7b.
[3] G.R. Whittell, I. Manners, Metallopolymers: New multifunctional materials, Adv. Mater. 19 (2007) 3439–3468, https://doi.org/10.1002/adma.200702876.
[4] Y. Liu, C. Li, Z. Ren, S. Yan, M.R. Bryce, All-organic thermally activated delayed fluorescence materials for organic light-emitting diodes, Nat. Rev. Mater. 3 (2018) 18020, https://doi.org/10.1038/natrevmats.2018.20.
[5] T.-L. Wu, M.-J. Huang, C.-C. Lin, P.-Y. Huang, T.-Y. Chou, R.-W. Chen-Cheng, H.-W. Lin, R.-S. Liu, C.-H. Cheng, Diboron compound-based organic light-emitting diodes with high efficiency and reduced efficiency roll-off, Nat. Photonics 12 (2018) 235–240, https://doi.org/10.1038/s41566-018-0112-9.
[6] Y. Kondo, K. Yoshiura, S. Kitera, H. Nishi, S. Oda, H. Gotoh, Y. Sasada, M. Yanai, T. Hatakeyama, Narrowband deep-blue organic light-emitting diode featuring an organoboron-based emitter, Nat. Photonics 13 (2019) 678–682, https://doi.org/10.1038/s41566-019-0476-5.
[7] Z. Yang, Z. Mao, Z. Xie, Y. Zhang, S. Liu, J. Zhao, J. Xu, Z. Chi, M.P. Aldred, Recent advances in organic thermally activated delayed fluorescence materials, Chem. Soc. Rev. 46 (2017) 915–1016, https://doi.org/10.1039/C6CS00368K.
[8] D. de Sa Pereira, D.R. Lee, N.A. Kukhta, K.H. Lee, C.L. Kim, A.S. Batsanov, J.Y. Lee, A.P. Monkman, The effect of a heavy atom on the radiative pathways of an emitter with dual conformation, thermally-activated delayed fluorescence and room temperature phosphorescence, J. Mater. Chem. C. 7 (2019) 10481–10490, https://doi.org/10.1039/C9TC02477H.
[9] Z.G. Wu, Z.P. Yan, X.F. Luo, L. Yuan, W.Q. Liang, Y. Wang, Y.X. Zheng, J.L. Zuo, Y. Pan, Non-doped and doped circularly polarized organic light-emitting diodes with high performances based on chiral octahydro-binaphthyl delayed fluorescent luminophores, J. Mater. Chem. C. 7 (2019) 7045–7052, https://doi.org/10.1039/c9tc01632e.
[10] Y. Chen, S. Wang, X. Wu, Y. Xu, H. Li, Y. Liu, H. Tong, L. Wang, Triazatruxene-based

small molecules with thermally activated delayed fluorescence, aggregation-induced emission and mechanochromic luminescence properties for solution-processable nondoped OLEDs, J. Mater. Chem. C 6 (2018) 12503–12508, https://doi.org/10.1039/c8tc04721a.
[11] J. Hu, X. Zhang, D. Zhang, X. Cao, T. Jiang, X. Zhang, Y. Tao, Linkage modes on phthaloyl/triphenylamine hybrid compounds: Multi-functional AIE luminogens, non-doped emitters and organic hosts for highly efficient solution-processed delayed fluorescence OLEDs, Dyes Pigm. 137 (2017) 480–489, https://doi.org/10.1016/j.dyepig.2016.10.029.
[12] J. Zhao, Recent progress in the mechanofluorochromism of cyanoethylene derivatives with aggregation-induced emission, J. Mater. Chem. C (2018), https://doi.org/10.1039/C8TC01648H.
[13] Y. Sagara, S. Yamane, M. Mitani, C. Weder, T. Kato, Mechanoresponsive luminescent molecular assemblies: an emerging class of materials, Adv. Mater. 28 (2016) 1073–1095, https://doi.org/10.1002/adma.201502589.
[14] C. Wang, Z. Li, Molecular conformation and packing: their critical roles in the emission performance of mechanochromic fluorescence materials, Mater. Chem. Front. 1 (2017) 2174–2194, https://doi.org/10.1039/c7qm00201g.
[15] Y. Sagara, T. Kato, Mechanically induced luminescence changes in molecular assemblies, Nat. Chem. 1 (2009) 605–610, https://doi.org/10.1038/nchem.411.
[16] B. Huang, W.-C. Chen, Z. Li, J. Zhang, W. Zhao, Y. Feng, B.Z. Tang, C.-S. Lee, Manipulation of molecular aggregation states to realize polymorphism, AIE, MCL, and TADF in a single molecule, Angew. Chemie. 130 (2018) 12653–12657, https://doi.org/10.1002/ange.201806800.
[17] S. Zheng, T. Liu, Z. Song, Z. He, Z. Yang, H. Wang, Z. Zeng, Acetenyl bridged diphenyl sulfones: a gate way to AIE / MCL / TADF multifunctional white-light emission molecule, Dyes Pigm. 176 (2020) 108204, , https://doi.org/10.1016/j.dyepig.2020.108204.
[18] Z. Xie, C. Chen, S. Xu, J. Li, Y. Zhang, S. Liu, J. Xu, Z. Chi, White-light emission strategy of a single organic compound with aggregation-induced emission and delayed fluorescence properties, Angew. Chemie Int. Ed. 54 (2015) 7181–7184, https://doi.org/10.1002/anie.201502180.
[19] R. Pashazadeh, P. Pander, A. Lazauskas, F.B. Dias, J.V. Grazulevicius, Multicolor luminescence switching and controllable thermally activated delayed fluorescence turn on/turn off in carbazole–quinoxaline–carbazole triads, J. Phys. Chem. Lett. 9 (2018) 1172–1177, https://doi.org/10.1021/acs.jpclett.8b00136.
[20] R. Pashazadeh, P. Pander, A. Bucinskas, P.J. Skabara, F.B. Dias, J.V. Grazulevicius, An iminodibenzyl-quinoxaline-iminodibenzyl scaffold as a mechanochromic and dual emitter: donor and bridge effects on optical properties, Chem. Commun. 54 (2018) 13857–13860, https://doi.org/10.1039/C8CC06981F.
[21] H. Li, Y. Zhi, Y. Dai, Y. Jiang, Q. Yang, M. Li, P. Li, Y. Tao, H. Li, W. Huang, R. Chen, Asymmetric thermally activated delayed fluorescence materials with aggregation-induced emission for high-efficiency organic light-emitting diodes, Front. Chem. 8 (2020), https://doi.org/10.3389/fchem.2020.00049.
[22] L. Huang, J. Liu, L. Liu, Q. Yang, Z. Ma, X. Jia, A D-A-D' type organic molecule with persistent phosphorescence exhibiting dual-mode mechanochromism, Dyes Pigm. 173 (2020) 107963, , https://doi.org/10.1016/j.dyepig.2019.107963.
[23] S.H. Choi, C.H. Lee, C. Adachi, S.Y. Lee, Highly effective nicotinonitrile-derivatives-based thermally activated delayed fluorescence emitter with asymmetric molecular architecture for high-performance organic light-emitting diodes, Dyes Pigm. 172 (2020) 107849, , https://doi.org/10.1016/j.dyepig.2019.107849.
[24] D. Song, Y. Yu, L. Yue, D. Zhong, Y. Zhang, X. Yang, Y. Sun, G. Zhou, Z. Wu, Asymmetric thermally activated delayed fluorescence (TADF) emitters with 5,9-dioxa-13 b -boranaphtho[3,2,1- de]anthracene (OBA) as the acceptor and highly efficient blue-emitting OLEDs, J. Mater. Chem. C. 7 (2019) 11953–11963, https://doi.org/10.1039/C9TC04115J.
[25] S. Xu, T. Liu, Y. Mu, Y.F. Wang, Z. Chi, C.C. Lo, S. Liu, Y. Zhang, A. Lien, J. Xu, An organic molecule with asymmetric structure exhibiting aggregation-induced emission, delayed fluorescence, and mechanoluminescence, Angew. Chemie – Int. Ed. 54 (2015) 874–878, https://doi.org/10.1002/anie.201409767.
[26] Z. Yang, Z. Mao, C. Xu, X. Chen, J. Zhao, Z. Yang, Y. Zhang, W. Wu, S. Jiao, Y. Liu, M.P. Aldred, Z. Chi, A sterically hindered asymmetric D-A–D′ thermally activated delayed fluorescence emitter for highly efficient non-doped organic light-emitting diodes, Chem. Sci. (2019), https://doi.org/10.1039/c9sc01686d.
[27] B. Xu, Y. Mu, Z. Mao, Z. Xie, H. Wu, Y. Zhang, C. Jin, Z. Chi, S. Liu, J. Xu, Y.-C. Wu, P.-Y. Lu, A. Lien, M.R. Bryce, Achieving remarkable mechanochromism and white-light emission with thermally activated delayed fluorescence through the molecular heredity principle, Chem. Sci. 7 (2016) 2201–2206, https://doi.org/10.1039/C5SC04155D.
[28] J. Guo, X. Li, H. Nie, W. Luo, S. Gan, S. Hu, Achieving high-performance nondoped OLEDs with extremely small efficiency roll-off by combining aggregation-induced emission and thermally activated delayed fluorescence, (2017). doi: 10.1002/adfm.201606458.
[29] D. Gudeika, O. Bezvikonnyi, D. Volyniuk, J.V. Grazulevicius, Dyes and pigments differently substituted benzonitriles for non-doped OLEDs, Dyes Pigm. 172 (2020) 107789, , https://doi.org/10.1016/j.dyepig.2019.107789.
[30] G. Sych, J. Simokaitiene, R. Lygaitis, E. Jatautiene, R. Pashazadeh, Structure-properties relationship of tetra fl uorostyrene-based monomers and polymers containing di ff erent donor moieties, React. Funct. Polym. 104323 (2019), https://doi.org/10.1016/j.reactfunctpolym.2019.104323.
[31] M.-S. Yuan, D.-E. Wang, P. Xue, W. Wang, J.-C. Wang, Q. Tu, Z. Liu, Y. Liu, Y. Zhang, J. Wang, Fluorenone organic crystals: two-color luminescence switching and reversible phase transformations between π–π stacking-directed packing and hydrogen bond-directed packing, Chem. Mater. 26 (2014) 2467–2477, https://doi.org/10.1021/cm500441r.
[32] K. Isayama, N. Aizawa, J.Y. Kim, T. Yasuda, Modulating photo- and electro-luminescence in a stimuli-responsive π-conjugated donor-acceptor molecular system, Angew. Chem. 130 (2018) 12158–12162, https://doi.org/10.1002/ange.201806863.
[33] B. Huang, D. Jiang, Y. Feng, W.-C. Chen, Y. Zhang, C. Cao, D. Shen, Y. Ji, C. Wang, C.-S. Lee, Mechanochromic luminescence and color-tunable light-emitting devices of triphenylamine functionalized benzo[d, e]benzo[4,5]imidazo[2,1-a]isoquinolin-7-one, J. Mater. Chem. C 7 (2019) 9808–9812, https://doi.org/10.1039/C9TC02592H.

SL344. 2020-12-09. 17,25 leidyb. apsk. l. Tiražas 12 egz. Užsakymas 270.
Išleido Kauno technologijos universitetas, K. Donelaičio g. 73, 44249 Kaunas
Spausdino leidyklos „Technologija“ spaustuvė, Studentų g. 54, 51424 Kaunas